

2017

Regulated Recruitment of the Chromosomal Passenger Complex to Chromatin and Microtubules Promotes Accurate Cell Division

Michael Wheelock

Follow this and additional works at: http://digitalcommons.rockefeller.edu/student_theses_and_dissertations



Part of the [Life Sciences Commons](#)

Recommended Citation

Wheelock, Michael, "Regulated Recruitment of the Chromosomal Passenger Complex to Chromatin and Microtubules Promotes Accurate Cell Division" (2017). *Student Theses and Dissertations*. 399.
http://digitalcommons.rockefeller.edu/student_theses_and_dissertations/399

This Thesis is brought to you for free and open access by Digital Commons @ RU. It has been accepted for inclusion in Student Theses and Dissertations by an authorized administrator of Digital Commons @ RU. For more information, please contact mcsweej@mail.rockefeller.edu.



REGULATED RECRUITMENT OF THE CHROMOSOMAL PASSENGER
COMPLEX TO CHROMATIN AND MICROTUBULES PROMOTES ACCURATE
CELL DIVISION

A Thesis Presented to the Faculty of
The Rockefeller University
in Partial Fulfillment of the Requirements for
the degree of Doctor of Philosophy

by
Michael S. Wheelock
June 2017

REGULATED RECRUITMENT OF THE CHROMOSOMAL PASSENGER
COMPLEX TO CHROMATIN AND MICROTUBULES PROMOTES ACCURATE
CELL DIVISION

Michael S. Wheelock, Ph.D.

The Rockefeller University 2017

Aurora B, the kinase subunit of the chromosomal passenger complex (CPC), promotes accurate cell division by destabilizing erroneous kinetochore-microtubule attachments and activating the spindle assembly checkpoint (SAC). Both functions require Aurora B activation, which is promoted by its binding to the C terminus of the CPC subunit INCENP, and by localization to the inner centromere, which requires the N terminus of INCENP. Inner centromere localization also requires phosphorylation of histone 3 threonine 3 (H3T3ph). While H3T3ph is required for CPC localization and the SAC during early mitosis, it must be dephosphorylated at anaphase to facilitate mitotic exit. However, the H3T3 kinase Haspin is predicted to be constitutively active, raising questions as to how H3T3ph is regulated with the cell cycle. Additionally, a single alpha helix (SAH) domain in INCENP is required to maintain the SAC elicited by the microtubule stabilizing drug taxol. While the SAH domain binds microtubules and is required for targeting the CPC to the spindle-midzone during anaphase, its role in the SAC during early mitosis remains unknown.

Here we uncover the molecular mechanism that couples H3T3ph to the cell cycle and elaborate how the INCENP SAH domain supports the SAC. Using

Xenopus egg extract and human tissue culture cells, we show that the kinase domain of Haspin is autoinhibited during interphase by a previously unidentified Haspin basic inhibitory segment (HBIS) downstream of the kinase domain. Upon entry into mitosis, Cdk1- and Polo-dependent multisite phosphorylation of the Haspin N terminus displace the HBIS from the kinase domain, resulting in Haspin activation and H3T3ph during mitosis. We also demonstrate that the INCENP SAH domain binds chromatin and supports CPC localization and stability at the centromere. Deleting the SAH domain reduces Aurora B-dependent phosphorylation at the kinetochore and attenuates the taxol-mediated SAC in human cells. We show that the microtubule-binding capacity of the SAH domain, rather than its role in localization, is required for the SAC in taxol. The microtubule-binding affinity of the SAH domain is also regulated by Cdk1-dependent phosphorylation in a phospho-regulatory domain (PRD) adjacent to the SAH domain, which we demonstrate also contributes to the checkpoint. Finally, while targeting INCENP to the centromere/kinetochore or microtubules supports the SAC in taxol, neither activity alone is sufficient for a robust checkpoint arrest. We propose a model wherein INCENP interacts with chromatin and microtubules during early mitosis to support local activation of Aurora B and the SAC. This work has implications for understanding how the CPC promotes the checkpoint and how Aurora B activity is regulated to ensure accurate chromosome segregation.

Acknowledgements

I want to start by thanking **Dr. Hironori Funabiki** for his mentorship, guidance and insightful discussion over the last 6 years. I admire his genuine love of science, open-mindedness and integrity. I greatly enjoyed the hours we spent discussing the CPC in his office and I thank him for his positivity and encouragement without which I would not be here today.

I would like to thank my committee members **Dr. Titia de Lange** and **Dr. Tarun Kapoor** for taking the time each year to meet and discuss my project. Their expertise, critical feedback, and support have been invaluable. I would also like to thank **Dr. Prasad Jallepalli** for serving as my external examiner.

I would like to thank all past and present members of **the Funabiki lab** for their insight, patience, camaraderie and snacks throughout the years. Thank you to **Dr. Boo Shan Tseng** for teaching me the *Xenopus* egg extract system and for pioneering the work on the INCENP SAH domain in our lab. Thanks to **Dr. Jessica Kumar** for teaching me about Budding yeast and for an incomparable level of energy and enthusiasm. To **Dr. John Xue**, thank you for a memorable experience purifying tubulin from cow brains and for always having some insight into current events. I would like to thank **Dr. Dave Wynne** for his optimism, sincerity and support during lab meetings. To my baymate **Dr. Simona Giunta-Field**, thank you for lending me your expertise in tissue culture, your pipettes (even when I did not ask), and your ear. Thanks to **Dr. Christian Zierhut** for organizing lab soccer games, for always bringing back marzipan, and for the best

thesis talk titles I could never use. I would like to thank future Ph.Ds **Pavan Choppakatla** and **Chris Jenness** for humoring my interest in basketball analytics and always being up to chat when I needed a break. Pavan, thank you for the thoughtful discussion on statistical distributions. Chris, thanks for letting me win (occasionally) in chess. A special thank you to **Adriana Garzon** for being the absolute best lab manager. Thank you to **Dr. Atanas Kaykov** for always being supportive and friendly, and to **Dr. Jun Funabiki** for your kindness and hospitality. I would also like to acknowledge **Dr. Cristoph Sommer** for having the patience to help me adapt CellCognition for my live imaging work. Finally, I would like to thank **Ali Smith** for a fun summer of cloning and setting up yeast cultures.

I would like to give a tremendous thank you to **Dr. Cristina GhenoIU** for taking me under her wing, giving me the opportunity to work on the Haspin project, and inspiring me to be a better scientist. I admire your fearlessness and sincerity, and thank you for your unwavering belief in my potential.

Thank you to **the Dean's office** for helping make Rockefeller the best graduate program in the world, including **Dr. Sid Stickland**, **Dr. Emily Harms**, **Marta Delgado**, **Kristen Cullen**, **Stephanie Fernandez** and **Cris Rosario**. Thank you for your kindness and assistance throughout the years. In particular, I would like to thank Dr. Strickland and Dr. Harms for inviting me to the genetics journal club, and Dr. Harms for inviting me to participate in SURF.

Thank you to the entire **Rockefeller Bioimaging Facility**, including **Dr. Alison North**, **Dr. Kaye Thomas**, **Dr. Pablo Ariel**, and **Tao Tong**. Your

expertise and patience were essential to my project and my success. Thank you also to **the Rockefeller Proteomics Resource Center**, especially **Dr. Henrik Molina, Dr. Joseph Fernandez** and **Dr. Milica Tesic Mark**.

To **Dr. Rachel O’neill**, your mentorship and encouragement inspired me to pursue science. Thank you for always believing in me. **Dr. Barbara Mellone**, thank you for introducing me to Aurora B, the SAC and Dr. Funabiki’s work.

Love and gratitude to my parents Donna and Steven Wheelock. **Mom**, your selflessness, perseverance and optimism are an inspiration to me. Thank you for your unconditional love, for worrying about the small things, and for making me who I am today. **Dad**, thank you for putting my education first, your strength, and your dry humor. To my **grandparents**, your lessons and love forever live in my heart. To the countless others who have accompanied and shepherded me throughout life; **friends, family** and **faculty**, thank you.

A special thank you to **Jennifer Peeler**. Your companionship has filled my life with joy and your strength and steady hand helped make this thesis possible. Thank you for your patience, your thoughtfulness and your willingness to listen. Thank you for filling graduate school with fond memories, lasting friendships and CSA veggies. I love and appreciate your unwavering support. I am tremendously proud of your personal and professional accomplishments and am excited for our life in Boston.

Finally, to **Buddy**, thank you for long walks through the city, late night romps and enthusiastic greetings.

Table of Contents

List of Figures	ix
List of Tables	xii
Chapter 1: General Introduction	1
1.1 Cell Division	1
1.2 The Spindle Assembly Checkpoint.....	12
Formation of the MCC	14
SAC silencing	18
SAC activation: Attachment versus Tension	20
1.3 The Chromosomal Passenger Complex (CPC)	25
CPC discovery, composition and activation	25
CPC localization during early mitosis	30
CPC functions during early mitosis	36
Coupling CPC function to kMT attachment status.....	41
Localization and function in late mitosis	49
1.4 Haspin	51
Atypical features of Haspin kinase	52
Coupling H3T3ph to the cell cycle.....	52
1.5 <i>Xenopus</i> egg extract.....	55
1.6 Goals of this dissertation	57
Chapter 2: Autoinhibition and Polo-dependent Multisite Phosphorylation	
Restrict Activity of the Histone H3 Kinase Haspin to Mitosis.....	58
2.1 Introduction:.....	58
2.2 Results	61
Cdk1- and Plx1-dependent phosphorylation activate Haspin in mitosis	61
Haspin is activated in mitosis by multisite phosphorylation of its N terminus.....	72
The Haspin Basic Inhibitory Sequence (HBIS) prevents Haspin activation in	
interphase	77
The HBIS interacts with importin- β but this does not regulate H3T3ph	80
The HBIS directly inhibits Haspin kinase <i>in vitro</i>	85
The HBIS peptide is unable to inhibit Haspin in extract	87
The HBIS binds the Haspin kinase domain in a Plx1-dependent manner.....	93
Plk1 and Aurora B activate Haspin during mitosis in human cells	105
Human Haspin is regulated by Polo-dependent activation and HBIS-dependent	
inhibition	111
2.3 Discussion	115
A model for coupling Haspin activation to the cell cycle.....	115
The mechanism of Haspin auto-inhibition in interphase	118
The mechanism of Haspin activation in mitosis	119
Polo and Aurora B support hHaspin activation in mitosis	123
Chapter 3: INCENP Detects Chromatin and Microtubules to Sustain the	
Mitotic Checkpoint and Alter Cell Fate.....	126
3.1 Introduction	126
3.2 Results	130

The INCENP SAH domain is required for CPC localization and the SAC in <i>Xenopus</i> egg extracts.....	130
The SAH domain is required for CPC localization and dynamics in human cells ..	136
The SAH domain is required for the SAC and cell death in taxol-treated human cells	144
The SAH domain is required for SAC protein recruitment and kinetochore phosphorylation in taxol-treated human cells	150
Neither cytoplasmic activation of Aurora B nor tethering INCENP to the centromere/kinetochore support a robust SAC	155
The SAH domain is a Cdk1-regulated microtubule-binding domain.....	165
The SAH domain binds microtubules to maintain the SAC in taxol-treated cells ..	178
3.3 Discussion	194
The INCENP SAH domain maintains the CPC on chromatin.....	194
The INCENP SAH domain binds microtubules prior to anaphase to support the SAC in taxol-treated cells	197
INCENP chromatin- and microtubule-binding independently contribute to the SAC in taxol.....	199
Cdk1-dependent regulation of the INCENP SAH domain	200
The CPC sustains the SAC to promote death in mitosis.....	202
Chapter 4: Perspectives	204
4.1 Broader Implications	204
Haspin detects Plk1 activity to regulate cohesion during mitosis	204
Positive feedback in CPC localization: The chicken and the egg.....	206
An additional mechanism supports CPC localization to the centromere	208
Why are there different requirements of the SAH domain in nocodazole versus taxol in human cells and <i>Xenopus</i> egg extract?	213
CPC localization dynamics at the centromere.....	216
Localization and function of the CPC on microtubules in early mitosis	220
Regulation of the CPC at the kinetochore and on microtubules.....	224
4.2 Concluding Remarks: CPC at the centromere and beyond.....	228
Chapter 5: Material and Methods	229
5.1 General Techniques	229
Plasmid construction	229
Immunoblotting.....	230
Immunofluorescence image acquisition and processing	231
Data presentation.....	232
5.2 Human Tissue Culture	233
Cell culture, siRNA and drug treatments	233
Immunoprecipitation.....	234
Live cell imaging and analysis.....	235
Immunofluorescence	236
Fluorescence recovery after photobleaching (FRAP)	238
5.3 <i>Xenopus</i> egg extract.....	239
<i>Xenopus</i> egg extract depletion and reconstitution	239
Immunofluorescence	240
Spindle assembly checkpoint.....	241
Microtubule pelleting assay	241

Phosphatase treatment	242
CENP-A nucleosome arrays	242
Immunoprecipitation.....	243
Synthetic peptides and bead pulldowns	245
Mass spectrometry.....	246
5.4 Recombinant proteins/ <i>in vitro</i> assays:	249
Recombinant proteins	249
Far western blots.....	250
Kinetic analysis of H3T3ph.....	251
<i>In vitro</i> kinase assays with recombinant proteins.....	252
Antibody beads kinase assay.....	253
Quantification of H3T3ph activity exhibited by xHaspin phosphorylation mutants	254
Appendix: Tables.....	255
References	261

List of Figures

Figure 1-1: Stages of mitosis	3
Figure 1-2: The vertebrate kinetochore	6
Figure 1-3: Configurations of kMT attachment during mitosis	9
Figure 1-4: The spindle assembly checkpoint prevents anaphase onset until all chromosomes are bi-oriented on the spindle	11
Figure 1-5: Molecular details of SAC activation.....	16
Figure 1-6: Components and structure of the CPC	27
Figure 1-7: INCENP regulates the kinase activity of Aurora B	29
Figure 1-8: Localization of the CPC during mitosis.....	32
Figure 1-9: Regulating Aurora B-dependent phosphorylation at the kinetochore with kMT attachment status.....	43
 Figure 2-1: H3T3 phosphorylation is not dependent on Aurora B in <i>Xenopus</i> egg extracts	62
Figure 2-2: The activity of Polo kinase is required for H3T3ph in <i>Xenopus</i> egg extract.....	64
Figure 2-3: Plx1 interacts with and phosphorylates the xHaspin N terminus dependent on priming phosphorylation of xHaspin T206 by Cdk1	67
Figure 2-4: Cdk1 activity is required for H3T3ph in <i>Xenopus</i> egg extract	71
Figure 2-5: Multisite phosphorylation of the xHaspin N terminus is required for robust H3T3ph in metaphase <i>Xenopus</i> egg extract	73
Figure 2-6: The HBIS restricts H3T3ph to interphase.....	79
Figure 2-7: Plx1 prevents binding of Importin β to xHaspin in metaphase <i>Xenopus</i> egg extracts.....	82
Figure 2-8: Importin β binding to xHaspin does not restrict H3T3ph to interphase	83
Figure 2-9: The xHaspin HBIS inhibits the kinase activity of xHaspin <i>in vitro</i>	86
Figure 2-10: The HBIS peptide is unable to inhibit H3T3ph in <i>Xenopus</i> egg extract.....	89
Figure 2-11: Plx1-mediated phosphorylation of the xHaspin N terminus regulates HBIS binding to the xHaspin N terminus and kinase domain	95
Figure 2-12: xHaspin residues 675-730 are critical for the xHaspin N terminus to bind the HBIS	99
Figure 2-13: The conserved acidic triplet in the xHaspin kinase domain does not mediate interaction with the HBIS	103
Figure 2-14: Plk1 is required for H3T3ph in mitosis in human cells.....	106
Figure 2-15: Aurora B and Plk1 stimulate H3T3ph in mitosis in human cells ...	107
Figure 2-16: Aurora B and Plk1 independently promote H3T3ph on mitotic chromatin and Aurora B localization to the centromere in human cells.....	109
Figure 2-17: hHaspin T128 supports the majority of Plk1-mediated hHaspin mobility shift and Plk1-dependent H3T3ph.....	112
Figure 2-18: The hHaspin HBIS antagonizes H3T3ph in interphase	114

Figure 2-19: Molecular mechanism coupling activation of Haspin to the cell cycle	117
Figure 3-1: The xINCENP SAH domain supports the nocodazole-induced SAC in <i>Xenopus</i> egg extract.....	131
Figure 3-2: The xINCENP SAH domain supports CPC localization to chromatin in <i>Xenopus</i> egg extract.....	133
Figure 3-3: The xINCENP SAH domain interacts with chromatin independent of the INCENP CEN domain.....	134
Figure 3-4: The CPC forms independent of the hINCENP SAH domain in HeLa cells.	137
Figure 3-5: The hINCENP SAH domain is not required for the spatiotemporal distribution of the CPC in HeLa cells.	139
Figure 3-6: The hINCENP SAH domain is necessary for robust enrichment of the CPC at the centromere in HeLa cells.	140
Figure 3-7: The hINCENP SAH domain stabilizes the CPC at the centromere in HeLa cells.....	143
Figure 3-8: The hINCENP SAH domain is required for the taxol- and monastrol-induced SAC in HeLa cells.	145
Figure 3-9: The hINCENP SAH domain promotes mitotic cell death in taxol. ..	148
Figure 3-10: The hINCENP SAH domain supports SAC protein recruitment to the kinetochore.....	152
Figure 3-11: The hINCENP SAH domain is required for Aurora B-dependent kinetochore phosphorylation in taxol.	153
Figure 3-12: Artificially activating Aurora B in the absence of the SAH domain is insufficient to support the taxol-mediated SAC.....	156
Figure 3-13: Artificially targeting hINCENP to the centromere or kinetochore independent of the CEN domain.	159
Figure 3-14: Targeting hINCENP to the centromere or kinetochore does not bypass the hINCENP CEN domain in the taxol-mediated SAC.....	161
Figure 3-15: Targeting hINCENP to the centromere or kinetochore promotes the taxol-mediated SAC independent of the hINCENP SAH domain.	162
Figure 3-16: Targeting hINCENP to the kinetochore induces a prolonged mitotic delay independent of the SAH domain.	164
Figure 3-17: The xINCENP SAH domain associates with the spindle dependent on its N terminus in <i>Xenopus</i> egg extract.....	167
Figure 3-18: Vertebrate INCENP contains six highly conserved putative Cdk1 phosphorylation sites flanking the SAH domain.	168
Figure 3-19: Alignment of human INCENP and the Budding yeast INCENP homolog Sli15.....	170
Figure 3-20: The xINCENP SAH domain is phosphorylated on the PRD in a cell-cycle-dependent manner in <i>Xenopus</i> egg extract.	175
Figure 3-21: Phosphorylation of the PRD regulates xINCENP SAH domain binding to the spindle in <i>Xenopus</i> egg extract.....	175

Figure 3-22: Phosphorylation of the PRD regulates xINCENP binding to microtubules and Aurora B activation.....	177
Figure 3-23: The hINCENP SAH domain binds microtubules to support the taxol-mediated SAC in HeLa cells.	180
Figure 3-24: The C terminus of the hINCENP SAH domain is dispensable for the taxol-mediated SAC in HeLa cells.	182
Figure 3-25: Phosphorylation of the hINCENP PRD regulates hINCENP microtubule binding and the taxol-mediated SAC in HeLa cells.	184
Figure 3-26: Targeting hINCENP to microtubules supports the taxol-mediated SAC independent of centromere targeting.	186
Figure 3-27: The hINCENP SAH domain is mostly dispensable for the SAC, SAC protein recruitment and kinetochore phosphorylation in nocodazole.	188
Figure 3-28: The N terminus of the xINCENP SAH domain supports CPC localization on chromatin to maintain the nocodazole-mediated SAC in <i>Xenopus</i> egg extract.....	192
Figure 3-29: A model for the CPC in the taxol-mediated SAC.....	196
 Figure 4-1: Summary of FRAP recovery data for CPC componenets from previous publications	218

List of Tables

Table 1: Identification of phosphorylation sites on Haspin.....	255
Table 2: Constructs.....	258
Table 3: Primary antibodies.....	259
Table 4: Secondary antibodies.....	260

Chapter 1: General Introduction

1.1 Cell Division

Cell division is a fundamental process required for organismal development, reproduction, and homeostasis. Cell division in somatic tissues (**Mitosis**) is a complex and coordinated series of events that equally partitions the genome of a mother cell into two daughter cells. Since Walther Flemming's seminal drawing in the 1880's (**Figure 1-1**), scientists have been fascinated with understanding the molecular determinants that govern this dramatic and essential process.

Mitosis can be partitioned into five stages based on obvious changes in chromosome structure and distribution within the vertebrate cell. These stages typically occur in the following sequence in vertebrates. During **prophase**, replicated genetic material begins to condense into individual chromosomes. Additionally, a pair of centrioles located outside of the nucleus begins to nucleate microtubules and separate towards opposite ends of the cell. This is followed by **prometaphase** in which nuclear envelope breakdown (NEB) occurs and the mitotic spindle takes shape. Chromosomes begin attaching to the spindle and align at the center of the cell. When every chromosome has aligned, the cell is in **metaphase**. These first three stages are collectively known as early mitosis (Rieder & Khodjakov 2003).

Chromosome segregation begins in **anaphase**, with sister chromatids moving towards opposite poles of the cell as the microtubules attached to each

chromatid shorten (anaphase A) and the spindle poles separate (anaphase B). These coordinated movements equally partition the genetic material into two separate masses at opposite ends of the mother cell. During **telophase**, the spindle is disassembled and each mass of chromatids begins to decondense and form its own nuclear envelope. These last two stages are known collectively as late mitosis (Rieder & Khodjakov 2003).

Cytokinesis, though a distinct process from mitosis, begins concomitant with the initiation of anaphase. A contractile ring forms at the cell cortex perpendicular to the direction of chromosome segregation and slowly contracts to pinch the mother cell into two daughter cells. This ultimately leads to a visible cleavage furrow and the production of a midbody, a small bridge of proteins and microtubules that connects the daughters. The midbody is severed during **abscission** to create two independent and genetically identical cells (Rieder & Khodjakov 2003).

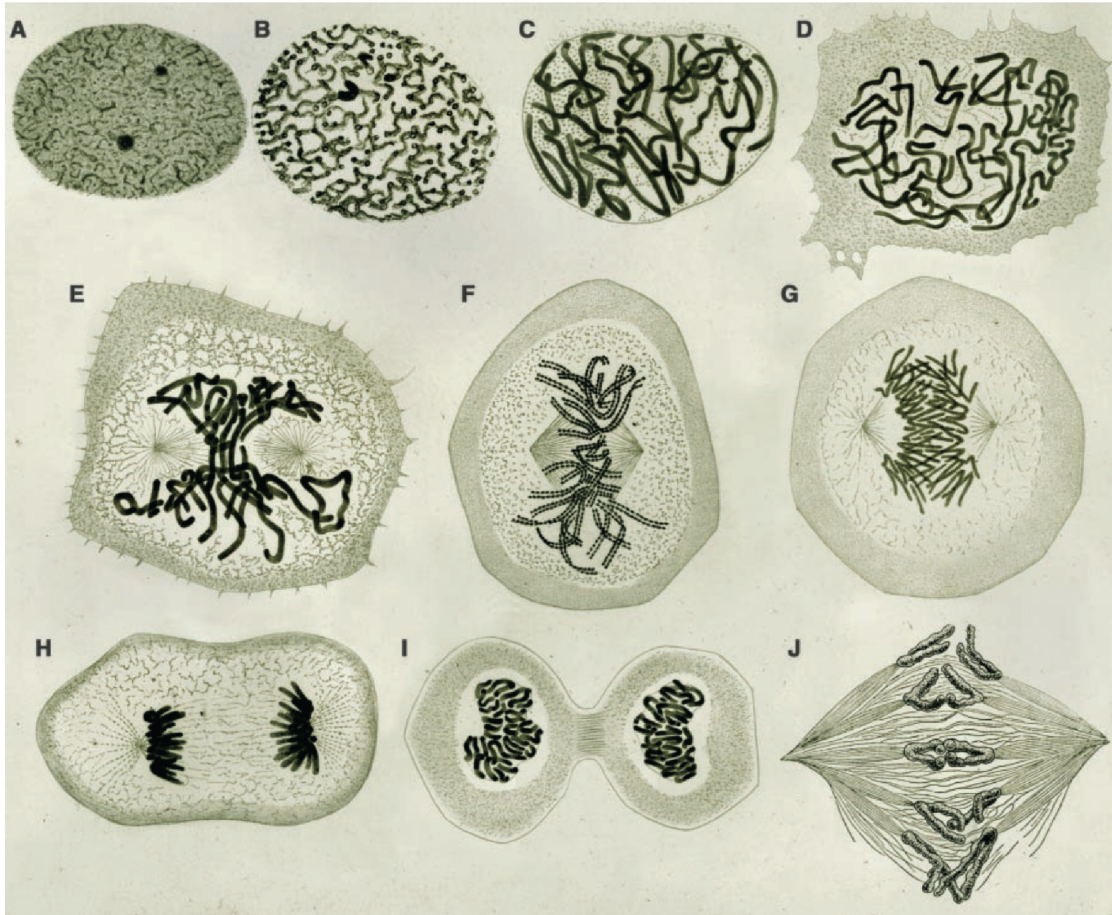


Figure 1-1: Stages of mitosis

A-I) Drawings of Newt cells undergoing mitosis by Walther Flemming. A-C: prophase: interphase chromatin compaction; D-E: prometaphase: nuclear envelop breakdown and spindle assembly; F: metaphase, chromosomes align at the center of the spindle/ cell; G: early anaphase (anaphase I), sister chromatids separate as the microtubules they're attached to depolymerize towards opposite poles; H: late anaphase (anaphase II), sister chromatids continue to separate as the spindle poles separate in opposite directions; I: cytokinesis/ telophase, chromosomes decompact, the nuclear envelop reforms, and the cleavage furrow ingresses; reproduced from (Rieder & Khodjakov 2003).

J) Drawing of chromosomes and the mitotic spindle in the Lilly by F. Schrader; reproduced from (Rieder & Khodjakov 2003).

During early mitosis, the goal for each chromosome is to align and form stable attachments to the mitotic spindle. This process is governed by the **kinetochore**, a proteinaceous adaptor linking centromeric chromatin to spindle microtubules. The kinetochore directly binds the plus-end of microtubules, forming **kinetochore-microtubule** (kMT) attachments. The kinetochore's ability to maintain this attachment, even as the microtubule alternates between polymerizing and depolymerizing states, helps power chromosome movement during early and late mitosis (Santaguida & Musacchio 2009).

The kinetochore is broadly organized into at least two layers: the **inner kinetochore** and **outer kinetochore** (Santaguida & Musacchio 2009) (**Figure 1-2**). The inner kinetochore contains the **constitutive centromere associated network** (CCAN) of proteins, which anchor the kinetochore to centromeric chromatin. Two proteins important for this function are **CENP-C**, which interacts with the CENP-A nucleosome (Kato et al. 2013), and **CENP-T**, which interacts with CENP-S, -X, and -W and forms a histone-fold domain that may directly bind centromeric DNA (Nishino et al. 2012). The outer kinetochore directly binds microtubules through the Knl1/Mis12/Ndc80 (**KMN**) complexes (Cheeseman et al. 2006). While components from all three complexes support microtubule binding, it is the **Ndc80 complex** that is most important for end-on microtubule binding in vertebrates. **Knl1** primarily acts as a protein recruitment and signaling platform for the spindle assembly checkpoint (SAC; see below) while the **Mis12 complex** recruits Knl1 and the Ndc80 complex. The inner and outer kinetochore

are connected by the N terminus of CENP-C, which binds the Mis12 complex (Przewloka et al. 2011; Screpanti et al. 2011). Independently of the Mis12 complex, CENP-T also provides an additional recruitment site for the Ndc80 complex (Nishino et al. 2013; Malvezzi et al. 2013).

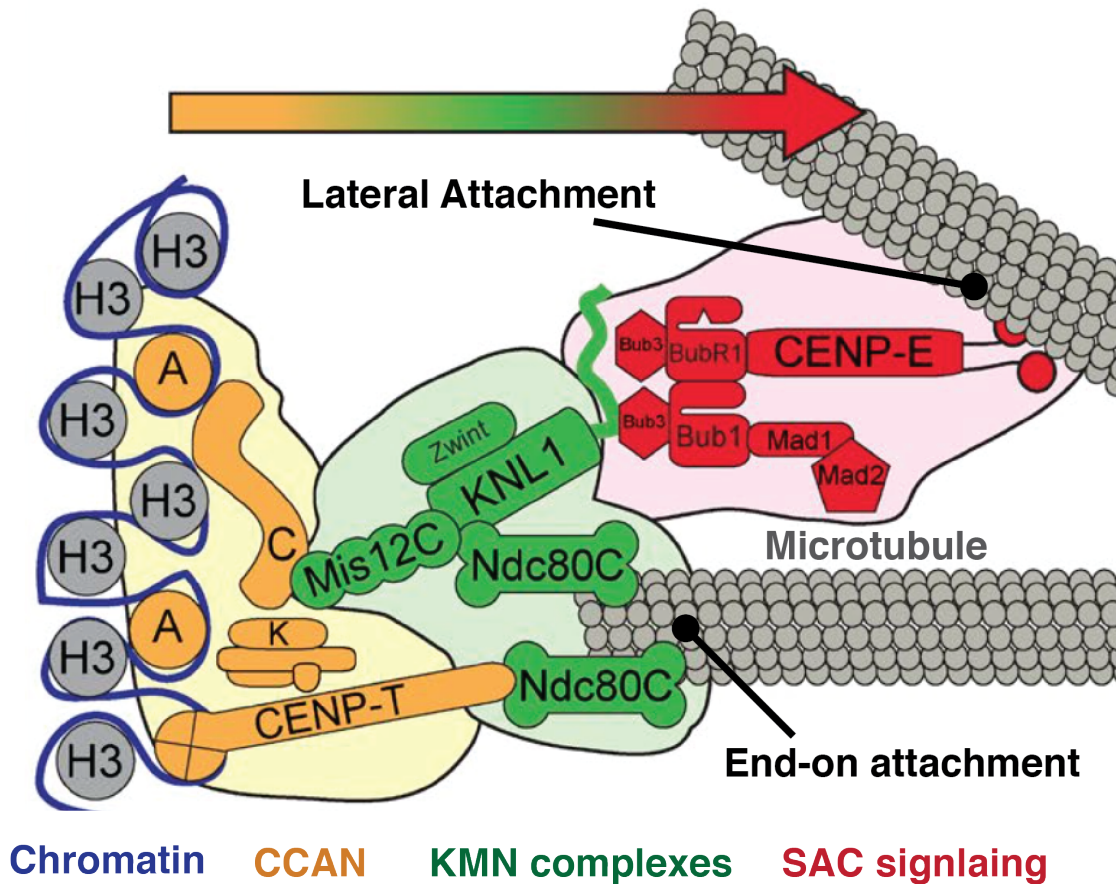


Figure 1-2: The vertebrate kinetochore

Diagram of the vertebrate kinetochore, highlighting centromeric chromatin (blue), the constitutive centromere associated network (CCAN, yellow), Knl1/Mis12/Ndc80 (KMN) complexes (green), the spindle assembly checkpoint (SAC) signaling machinery (red) and microtubules (gray). CENP-C (C) and CENP-T bridge centromeric chromatin to the KMN complexes, which bind microtubules. Efficient chromosome segregation requires the kinetochore to form end-on attachments. Lateral attachments support chromosome alignment, but must be released or converted to end-on attachment for efficient chromosome segregation. Adapted from (Wynne & Funabiki 2015).

For accurate chromosome segregation to occur, sister kinetochores must be oriented towards opposite poles and attached to microtubules exclusively from that pole (**Figure 1-3**). This **bipolar attachment** ensures efficient segregation of sister chromatids in opposite directions. However, formation of kMT attachments occurs by a stochastic **search-and-capture** process and can generate configurations prone to chromosome missegregation (Kirschner & Mitchison 1986). These include failure to form kMT attachment (**unattached**), attachment of sister kinetochores to microtubules from a single pole (**syntelic attachment**) or attachment of a single kinetochore to microtubules from both poles (**merotelic attachment**) (Santaguida & Musacchio 2009).

The cell has a robust **error correction** machinery that limits the frequency of chromosome segregation in the presence of attachment errors. In vertebrates, this depends on the protein kinase **Aurora B** (Chapter 1.3) (Ruchaud et al. 2007; Carmena et al. 2014). Aurora B phosphorylates multiple components of the KMN network, lowering their affinity for microtubules *in vitro* and contributing to kMT destabilization *in vivo* (Welburn et al. 2010). This process is thought to release erroneous attachments, generating an unattached kinetochore that can reinitiate search-and-capture. Consistent with this idea, chemical inhibition of Aurora B stabilizes syntelic and merotelic attachments and results in chromosome missegregation (Cimini et al. 2006; Lampson et al. 2004; Ditchfield et al. 2003; Hauf et al. 2003). Levels of Aurora B phosphorylation are high on substrates at unattached kinetochores and decreases following bi-orientation (Deluca et al.

2011; Welburn et al. 2010; D. Liu et al. 2009). How Aurora B-substrate phosphorylation is regulated with microtubules attachment status remains unclear, but this process seems critical. Failure to regulate Aurora B activity with microtubule attachment, for example by mimicking constitutive phosphorylation of Ndc80 with glutamic acid, destabilizes kMT attachments and impairs chromosome alignment (Welburn et al. 2010; Guimaraes et al. 2008). Understanding the molecular basis for Aurora B regulation is a central topic in this dissertation.

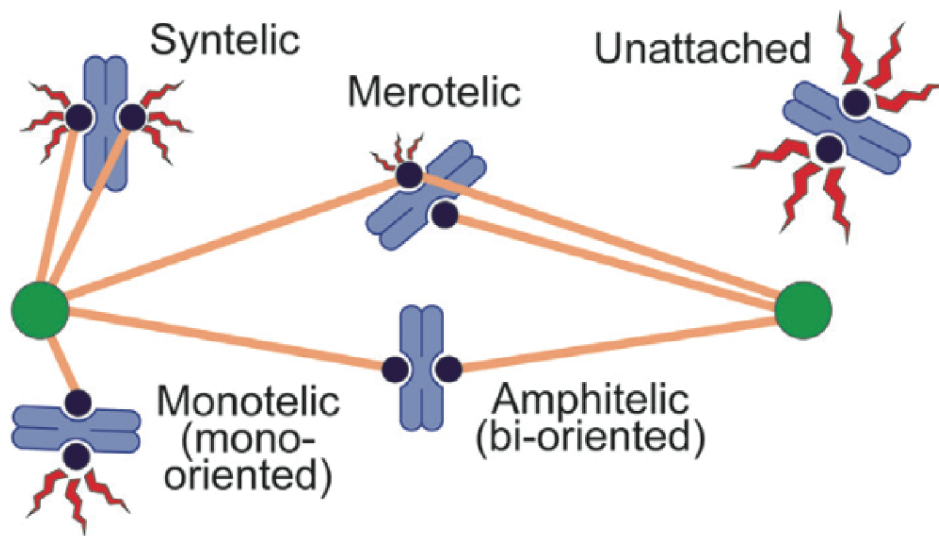


Figure 1-3: Configurations of kMT attachment during mitosis

Accurate chromosome segregation requires each chromosome achieve bi-oriented (amphitelic) attachment to the spindle. Unattached kinetochores or erroneous kMT attachment configurations (syntelic, monotelic or merotelic) can lead to lagging chromosomes, chromosome missegregation and aneuploidy. These aberrant states can signal the SAC (red waves) to different extents. While unattached kinetochores generate a robust SAC signal, merotelic attachments only weakly, if at all, activate the checkpoint. Thus, an efficient error correction mechanism, centered on the protein kinase Aurora B, is required to prevent chromosome segregation in the presence of erroneous attachments. Reproduced from (Krenn & Musacchio 2015).

An additional mechanism that promotes accurate cell division is the **spindle assembly checkpoint** (SAC) (**Figure 1-4**; Section 1.2). This signaling cascade can be activated by a single unattached kinetochore (Rieder et al. 1994) and is capable of delaying the onset of anaphase for over 50 hrs in certain cell types and conditions (Gascoigne & Taylor 2008). This provides time for an unattached kinetochore to form bipolar attachments to the spindle. The SAC works by inhibiting the **Anaphase Promoting Complex** (APC), an E3 ubiquitin ligase that targets multiple substrates for proteasome-dependent degradation, most importantly Cyclin B and Securin. Degradation of Cyclin B decreases Cdk1-Cyclin B activity, which initiates anaphase onset. Meanwhile degradation of Securin activates separase, which degrades cohesin and allows sister chromatid separation. The major effector of the SAC that inhibits the APC is the **mitotic checkpoint complex** (MCC, see below). The MCC is also generated during interphase (Sudakin et al. 2001), which slows Cyclin B/Securin degradation during mitotic entry (Rodriguez-Bravo et al. 2014). During mitosis, the MCC is locally generated by unattached kinetochores to inhibit the APC (Kulukian et al. 2009). Continued production of the MCC dramatically attenuates the rate of Cyclin B/ Securin degradation, providing time for the unattached kinetochore to form bipolar attachments to the spindle. Once all chromosomes are bi-oriented, the SAC signal is **silenced**, resulting in the cessation of MCC production, disassembly of residual MCC, and subsequent APC activation and entry into anaphase (Musacchio & Salmon 2007).

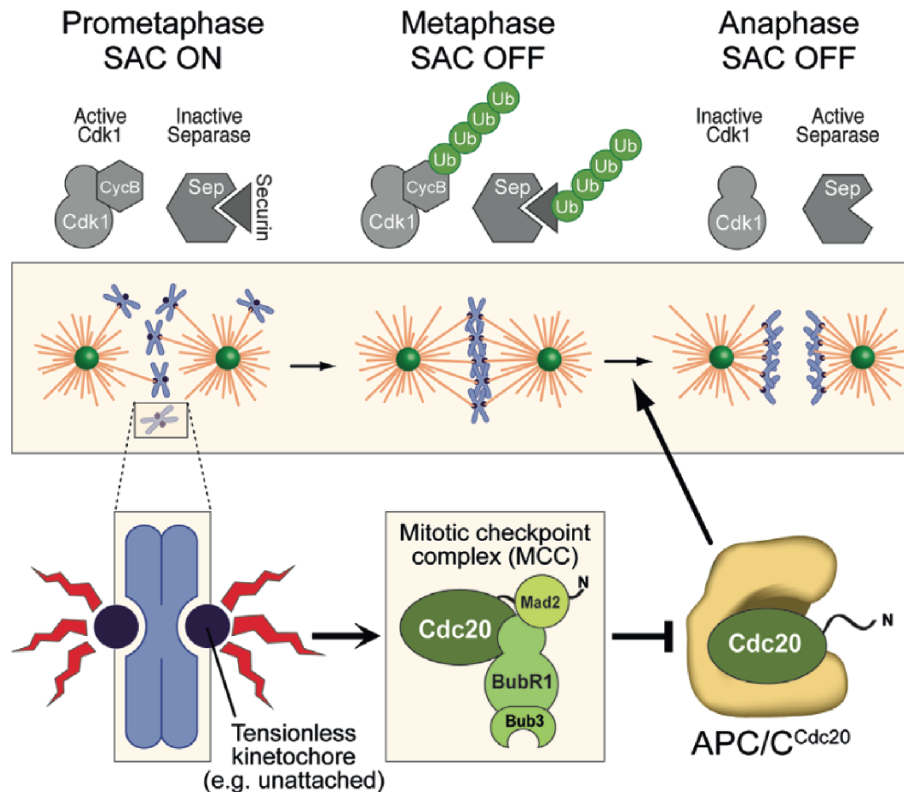


Figure 1-4: The spindle assembly checkpoint prevents anaphase onset until all chromosomes are bi-oriented on the spindle

The initiation of anaphase requires ubiquitin-mediated (Ub) degradation of Cyclin B and Securin (top) by the 26S proteasome. This process is initiated by the E3 ubiquitin ligase Anaphase Promoting Complex/ Cyclosome (APC/C, bottom right). Degradation of Cyclin B inactivates Cdk1, triggering anaphase, while degradation of Securin activates Separase, which promotes removal of centromeric cohesion to facilitate sister chromatid separation. Unattached kinetochores (bottom left) locally activate the spindle assembly checkpoint (SAC, red waves) and produce the mitotic checkpoint complex (MCC, bottom middle), which inhibits the function of the APC/C. This attenuates the degradation of Cyclin B and Securin, maintaining cells in mitosis until the SAC signal is exterminated by chromosome bi-orientation. Reproduced from (Krenn & Musacchio 2015).

1.2 The Spindle Assembly Checkpoint

Anaphase onset requires ubiquitination of Cyclin B by the E3-ubiquitin ligase Anaphase Promoting Complex/ Cyclosome (APC/C; referred to in this dissertation as the **APC**) and subsequent degradation by the 26S proteasome (**Figure 1-4**). The ubiquitin ligase activity of the APC is stimulated by Cdc20, which acts both as an allosteric activator and an APC substrate recognition protein via interaction with the destruction box on APC substrates. Quantitatively measuring the abundance of fluorescently labeled Cyclin B during mitosis reveals that its rate of degradation is slow during early mitosis and accelerates after chromosomes align at the metaphase plate (Clute & Pines 1999). Once Cyclin B abundance dips below a threshold level, anaphase chromosome movement is initiated regardless of chromosome alignment. Thus, degradation of Cyclin B must be coupled to chromosome alignment to prevent anaphase onset in the absence of bi-oriented chromosomes (Musacchio & Salmon 2007).

This coupling is accomplished by the spindle assembly checkpoint (**SAC**) (Musacchio & Salmon 2007). The SAC promotes assembly of the mitotic checkpoint complex (**MCC**), composed of the proteins **Mad2**, BubR1, Bub3 and **Cdc20** (Sudakin et al. 2001) (**Figure 1-4**). The MCC is the primary effector of the SAC and inhibits APC activation in at least three ways: first, by sequestering Cdc20 from the APC, second, by binding the APC and allosterically inhibiting it, and finally, by acting as a pseudocompetitive inhibitor through the interaction of a KEN box on BubR1 with Cdc20 (Musacchio & Salmon 2007; Alfieri et al. 2016).

By preventing full activation of the APC, the MCC decreases the rate of Cyclin B and Securin degradation, delaying the onset of anaphase to allow time for chromosome bi-orientation.

The SAC is activated by unattached kinetochores and silenced when all kinetochores accomplish bi-oriented attachment. Preventing microtubule attachment by depolymerizing microtubules with drugs such as nocodazole or benomyl results in a robust SAC-dependent arrest from yeasts to humans. During an unperturbed mitosis, even a single unattached kinetochore is sufficient to induce a mitotic delay (Rieder et al. 1994). Consistent with the kinetochore generating the SAC signal, the number of unattached kinetochores inversely correlates with the rate of Cyclin B degradation (Clute & Pines 1999; Dick & Gerlich 2013; Collin et al. 2013) while laser-ablation of the last unattached kinetochore rapidly induces anaphase (Rieder et al. 1995). Many of the proteins involved in the SAC localize to the kinetochore upon mitotic entry and are decreased in abundance or absent when chromosome segregation initiates. Recruiting SAC proteins to the kinetochore is critical for their function. For example, preventing kinetochore localization of the upstream SAC activator Mps1 attenuates the checkpoint in nocodazole (Nijenhuis et al. 2013), while artificially targeting it to the kinetochore can stimulate a SAC-dependent arrest even after chromosome alignment (Jelluma et al. 2010). Understanding how SAC protein recruitment and checkpoint activation is coupled to kMT attachment is a central question in the field.

Formation of the MCC

During mitosis, formation of the MCC occurs primarily at the kinetochore and requires several proteins including the serine/threonine kinase Mps1, mitotic arrest deficient 1 (**Mad1**) and the MCC component Mad2 (**Figure 1-5A**).

Formation of the MCC is complex, but a critical first step is the binding of Mad2 to the APC activator Cdc20. This binding requires Mad2 to adopt a 'closed' conformation (C-Mad2), which is biochemically and structurally distinct from its 'open' conformation (O-Mad2) that predominates in solution (Luo et al. 2004). It has been proposed that Mad1 at the kinetochore promotes formation of the MCC through a templating model (Kulukian et al. 2009; De Antoni et al. 2005; Mapelli et al. 2007; Simonetta et al. 2009). First, a 2:2 complex of Mad1/C-Mad2 is recruited to the kinetochore. Then, Mad1/C-Mad2 acts as a template to catalyze the production of soluble O-Mad2, which is capable of binding Cdc20 and initiating formation of the MCC. While this model is still under investigation, it provides an explanation for how the signal from a single kinetochore could be amplified enough to arrest the entire cell.

Mad1 must localize to the kinetochore to support formation of the MCC. This depends on the kinetochore recruitment and kinase activity of Mps1 (**Figure 1-5B**). Mps1 binds the N terminus of the kinetochore protein Ndc80 adjacent to its microtubule-binding calponin homology (CH) domain (Ji et al. 2015; Hiruma et al. 2015). Mps1 then phosphorylates a series of MELT motifs (M[D/E][I/L/V/M][S/T]) on the kinetochore protein **Knl1**, which directly interact with

and recruit the proteins **Bub1**/Bub3 (London et al. 2012; Yamagishi et al. 2012; Sheppard et al. 2012; Primorac et al. 2013). This complex then supports kinetochore recruitment of the MCC components BubR1/Bub3 (Zhang et al. 2015; Overlack et al. 2015). Mps1 activity and MELTph are required for Mad1 recruitment. In *C. elegans*, Bub1 directly binds Mad1 to promote the SAC (Moyle et al. 2014), while in yeast, this interaction requires Mps1-dependent phosphorylation of Bub1 (London & Biggins 2014; Heinrich et al. 2014). It remains to be established how Mad1 is recruited in vertebrates. It is known that the Rod/ZW10/Zwilch (**RZZ**) complex is required for Mad1/Mad2 targeting to the kinetochore (Kops et al. 2005; Buffin et al. 2005), and while the molecular details remain unclear, it has been suggested that this complex recruits Mad1/Mad2 independent of Knl1 (Silió et al. 2015). Regardless of the specific mechanism, Mps1 supports recruitment of Mad1/Mad2 to the kinetochore to activate the checkpoint during mitosis (**Figure 1-5C**). Consistent with this, constitutive targeting of Mps1 or Mad1, or C-Mad2 to the kinetochore stimulates a mitotic arrest even when chromosomes are aligned at the metaphase plate (Kruse et al. 2014; Maldonado & Kapoor 2011; Jelluma et al. 2010). Interestingly, inhibiting Mps1 activity induces checkpoint silencing even when Mad1 is constitutively recruited to the kinetochore, indicating it is required downstream of Mad1/Mad2 recruitment for the checkpoint (Maldonado & Kapoor 2011). Thus, it is still unclear exactly how the MCC is generated during mitosis.

Figure 1-5: Molecular details of SAC activation

A) A 2:2 heterodimer of Mad1 (dark yellow) and C-Mad2 (dark red) recruited to an unattached kinetochore (red) initiates formation of the MCC by “templating” the conversion of soluble O-Mad2 (light yellow) into C-Mad2. C-Mad2 binds the APC activator Cdc20 (green), which is the first step in formation of the MCC.

B) Mps1 (dark red) binds the calponin homology (CH) domain of Ndc80 (Ndc80-C, orange) and phosphorylates (black “P”) the N-terminal tail of Knl1 on multiple MELT motifs (dark red circles) to recruit the SAC signaling machinery (see C). The kinase Aurora B (AurB) phosphorylates (red “P”) multiple kinetochore proteins to promote the SAC, including the Mis12 complex (Mis12-C) to recruit Knl1 to the kinetochore, the N terminus of Knl1 to prevent recruitment of PP1, and the N-terminal tail of Ndc80 (near the CH domain) to promote unattached kinetochores and recruit Mps1.

C) The SAC signaling machinery (“Catalytic Platform”) recruited by Mps1-dependent phosphorylation of Knl1 MELT motifs (P-MELT). Bub1/Bub3 (dark blue) directly bind a phosphorylated MELT motif and recruits both a dimer of BubR1/Bub3 (light blue) and the dimer of Mad1/Mad2 (at least in yeast and nematode). This platform then generates the SAC signal (see A).

Reproduced from (Musacchio 2015).

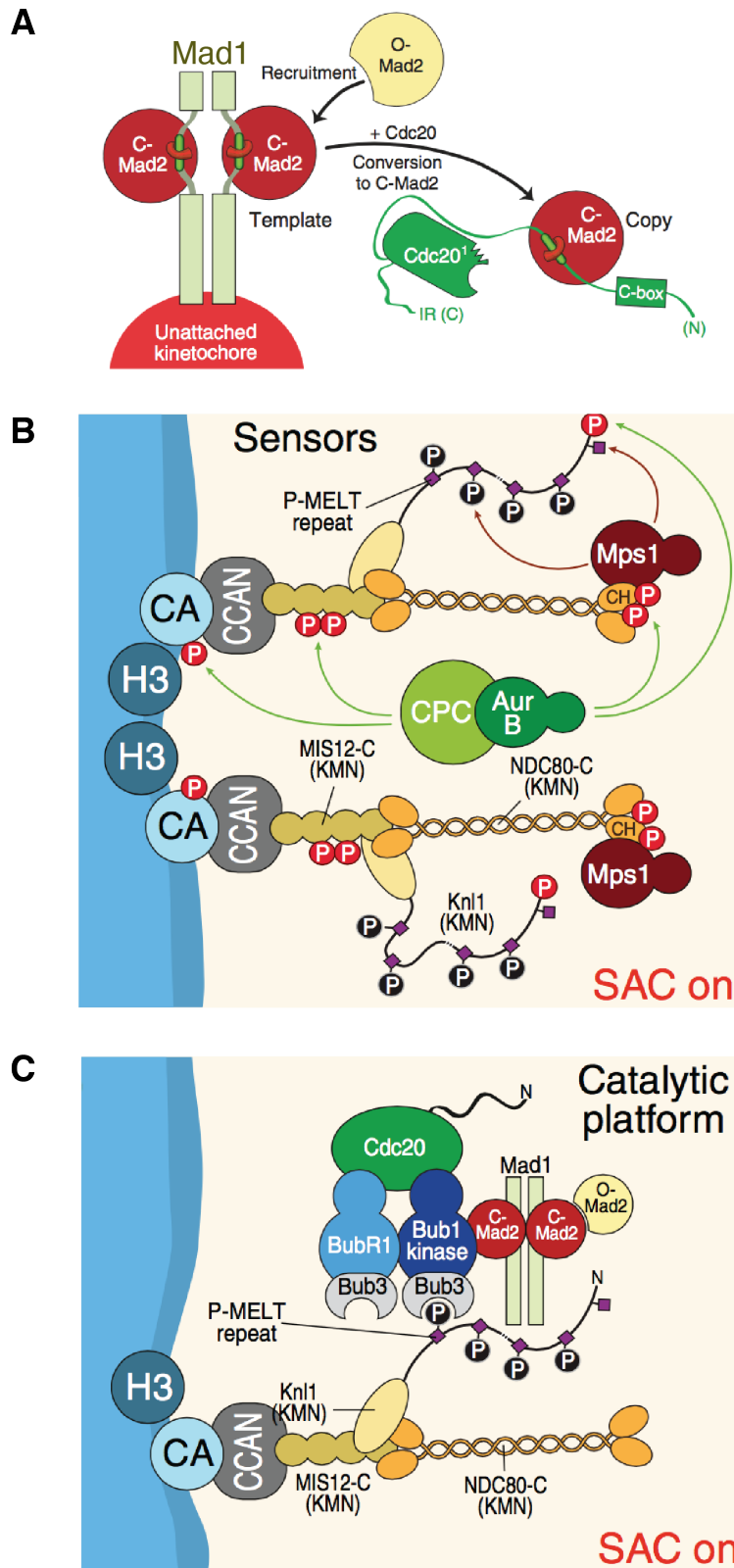


Figure 1-5: Molecular details of SAC activation

Interestingly, MCC is also present during interphase (Sudakin et al. 2001), even though Knl1 and other components important for its formation are absent from the interphase kinetochore (Nagpal & Fukagawa 2016). Instead, it has been shown that the nuclear pore complex (**NPC**) recruits Mad1 during interphase and supports Mps1-dependent formation of the MCC (Rodriguez-Bravo et al. 2014; Maciejowski et al. 2010). Preventing MCC formation during interphase, for example through inhibition of Mps1, leads cells to rapidly exit mitosis after NEB (Maciejowski et al. 2010). This suggests that MCC synthesized during interphase defines a mitotic timer that determines the minimum amount of time a cell spends in mitosis, measured to be between 10-20 minutes. This maybe physiologically important to provide time to recruit mitosis-specific kinetochore components required for microtubule attachment and SAC activation.

SAC silencing

Once chromosome bi-orientation is achieved, the checkpoint must be **silenced** to promote anaphase onset (Bokros & Y. Wang 2016). SAC proteins including Mad1 and Mad2 are absent from the kinetochore of bi-oriented chromosomes. This is important for checkpoint silencing as constitutively targeting any of these components to the kinetochore activates the checkpoint even when chromosome are aligned (Kruse et al. 2014; Maldonado & Kapoor 2011; Jelluma et al. 2010). It has been demonstrated that microtubule binding by Ndc80 directly displaces Mps1 from the kinetochore (Hiruma et al. 2015; Ji et al.

2015), thus directly coupling checkpoint kMT attachment to silencing.

Recruitment of **PP1** phosphatase to the kinetochore upon chromosome bi-orientation has also been implicated in removing SAC proteins. During early mitosis, Aurora B prevents PP1 recruitment by phosphorylating the PP1 binding motif on Knl1 (RVSF and SILK) (D. Liu et al. 2010; Rosenberg et al. 2011). PP1 contributes to checkpoint silencing in part by dephosphorylating the MELT motifs on Knl1 (London et al. 2012). Another kinetochore phosphatase is **PP2A**, which binds to the MCC component BubR1 (Suijkerbuijk et al. 2012). It was recently shown that PP2A also contributes to checkpoint silencing by dephosphorylating the MELT and RVSF motifs on Knl1 (Espert et al. 2014; Nijenhuis et al. 2014) and by stabilizing kMT attachment (Foley et al. 2011). How phosphatase recruitment is coupled to kMT attachment to regulate silencing remains unclear.

Another mechanism to remove SAC proteins from the kinetochore is **Dynein**-dependent 'stripping' along microtubules. This activity can be visualized by depleting cellular ATP levels in metaphase cells, revealing a pool of Dynein-associated checkpoint proteins on the spindle and at spindle poles (Wojcik et al. 2001; Howell et al. 2001). Dynein recruitment to the kinetochore is regulated through binding the RZZ complex and Spindly (Gassmann et al. 2008; Griffis et al. 2007; Y. W. Chan et al. 2009; Barisic et al. 2010). Given the role of Dynein in chromosome congression and kMT attachment stability however, Dynein's role in checkpoint silencing remains controversial (Y. Wang et al. 2014).

Finally, preformed MCC must be disassembled and/or displaced from the APC to allow APC activation once the checkpoint is silenced. In vertebrates, the protein **p31^{comet}**, which contains a HORMA domain similar to Mad2, forms a dimer with Mad2 that can drive dissociation of Mad2 from Cdc20 (M. Yang et al. 2007). It has been proposed that this could have at least two roles in silencing: first, preventing MCC production by 'capping' Mad2 at the kinetochore to prevent it from templating additional C-Mad2 and second, dissociating Mad2 from Cdc20 to initiate disassembly of the MCC (Musacchio & Salmon 2007). In addition, the APC subunit APC15 is important for releasing the MCC from its inhibitory interaction with the APC (Mansfeld et al. 2011). Future work is necessary to elucidate the molecular basis of MCC disassembly and APC activation.

SAC activation: Attachment versus Tension

How do unattached kinetochores activate the SAC? One hypothesis is that the checkpoint is activated by lack of microtubule **attachment** to the kinetochore. Alternatively, the checkpoint may detect the absence of **tension**, the microtubule-dependent pulling force that generates an increased distance between sister kinetochores on a bi-oriented chromosome (inter-kinetochore stretch). This hypothesis was bolstered by Bruce Nicklas's observation that artificially applying tension to a chromosome with syntelic attachments could silence the checkpoint (Li & Nicklas 1995). Distinguishing whether the SAC is activated by lack of attachment or lack of tension is difficult to do experimentally and has been

historically contentious (Maresca & Salmon 2010). Below, I address evidence for each mechanism independently, concluding on more recent work that may provide a solution to this debate.

In budding yeast, unreplicated chromatids attach to microtubules and elicit a SAC-dependent arrest, assumed to result from inability to generate tension (Stern & Murray 2001). Mutating subunits of cohesin leads to a similar SAC arrest that depends on the Aurora B homolog Ipl1 (Biggins & Murray 2001). Interestingly, Ipl1 is dispensable for the SAC arrest in nocodazole (Biggins & Murray 2001), suggesting that Aurora B activates the checkpoint specifically in response to defective tension, at least in this system. In vertebrates, early arguments for tension involved studying the SAC induced by the drug taxol, which hyperstabilizes microtubules and decreases tension, but was observed not to affect the number of kMT attachments (McEwen et al. 1997). The SAC in taxol also depends on Aurora B (Ditchfield et al. 2003), which at the time was viewed as mostly dispensable for the checkpoint in nocodazole, again in line with a specific tension-sensing pathway. Suppressing microtubule dynamics by treating human cells with a low dose of the drug vinblastine decreased inter-kinetochore tension and induced a SAC-dependent arrest even though kMT attachment appeared unchanged (Skoufias et al. 2001). Subsequent work correlated silencing of the checkpoint with increased microtubule-dependent separation of the inner and outer layers of a single kinetochore (intra-kinetochore

tension), rather than the distance between sister kinetochores (Maresca & Salmon 2009; Uchida et al. 2009).

How would tension activate the checkpoint? One longstanding model is that intra-kinetochore stretch increases the distance between Aurora B kinase, located at the inner centromere, and its substrates at the outer kinetochore (Lampson & Cheeseman 2011; T. U. Tanaka et al. 2002). Aurora B supports the SAC through multiple mechanisms, (discussed in detail later) including generating unattached kinetochores, recruiting Mps1, assembling the kinetochore and preventing recruitment of PP1, all of which require Aurora B-dependent phosphorylation of kinetochore proteins. Thus, physically separating Aurora B from its substrates could trigger anaphase onset through preventing checkpoint activation and promoting checkpoint silencing.

Arguing the importance of attachment versus tensions rests on the ability to manipulate these states independently. However, this separation is not achieved by treating cells with taxol. A recent study has confirmed the longstanding hypothesis that a subset of kinetochores are unattached in taxol and that checkpoint silencing only occurs after these kinetochores are bi-oriented (Waters et al. 1998; Magidson et al. 2016). Additionally, the duration of mitotic arrest increases with the concentration of taxol until 1 μ M, at which point increasing the concentration further shortens the mitotic arrest (Z. Yang et al. 2009). This result is inconsistent with taxol activating the checkpoint by a defect in tension and is consistent with increased stability/number of microtubules

allowing the checkpoint to become silenced by kMT attachment more rapidly. While Aurora B may couple lack of tension to activation of the checkpoint, this is correlated with its ability to generate unattached kinetochores (Pinsky et al. 2006; Z. Yang et al. 2009). Moreover, an Ndc80 mutant that forms hyperstable kMT attachments is unable to bi-orient chromosomes or support intra-kinetochore stretch, but can none-the-less silence the SAC (Tauchman et al. 2015; Etemad et al. 2015).

How could attachment regulate the SAC? Its been demonstrated in human cells that kinetochore recruitment of Mps1 to Ndc80 is mutually exclusive with microtubule binding (Hiruma et al. 2015; Ji et al. 2015), providing a mechanism to directly couple microtubule attachment status to recruitment of an upstream SAC activator. The ability of Knl1 to bind microtubules is important for checkpoint silencing in *C. elegans*, though the mechanism is unclear (Dumont et al. 2010). It has also been suggested that microtubule binding increases the distance between Mps1 and the Knl1 MELT motifs and contributes to SAC regulation (Aravamudhan et al. 2015). The yeast-specific microtubule-binding Dam1 complex was also suggested to create a physical barrier to reinforce the separation of Mps1 and Knl1 upon kMT attachment (Aravamudhan et al. 2015). Thus, microtubule-dependent changes in kinetochore architecture may underlie checkpoint silencing and activation. This is consistent with studies demonstrating reorganization of the kinetochore upon microtubule binding (Wan et al. 2009;

Magidson et al. 2015; Wynne & Funabiki 2015; Hoffman et al. 2001; Suzuki et al. 2011; Suzuki et al. 2014).

Current research is consistent with the SAC being activated by lack of kMT attachment rather than defective tension. While the 'tension sensing' mechanism may not exist, the checkpoint is none-the-less 'tension sensitive'. Elegant experiments using purified budding yeast kinetochores indicate that tension directly stabilizes kMT attachment (Akiyoshi et al. 2010). Kinetochores under low tension are more likely to become detached from microtubules, suggesting the mechanical properties of kMT attachment can result in the conversion of defective tension to a checkpoint signal. Moreover, Aurora B maintains the SAC in response to defective tension by generating unattached kinetochores (Pinsky et al. 2006; Z. Yang et al. 2009), suggesting that the error correction machinery also makes the checkpoint tension sensitive. Understanding how Aurora B activity is coupled to kMT attachment status is thus critical to understand how defective tension is converted into a SAC signal.

1.3 The Chromosomal Passenger Complex (CPC)

In 1991, William Earnshaw posited that a subset of anaphase midzone proteins are positioned by traveling with chromosomes to the metaphase plate (Earnshaw & Cooke 1991). This chromosomal passenger hypothesis arose following the identification of an inner centromere protein (**INCENP**) in 1987 that was located at the (previously unidentified) inner centromere during early mitosis and transferred to the midzone at anaphase (Cooke et al. 1987). Research conducted over the past 25 years has confirmed and refined this hypothesis, elaborating INCENP as part of a four protein Chromosomal Passenger Complex (**CPC**) conserved from yeasts to humans (Ruchaud et al. 2007; Carmena, Wheelock, et al. 2012). The CPC not only transfers from chromosomes to the spindle midzone to support anaphase and cytokinesis, it is also required for accurate chromosome segregation during early mitosis.

CPC discovery, composition and activation

Following the identification of INCENP, it was soon discovered that the serine/threonine kinase **Aurora B** formed a protein complex with INCENP (Adams et al. 2000; Kaitna et al. 2000; J.-H. Kim et al. 1999) (**Figure 1-6A**). The baculovirus inhibitor of apoptosis repeat (BIR)-domain containing protein **Survivin** was subsequently identified as a passenger protein required for the proper localization of INCENP and Aurora B to chromatin and microtubules (Uren et al. 2000; Speliotes et al. 2000; Wheatley et al. 2001). The final CPC

component, referred to as **Borealin** throughout this dissertation, was simultaneously identified in *Xenopus* egg extract by our group (Dasra) and in human cells (Borealin) (Gassmann et al. 2004; Sampath et al. 2004). Unlike other CPC components in which homologs were readily identified in other systems, it took five years to identify the yeast homologs of Borealin (Nakajima et al. 2009; Bohnert et al. 2009) and for the previously discovered nematode protein CSC-1 to be identified as a Borealin homolog (Romano et al. 2003). Borealin, Survivin, INCENP and Aurora B form a complex that co-localizes throughout mitosis and define the canonical CPC.

The CPC is composed of a kinase module and a localization module connected by the central region of INCENP (**Figure 1-6B**). The **kinase module** is composed of Aurora B bound to the INCENP (IN)-box in the C terminus of INCENP. A crystal structure of this complex reveals this interaction is essential for allosterically activating Aurora B (Sessa et al. 2005), which in turn is essential for all known functions of the CPC. The **localization module** has also been crystalized, revealing a triple-helix bundle with one helix each from Survivin, Borealin and the CEN-box in the N terminus of INCENP (Jeyaparakash et al. 2007). This interaction is required for the CPC to localize to the centromere during early mitosis and to transfer to the spindle midzone during late mitosis. INCENP connects the kinase and localization module through its poorly characterized central region, which includes a single alpha helix (**SAH**) domain (previously misclassified as a coiled-coil domain).

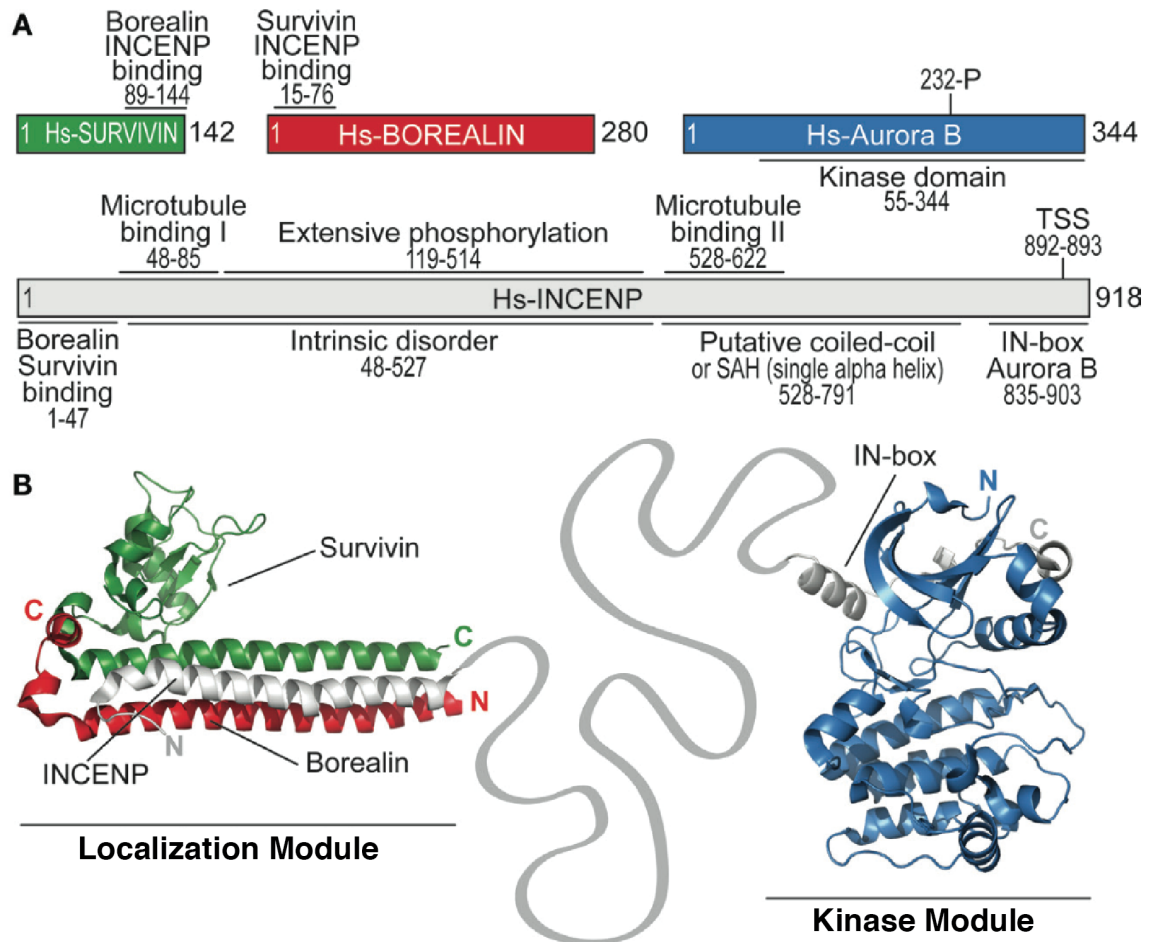


Figure 1-6: Components and structure of the CPC

A) Individual components of the CPC, highlighting regions important for function. Survivin (green), Borealin (red), Aurora B (blue), INCENP (gray).

B) The CPC is composed of two modules. The localization module (left) is composed of a triple helix bundle formed by Survivin, Borealin and the N-terminal CEN domain of INCENP (residues 1-47). The kinase module (right) is formed by Aurora B in complex with the INCENP C-terminal IN-box (residues 835-903). The central region of INCENP (gray strand) connects the two modules. It also contains a stable alpha helix (SAH) domain that binds microtubules. Hs= *Homo sapien*, TSS= threonine-threonine-serine motif, N= N terminus, C= C terminus. Reproduced from (Krenn & Musacchio 2015).

INCENP regulates Aurora B activation in at least three ways (**Figure 1-7**). First, the INCENP IN-box forms a crown around the N-terminal lobe of Aurora B that alters the conformation of the kinase domain and partially activates kinase activity (Sessa et al. 2005) (**Figure 1-7A**). Second, full activation requires both autophosphorylation of the Aurora B activation loop and Aurora B-mediated phosphorylation of a threonine-threonine-serine (TSS) motif downstream of the IN-box on INCENP, both of which must happen in trans (Sessa et al. 2005; Honda et al. 2003; Bishop & Schumacher 2002) (**Figure 1-7A**). Finally, our group has shown that artificially clustering the CPC, for example with antibodies against the C terminus of INCENP or inclusion of a dimerization domain within INCENP, stimulates Aurora B autophosphorylation and activation (Kelly et al. 2007). This **cluster-dependent activation** suggests that Aurora B activation is directly coupled to its localization, which is wholly dependent on binding to INCENP (**Figure 1-7B**).

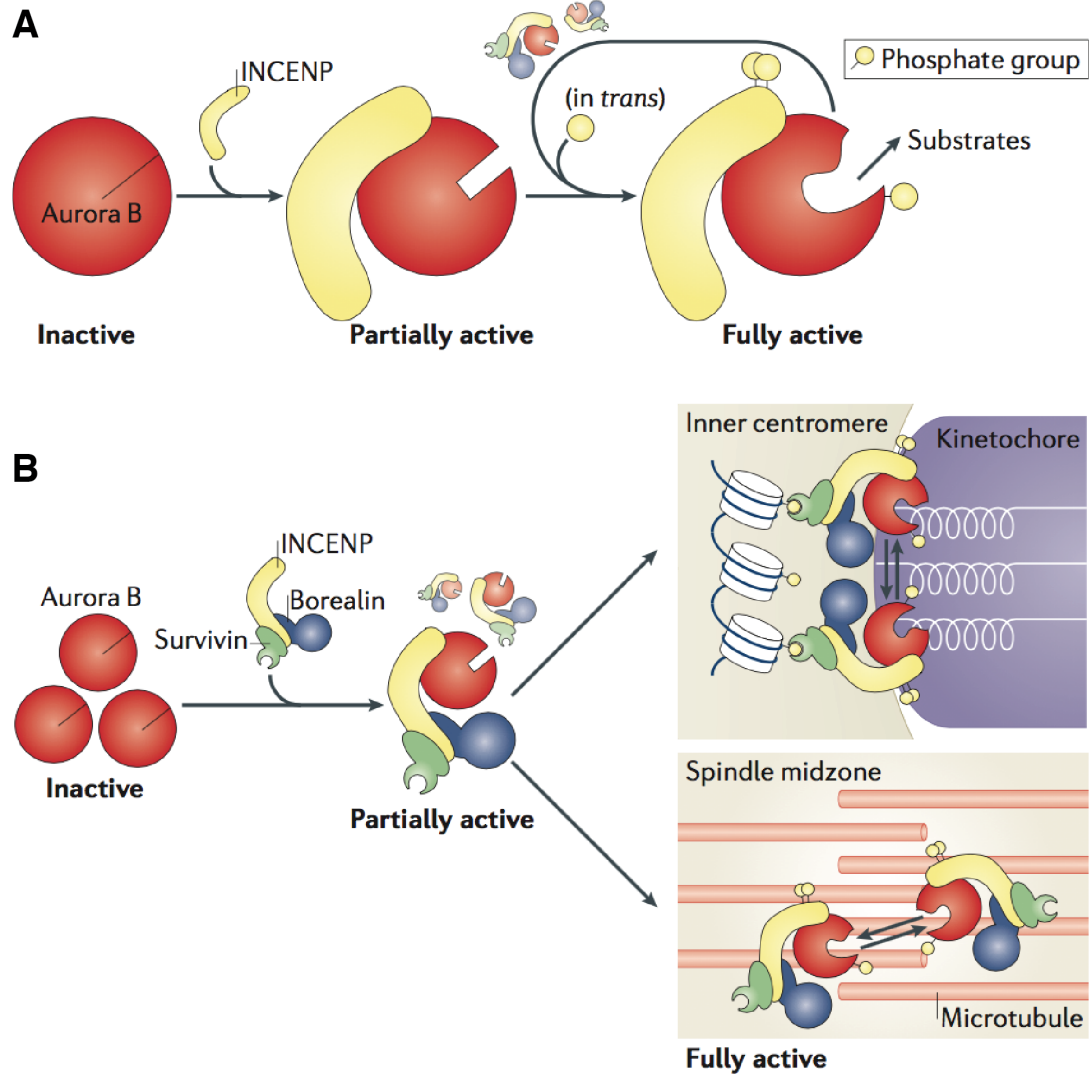


Figure 1-7: INCENP regulates the kinase activity of Aurora B

A) Aurora B (red) is intrinsically inactive (left). Binding to the C-terminal IN-box of INCENP (yellow) induces a conformational change that partially activates kinase activity (middle). Full activation requires Aurora B autophosphorylation of its activation segment and phosphorylation of the TSS motif on the N terminus of INCENP (right). This autophosphorylation must occur *in trans*.

B) Localization clusters the CPC at the inner centromere (early mitosis) or spindle midzone (late mitosis) and promotes Aurora B activation by supporting autophosphorylation *in trans*. Reproduced from (Carmena, Wheelock, et al. 2012).

CPC localization during early mitosis

The CPC shows a dynamic distribution during early mitosis in vertebrates (**Figure 1-8A**). During prophase, the CPC is broadly distributed on chromosomes with particular enrichment at the **inner centromere**, the region of centromeric DNA between adjacent sister chromatids (Ruchaud et al. 2007). CPC localization on chromosome arms is poorly understood but depends in part on the binding of INCENP to HP1 (Nozawa et al. 2010). This localization is transient, and by prometaphase the majority of the CPC is concentrated at the inner centromere.

Survivin and Borealin each interact with a distinct, mitosis-specific histone phosphorylation to target the CPC to the inner centromere (**Figure 1-8B, C**). The BIR-domain of Survivin directly binds histone H3 phosphorylated at threonine 3 (**H3T3ph**) (Kelly et al. 2010; Du et al. 2012; Jeyaparakash et al. 2011; F. Wang et al. 2010; Yamagishi et al. 2010; Niedzialkowska et al. 2012). H3T3ph is enriched between sister chromatids at the centromere and is catalyzed by the atypical protein kinase **Haspin** (discussed below) (Dai et al. 2005). Borealin indirectly binds phosphorylated histone H2A threonine 120 (**H2A T120ph**) (Yamagishi et al. 2010). H2A T120ph is enriched between sister kinetochores and is phosphorylated by **Bub1** at the kinetochore (Kawashima et al. 2010). H2A T120ph recruits **Shugoshin** proteins to the inner centromere (Kawashima et al. 2010), which in vertebrates interacts with Borealin phosphorylated at Ser132 by Cdk1 (H. Liu et al. 2015; Kawashima et al. 2007; Yamagishi et al. 2010). The

CPC is maximally enriched on the region of chromatin defined by the overlap of H3T3ph and H2A T120ph (Yamagishi et al. 2010) (**Figure 1-8B**).

CPC localization is reinforced by positive feedback loops (**Figure1-8D**).

Aurora B promotes rapid accumulation of Mps1 at the kinetochore during mitotic entry (Saurin et al. 2011), while Mps1 is required for rapid accumulation of Aurora B at the inner centromere (Van Der Waal et al. 2012) by supporting Bub1-dependent H2A T120ph. Additionally, Aurora B-dependent phosphorylation of the RVSF motif of Knl1 prevents recruitment of PP1 (Rosenberg et al. 2011; D. Liu et al. 2010), which dephosphorylates the Knl1 MELT motifs (London et al. 2012), suggesting the CPC promotes Bub1 recruitment and prevents its removal.

A similar pathway exists between Aurora B and Haspin in human cells (F. Wang et al. 2011). Aurora B inhibition reduces H3T3ph in mitosis. Mutating several Aurora B-dependent phosphorylation sites on Haspin to alanine phenocopied this decrease in H3T3ph, consistent with positive feedback. More indirectly, Aurora B-dependent recruits Shugoshin and PP2A (Tanno et al. 2010) to the centromere to protect centromeric cohesion, which may support Haspin localization. In fission yeast, the Haspin homolog Hrk1 requires the cohesion-interacting protein **Pds5** to support H3T3ph (Yamagishi et al. 2010) while in mouse, a centromere specific form of Pds5 (Pds5B) is required to protect centromeric cohesion and promote Aurora B localization at the centromere (Carretero et al. 2013). Thus, Aurora B may directly and indirectly support H3T3ph, though the molecular basis for this function remains unclear.

Figure 1-8: Localization of the CPC during mitosis

A) Distribution of the CPC (green) on chromatin (blue) and microtubules (red) during mitosis. During early mitosis, the CPC is enriched at the inner centromere (inset “Ba”). At anaphase, the CPC transfers to the spindle midzone. Reproduced from (Ruchaud et al. 2007).

B) Phosphorylation of two histone tails targets the CPC to the inner centromere (top): H3T3ph (blue) and H2A T120ph (yellow). The CPC is maximally enriched where these marks overlap at the inner centromere (green). Cohesin (orange) at the inner centromere recruits Haspin, the H3T3 kinase (bottom, left). Mps1-dependent phosphorylation of Knl1 (purple) supports kinetochore-recruitment of Bub1, the H2A T120 kinase (bottom, right). Reproduced from (Carmena, Wheelock, et al. 2012).

C) The CPC interacts with H3T3ph (T3) and H2A T120ph (T120) to localize to the centromere. The BIR domain of Survivin (Sur, green) directly binds H3T3ph. Borealin (Bor, blue) phosphorylated by Cdk1 (yellow sphere) binds Shugoshin (Sgo, gray), which interacts with H2A T120ph.

D) Two positive feedback loops promote CPC localization to the centromere. Haspin and Bub1 recruit the CPC to the centromere by supporting H3T3ph and H2A T120ph, respectively. The CPC phosphorylates Haspin to activate its kinase activity and support H3T3ph (left). The CPC also recruits Mps1, which in turn recruits Bub1 to support H2A T120ph (right). Reproduced from (Trivedi & Stukenberg 2016).

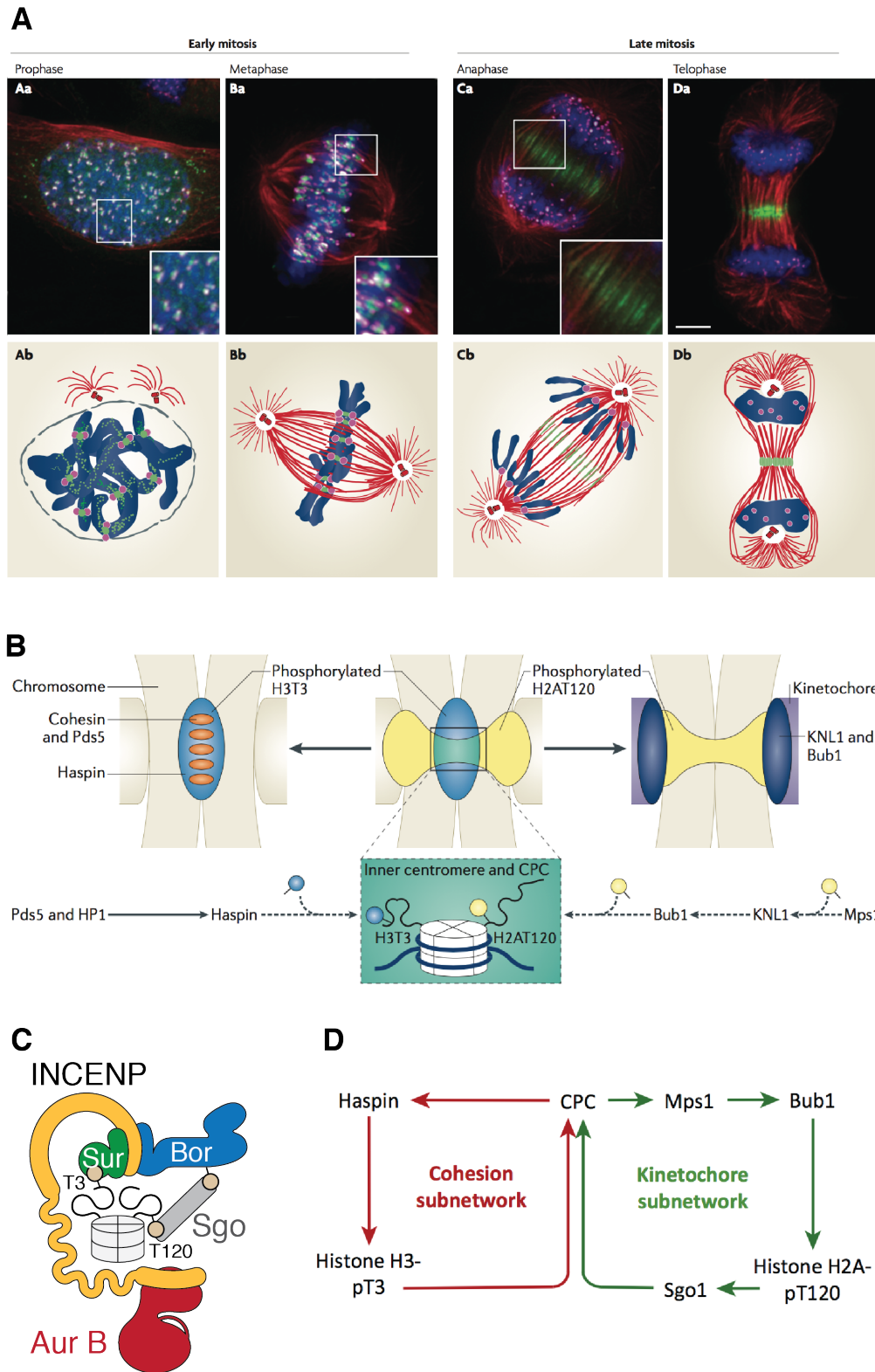


Figure 1-8: Localization of the CPC during early mitosis

Localization of the CPC to structures other than chromatin has been reported during early mitosis. In early embryonic *Xenopus* egg extracts, the CPC binds spindle microtubules through the INCENP SAH domain (Tseng et al. 2010). This interaction promotes activation of Aurora B on microtubules and is required to assemble the spindle in this system (Tseng et al. 2010). Two studies recently identified interactions of the CPC on microtubules during early mitosis in human cells. First, it was shown that Aurora B interacts with End-binding 1 (**EB1**), a plus-end microtubule tracking protein (Banerjee et al. 2014). Human cells depleted of EB1 or reconstituted with an EB1 point mutant that does not bind microtubules show reduced abundance of the CPC, H3T3ph and H2A T120ph at the centromere. It was suggested that a complex of EB1/ Aurora B on kinetochore proximal microtubules promotes Bub1 recruitment, initiating H2A T120ph dependent CPC recruitment to the inner centromere. Second, it was reported that ubiquitinated Aurora B interacts with the ubiquitin receptor protein **UBASH3B** on microtubules (Krupina et al. 2016). Depleting UBASH3B or preventing its targeting to microtubules resulted in robust and uniform distribution of the CPC on chromatin. Over-expressing UBASH3B targeted Aurora B to microtubules, while super-resolution microscopy of untreated cells identified Aurora B on kinetochore proximal microtubule fibers, albeit ambiguously. The authors posit that the Aurora B/ UBASH3B interaction supports microtubule-dependent ‘focusing’ of the CPC from chromosome arms to the centromere to facilitate localization and transfer to the spindle midzone. While future work is necessary

to validate these models, they indicate that the interaction of the CPC with microtubules is important prior to anaphase.

Lastly, it has been reported that an antibody detecting Aurora B phosphorylated on its activation loop (**T232**) specifically stains the outer kinetochore even though total Aurora B cannot be detected at this location (Deluca et al. 2011; Posch et al. 2010). This epitope is sensitive to Aurora B inhibition, consistent with it being T232 autophosphorylation, though it is possible this antibody crossreacts with other Aurora B substrates at the kinetochore. It was recently reported that Borealin dimerization is required to target the CPC to the kinetochore, though this localization was only revealed by removing the centromeric pool of CPC by inhibiting Haspin (Bekier et al. 2015). Additionally, depletion of the PP1 regulatory subunit Sds22 reveals a pool of active Aurora B at the kinetochore, suggesting the CPC is regulated by PP1 at this location (Posch et al. 2010). These observations are consistent with the hypothesis that a small but active pool of Aurora B at the kinetochore may locally phosphorylate Aurora B substrates at the kinetochore; however, supporting evidence for this model is lacking and no protein is currently a candidate for an Aurora B 'kinetochore receptor'.

Two unrelated observations are interesting to note. First, both UBASH3B and EB1 target Aurora to kinetochore proximal microtubules (Banerjee et al. 2014; Krupina et al. 2016), suggesting that the active Aurora B at the kinetochore may result from microtubule-dependent activation, similar to what we see in

Xenopus egg extract (Tseng et al. 2010). Second, acetylation of Aurora B adjacent to its activation loop by the microtubule-associated protein TIP-60 was shown to prevent dephosphorylation of T232 by PP2A and promote accurate chromosome segregation (Mo et al. 2016). This mechanism could make active Aurora B refractory to deactivation by kinetochore localized PP2A, thus helping to retain the small pool of kinetochore Aurora B in an active state.

CPC functions during early mitosis

Before its identification as a chromosomal passenger, Aurora B was implicated in correcting aberrant kMT attachments during mitosis. In budding yeast, a screen for proteins that when mutated lead to an increase-in-ploidy identified **Ipl1**, a homolog to mammalian Aurora B (C. S. Chan & Botstein 1993). Subsequent work indicated that Ipl1 was critical for accurate chromosome segregation by regulating kinetochore-microtubule attachment (Biggins et al. 1999; J.-H. Kim et al. 1999; T. U. Tanaka et al. 2002). In human cells, chemical inhibition of Aurora B leads to the persistence of syntelic and merotelic kMT attachments and an increase in chromosome missegregation (Cimini et al. 2006; Lampson et al. 2004; Ditchfield et al. 2003; Hauf et al. 2003). Merotelic attachments do not activate the SAC because they satisfy both kMT attachment and tension, thus an important role for Aurora B is correcting these otherwise invisible attachment errors.

How does Aurora B-dependent phosphorylation correct erroneous kMT attachments? Aurora B phosphorylates a number of proteins in the **KMN network** important for establishing kMT attachment, the most well-studied of which in vertebrates is the N-terminal tail of **Ndc80** (known as Hec1 in human cells). This region supports microtubule binding through a number of positively charged residues that electrostatically interact with the negatively charged C terminus of tubulin, E-hook (Guimaraes et al. 2008; Tooley et al. 2011; Miller et al. 2008). Aurora B phosphorylation imparts a negative charge thought to disrupt this interaction and thus destabilize microtubule binding by Ndc80 (Ciferri et al. 2008; Cheeseman et al. 2006; Welburn et al. 2010; DeLuca et al. 2006; Guimaraes et al. 2008). Consistent with this, phosphomimetic Ndc80 mutants are unable to form stable kMT attachments, creating unattached kinetochores that activate the SAC (Welburn et al. 2010; Guimaraes et al. 2008). Conversely, unphosphorylatable Ndc80 mutants form hyperstable kMT attachments and demonstrate an increased frequency of syntelic and merotelic attachments (DeLuca et al. 2006; Guimaraes et al. 2008; Deluca et al. 2011). Phosphorylation of multiple KMN proteins has been shown to synergistically lower their binding affinity *in vitro* (Welburn et al. 2010), suggesting that Aurora B antagonizes the microtubule binding capacity of the entire KMN network. While Aurora B phosphorylates Ndc80 in budding yeast, it primarily regulates kMT attachment through phosphorylation of the yeast specific microtubule-binding **Dam1** complex (Akiyoshi et al. 2009). Additionally, Aurora B prevents kinetochore recruitment of

PP1 (D. Liu et al. 2010; Rosenberg et al. 2011), which oppose Aurora B-dependent phosphorylation to promote KMT stability. Phosphorylation of KMN proteins is high on unattached kinetochores and low on the kinetochores of bi-oriented chromosomes, indicating that Aurora B substrate phosphorylation is coupled to microtubule attachment status. How this regulation is achieved remains unclear.

The second major function of the CPC during early mitosis is activating the SAC. The history of Aurora B in the checkpoint is complex. Early experiments in budding yeast and human cells found that Aurora B (Ipl1 in yeast) was not required to maintain the SAC in nocodazole (Biggins & Murray 2001), a drug that depolymerizes microtubules and generates unattached kinetochores. Conversely, Ipl1 is required for the SAC in the presence of unreplicated chromatids or defective cohesion (Biggins & Murray 2001), both of which are thought to allow KMT attachment but not microtubule-dependent tension (Stern & Murray 2001; T. Tanaka et al. 2000). This ‘tension sensing’ mechanism relied on the ability of Ipl1 to generate unattached kinetochore by phosphorylating the Dam1 complex (Pinsky et al. 2006), thus converting lack of tension into lack of attachment. This ‘tension-sensing’ mechanism maybe important in the case of syntelic attachments, where KMT attachment is present but tension is not. Indeed, inhibiting Aurora B in human cells increases the frequency of syntelic attachments (Hauf et al. 2003; Ditchfield et al. 2003; Lampson et al. 2004). The

ability of Aurora B to destabilize syntelic attachments and generate unattached kinetochores is critical to maintain the SAC arrest in taxol (Z. Yang et al. 2009).

In addition to generating unattached kinetochores, Aurora B more directly contributes to the SAC (**Figure1-5B**). Chemical inhibition of Aurora B in *Xenopus* egg extracts prevents kinetochore assembly and checkpoint protein recruitment (Emanuele et al. 2008; Wynne & Funabiki 2015) and rapidly silences the nocodazole-induced SAC (Gadea & Ruderman 2005). While similar experiments in human cells were initially inconclusive (Maresca & Salmon 2010), it was eventually demonstrated that penetrant inhibition of Aurora B silenced the SAC even in a dose of nocodazole in which all kinetochores were unattached (Santaguida et al. 2011). Under these conditions, inhibiting both Aurora B and Mps1, a *bona fide* SAC activator, has an additive effect on silencing the SAC, strongly arguing for a direct role in checkpoint activation independent of generating unattached kinetochores. A number of subsequent studies have demonstrated the CPC activates the SAC through multiple mechanisms in human cells. First, Aurora B promotes rapid recruitment of Mps1 to the kinetochore during mitotic entry in nocodazole (Saurin et al. 2011). While the molecular mechanism is unclear, it has been proposed that this is through either Aurora B-mediated phosphorylation of the Ndc80 tail (Zhu et al. 2013) or Aurora B-dependent stimulation of the Mps1 TPR domain (Nijenhuis et al. 2013). Second, Aurora B phosphorylates the Mis12 subunit Dsn1 to promote kinetochore recruitment of Ndc80 and the checkpoint signaling platform Knl1 (S.

Kim & Yu 2015; Y. Yang et al. 2008; Akiyoshi et al. 2013)3. Third, Aurora B phosphorylates the RVSF motif of Knl1 to prevent PP1 recruitment to the kinetochore (D. Liu et al. 2010; Rosenberg et al. 2011), which contributes to both kMT attachment stability and SAC silencing. Fourth, phosphorylation of Zwint-1 by Aurora B promotes binding and retention of Dynein to the kinetochore, preventing it from silencing the checkpoint by 'stripping' SAC proteins from the kinetochore along microtubules (Kasuboski et al. 2011). Thus, Aurora B promotes the SAC both by recruiting Mps1 and Knl1 to the kinetochore and by preventing PP1- and Dynein-mediated checkpoint silencing.

It has been suggested that INCENP supports the SAC independent of regulating Aurora B. Deleting the INCENP **SAH domain** impairs the SAC in taxol without affecting CPC localization or Aurora B-mediated error correction (Vader et al. 2007). While the molecular requirement for the SAH domain was not determined, it has been shown to support microtubule binding in human cells, chicken cells and *Xenopus* egg extracts (van der Horst et al. 2015; Samejima et al. 2015; Tseng et al. 2010). Given that the CPC may interact with kinetochore-proximal microtubules (Krupina et al. 2016; Banerjee et al. 2014), this raises the possibility that the INCENP SAH domain directly couples Aurora B-dependent signaling to the presence of kinetochore-proximal microtubules. Thus, determining how the INCENP SAH domain supports the checkpoint may provide a molecular understanding of how Aurora B activity is coordinated with kMT

attachment status. In **Chapter 3** of my dissertation, I dissect the molecular function of the SAH domain in *Xenopus* egg extract and human cells.

Coupling CPC function to kMT attachment status

Levels of phosphorylation of Aurora B substrates at the kinetochore are high on unattached kinetochores and low following bi-orientation (DeLuca et al. 2011; Welburn et al. 2010; D. Liu et al. 2009). Regulating Aurora B phosphorylation with kMT attachment is critical to balance error correction with formation of end-on kMT attachments to promote accurate chromosome segregation (Welburn et al. 2010; Guimaraes et al. 2008; DeLuca et al. 2006; DeLuca et al. 2011). How this coupling is achieved remains an outstanding question in the field.

The extent of Aurora B substrate phosphorylation is determined by the balance of Aurora B activity against its opposing phosphatases PP1 and PP2A (Foley & Kapoor 2013). In vertebrates, localization of PP1 and PP2A to the kinetochore stabilizes kMT attachment by opposing Aurora B activity (D. Liu et al. 2010; Foley et al. 2011), presumably by dephosphorylating the KMN network. PP1 is enriched on bi-oriented kinetochores through binding the RVSF motif of Knl1 (D. Liu et al. 2010); conversely, PP2A in complex with a B56 regulatory subunit (B56-PP2A) is enriched on unattached kinetochores via binding BubR1 phosphorylated by Polo (Suijkerbuijk et al. 2012; Foley et al. 2011). Its been

suggested that this dynamic localization regulates Aurora B activity to balance error correction and chromosome bi-orientation (Foley & Kapoor 2013).

One model for regulating Aurora B phosphorylation with kMT attachment involves regulating Aurora B's accessibility to kinetochore substrates (Lampson & Cheeseman 2011; T. U. Tanaka et al. 2002) (**Figure 1-9A, B**). A large pool of active Aurora B is located at the inner centromere, presumably due to localization-dependent activation of Aurora B (Kelly & Funabiki 2009).

Microtubule attachment generates tension that pulls the kinetochore away from the inner centromere, thus increasing the distance between Aurora B and its kinetochore substrates. In this way, the presence or absence of kMT attachment dictates the proximity of Aurora B to its kinetochore substrates. In combination with regulated recruitment of PP1 and B56-PP2A, this mechanism would directly couple the extent of Aurora B substrate phosphorylation with kMT attachment status. Consistent with this model, FRET sensors indicate that the steady-state level of Aurora B phosphorylation decreases with increasing distance from the inner centromere (Welburn et al. 2010). These sensors also detect progressively lower amounts of phosphorylation throughout the kinetochore as cells form kMT attachment following nocodazole washout (Welburn et al. 2010). Artificially recruiting INCENP to the kinetochore supports a higher level of Aurora B substrate phosphorylation than targeting it to the centromere (D. Liu et al. 2009), consistent with the proximity of Aurora B to its substrates determining the steady-state level of phosphorylation.

Figure 1-9: Regulating Aurora B-dependent phosphorylation at the kinetochore with kMT attachment status

A, B) Spatial separation model for regulating Aurora B with kMT attachment status. Unattached kinetochores (A) are in close proximity to the sphere of Aurora B activity (red) emanating from its location at the inner centromere. This promotes phosphorylation (orange P) of the Ndc80 complex, which functions in error correction, and of Knl1, which prevents PP1 (green) recruitment to the kinetochore. Upon microtubule attachment (B), tension increases the distance between the centromere and kinetochore (spatial separation), preventing efficient phosphorylation by Aurora B. This leads to a host of events including recruitment of PP1, which counteracts Aurora B-dependent phosphorylation and stabilizes kMT attachment (green). Reproduced from (Lampson & Cheeseman 2011).

C) The dog leash model. The CPC (blue) is anchored at the centromere (green) by the localization module of the CPC. INCENP acts as a tether, the length of which physically limits the accessibility of Aurora B to kinetochore substrates (red). In the absence of attachment (top), Aurora B can phosphorylate substrates at the centromere (orange P) and kinetochore (gray P); however, upon attachment and tension (bottom), Aurora B is unable to reach kinetochore substrates (open gray circles), though it can still locally phosphorylate substrates at the centromere. Reproduced from (Lampson & Cheeseman 2011).

D) The reaction-diffusion model. The CPC localizes to the centromere where it undergoes cluster-mediated activation (dark red). It then diffuses away, creating a physical gradient of CPC emanating from the centromere. The radius of this gradient is determined by the rate of CPC inactivation (light red) by dephosphorylation. Tension-dependent separation of the centromere and kinetochore pulls kinetochore substrates away from the centromere, placing it outside the gradient of active CPC. Reproduced from (Santaguida & Musacchio 2009).

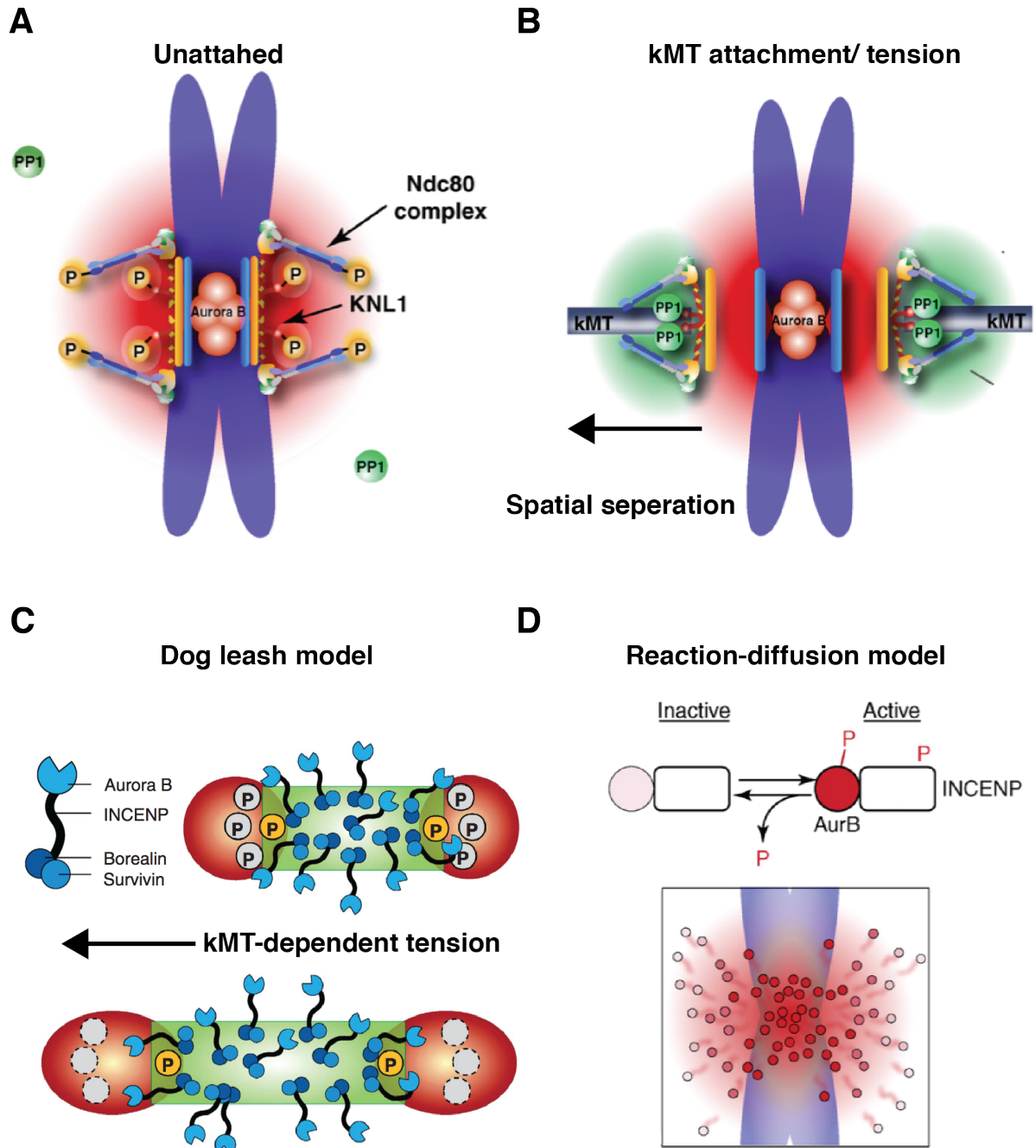


Figure 1-9: Regulating Aurora B-dependent phosphorylation at the kinetochore with kMT attachment status

If microtubule-dependent tension determines the distance between the inner centromere and kinetochore, what determines the outward 'reach' of Aurora B towards its substrates? The 'dog-leash' model posits that INCENP acts as a centromere-bound tether, the length of which physically limits Aurora B's proximity to the kinetochore (Krenn & Musacchio 2015) (**Figure1-9C**). Consistent with this, biochemical work suggests the INCENP SAH domain is theoretically capable of extending up to 50 nm (Samejima et al. 2015), approximately the distance from CENP-A to the base of the KMN network (Wan et al. 2009). However, deletion of the SAH domain fails to compromise Aurora B-dependent error correction (Vader et al. 2007), suggesting the length of INCENP does not regulate Aurora B-dependent phosphorylation at the kinetochore.

Alternatively, the 'reaction-diffusion' model states that Aurora B becomes activated by binding the centromere before rapidly diffusing outwards, creating a gradient of active Aurora B centered on the centromere (Kelly & Funabiki 2009) (**Figure 1-9D**). Consistent with this, FRAP data indicates that Aurora B, INCENP and Survivin bind dynamically at the centromere with $t_{1/2}$ between 0.5- 50 sec (Ahonen et al. 2009; Delacour-Larose et al. 2004; Delacour-Larose et al. 2007; Beardmore et al. 2004). Artificially tuning CPC dynamics at the centromere alters the steady-state level of Aurora B phosphorylation along mitotic chromosomes as measured by a FRET-sensor (E. Wang et al. 2011). While the same sensor normally shows a uniformly high level of Aurora B-dependent phosphorylation along chromosomes during early mitosis, partial or transient inhibition of Aurora B

reveals a micron-scale gradient of activity centered on the centromere (E. Wang et al. 2011). Given the inability to detect a micron-scale gradient of Aurora B activity under unperturbed conditions, it is surprising that a nanometer-scale gradient can be detected within the kinetochore (Welburn et al. 2010). This difference may be explained by PP1 and/or PP2A opposing Aurora B activity and sensor saturation at the kinetochore, whereas low phosphatase activity on chromosome arms, for example by Aurora B-mediated inhibition of Repoman/PP1 (Qian et al. 2013), results in persistent substrate phosphorylation. Thus, while it is unclear if a physical gradient of Aurora B exists, it is likely that the gradient of Aurora B activity at the kinetochore is at least partly defined by regulated recruitment of counteracting phosphatases.

It is important to note that mechanisms other than ‘reaction-diffusion’ can contribute to gradient formation and that even if a gradient of Aurora B does exist, it is not necessarily required for CPC function. For example, Ras-related nuclear protein (Ran) forms an activity gradient around chromosomes during early mitosis and is required for spindle assembly (Kalab et al. 2002). Global activation of Ran can support spindle assembly in *Xenopus* egg extract even though this abolishes the Ran gradient around chromatin, indicating the gradient is dispensable under these conditions (Maresca et al. 2009). Additionally, Ran activates spindle assembly factors (SAFs) to promote spindle assembly. While a reaction-diffusion process is believed to generate the Ran gradient, it has been suggested that the spatial distribution of microtubules depends on a more

complicated process involving feedback with SAFs, which both nucleate and bind microtubules (Oh et al. 2016).

Regardless of the particular model describing how CPC function is coupled to kMT attachment status, each assumes that CPC localized to the inner centromere supports Aurora B-dependent phosphorylation at the kinetochore. This seems reasonable given that, for example, chemically inhibiting Haspin in human cells displaces the CPC from the centromere and impairs kinetochore phosphorylation, chromosome alignment and the SAC in taxol (F. Wang et al. 2012). However, the importance of CPC localization at the centromere may not be universal. In budding yeast, lethality from deleting the Survivin homolog Bir1 can be rescued by deleting the CEN domain of the INCENP homolog Sli15 (Campbell & Desai 2013). This Sli15 mutant localizes to the mitotic spindle and is fully capable of supporting error correction and the SAC; however, deleting both the CEN domain and the region of Sli15 required for microtubule binding resulted in lethality in the absence of Bir1 (Campbell & Desai 2013). These results suggest that localization of the CPC to locations other than the centromere, for example microtubules, can support CPC function at least under certain conditions. Thus, our current model of Aurora B regulation may be incomplete or at least not universal across species.

One hypothesis that reconciles these observations is that Aurora B function only requires a kinetochore-proximal pool of active Aurora B whose activity can be regulated with kMT attachment. While this pool of Aurora B is

normally generated by the inner centromere, it may be locally generated by other means, for example activation on microtubules. Regulation may be achieved by virtue of this Aurora B pool being small and/or transiently associated with the kinetochore, which would both prevent continuous cluster-mediated activation of Aurora B and provide the opportunity for counteracting phosphatase to regulate the level of Aurora B substrate phosphorylation. This idea is conceptually consistent with the reaction-diffusion model, where the CPC participating in kinetochore phosphorylation is active but no longer associated with the centromere. The major difference is that it does not assume Aurora B activation happens exclusively at the inner centromere.

Several observations are consistent with this hypothesis, including the presence of active Aurora B at the kinetochore (Deluca et al. 2011; Posch et al. 2010) (Bekier et al. 2015), the presence of Aurora B on kinetochore-proximal microtubules (Banerjee et al. 2014; Krupina et al. 2016) and the detection of Aurora B-dependent phosphorylation on the mitotic spindle (Tseng et al. 2010). This mechanism may also explain how the microtubule-binding capacity of Sli15 supports error correction in the absence of its centromere-targeting domain. While this model remains speculative, it will be critical to determine if CPC localization at regions other than the centromere contributes to CPC function in vertebrates during early mitosis.

Localization and function in late mitosis

Following anaphase onset, the CPC transfers from the inner centromere to the spindle midzone (Cooke et al. 1987). This process requires active removal of the CPC from chromatin and active recruitment to the spindle midzone. CPC removal depends on several mechanisms, including dephosphorylation of H3T3ph by Repo-man/PP1 (Qian et al. 2011) and stripping of ubiquitinated Aurora B from chromatin by the AAA+ ATPase Cdc48/p97 (Ramadan et al. 2007). Failure to remove the CPC from chromatin, for example by depleting Cdc48/p97 in human cells, inhibits chromosome decondensation and nuclear envelope reformation (Ramadan et al. 2007), indicating that timely recruitment and removal of the CPC from chromatin is necessary for proper cell division.

Multiple mechanisms also control targeting to the spindle midzone. In budding yeast, Sli15 associates with the anaphase spindle directly through its central microtubule-binding region. Cdk1-dependent phosphorylation in this region prevents microtubule binding in early mitosis and is reversed by release of the phosphatase Cdc14 at anaphase onset (Pereira & Schiebel 2003; Mirchenko & Uhlmann 2010). In human cells, removal of Cdk1-dependent phosphorylation on INCENP Thr59 promotes CPC binding to MKLP2 and co-targeting of this complex to the spindle midzone (Hummer & Mayer 2009; Gruneberg et al. 2004). Additionally, the INCENP SAH domain directly binds microtubules and supports midzone localization (van der Horst et al. 2015), though unlike in budding yeast, this region appears not to be regulated by phosphorylation.

Once at the midzone, the CPC contributes to anaphase and is essential for completion of cytokinesis (Ruchaud et al. 2007; Carmena, Wheelock, et al. 2012). Indeed, the most obvious phenotype from chemically inhibiting Aurora B in human cells is cleavage furrow regression and binucleation. Aurora B phosphorylates a variety of proteins to promote contractile ring assembly and maturation. Aurora B also regulates spindle microtubule dynamics to promote efficient chromosome segregation during anaphase. Finally, Aurora B activity is required for the abscission/NoCut checkpoint, a poorly understood pathway that delays abscission in response to chromatin near the spindle midzone to prevent cleavage by the contractile ring (Norden et al. 2006; Steigemann et al. 2009). Thus, Aurora B has an evolutionarily conserved role as a master regulator of both early and late mitosis.

1.4 Haspin

Haploid germ cell-specific nuclear protein kinase (**Haspin**) was discovered in 1999 from a cDNA cloned from mouse testis (H. Tanaka et al. 1999). Cloning of human Haspin and alignment with its murine homolog revealed a conserved yet atypical kinase domain lacking several key sequences features present in the eukaryotic protein kinase (**ePK**) family (H. Tanaka et al. 2001; Higgins 2001a; Higgins 2001b). Subsequent identification of additional Haspin homologs in animals and plants confirmed that Haspin was the prototypical member of a conserved family of atypical kinases of unknown function (Higgins 2003). It also displayed a conserved and unique genomic architecture including the absence of introns and being located in an intron of the integrin α E gene (Higgins 2001b; Yoshimura et al. 2001; H. Tanaka et al. 2001).

In 2005, Haspin was shown to phosphorylate histone 3 threonine 3 (H3T3ph) (Dai et al. 2005), a mitosis-specific histone modification enriched at the inner centromere (Polioudaki et al. 2004). The original phenotype of depleting Haspin protein in human cells was loss of centromeric Shugoshin and sister chromatid cohesion (Dai et al. 2006). It was not until four years later that three labs, including our own, determined that Haspin and H3T3ph were critical for CPC localization and function (F. Wang et al. 2010; Kelly et al. 2010; Yamagishi et al. 2010). These studies demonstrated in human cells, fission yeast and *Xenopus* egg extracts that Haspin-dependent H3T3ph was directly bound by the BIR domain of Survivin and that this interaction was required to localize the CPC

to chromatin. This pathway was required for CPC function as depletion of Haspin perturbed Aurora B-dependent spindle assembly in *Xenopus* egg extracts and attenuated the taxol-mediated SAC response in human cells. This later result was subsequently verified using the haspin inhibitor 5-iodotubercin (F. Wang et al. 2012), confirming that H3T3ph is required for CPC localization and function.

Atypical features of Haspin kinase

The primary structure of Haspin revealed several deviations from the canonical ePK family of serine/threonine kinases (Higgins 2003). Most obvious were two alterations to the activation segment involved in substrate binding and catalysis. First, the DFG-motif, which typically coordinates and orients binding of the γ -phosphate of Mg^{2+} -ATP, was mutated to DYT. Second, the APE motif present near the P+1 site of almost all ePK family proteins was absent. Solving the structure of the Haspin kinase domain identified a number of unique features predicted to render the kinase domain constitutively active (Eswaran et al. 2009; Villa et al. 2009). For example, several insertions stabilized the typically mobile α C helix in proximity to the β 3-strand, a placement typically seen in activated kinase domains.

Coupling H3T3ph to the cell cycle

Phosphorylation of H3T3 must be tightly regulated to facilitate proper cell division. Preventing H3T3ph by chemical inhibition of Haspin in human cells

displaces the CPC from the centromere, resulting in defects in kinetochore phosphorylation and chromosome alignment (F. Wang et al. 2012). Conversely, failure to dephosphorylate H3T3ph at anaphase retains the CPC on chromatin, resulting in Aurora B-dependent defects in chromosome decondensation and nuclear envelope reformation (Kelly et al. 2010). Thus, cell cycle regulated phosphorylation of H3T3 promotes timely recruitment and removal of the CPC from chromatin to facilitate mitosis.

This raises an important question: if the Haspin kinase domain is constitutively active, how is H3T3ph regulated? It is known that PP1 in complex with the regulatory subunit Repo-man (Repo-man/PP1) dephosphorylates H3T3ph on chromosome arms during early mitosis and at the centromere following anaphase onset (Qian et al. 2011; Qian et al. 2013). While this mechanism restricts H3T3ph to the centromere prior to anaphase and ensures global dephosphorylation through the end of mitosis, it is unclear if it suppresses H3T3ph during interphase. A second mechanism of regulation might be controlling Haspin localization. Work in fission yeast identified the cohesin-interacting protein Pds5 as binding the N terminus of Haspin and being required for Haspin localization and H3T3ph (Yamagishi et al. 2010). Cohesin is degraded at anaphase and is not loaded back onto chromatin until the following S-phase. Thus if Haspin kinase activity is coupled to its localization, this mechanism could prevent substantial H3T3ph until late-S/ G2 phase. Finally, it has been speculated that the N terminus of Haspin could regulate its kinase activity (Villa et

al. 2009). It has also been shown that Aurora B-dependent phosphorylation of the Haspin N terminus stimulates H3T3ph and supports CPC localization during mitosis (F. Wang et al. 2011). This raises the possibility that Aurora B-dependent phosphorylation of the N terminus during mitosis neutralizes an inhibitory affect that normally prevents Haspin kinase activity in interphase. Elaborating the molecular mechanism that couples H3T3ph to the cell cycle is critical to our understanding of the CPC and may yield a mechanism to regulate an otherwise atypical kinase. In **Chapter 2** of my dissertation, I present work in collaboration with a former Ph.D. student in the Funabiki lab, Cristina Ghenoiu, which demonstrates how Haspin's kinase activity is regulated with the cell cycle.

1.5 *Xenopus* egg extract

Xenopus egg extract is a powerful cell-free system to study processes related to the cell cycle and chromatin (Murray 1991). The extract is prepared by centrifugation of oocytes from the African clawed frog *Xenopus laevis* and subsequent removal of the layer enriched for cytoplasmic components. These extracts are transcriptionally silent and naturally arrested at meiotic prophase II by cytostatic factor (CSF), which was later identified as an APC inhibitor xErp1/Emi2 (Schmidt et al. 2005). These extracts are free of endogenous genomic DNA but do support chromatinization of exogenously added DNAs, including plasmids or demembranated *Xenopus* sperm. In M-phase, these chromatinized templates nucleate microtubules and assemble a spindle capable of aligning chromatin. It can also generate a SAC-dependent arrest when incubated with nocodazole, but only after addition of a high amount of sperm chromatin, equivalent to the chromosome/cytoplasm ratio of the mid-blastula transition (MBT) (Minshull et al. 1994). Adding calcium to M-phase extract degrades the CSF component xErp1 (Rauh et al. 2005) and releases (or ‘cycles’) the extract into anaphase and subsequently interphase, resulting in sister chromatid separation, nucleus formation, DNA replication, and a functional DNA damage response. *Xenopus* egg extract is also highly tractable for functional protein dissection: a protein of interest can be efficiently immunodepleted by incubation with and removal of antibody-coated magnetic beads and replaced by addition of mRNA produced *in vitro*, which is subsequently translated by the

extract, or the addition of purified recombinant protein. Thus, *Xenopus* egg extract combines a tractable system to manipulate proteins with the ability to study complex processes such as spindle assembly and DNA replication.

1.6 Goals of this dissertation

The goal of this dissertation is to understand how the CPC is regulated in time and space to promote accurate cell division. During early mitosis, the CPC localizes to the inner centromere and promotes accurate chromosome segregation through two mechanisms: destabilizing erroneous kMT attachments and activating the SAC. I am interested in understanding the molecular mechanisms that target the CPC to the inner centromere and how the CPC contributes to the SAC. In **Chapter 2**, I collaborate with Cristina Ghenoiu to determine how phosphorylation of H3T3 is coupled to the cell cycle to promote timely recruitment of the CPC to chromatin during mitosis. In **Chapter 3**, I demonstrate that the INCENP SAH domain supports CPC localization on chromatin and microtubules, and that these interactions support the SAC and mitotic cell death in taxol. In **Chapter 4**, I discuss the implications of this work in terms of regulating the events of early mitosis, specifically coordinating Aurora B activity with kMT attachment to promote accurate cell division.

Chapter 2: Autoinhibition and Polo-dependent Multisite

Phosphorylation Restrict Activity of the Histone H3 Kinase

Haspin to Mitosis

2.1 Introduction:

Accurate cell division requires localization of the CPC to chromatin during early mitosis and transfer to the spindle midzone following anaphase onset (Ruchaud et al. 2007; Carmena, Wheelock, et al. 2012). Phosphorylation of H3T3 is a critical regulator of CPC localization. H3T3 is phosphorylated by the atypical protein kinase Haspin during early mitosis (Dai et al. 2005) and dephosphorylated at anaphase onset by Repo-man/PP1 (Qian et al. 2011). The activity of Repo-man/PP1 prior to anaphase prevents H3T3ph on chromosome arms and is one of the mechanisms to promote its enrichment at the inner centromere (Qian et al. 2013). The BIR-domain of the Survivin subunit of the CPC directly binds H3T3ph and is required to target the CPC to the centromere (Kelly et al. 2010; F. Wang et al. 2010; Yamagishi et al. 2010; Jeyaparakash et al. 2011). Depletion of Haspin protein in *Xenopus* egg extract reduces H3T3ph and CPC recruitment to chromatin, leading to defects in spindle size (Kelly et al. 2010). In human cells, chemical inhibition of Haspin (F. Wang et al. 2012) or siRNA depletion of Haspin protein (F. Wang et al. 2010; Yamagishi et al. 2010) also reduces H3T3ph and the CPC on chromatin, leading to chromosome segregation errors and an inability to activate the SAC. Conversely, failure to dephosphorylate H3T3 at anaphase increases CPC abundance on chromatin,

resulting in defects in chromosome condensation and nuclear envelope reformation (Qian et al. 2011). While we know that Repo-man/PP1 is important for dephosphorylating H3T3 at anaphase, the molecular mechanisms governing its inhibition during interphase and activation during mitosis remain unclear.

Many kinases, including Aurora B, are activated by phosphorylation of their activation segment (also called the t-loop). This phosphorylation helps structure the catalytic pocket for productive substrate phosphorylation (Bayliss et al. 2012). Interestingly, the crystal structure of the Haspin kinase domain revealed that a segment in the C-terminal lobe intrinsically structures the activation segment such that phosphorylation should be dispensable for its activation (Villa et al. 2009). Given that the Haspin kinase domain is intrinsically active, how is phosphorylation of H3T3 restricted to mitosis? One idea is that counteracting phosphatases suppress phosphorylation of H3T3 during interphase. It has been shown that during mitosis, H3T3ph is dephosphorylated on chromatin by Repo-man/PP1, but retained at the centromere through Aurora B-dependent inhibition of Repo-man recruitment (Qian et al. 2013). Given that Aurora B is not present on chromatin during G1- and early S-phase, this mechanism could help prevent H3T3ph during interphase. An alternative hypothesis is that the N terminus of Haspin, which was not present in the crystal structure, regulates the activity of the kinase domain. In line with Haspin being regulated through its N terminus, it has been shown that Aurora B-dependent phosphorylation of the human Haspin N terminus is required for H3T3ph during

mitosis (F. Wang et al. 2011). Identifying the molecular mechanism that couples H3T3ph to the cell cycle is critical to understand how CPC localization is regulated to ensure proper cell division.

In collaboration with Cristina Ghenoïu, a previous graduate student in the Funabiki laboratory, I helped uncover the molecular mechanism that couples Haspin activation to the cell cycle to ensure timely phosphorylation of H3T3 and recruitment of the CPC. The work I will discuss below was published in *Molecular Cell* in 2013 in a paper entitled “Autoinhibition and Polo-dependent multisite phosphorylation restrict activity of the histone H3 kinase Haspin to mitosis” (Ghenoïu et al. 2013).

2.2 Results

Cdk1- and Plx1-dependent phosphorylation activate Haspin in mitosis

In *Xenopus* egg extract, Ghenoiu found that phosphorylation of H3T3 in M phase is correlated with a phosphorylation-dependent mobility shift in xHaspin. Aurora B-dependent phosphorylation of the human homolog of xHaspin (hHaspin) is required for H3T3ph in human cells (F. Wang et al. 2011). Thus, we hypothesized that cell-cycle dependent-phosphorylation of Haspin may regulate its kinase activity. To test this, we sought to identify the kinase(s) that phosphorylate Haspin and support H3T3ph in mitosis. Given the role of Aurora B in human cells, I tested whether activation or inhibition of xAurora B in *Xenopus* egg extract affected H3T3ph as monitored by western blot. xAurora B is typically inactive in CSF extract; however, its kinase activity can be stimulated by the addition of chromatin or taxol (Kelly et al. 2007; Tseng et al. 2010). While addition of sperm chromatin, plasmid DNA or taxol stimulated Aurora B-dependent phosphorylation of its canonical substrate Op18 (Gadea & Ruderman 2006), these treatments failed to enhance H3T3ph (**Figure 2-1**). This was not due to histones being pre-saturated with H3T3ph in mitosis, as treatment with the phosphatase inhibitor okadaic acid enhanced the abundance of H3T3ph. Conversely, depleting the CPC from extract did not reduce the level of H3T3ph, indicating the xAurora B is not required for Haspin activation in *Xenopus* egg extract.

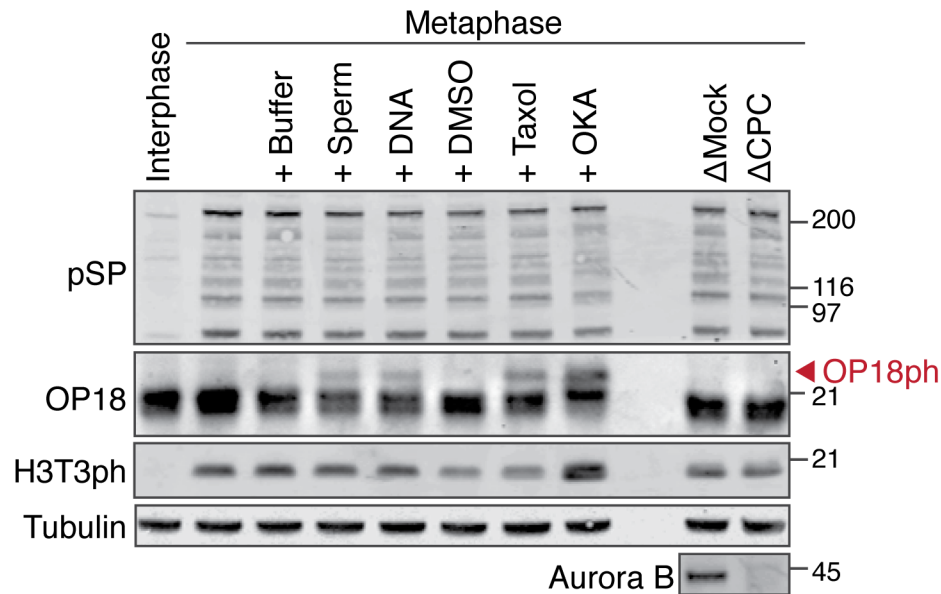


Figure 2-1: H3T3 phosphorylation is not dependent on Aurora B in *Xenopus* egg extracts

Aurora B activity in metaphase *Xenopus* egg extracts was stimulated by adding DNA, sperm chromosomes, or taxol. Maximum levels of substrate phosphorylation were revealed by addition of okadaic acid (OKA). The CPC was depleted from metaphase extracts using anti-iNCENP antibodies (Δ CPC). Western blot analysis of total extracts is shown. The hyperphosphorylated form of Op18, an Aurora B-dependent phosphorylation indicative of kinase activation, is indicated by an arrowhead. Anti-phosphoSP (pSP) was used to monitor M phase-specific Cdk1 substrate phosphorylation. While addition of DNA, sperm or taxol stimulates Aurora B activation, no change in H3T3ph is observed. Depleting the CPC also has no effect on H3T3ph.

Next, Ghenoïu tested whether Polo-like kinase (Plx1) supported Haspin activation in mitosis. She found that immunodepleting Plx1 from *Xenopus* egg extract reduced the level of H3T3ph and the xHaspin mobility-shift (**Figure 2-2A**). She also saw a dose-dependent decrease in H3T3ph using the Polo inhibitor BI2536 (**Figure 2-2B**), consistent with Haspin being activated by Plx1-dependent phosphorylation. Interestingly, recombinant human Polo-like kinase (Plk1) failed to phosphorylate the N terminus of xHaspin *in vitro*. Robust phosphorylation of Polo substrates often requires an interaction between the Polo box domain (PBD) of Polo and a phosphorylated PBD-binding motif (S[pS/pT]) on its substrate (Elia, Cantley, et al. 2003; Elia, Rellos, et al. 2003). The N terminus of xHaspin contains three potential PBD-binding motifs that overlap with a putative Cdk1 phosphorylation site ([S/T]P) and may serve to recruit Plx1 (ST¹²¹P, ST²⁰⁶P, SS⁴⁸⁶P) (**Figure 2-3A**). Only the ST²⁰⁶P motif (hereafter called T206) is conserved in vertebrate Haspin homologs outside of *Xenopus*.

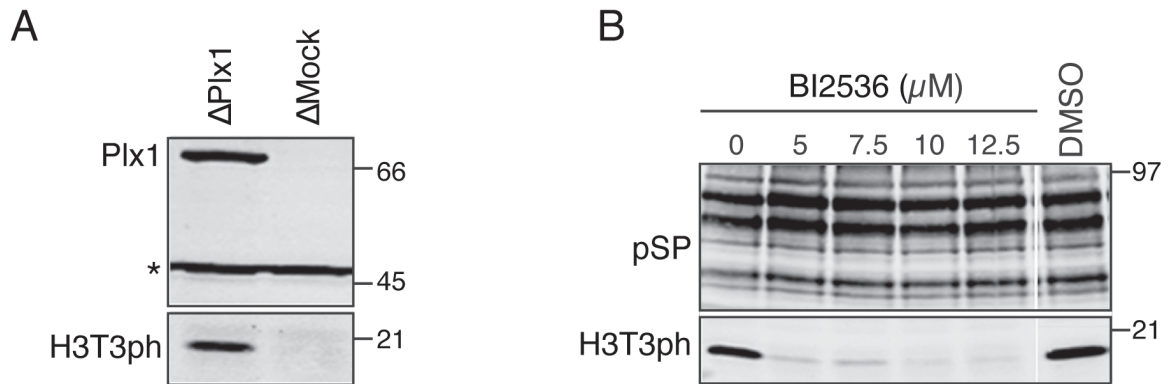


Figure 2-2: The activity of Polo kinase is required for H3T3ph in *Xenopus* egg extract

A) Metaphase *Xenopus* egg extracts were depleted with either an anti-Plx1 (Δ Plx1) or a control IgG (Δ Mock) antibody. Western blot analysis of extract proteins with anti-Plx1 and anti-H3T3ph is shown. The asterisk indicates a cross-reacting antigen used as a loading control. Depleting Plx1 dramatically reduces the level of H3T3ph.

B) The Plx1 inhibitor BI2536 was added to metaphase *Xenopus* egg extracts at the indicated concentrations. Western blot analysis of extract proteins with the indicated antibodies is shown. Inhibiting the kinase activity of Plx1 decreases H3T3ph in extract.

Experiments performed by C. GhenoIU.

To test the importance of T206 for Plx1-dependent xHaspin activation, Ghenoiu developed a system to immunodeplete xHaspin from *Xenopus* egg extract and reconstitute it with ³⁵S-labeled xHaspin produced by *in vitro* translation in reticulocyte lysates. She added back either xHaspin wild-type (xHaspin-WT) or a mutant where T206 was mutated to alanine to prevent phosphorylation and binding to Plx1 (xHaspin T206A) (**Figure 2-3B**). Extract depleted of endogenous xHaspin lost H3T3ph, but could be rescued by addition of xHaspin-WT. This construct also underwent a mobility shift consistent with phosphorylation-dependent activation. However, xHaspin T206A neither supported H3T3ph nor underwent a mobility shift, indicating this residue was critical to support Plx1-dependent phosphorylation and activation of xHaspin.

Several lines of evidence indicate that phosphorylation of T206 by Cdk-1 promotes binding of Plx1 to xHaspin and subsequent phosphorylation of xHaspin by Plx1. First, immunoprecipitation (IP) of GFP-tagged xHaspin from extract co-purified Plx1 during mitosis, but not interphase, indicating cell cycle-dependent binding to Haspin (**Figure 2-3C**). This interaction was dependent on T206 as IP of MBP-tagged xHaspin N terminus (N420) from extract co-purified Plx1, but not when T206 was mutated to alanine (N420^{T206A}) (**Figure 2-3D**). Second, the Plx1 PBD bound to a 34aa xHaspin peptide *in vitro* dependent on T206 and priming phosphorylation by Cdk1-Cyclin B (**Figure 2-3E**). Third, *in vitro* phosphorylation of the xHaspin N terminus by Plx1 was greatly enhanced by the addition of Cdk1, but not when T206 was mutated to alanine (**Figure 2-3F**). Fourth, M-phase

specific phosphorylation of xHaspin T206 in *Xenopus* egg extract was confirmed by mass spectroscopy (MS) and by western blot using a phosphospecific antibody against T206ph. Finally, I demonstrated that addition of the Cdk1 inhibitor roscovitine to extract resulted in rapid dephosphorylation of H3T3ph **(Figure 2-4)**. This was specific to Cdk1 inhibition, as addition of U0126, an inhibitor of MAP kinase which also phosphorylates [S/T]P motifs, did not reduce H3T3ph. Altogether, this data indicates that Cdk1-dependent phosphorylation of xHaspin at T206 directly recruits Plx1, which subsequently phosphorylates and activates xHaspin during mitosis.

Figure 2-3 (A-D): Plx1 interacts with and phosphorylates the xHaspin N terminus dependent on priming phosphorylation of xHaspin T206 by Cdk1

A) Multisequence alignment of Haspin proteins, focusing on residues adjacent to *Xenopus laevis* (Xl) ST¹²¹P (bottom) and ST²⁰⁶P (top). While ST²⁰⁶P is widely conserved among vertebrates, ST¹²¹P is specific to *Xenopus* species. Xt, *Xenopus tropicalis*; Dr, *Danio rerio*; Gg, *Gallus gallus*; Mm, *Mus musculus*; Hs, *Homo sapiens*.

B) Wild-type (WT) or indicated mutants of full-length xHaspin translated and labeled with ³⁵S in reticulocyte lysates were added to control or ΔxHaspin metaphase extracts. Total extracts were analyzed by autoradiography (³⁵S-labeled xHaspin) and western blotting (anti-Plx1 and anti-H3T3ph). Mutating the highly conserved T206, but not the *Xenopus*-specific T121, decreases the xHaspin mobility shift and fails to support H3T3ph in the absence of endogenous Haspin. This defect is similar to expressing an xHaspin kinase dead mutant (xHaspin K862A).

C) GFP or xHaspin-GFP were translated from exogenously added mRNA in metaphase *Xenopus* egg extracts and were either maintained in metaphase (M) or released into interphase (I) by calcium addition. GFP-fused proteins were immunopurified with anti-GFP beads. The bead fraction was probed with anti-GFP or anti-Plx1. Plx1 co-purifies with xHaspin-GFP in metaphase, but not in interphase.

D) Purified MBP, MBP-xHaspin-N420 with or without a T206A mutation, or MBP-xHaspin-ΔN729 were incubated with metaphase *Xenopus* egg extracts and immunopurified with anti-MBP beads. Coomassie staining (top) and a western blot of the bead fraction with an anti-Plx1 (bottom) are shown. Plx1 co-purifies with the Haspin N terminus dependent on the T206 residue being intact.

Experiments performed by C. Ghenoïu.

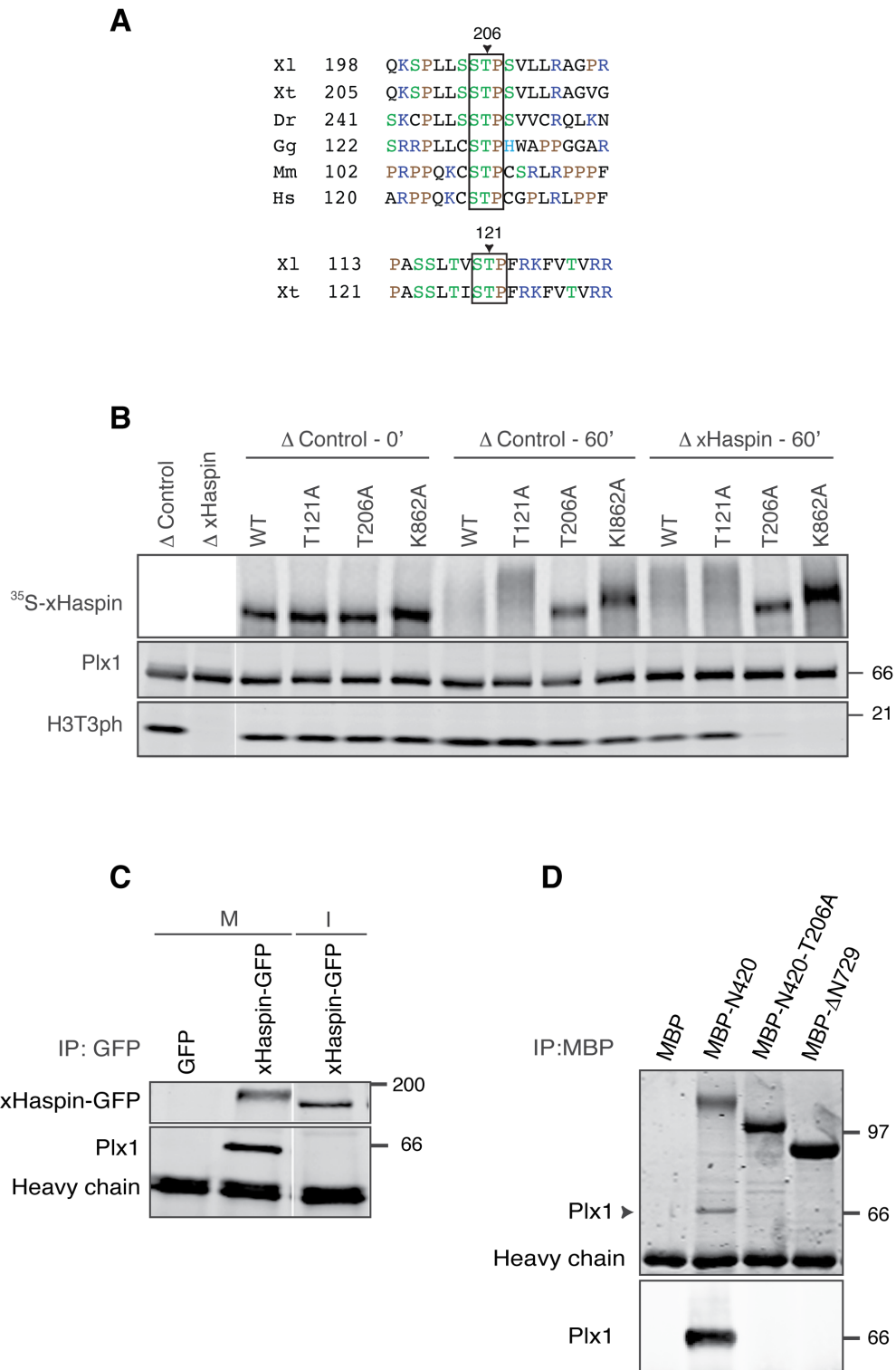
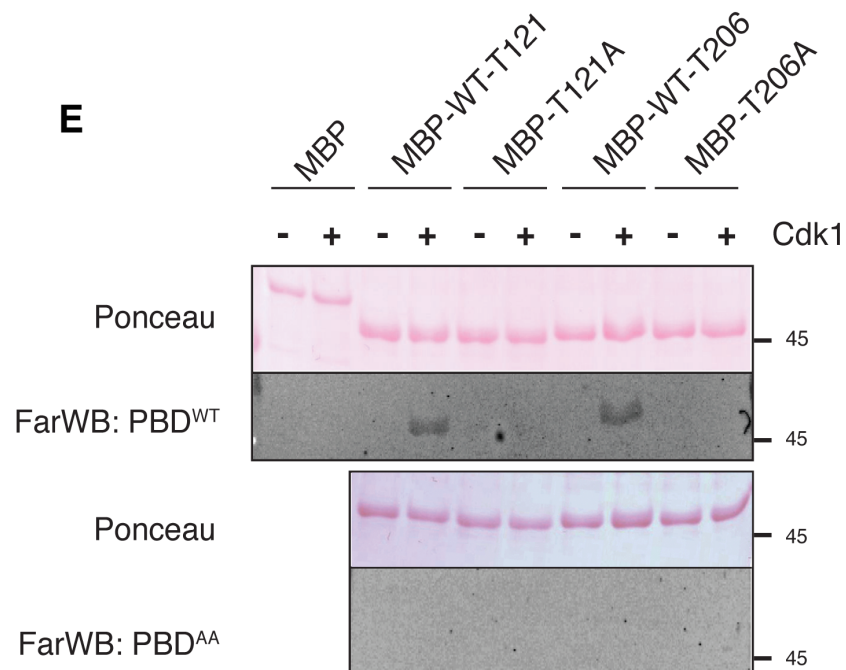


Figure 2-3 (A-D): Plx1 interacts with and phosphorylates the xHaspin N terminus dependent on priming phosphorylation of xHaspin T206 by Cdk1

Figure 2-3 (E-F): Plx1 interacts with and phosphorylates the xHaspin N terminus dependent on priming phosphorylation of xHaspin T206 by Cdk1

E) Far Western analysis detecting the phospho-dependent interaction between xHaspin N-terminal constructs and the PBD of Plx1. MBP-lacZ α (control) or MBP fused to the 34 amino acids surrounding T121 or T206 of xHaspin (top) were phosphorylated by Cdk1-cyclin B, and transferred to a nitrocellulose membrane (Ponceau), followed by incubation with recombinant PBD of Plx1. A PBD^{H532A/K534A} mutant defective in phospho-dependent binding (PBD^{AA}) was used as a negative control. Binding of the PBD on the membrane was monitored by anti-Plx1 antibody (FarWB). Binding of PBD^{WT} to both Haspin peptides upon Cdk1-dependent phosphorylation at T121 and T206 sites was detected.

F) Recombinant MBP-xHaspin-N520 (with or without T206A) was subjected to *in vitro* kinase reactions with γ -[³³P]-ATP and a combination of purified Cdk1-cyclin B, Plx1, and MBP-xHaspin- Δ N729. Coomassie staining (top) and autoradiography corresponding to MBP-xHaspin N520 proteins are shown. xHaspin is phosphorylated by Cdk1 on T206. This phosphorylation is required for robust Plx1-dependent phosphorylation of the xHaspin N terminus. Experiments performed by C. Ghenoïu.



MBP-WT-121: NGPPSERNPASSLTV**STP**FRKFVTVRRKAPTRCN

MBP-WT-T206: TEISHSPLQKSPLLS**STP**SVLLRAGPRARGAVGK

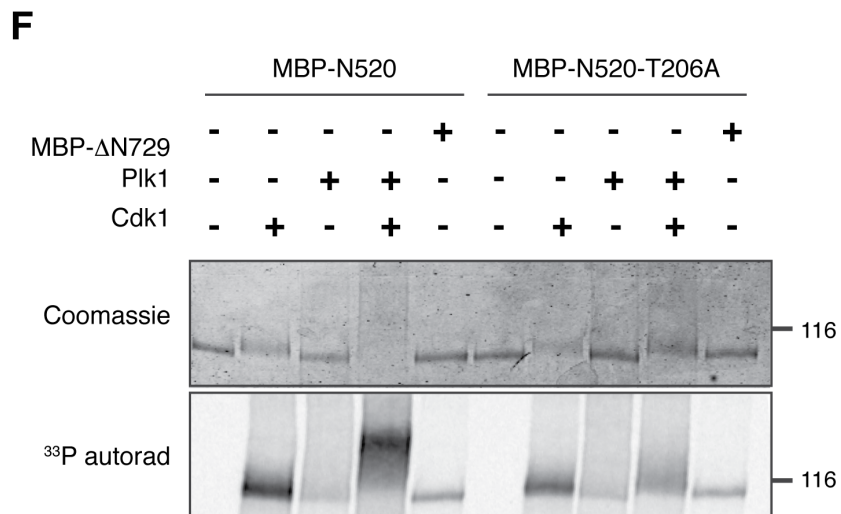


Figure 2-3 (E-F): Plx1 interacts with and phosphorylates the xHaspin N terminus dependent on priming phosphorylation of xHaspin T206 by Cdk1

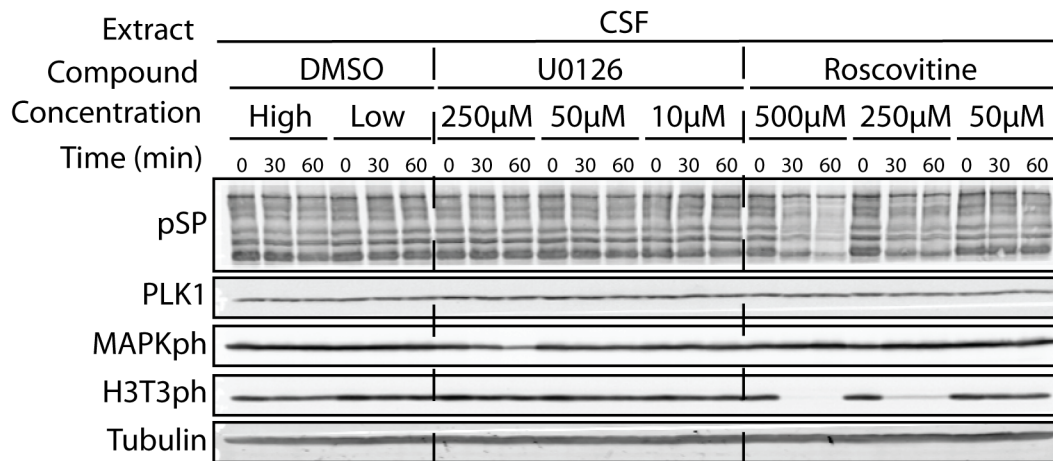


Figure 2-4: Cdk1 activity is required for H3T3ph in *Xenopus* egg extract

Western blot of the total level of H3T3ph in metaphase *Xenopus* egg extracts incubated with the indicated concentration of DMSO, the MAP kinase inhibitor U0126 and the Cdk1 inhibitor Roscovitine. H3T3ph levels were monitored for 60 min following addition of the inhibitors. 'High' and 'Low' DMSO concentration corresponds to a volume of DMSO equal to that present in 500 μm and 50 μm of Roscovitine, respectively. An antibody specific to phosphorylation of the MAP kinase t-loop (MAPKph) was used as a marker for MAPK activity. An antibody recognizing Cdk1-dependent phosphorylation of serine (pSP) was used as a marker for Cdk1 activity. Inhibiting the kinase activity of Cdk1, but not Map kinase, led to a decrease in H3T3ph.

Haspin is activated in mitosis by multisite phosphorylation of its N terminus

Plx1-dependent phosphorylation of xHaspin is correlated with its kinase activity. xHaspin contains multiple putative Plx1 sites ([D/E]x[S/T]) throughout its N terminus. While there is also a Plx1 site within the activation loop of the xHaspin kinase domain (S1054), Ghenoïu found that it was dispensable for Haspin's kinase activity, as mutating it to alanine did not affect H3T3ph in extract.

To identify phosphorylation sites in xHaspin important for its activation, Ghenoïu purified xHaspin-WT, xHaspin T206A and xHaspin K862A (xHaspin-kinase dead (KD)) from metaphase *Xenopus* egg extract and sent it for liquid chromatography tandem MS (LC-MS/MS). I used the software ScaffoldPTM to compile the results of this experiment and identify xHaspin residues that were phosphorylated during mitosis (**Figure 2-5A**). We identified over 30 residues in xHaspin phosphorylated during mitosis, the majority of which were in the N terminus (**Table 1**). By comparing the LC-MS/MS profiles of xHaspin-WT, xHaspin T206A, and xHaspin-KD, we identified at least two residues dependent on T206 (S304, Y307), two residues dependent on xHaspin kinase activity (T472, T675), and two residues dependent on both (S92, S753). We defined these based on each residue having at least 2 phosphorylated peptides in xHaspin-WT, at least 3 total peptides in each sample, and at least an 80% reduction in the percent of phosphorylated peptides relative to xHaspin-WT.

Figure 2-5: Multisite phosphorylation of the xHaspin N terminus is required for robust H3T3ph in metaphase *Xenopus* egg extract

A) Coverage map of xHaspin peptides identified by tandem mass spectroscopy (MS/MS) for full-length xHaspin (WT), xHaspin T206A (T206A) and xHaspin K862A (kinase dead). Residues are colored based on which samples they were identified in. A Venn diagram in the lower right explains the color-coding.

B) Quantitation of H3T3ph levels in metaphase Δ xHaspin extracts supported by various xHaspin phosphorylation site mutants. Within the schematic of xHaspin, black bars point to the relative location of the residue in the N terminus.

Constructs are numbered 1–13 on the left-hand side. A black square in the matrix indicates the presence of the indicated serine- and threonine-to-alanine mutation for a given construct. Phosphorylation sites matching to substrate consensus sequences for Plk1 and Cdk1 are marked in red and blue, respectively. Residues whose phosphorylation depends on T206 are bolded. Constructs were synthesized and labeled with ^{35}S in reticulocyte lysates and added to metaphase Δ xHaspin for 60 min before assessing the H3T3ph levels by western blot. The graph on the right displays the mean and SEM of relative H3T3ph levels divided by the input amount of ^{35}S -labeled xHaspin proteins and standardized to WT. “n” represents number of independent experiments. p values relative to xHaspin-WT are reported for all constructs and were determined with a one-way ANOVA followed by a Bonferroni post hoc test. ***p < 0.001; **p < 0.01; *p, < 0.05; ns = not significant.

Experiments in B performed by C. Ghenoiu, visualized by M. Wheelock.

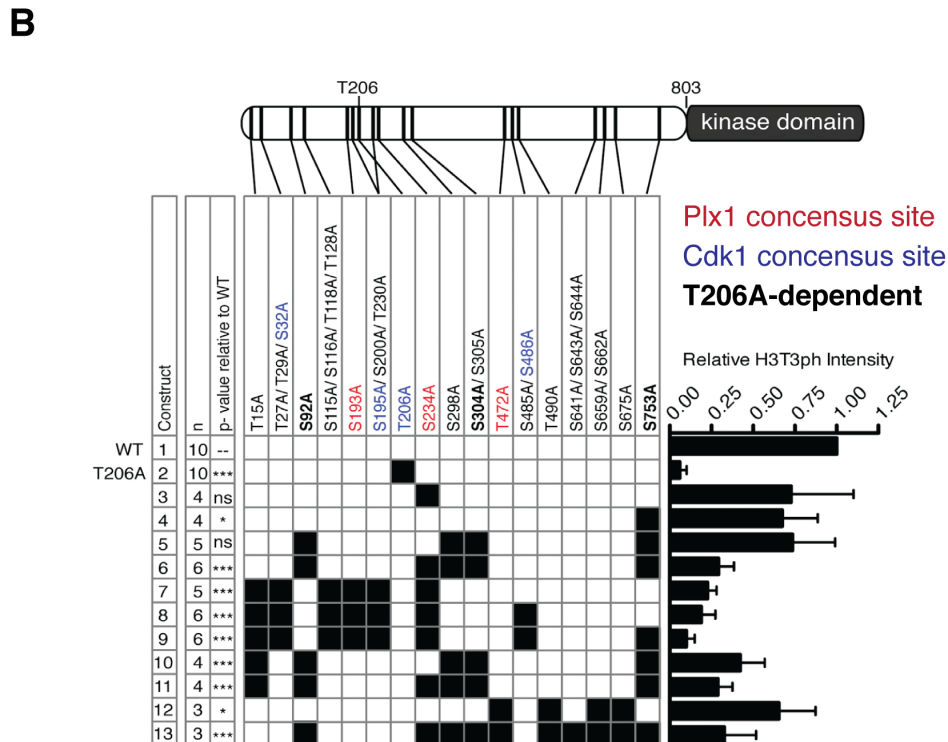
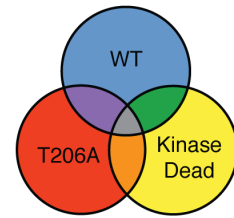
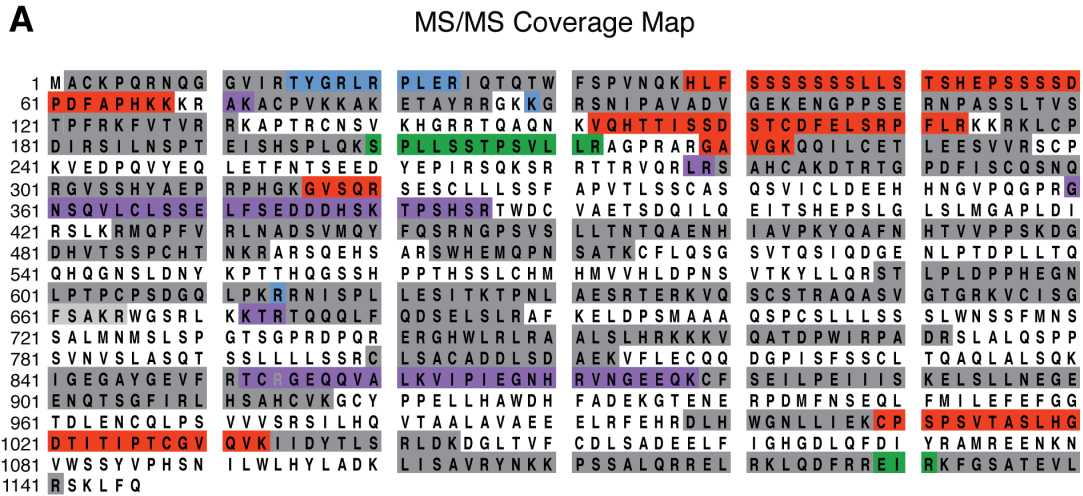


Figure 2-5: Multisite phosphorylation of the xHaspin N terminus is required for robust H3T3ph in metaphase *Xenopus* egg extract

Residues which depend on both T206 and xHaspin kinase activity (S92, S753) may be Haspin auto-phosphorylation sites that require initial xHaspin activation by Plx1-dependent phosphorylation. However, we find that Plx1 can phosphorylate S92 *in vitro* on an N-terminal fragment of xHaspin lacking the kinase domain (xHaspin N520). This raises the alternative possibility that S92 is phosphorylated by Plx1 in full-length xHaspin, but requires a priming auto-phosphorylation by xHaspin. Consistent with this idea, we find that xHaspin N520, which lacks the kinase domain, is not phosphorylated at S92 in CSF extract. It should be noted that while many sites in xHaspin N520 were phosphorylated in extract, the peptide coverage in this experiment was lower than our MS for full-length xHaspin and only two residues, both below our minimum cut off, were T206-dependent.

Candidate residues for priming auto-phosphorylation by xHaspin are T472 and T675, which depended only on xHaspin kinase activity; however, interpretation LC-MS/MS data for phosphorylation of these residues is complicated. Peptide coverage of T675 was just above our minimum cut off. Conversely, while T472 had high coverage and many phosphorylated peptides in xHaspin-WT and xHaspin T206A, it conforms to the Plk1 consensus motif and is phosphorylated by Plx1 *in vitro* on xHaspin N520, which lacks the xHaspin kinase domain. xHaspin N520 was also phosphorylated at T472 in extract, however; whether this depended on Plx1 binding or was catalyzed by endogenous xHaspin is unclear given that only one unphosphorylated peptide was detected for

xHaspin N520 T206A. Thus, while xHaspin is phosphorylated in a manner dependent on its own kinase activity, it is unclear if these are *bona fide* auto-phosphorylation sites or are indirectly supported by Haspin, for example by phosphorylating and activating Plx1 to promote phosphorylation of low affinity Plx1 sites on xHaspin.

Next, we determined whether any of these residues were important for xHaspin activation by measuring the ability of xHaspin phospho-site mutants to rescue H3T3ph following xHaspin depletion from extract (**Figure 2-5B**). Mutating five phosphorylation sites to alanine (S92, S298, S304, S305, S753), including those whose phosphorylation required T206, did not significantly decrease H3T3ph (construct #5). This is likely due to the contribution of other T206-dependent sites, which were either not identified by MS or below our peptide cut offs. Indeed, adding another alanine mutation at S234, a residue that conforms to the Plx1 consensus and was phosphorylated on xHaspin N520 by Plx1/Cdk1 *in vitro*, significantly reduced H3T3ph (construct #6). Mutation of S234 alone did not affect H3T3ph (construct #3), suggesting that phosphorylation at multiple sites, rather than a key residue, supports xHaspin activation. Several observations are consistent with this hypothesis. First, mutation of T15 instead of S234 reduces H3T3ph when mutated with the five residues in construct #6 (construct #10). Second, mutating S234 and T15 in addition to 12 other phosphorylation sites not mutated in #6 also reduces H3T3ph (construct #7). Finally, mutating five residues (T472, T490, S659, S662, S675) that were phosphorylated dependent on

xHaspin kinase activity and not present in the above constructs, mildly but significantly reduced the level of H3T3ph (construct #12). Taken together, these results indicate that multisite phosphorylation of the xHaspin N terminus, dependent on both Plx1 and xHaspin kinase activity, contribute to xHaspin activation in extract.

The Haspin Basic Inhibitory Sequence (HBIS) prevents Haspin activation in interphase

Why does xHaspin activation require N-terminal phosphorylation when the crystal structure of its kinase domain suggests it assumes an intrinsically active conformation? One possibility is that an inhibitory segment in the xHaspin N terminus prevents xHaspin activation but is antagonized by Plx1-dependent phosphorylation. If this hypothesis was true, deleting the inhibitory segment should activate xHaspin and bypass the recruitment for Plx1. Ghenoïu found that deletion of up to the first 729aa of the xHaspin N terminus (xHaspin Δ N729) diminished, rather than enhanced, H3T3ph in *Xenopus* egg extract, suggesting that if an inhibitory segment existed, it was likely located between residue 730 and the beginning of the kinase domain at residue 803. Within this region, Ghenoïu identified an evolutionarily conserved patch of basic residues that we termed the Haspin Basic Inhibitory Sequence (HBIS) based on the results below **(Figure 2-6A)**.

To determine if the HBIS negatively regulated xHaspin activity, Cristina deleted the RKKKVQ sequence in the HBIS from xHaspin Δ N729 and assessed its ability to support H3T3ph in *Xenopus* egg extract. Deletion of the HBIS not only restored H3T3ph in metaphase extract, it also supported H3T3ph in interphase, when H3T3 is normally dephosphorylated (**Figure 2-6B**). Deleting the HBIS from full-length xHaspin (xHaspin Δ HBIS) not only supported H3T3ph in metaphase and interphase, it did so in the absence of T206-dependent activation (xHaspin T206A Δ HBIS). Taken together, these results indicate that the HBIS prevents activation of xHaspin in interphase.

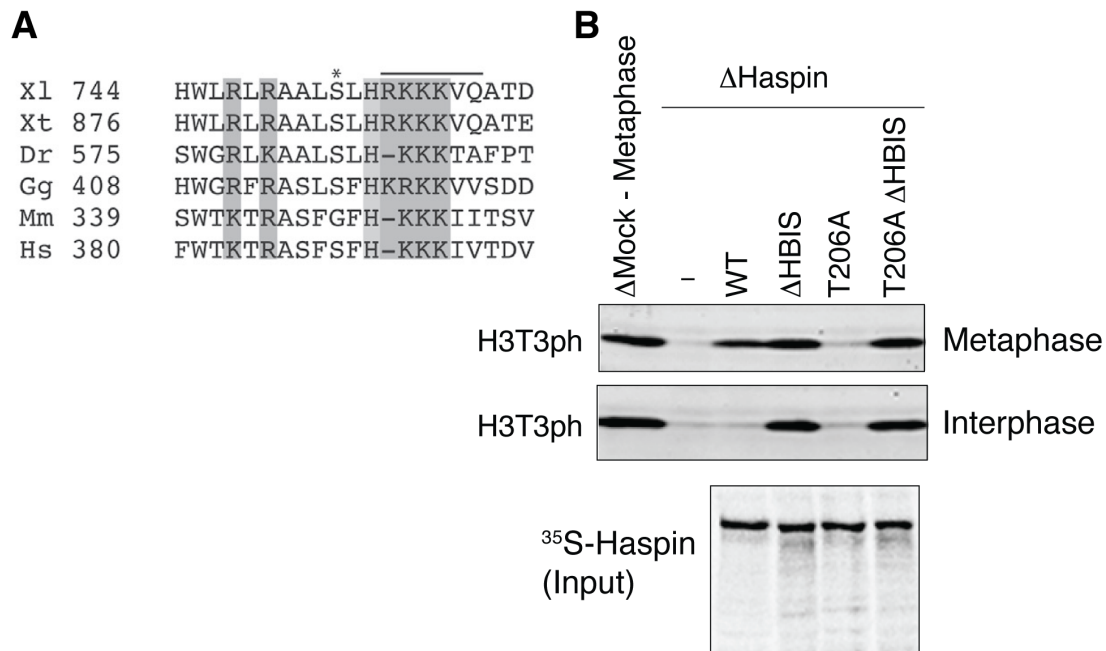


Figure 2-6: The HBIS restricts H3T3ph to interphase

A) Multisequence alignment of Haspin proteins showing conservation of the Haspin Basic Inhibitory Sequence (HBIS). A line indicates the amino acids that are deleted in Δ HBIS. An asterisk indicates S753, which is phosphorylated in metaphase *Xenopus* egg extracts. Xl, *Xenopus laevis*; Xt, *Xenopus tropicalis*; Dr, *Danio rerio*; Gg, *Gallus gallus*; Mm, *Mus musculus*; Hs, *Homo sapiens*.

B) Full-length xHaspin (WT), xHaspin- Δ HBIS, xHaspin^{T206A}, xHaspin^{T206A} Δ HBIS mutant protein, or N-terminally truncated xHaspin (Δ N729) with or without an HBIS deletion (Δ HBIS) were labeled with ³⁵S in reticulocyte lysates and incubated with metaphase (top) or interphase (middle) Δ xHaspin extracts. Western blot analyses (top and middle) with anti-H3T3ph and an autoradiography (bottom) of the input samples are shown. Whereas H3T3ph is normally restricted to metaphase extract, deletion of the HBIS promotes robust H3T3ph in both metaphase and interphase.

Experiments performed by C. Ghenoiu.

The HBIS interacts with importin- β but this does not regulate H3T3ph

How does the HBIS prevent H3T3ph in interphase? One possibility is that the HBIS binds a protein that inhibits xHaspin. We noticed that the HBIS resembles the basic nuclear localization signal (NLS) (Lange et al. 2007), a short amino acid sequence that promotes nuclear import through binding to a complex of importin- α and importin- β . Ghenoiu found that immunoprecipitation of xHaspin co-purified importin- β from interphase extract, but not metaphase extract (**Figure 2-7A**). Depleting Plx1 from metaphase extract not only reduced H3T3ph but also promoted binding of importin- β to xHaspin (**Figure 2-7B**), consistent with importin- β acting as a cell-cycle dependent xHaspin inhibitor.

If binding of importin- β to xHaspin prevents H3T3ph during interphase, then preventing this interaction should activate xHaspin. Importin- β binds to an importin- β binding (IBB) domain on importin- α , which directly binds the NLS through its N terminus (Lange et al. 2007). Addition of recombinant IBB can disrupt this interaction, displacing importin- β from its cargo and preventing nuclear import (Weis et al. 1996). Consistent with this, I found that adding 10 mM or more of IBB to interphase *Xenopus* egg extract prevented accumulation GFP-NLS into interphase sperm nuclei (**Figure 2-8A**). Next, I tested whether addition of 20 mM IBB could promote H3T3ph in interphase extract expressing GFP-xHaspin-WT. While addition of IBB successfully dissociated importin- β from GFP-xHaspin-WT, it failed to stimulate H3T3ph (**Figure 2-8B**), indicating that importin- β does not inhibit xHaspin kinase activity in interphase. While it is formally

possible that the HBIS inhibits Haspin through binding importin- α , our data below is consistent with a more direct mechanism of action.

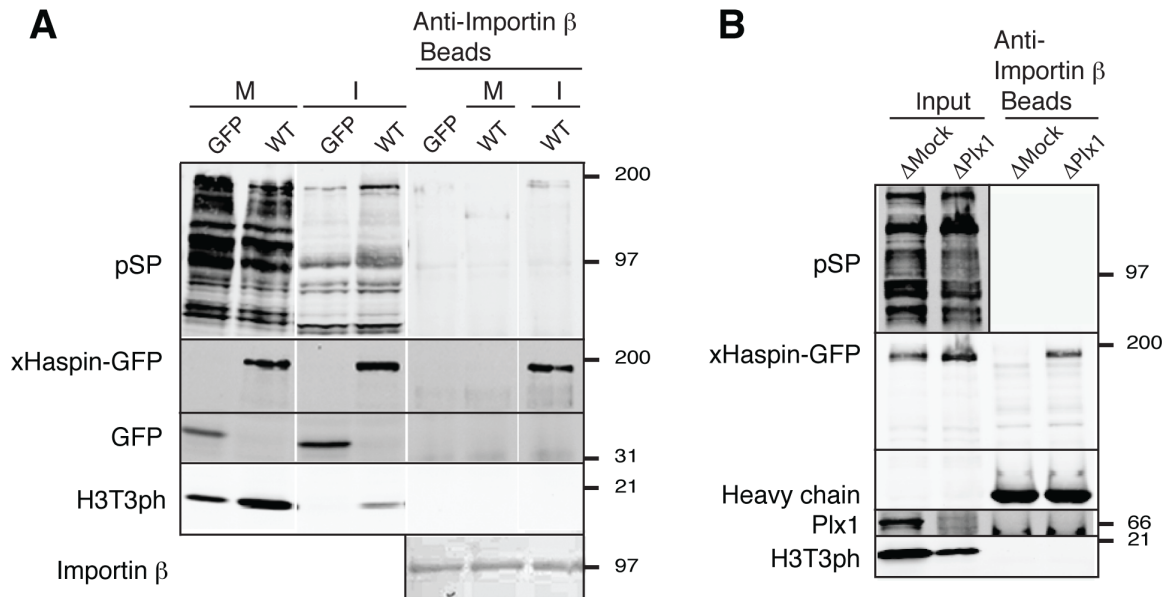


Figure 2-7: Plx1 prevents binding of Importin β to xHaspin in metaphase *Xenopus* egg extracts

A) Interphase-specific binding of xHaspin to Importin β. GFP (control) or Haspin-GFP were translated from exogenously added mRNA for 1 hour in metaphase *Xenopus* egg extracts, and then either maintained in M phase (M) or released into interphase (I) by calcium addition. Cyclohexamide was then added to stop translation. Anti-Importin β -beads were incubated with these extracts for 1hr at room temperature. Total fractions and bead fractions were analyzed by Western blot. The anti-pan phospho SP site (Cdk1 substrate) antibody was used to confirm the maintenance of cell cycle stages. The blots were probed with anti-GFP (to detect GFP and xHaspin-GFP) and anti-H3T3ph antibodies. The immunisolated Importin β was visible by Ponceau staining.

B) Binding of xHaspin to Importin β is inhibited by Plx1 in metaphase. GFP or xHaspin GFP translated in control (ΔMock) or Plx1-depleted (ΔPlx1) metaphase *Xenopus* egg extracts were subjected to immunisolation with anti-Importin b-beads.

Experiments performed by C. Ghenoiu.

Figure 2-8: Importin β binding to xHaspin does not restrict H3T3ph to interphase

A) Recombinant importin β - binding domain (IBB) was added at the indicated concentration to metaphase extract containing sperm chromatin and 1.5 μ M recombinant NLS-tagged GFP. Calcium was added at 0 min to release extract into interphase. Decondensation of sperm chromatin into interphase nuclei and import of GFP-nls, a marker for functional nuclear import, was monitored by immunofluorescence microscopy. Addition of 10 mM or more of IBB inhibited both chromatin decondensation and nuclear import.

B) Excess IBB dissociates xHaspin from Importin β in interphase extracts but does not re-activate Haspin kinase activity. Full-length xHaspin-GFP (FL), xHaspin Δ HBIS-GFP (Δ HBIS), or GFP (GFP) were translated in metaphase *Xenopus* egg extracts for 1 hour released into interphase for 30 minutes, then treated with either 20 μ M of IBB or buffer (-) for 1 hour while incubated with anti-Importin β beads. Beads were then subjected to Western blot analysis. Addition of IBB effectively inhibited binding of xHaspin-GFP and xKid to Importin β (beads), but did not promote H3T3 phosphorylation (input).

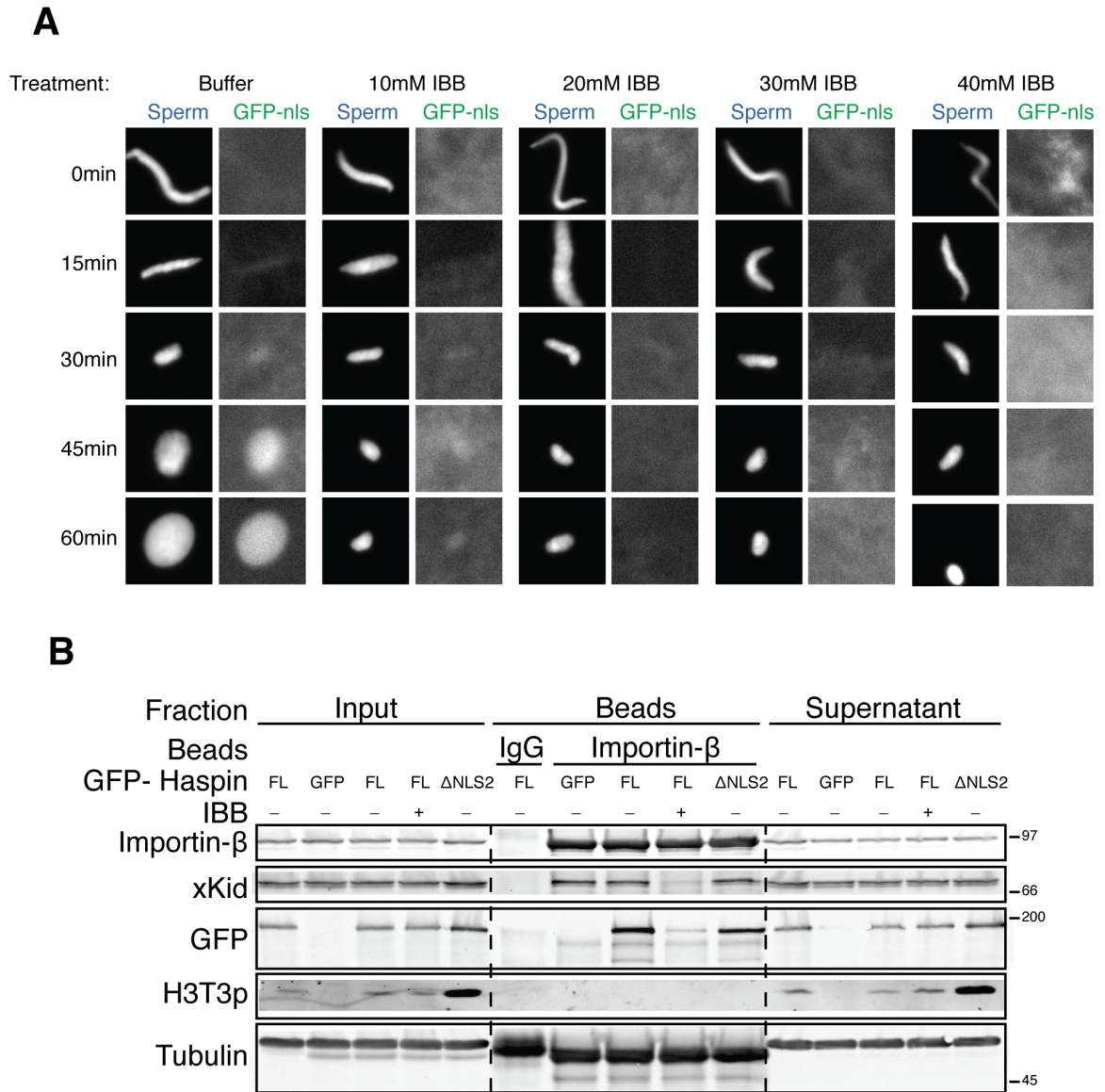


Figure 2-8: Importin β binding to xHaspin does not restrict H3T3ph to interphase

The HBIS directly inhibits Haspin kinase *in vitro*

The HBIS could act as an auto-inhibitory segment that prevents activation of xHaspin in interphase. To test this, Ghenoïu purified recombinant MBP-xHaspin N729 and MBP-xHaspin N729 Δ HBIS and performed *in vitro* kinase assays to measure the rate of H3T3ph on purified H3¹⁻⁴⁵-GST by western blot. She determined the initial velocity of H3T3 phosphorylation using a saturating amount of ATP (750 μ M) and increasing concentrations of substrate. While deletion of the HBIS had only a modest effect on K_m , it increased the V_{max} by 2-fold (**Figure 2-9A**). These changes are consistent with the HBIS being an allosteric inhibitor, which alters the rate of catalysis, rather than a competitive inhibitor, which decreases the affinity of the kinase for its substrate. Additionally, Ghenoïu found that addition of a synthetic 21aa peptide corresponding to the xHaspin HBIS reduced H3T3ph by xHaspin N729 *in vitro* (**Figure 2-9B**). A peptide containing the same amino acids but in a scrambled sequence (SCR) did not affect H3T3ph. Taken together, these data suggest that the HBIS allosterically inhibits the xHaspin kinase domain in a sequence-specific manner.

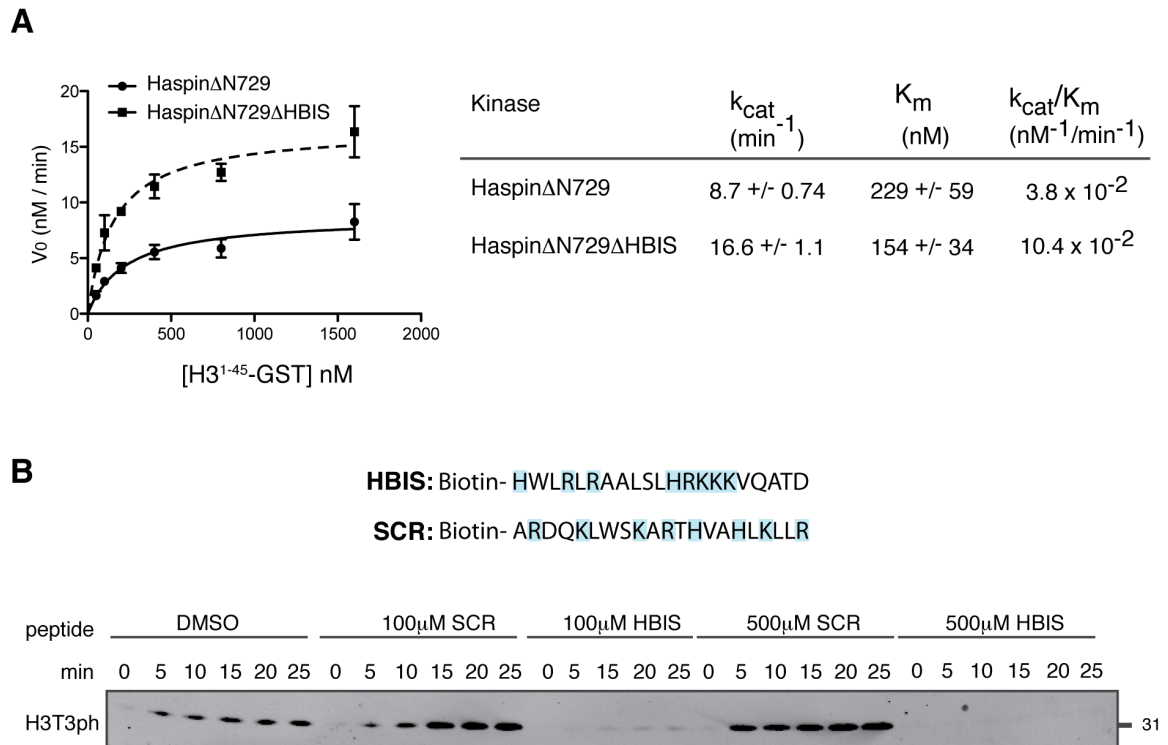


Figure 2-9: The xHaspin HBIS inhibits the kinase activity of xHaspin *in vitro*

A) Initial velocities of H3T3 phosphorylation reaction with 1 nM MBP-xHaspin- Δ N729 or MBP-xHaspin- Δ N729 Δ HBIS at various H3¹⁻⁴⁵-GST concentrations are shown (left). Triplicate data sets were fit to the Michaelis-Menten equation with the nonlinear least-square fit method. Error bars represent SEM. K_m and k_{cat} values (right) were obtained after fitting the data to the Michaelis-Menten equation.

B) Either HBIS or SCR peptides (top) were added at the indicated concentration to the *in vitro* kinase reaction with 1 nM xHaspin- Δ N729 and 200 nM H3¹⁻⁴⁵-GST. Substrate phosphorylation was detected by western blot with anti-H3T3ph (bottom). Basic residues are indicated in blue. Addition of HBIS peptide, but not the SCR peptide, inhibited xHaspin Δ N729-mediated phosphorylation of H3T3. Experiments performed by C. Ghenoiu.

The HBIS peptide is unable to inhibit Haspin in extract

Next, I attempted to inhibit H3T3ph in *Xenopus* egg extract by incubating it with varying amounts of the synthetic HBIS peptide. Addition of up to 350 μ M of HBIS peptide failed to reduce H3T3ph in metaphase extract (**Figure 2-10A**). Several other methods also failed to detect an inhibitory effect on the HBIS peptide on H3T3ph. Addition of soluble HBIS peptide didn't affect H3T3 phosphorylation kinetics as extract transitioned from interphase to mitosis (**Figure 2-10B**). It also failed to reduce H3T3ph when incubated with extract on ice, a condition that we have found lowers the steady-state level of phosphorylation (**Figure 2-10C**). Increasing the local concentration of HBIS peptide by binding it to streptavidin coated beads also failed to affect H3T3ph on ice (**Figure 2-10C**). Finally, soluble HBIS peptide failed to reduce H3T3ph when xHaspin N730 Δ HBIS was incubated with CSF or interphase extract on ice (**Figure 2-10D**). The failure of the HBIS peptide to affect H3T3ph may be due to the low abundance of xHaspin in *Xenopus* egg extract or low affinity/dynamic interaction of the HBIS peptide with the xHaspin kinase domain. While it is also possible that the peptide was degraded, proteins running at a similar size as the HBIS and SCR peptides (**Figure 2-10E**), were visualized in fixed gel slices after incubation in extract (**Figure 2-10D**). Interestingly, the HBIS peptide consistently stimulated activation of Aurora A at 22 °C (**Figure 2-10A,B**), but not 4 °C (**Figure 2-10C,D**). This is consistent with the peptide being stable enough to act as a functional NLS capable of displacing importin- α/β from spindle assembly factors,

which nucleate microtubules that can stimulate Aurora A. However, addition of HBIS peptide stimulated Aurora A activation even in the presence of nocodazole (**Figure 2-10F**), suggesting a more direct mechanism of activation.

Figure 2-10: The HBIS peptide is unable to inhibit H3T3ph in *Xenopus* egg extract

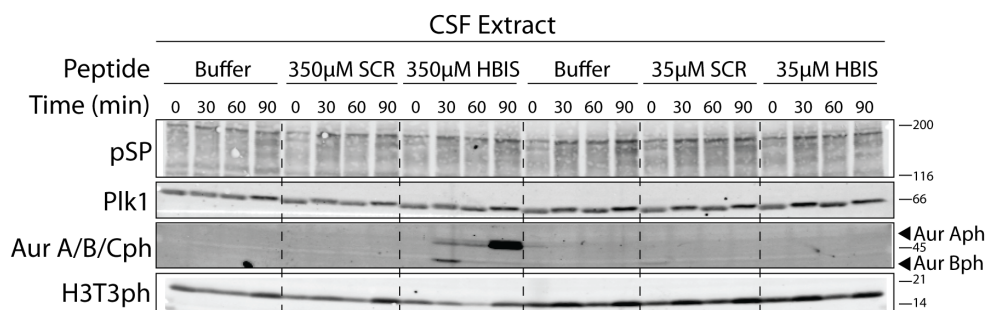
A, B, C, D, F) Western blot monitoring the level of H3T3ph under various conditions. An antibody that recognizes Cdk1-dependent serine phosphorylation (pSP) was used to monitor the cell cycle. An antibody against phosphorylation of the Aurora B/ Aurora B/ Aurora C t-loop (AurA/B/Cph) was used as a marker for activation of Aurora A (AurAph) and Aurora B (AurBph). SCR, scrambled peptide; HBIS, HBIS peptide.

A) Buffer (sperm dilution buffer), SCR-peptide or HBIS-peptide was added at the indicated concentration to metaphase *Xenopus* egg extract and incubated for 90min. A sample was taken every 30min following peptide addition. Addition of the SCR- or HBIS- peptide did not affect the level of H3T3ph.

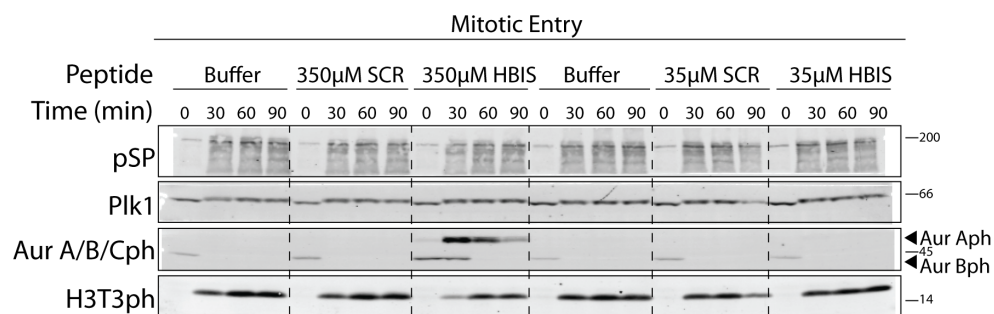
B) Buffer (sperm dilution buffer), SCR-peptide or HBIS-peptide was added at the indicated concentration to interphase *Xenopus* egg extract and mixed with fresh CSF to drive extract back into metaphase. A sample was taken every 30min following addition of fresh CSF extract. Addition of the SCR- or HBIS- peptide did not affect the kinetics of H3T3 phosphorylation during mitotic entry.

C) SCR- or HBIS- peptide alone (soluble) or prebound to beads (Beads) was added at the indicated concentration to interphase of metaphase *Xenopus* egg extract and incubated for 60min at 4°C. A sample was taken every 30min following peptide addition. Soluble peptide was added to a final concentration of 350 μ M. Beads were incubated with peptide in 10-fold excess to their binding capacity and 2mg of beads were added to extract (~15-50 μ M peptide). Addition of soluble or bead-bound peptides did not affect the level of H3T3ph in interphase of metaphase.

A



B



C

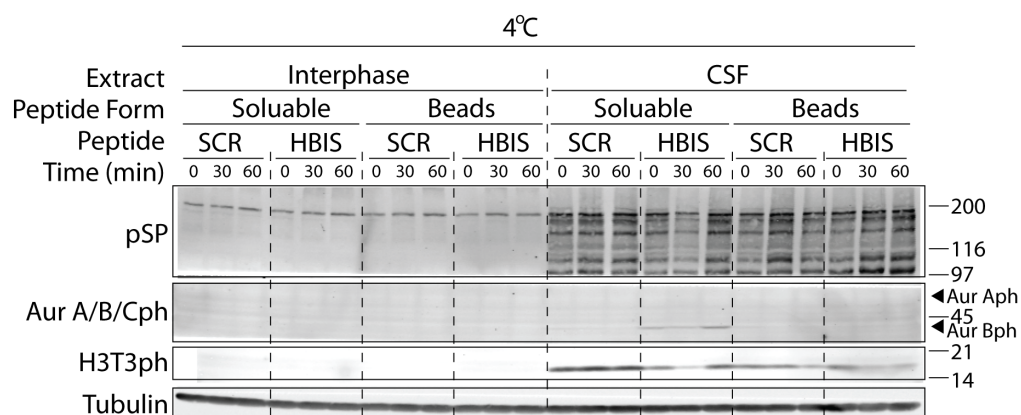


Figure 2-10 (A-C): The HBIS peptide is unable to inhibit H3T3ph in *Xenopus* egg extract

Figure 2-10 (D-F): The HBIS peptide is unable to inhibit H3T3ph in *Xenopus* egg extract

D) MBP-xHaspin kinase domain lacking the HBIS (N730 Δ HBIS) was added to interphase or CSF extract to 30 nM and incubated at 22°C for 60min. SCR-peptide or HBIS-peptide was added at the indicated concentration and incubated for 60 min at 4°C. A sample was taken every 30min following peptide addition. Ponceau staining of a nitrocellulose membrane detects protein of the appropriate size for the added peptide (see E). Addition of SCR- or HBIS-peptide did not affect the level of H3T3ph in interphase or metaphase.

E) Coomassie-stained SDS-PAGE gel of the indicated amount of either HBIS- or SCR- peptide. The SCR- peptides runs at a lower apparent molecular weight than the HBIS peptide.

F) Buffer (sperm dilution buffer), SCR-peptide or HBIS-peptide was added at the indicated concentration to metaphase *Xenopus* egg extract preincubated for 30min with either DMSO or nocodazole (Noc.). A sample was taken every 30min for 90min following addition peptide addition. Activation of Aurora A, as monitored by Aurora A/B/Cph, was unaffected by addition of nocodazole.

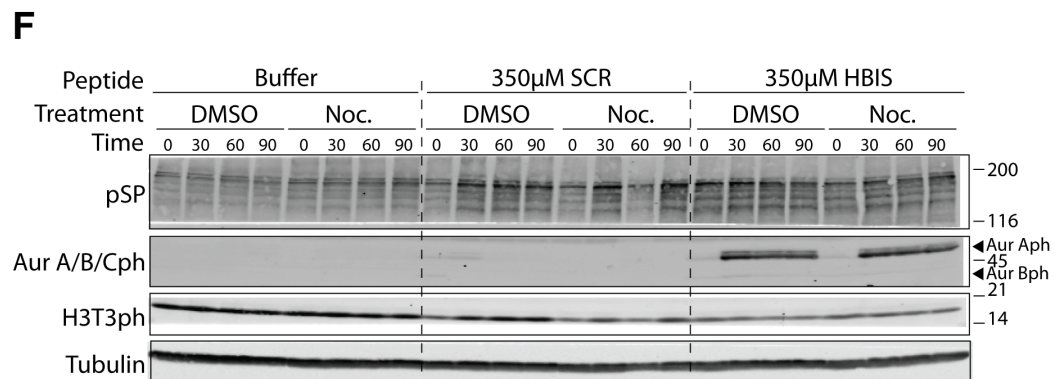
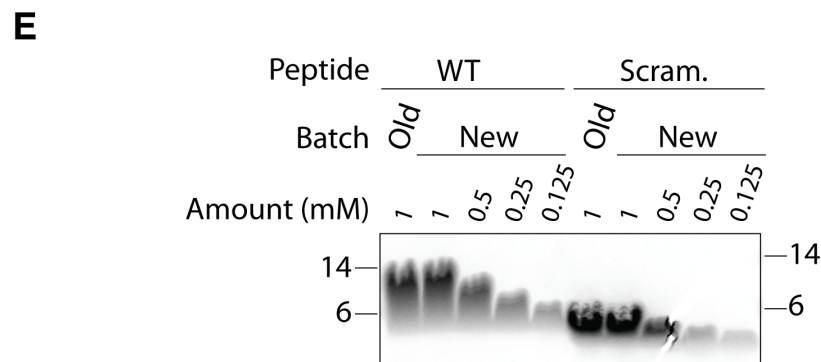
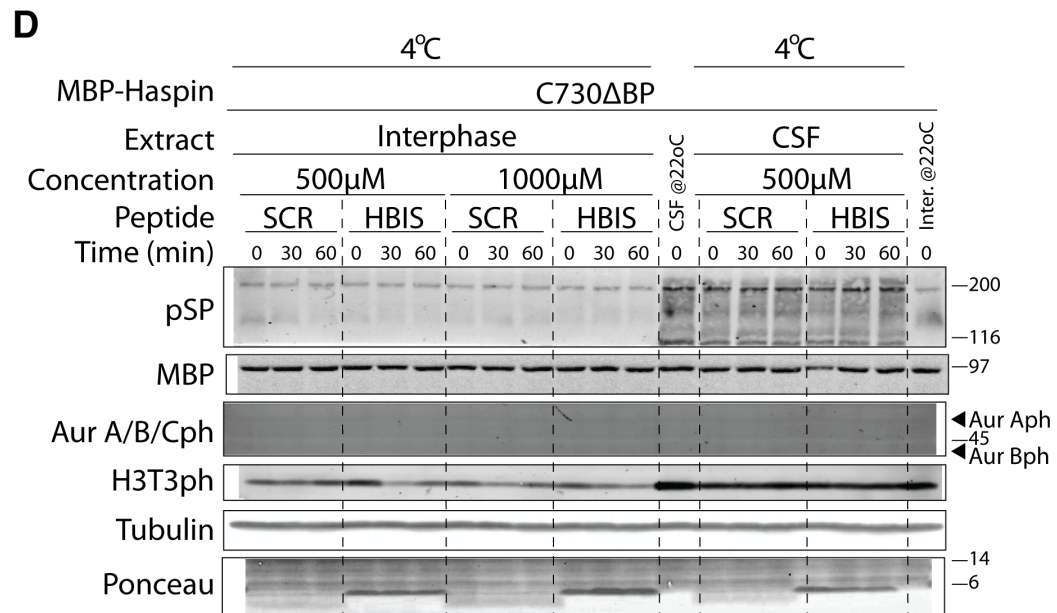


Figure 2-10 (D-F): The HBIS peptide is unable to inhibit H3T3ph in *Xenopus* egg extract

The HBIS binds the Haspin kinase domain in a Plx1-dependent manner

xHaspin is activated by Plx1-dependent phosphorylation and inhibition by the HBIS, but are these mechanisms connected? The HBIS contains S753, which we identified as phosphorylated in a T206-dependent manner in full-length xHaspin. Ghenoiu demonstrated that mutating this residue to alanine resulted in only a minor decrease in H3T3ph in mitosis, suggesting that while Plx1-dependent phosphorylation of S753 may antagonize the inhibitory affect of the HBIS, it is insufficient to completely relieve inhibition.

Given that multisite phosphorylation of xHaspin is required for robust H3T3ph in mitosis, it is likely that phosphorylation of additional sites antagonize HBIS-mediated inhibition. We hypothesized that the negative charge from Plx1-dependent phosphorylation of the xHaspin N terminus could interact with the basic patch in the HBIS, displacing it from the Haspin kinase domain to relieve inhibition in mitosis. To test this, I first determined how the HBIS peptide interacts with full-length xHaspin. Full-length ³⁵S-labeled xHaspin-WT, T206A, ΔHBIS, or T206A ΔHBIS were incubated in metaphase extract containing magnetic beads coupled to either HBIS or SCR peptides (**Figure 2-11A**). While xHaspin-WT co-purified with both the SCR and HBIS beads, the T206A mutant bound poorly to both. Binding of xHaspin-WT was dependent on the presence of peptide, as beads alone did not purify any xHaspin construct. Thus, this result suggests that the interaction of the HBIS with full-length xHaspin is dependent on T206-mediated phosphorylation and is mostly independent of peptide sequence. While

xHaspin Δ HBIS also bound both types of peptide beads, xHaspin T206A Δ HBIS showed robust binding to only the HBIS beads. Given that xHaspin T206A alone showed weak binding to either peptide, this suggests that deletion of the endogenous xHaspin HBIS opened a sequence-specific HBIS binding site. These results are consistent with the HBIS binding xHaspin through two distinct mechanisms: the first is phosphorylation-dependent while the second is sequence-dependent.

To determine if these modes of binding are supported by different regions of xHaspin, I repeated the peptide binding assay using xHaspin N terminus with or without T206 (xHaspin N730, xHaspin N730 T206A) and xHaspin kinase domain with or without the HBIS (xHaspin Δ N729, xHaspin Δ N729 Δ HBIS) (**Figure 2-11B**). While the xHaspin kinase domain showed weak binding to HBIS beads, deletion of the endogenous HBIS greatly enhanced this interaction, consistent with the sequence dependent mode of interaction. Conversely, while the xHaspin N terminus bound equally to both peptides, introduction of T206A abrogated binding, consistent with the phosphorylation-dependent mode of interaction. Depleting Plx1 activity also diminished binding of the N terminus of HBIS and SCR beads (**Figure 2-11C**), reinforcing the idea that Plx1-dependent phosphorylation mediates the interaction between the N terminus and the HBIS.

Figure 2-11: Plx1-mediated phosphorylation of the xHaspin N terminus regulates HBIS binding to the xHaspin N terminus and kinase domain

A) ^{35}S -labeled full-length xHaspin WT, a T206A mutant (T206A), a mutant lacking the HBIS (ΔHBIS), or a construct with both mutations (T206A ΔHBIS) were preincubated in metaphase *Xenopus* egg extract. This extract was then incubated for 60 min with uncoupled control beads or beads coated in the HBIS or SCR peptide. Input and bead fractions (treated with phosphatase in order to reduce the mobility shifts) were analyzed by autoradiography. SCR beads interact with xHaspin dependent on T206. HBIS beads interact with xHaspin dependent on T206 and the presence of an endogenous HBIS.

B) ^{35}S -labeled xHaspin N terminus (N730), the N terminus with a T206A mutation (N730^{T206A}), xHaspin kinase domain (ΔN729), or a kinase domain mutant without the HBIS ($\Delta\text{N729}^{\Delta\text{HBIS}}$) were processed as in (A). SCR and HBIS beads interact with the xHaspin N terminus dependent on T206. Unlike SCR beads however, the HBIS also interacts with the xHaspin kinase domain, dependent on the presence of an endogenous HBIS.

C) Plx1 was inhibited by immunodepletion (ΔPlx1) and by adding the Plx1 inhibitor BI2536 (BI) to metaphase *Xenopus* egg extracts. Extract that was mock depleted (ΔMock) is shown as a control (left). ^{35}S -xHaspin N730 (WT) or xHaspin N730T206A (T206A) was incubated with these extracts, as well as SCR- or HBIS- coated peptide beads. Autoradiographs are of pulldowns of peptide-coated beads treated with lambda phosphatase to reduce mobility shift and visualize ^{35}S -labeled protein co-purification (pulldown + λ). Relative intensity co-purified xHaspin protein in each lane was calculated by integrating the total intensity of ^{35}S protein in each lane, and dividing it by the total intensity of xHaspin-WT co-purifying with SCR-beads in ΔMock extract. Binding of the HBIS and SCR beads to the xHaspin N terminus depends on Plx1-dependent phosphorylation.

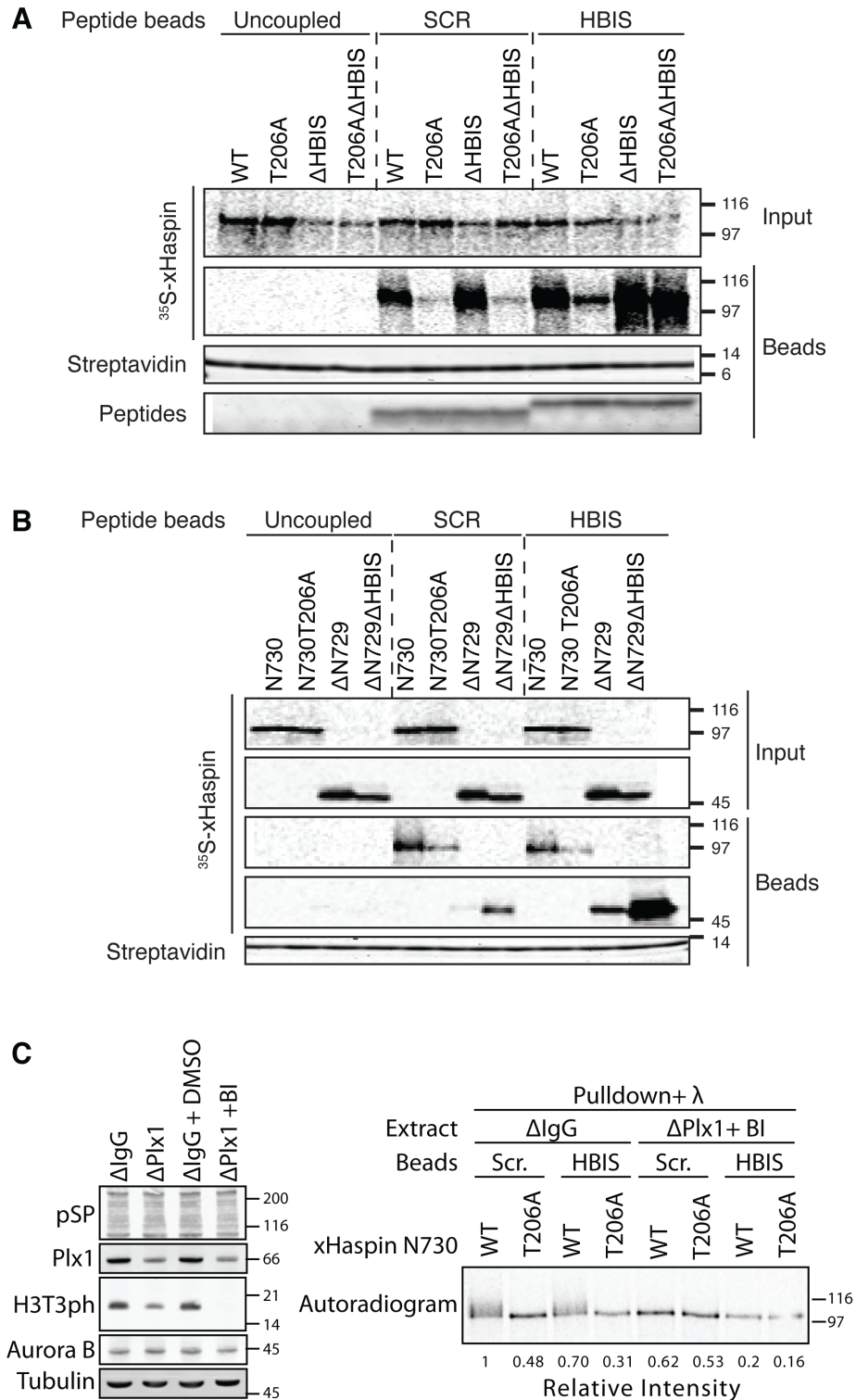


Figure 2-11: Plx1-mediated phosphorylation of the xHaspin N terminus regulates HBIS binding to the xHaspin N terminus and kinase domain

Next, I wanted to identify regions of the xHaspin N terminus important for the phosphorylation-dependent interaction with the HBIS. While xHaspin N730 co-purified equally with HBIS- and SCR-beads as before, a shorter construct containing only the first 530 residues of xHaspin (xHaspin N530) did not, suggesting that residues from 530-730 mediate the phosphorylation-dependent interaction with the HBIS (**Figure 2-12A**). To more precisely map the interaction site, I generated a series of four partially overlapping scanning deletions from residues 530 to 730 within the xHaspin N730 construct (**Figure 2-12B**). For simplicity, I performed the peptide-binding assay with the SCR-coated beads to look specifically at the charge-dependent interaction of the HBIS with the xHaspin N terminus. While the three deletions spanning residue 530-684 did not attenuate binding with SCR-beads, the final deletion from 675-730 bound as weakly as xHaspin N530, suggesting this may be a 'critical region' for phosphorylation-dependent binding (**Figure 2-12C**). Failure to bind was not due to a lack of phosphorylation on the xHaspin fragment, as all truncation constructs demonstrated a phosphorylation-dependent mobility shift (**Figure 2-12D**). The region from residue 675-740 is just upstream of the HBIS and contains 15 serine/threonine residues, including 7 that fit the canonical Plk1 consensus motif. Our MS analysis of full-length xHaspin identified T675 as an hHaspin auto-phosphorylation site; however, T675 was also deleted in xHaspin N606-684, suggesting it is not sufficient for binding to SCR beads. Peptide coverage outside the first 4 residues of the critical region was low, with over 75% of the region not

registering a single peptide by MS. Taken together, this suggests that the phosphorylation-dependent interaction between the xHaspin N terminus and HBIS may be mediated by as yet unidentified phosphorylations proximal to the HBIS.

Figure 2-12: xHaspin residues 675-730 are critical for the xHaspin N terminus to bind the HBIS

A) ^{35}S -labeled xHaspin N terminus cooresponding to residues 1-530 (N530) or 1-730 (N730) containing residue T206 (T) or T206A (A) were incubated in metaphase *Xenopus* egg extracts for 60 min with beads coated in the HBIS or SCR peptide. Autoradigograms of the input and bead fractions (Pulldown; treated with phosphatase to reduce mobility shift) are shown. xHaspin N730, but not xHaspin N530, co-purifies with peptide-coated beads

B) Diagram of the xHaspin N terminus deletion mutants in C and D (top) and a zoom in of xHaspin residues 675-730 (bottom) indicating consensus sites for Plk1 (red).

C) ^{35}S -xHaspin N730 (WT), xHaspin N730 T206A (T206A), or xHaspin N730 containing various deletions, was incubated for 60min in extract containing beads coated in SCR-peptide. Autoradiographs are of crude extracts (Input) or SCR-bead pulldowns (Pulldown), both treated with lambda phosphatase to reduce the mobility shift and visualize the abundance of co-purifying ^{35}S -xHaspin N-terminal constructs. Relative intensity was calculated by integrating the total intensity of ^{35}S protein in each lane and dividing it by the total intensity of xHaspin N730 (WT). xHaspin residues 675-730 mediate binding of xHaspin N730 to SCR-beads.

D) Autoradiogram of samples from C, visualizing the abundance of ^{35}S -xHaspin proteins in input extract (Input), extract following removal of SCR-beads (Soup) and input extract treated with lambda phosphatase to reduce the mobility shift and visualize protein abundance (Input + λ , corresponds to 'Input' in C).

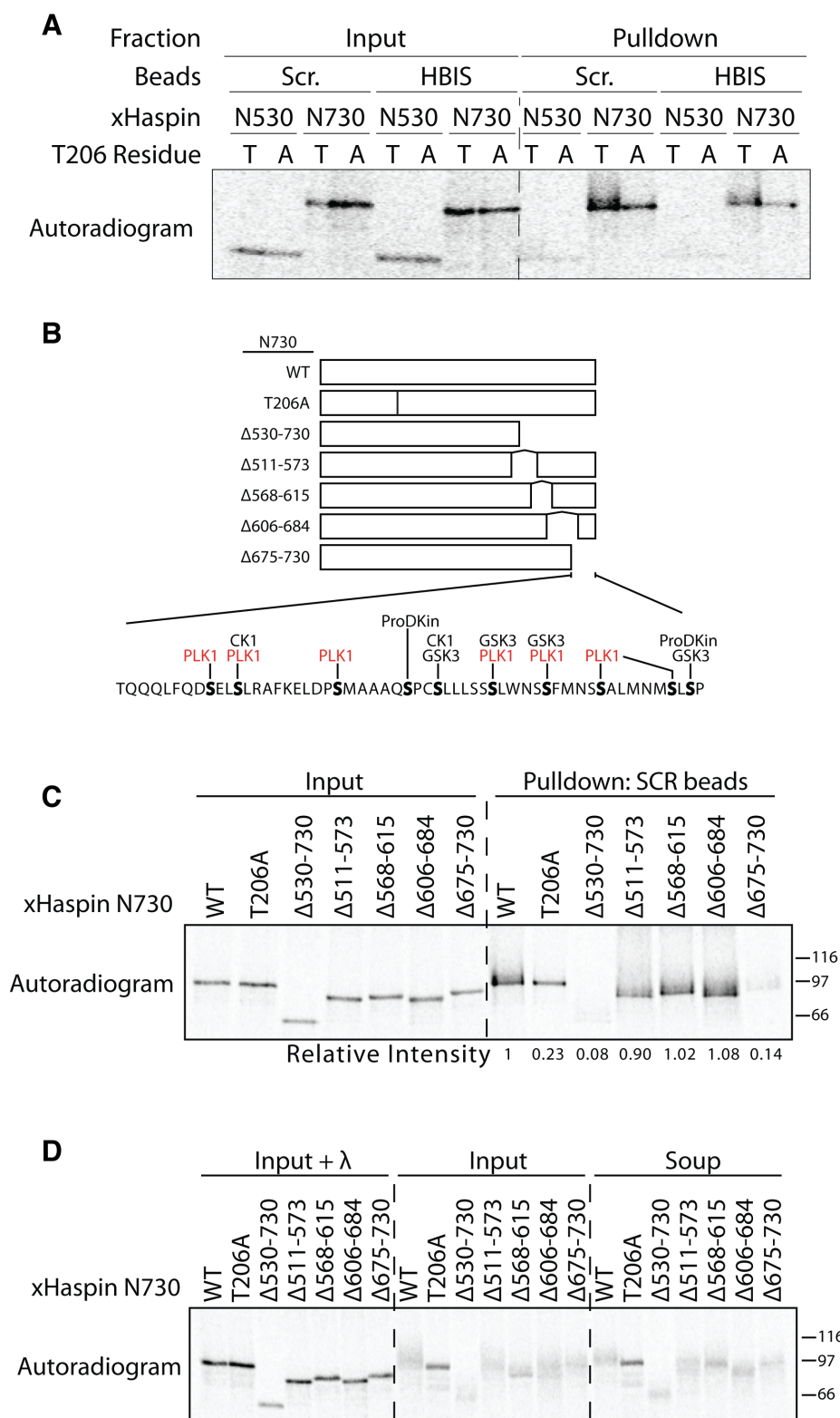


Figure 2-12: xHaspin residues 675-730 are critical for the xHaspin N terminus to bind the HBIS

Next, I sought to identify the binding site for the HBIS to the xHaspin kinase domain. Given that the HBIS contains a basic patch, we hypothesized that it may bind a highly conserved acidic triplet (1056-DED-1058) in the xHaspin kinase domain (**Figure 2-13A**). Mutating two or three of these acidic residues to alanine to negate their charge (xHaspin DAA, xHaspin AAA) showed a mild reduction in binding to the HBIS-peptide, suggesting this acidic region may contribute to HBIS binding (**Figure 2-13B**). However, neither xHaspin DAA nor AAA stimulated H3T3ph in interphase, indicating these constructs were still subject to HBIS-mediated inhibition (**Figure 2-13C**). Lack of H3T3ph was not due to xHaspin kinase inactivation, as deleting the HBIS in xHaspin DAA or AAA stimulated robust H3T3ph in interphase. Thus, while the acidic triplet in the xHaspin kinase domain may contribute to HBIS binding, it is not the major determinant.

In summary, the HBIS can bind the xHaspin kinase domain or the xHaspin N terminus after Plx1-dependent phosphorylation. Without Plx1, the majority of xHaspin exists in a conformation where the HBIS is bound to the kinase domain, thus preventing interaction with exogenous HBIS peptide. Deleting the endogenous HBIS liberates this binding site, allowing efficient interaction with HBIS beads even in the absence of Plx1-dependent phosphorylation. Based on these results, we propose that the HBIS binds the xHaspin kinase domain in a sequence-dependent manner to inhibit its activation in interphase. Upon entry into mitosis, Plx1-dependent multisite phosphorylation of the xHaspin N terminus

introduces negative charges that interact with and displace the HBIS from the kinase domain, promoting H3T3ph in mitosis. In support of Plx1-dependent phosphorylation directly antagonizing the HBIS, Ghenoiu demonstrated that Cdk1/Plk1-dependent phosphorylation of full-length hHaspin *in vitro* stimulated phosphorylation of an H3¹⁻⁴⁵-GST substrate.

Figure 2-13: The conserved acidic triplet in the xHaspin kinase domain does not mediate interaction with the HBIS

A) Multisequence alignment of Haspin proteins, focusing on residues adjacent to the acidic triplet (Xenopus residues 1056-1058). Residue number is indicated at the beginning and ending of the peptide. Acidic residues (red), Basic residues (blue). The Acidic triplet is highly conserved in animal homologs of Haspin.

Xenopus, laevis; Human, *Homo sapien*; Drosophila, *Drosophila melanogaster*; Mouse, *Mus musculus*; Chicken, *Gallus galulus*; Zebrafish, *Danio rerio*; Fission yeast, *Schizosaccharomyces pombe*; Arabidopsis, *Arabidopsis thaliana*.

B) ³⁵S-labeled full-length xHaspin (FL) or full-length xHaspin lacking the HBIS (ΔHBIS) containing an intact acidic triplet (DEE) or mutation of residues in the triplet to alanine (DAA, AAA) were incubated in metaphase *Xenopus* egg extracts for 60 min with beads coated in the HBIS or SCR peptide. Autoradigograms of the input and bead fractions (Pulldown), both treated with phosphatase to reduce mobility shift, are shown. Mutation of the acidic triplet does not affect the amount of ³⁵S-labeled xHaspin co-purifying with SCR- or HBIS-coated beads.

C) The level of H3T3ph in interphase extract containing ³⁵S-labeled constructs from B was measured after addition of the protein (T0) and after a 60 min incubation (T60). An antibody against Cdk1-phosphorylated serines and threonines (Pan Cdk1 S/Tph) was used as a cell cycle marker. Mutating the acidic triplet does not stimulate H3T3ph in interphase.

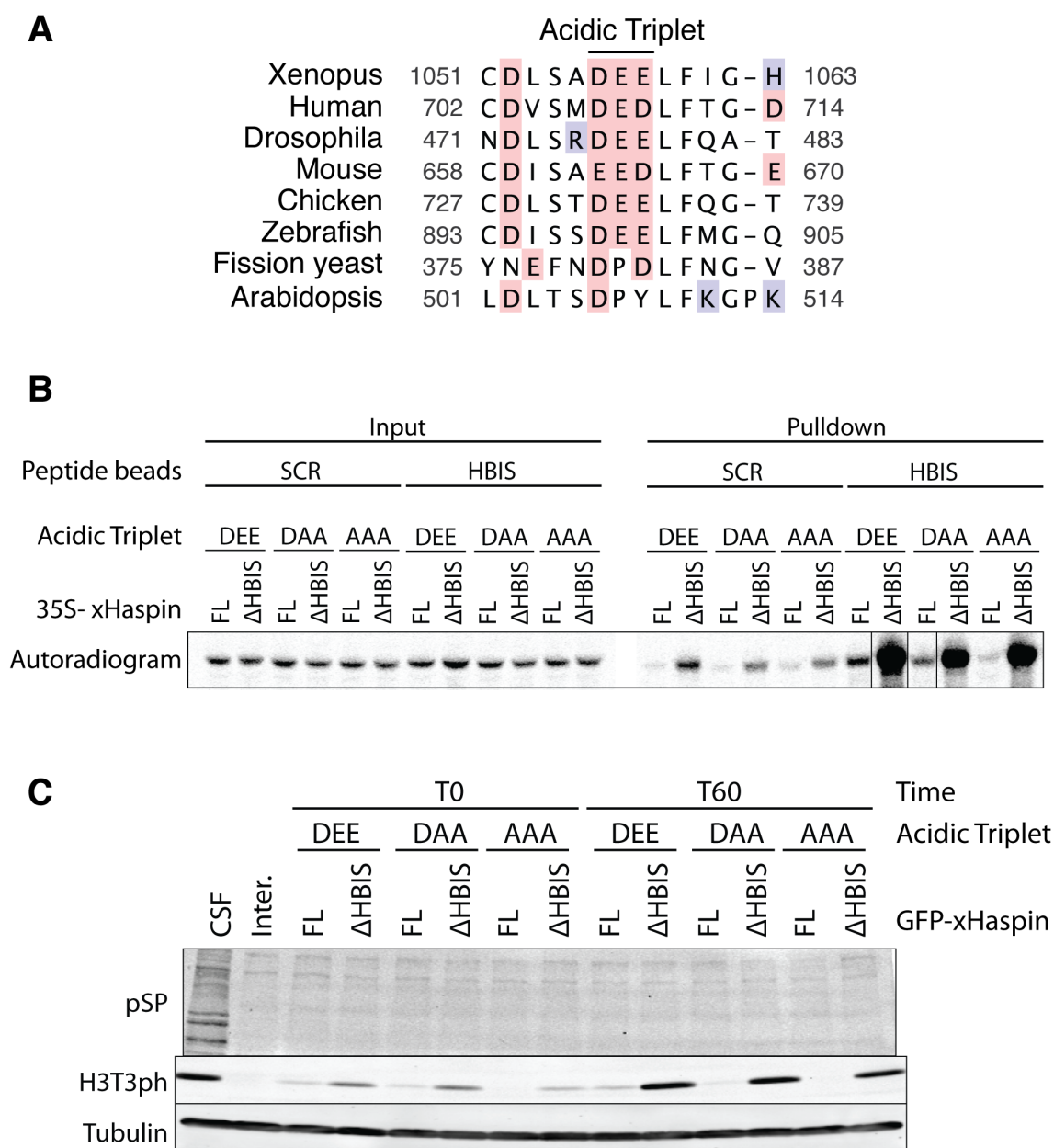


Figure 2-13: The conserved acidic triplet in the xHaspin kinase domain does not mediate interaction with the HBIS

Plk1 and Aurora B activate Haspin during mitosis in human cells

To determine whether Polo-dependent Haspin activation is conserved in human cells, I synchronized RPE1-hTERT and HeLa cells in mitosis with a thymidine-nocodazole block, then treated them with the Plk1-inhibitor BI2536 and monitored H3T3ph by western blot. I observed a time-dependent decrease in H3T3ph, consistent with Plk1 supporting Haspin activation in human cells **(Figure 2-14)**.

It was previously reported that Aurora B-dependent phosphorylation of human Haspin also promotes H3T3ph during mitosis (F. Wang et al. 2011). To assess how Plk1 and Aurora B may coordinate Haspin activation, I synchronized RPE1-hTERT and HeLa cells in mitosis and treated them with either DMSO, BI2536, the Aurora B inhibitor ZM447439, or both kinase inhibitors simultaneously **(Figure 2-15)**. Plk1-inhibition dramatically reduced H3T3ph without affecting phosphorylation of the Aurora B substrate H3S10. Inhibition of Aurora B reduced both H3S10p and H3T3ph, consistent with previous reports. Simultaneous inhibition of Plk1 and Aurora B had an additive effect and abolished H3T3ph, indicating that unlike in *Xenopus*, both kinases contribute to Haspin activation during mitosis in human cells.

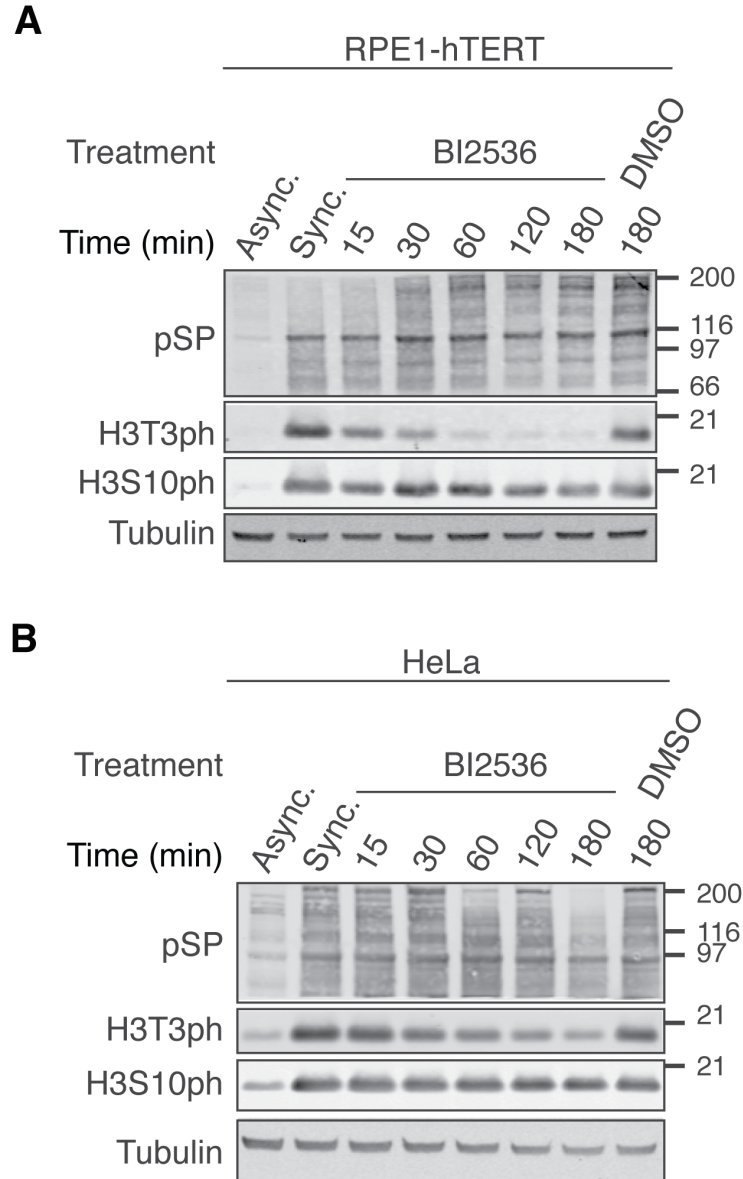


Figure 2-14: Plk1 is required for H3T3ph in mitosis in human cells

A, B) RPE1-hTERT (left) or HeLa cells (right) were synchronized in mitosis by a thymidine-nocodazole block, collected by mitotic shake-off, placed in media containing nocodazole and treated with either DMSO or a Plk1 inhibitor (BI2536). Samples were then collected at the indicated time points (in minutes) by mitotic shake-off and levels of H3T3ph were monitored by Western blot. While levels of H3S10ph remained constant, Plk1 inhibition resulted in a gradual decrease in H3T3ph levels beginning 15-30 minutes after treatment.

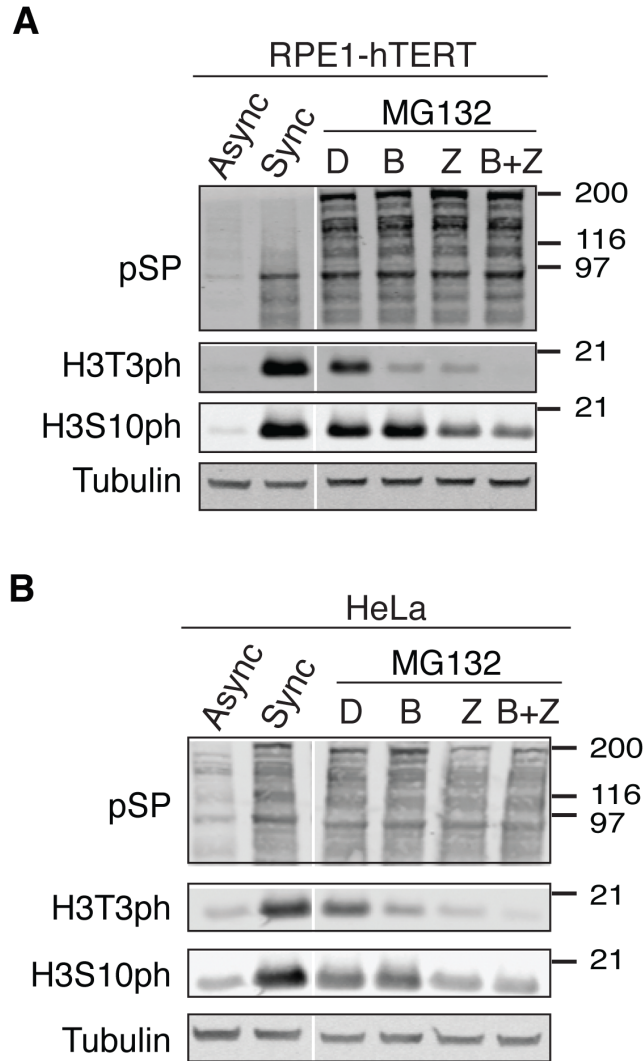


Figure 2-15: Aurora B and Plk1 stimulate H3T3ph in mitosis in human cells

A, B) RPE1-hTERT (left) or HeLa (right) cells were synchronized in mitosis with a thymidine-nocodazole block followed by mitotic shake-off. Mitotic cells were placed in media containing nocodazole and the proteasome inhibitor MG132, which prevents mitotic slippage. Cells were then treated with either 100 nM of the Plk1 inhibitor BI2536 (B), 2 μ M of the Aurora B inhibitor ZM447439 (Z), both inhibitors (B+Z), or DMSO (D). Western blots using indicated antibodies are shown. Inhibition of either Plk1 or Aurora B reduces the level of H3T3ph and show an additive affect on H3T3ph levels when added together.

Next, I assessed the impact of Plk1 and Aurora B inhibition on the distribution and abundance of H3T3ph on mitotic chromatin using immunofluorescence (**Figure 2-16**). While H3T3ph was broadly distributed on chromatin with enrichment near the centromere in control cells, inhibition of Plk1 or Aurora B lead to a dramatic reduction in H3T3ph. Simultaneous inhibition of both kinases further reduced H3T3ph to background levels. Additionally, we monitored the distribution of Aurora B on chromatin. Consistent with published studies, we found that inhibition of Plk1 (Salimian et al. 2011) or Aurora B (F. Wang et al. 2011) individually or in combination reduced the abundance of Aurora B at the centromere. Together, this data indicates that both kinases support Haspin activation and CPC localization during mitosis.

Figure 2-16: Aurora B and Plk1 independently promote H3T3ph on mitotic chromatin and Aurora B localization to the centromere in human cells

A, B) RPE1-hTERT cells were synchronized in mitosis for 3 hr with nocodazole, collected by mitotic shake off, and transferred to media containing MG132 and nocodazole for 1 hr. Then, cells were treated with either DMSO, BI2536 (BI), ZM447439 (ZM), or both inhibitors (BI/ZM) for 3 hr, collected by mitotic shake off, and processed for indirect immunofluorescence with the indicated antibodies. Inhibiting the kinase activity of Plx1 or Aurora B leads to a reduction in H3T3ph and Aurora B localization at the centromere.

A) Representative maximum projections. Scale bar, 5 μ m.

B) Integrated intensity was calculated in MetaMorph on deconvolved images and standardized to the average intensity of the control. Mean and SEM are shown. Statistics were calculated using a two-tailed Mann-Whitney test. *** $p \leq 0.001$; ** $p \leq 0.01$; * $p \leq 0.05$.

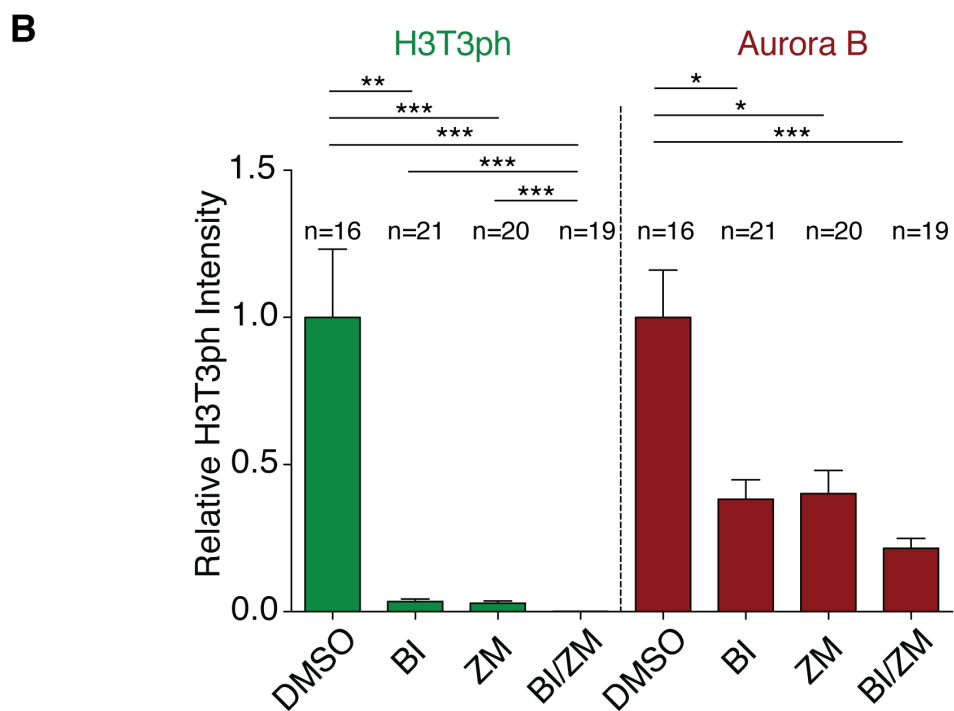
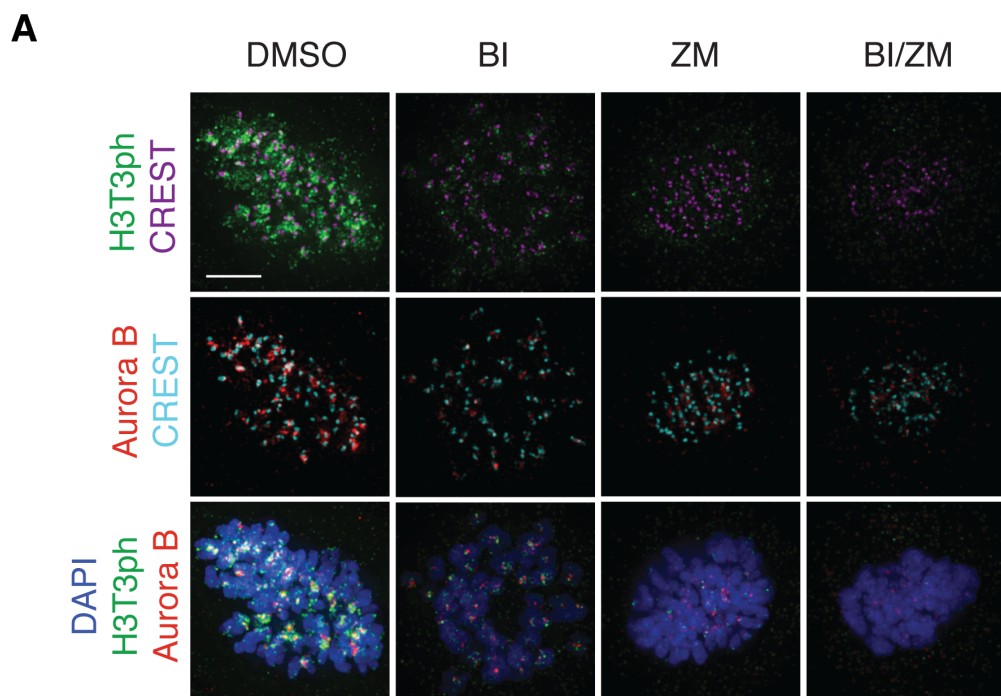


Figure 2-16: Aurora B and Plk1 independently promote H3T3ph on mitotic chromatin and Aurora B localization to the centromere in human cells

Human Haspin is regulated by Polo-dependent activation and HBIS-dependent inhibition

To evaluate the conservation of Polo-dependent Haspin activation in human cells, I used the T-REx tissue culture system to generate inducible, single-site integrations of LAP-tagged hHaspin-WT or hHaspin T128A (the equivalent residue to xHaspin T206) in HeLa and DLD1 cells. I induced expression of these constructs by addition of doxycycline and synchronized cells in S-phase or mitosis (**Figure 2-17**). hHaspin-WT demonstrated a large mobility shift in mitosis relative to S-phase. Treatment with either BI2536 or ZM447439 reduced this mobility shift as well as the level of H3T3ph, consistent with Plk1- and Aurora B-mediated phosphorylation of hHaspin, respectively. Simultaneous treatment with both inhibitors reduced the mobility shift even further, suggesting these kinases may phosphorylate distinct sites on hHaspin. Cells expressing hHaspin T128A demonstrated a reduction in mobility shift and H3T3ph relative to hHaspin-WT; however, they were insensitive to BI2536 treatment, consistent with T128 supporting Plk1-dependent activation of hHaspin. Treating hHaspin T128A with ZM447439 reduced the hHaspin mobility shift and levels of H3T3ph to levels similar to hHaspin-WT treated with both ZM447439 and BI2536. These results are consistent with T128 supporting Plx1-dependent activation of hHaspin independent of Aurora B-mediated activation.

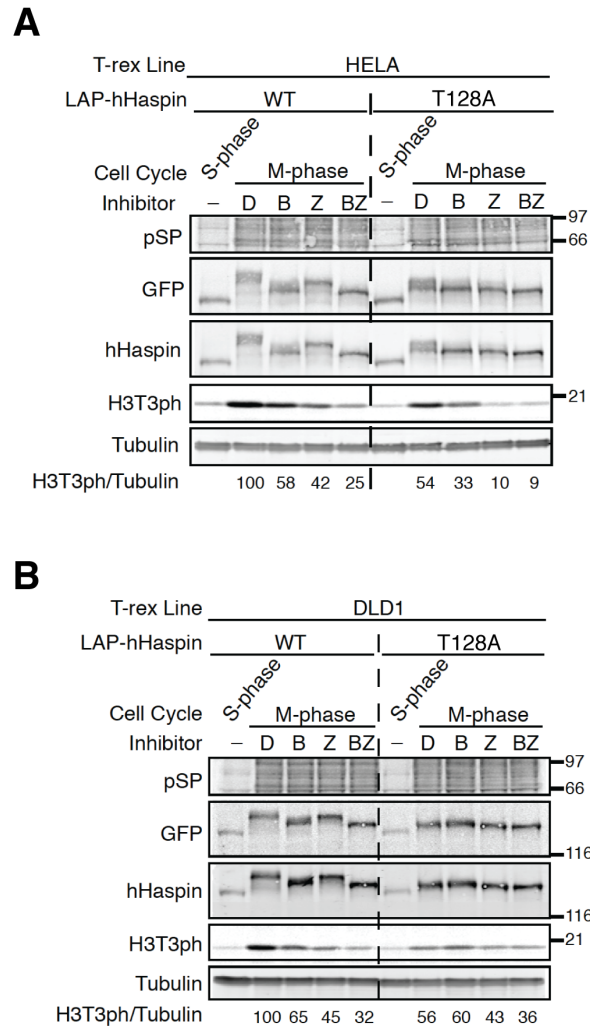
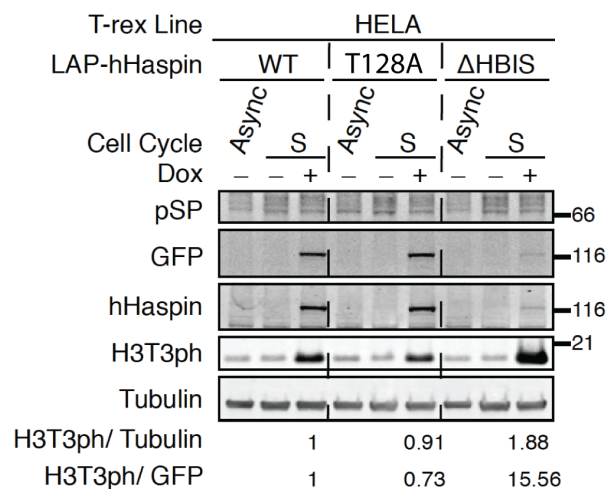


Figure 2-17: hHaspin T128 supports the majority of Plk1-mediated hHaspin mobility shift and Plk1-dependent H3T3ph

A, B) HeLa (A) and DLD1 (B) T-REx Flp-In cell lines expressing either LAP-hHaspin (WT) or LAP-hHaspin^{T128A} were synchronized in mitosis with nocodazole for 16 hr, then collected by mitotic shake off and transferred to media containing MG132 and nocodazole for 1 hr. Cells were then treated with either DMSO (D), the Plk1 inhibitor BI2536 (B), the Aurora B inhibitor ZM447439 (Z) or both inhibitors simultaneously (BZ) for 3 hrs. The ratio of H3T3ph/tubulin is reported relative to LAP-hHaspin (WT) incubated with DMSO. LAP-hHaspin was detected by anti-GFP. hHaspin T128 is required for the Plk1-mediated mobility shift of hHaspin and stimulation of H3T3ph.

To demonstrate that the HBIS auto-inhibits hHaspin in interphase, we synchronized DLD1 cells in S-phase and compared the level of H3T3ph in cells expressing hHaspin-WT, T128A or Δ HBIS (deletion of KKKIV in hHaspin, homologous to the basic patch in xHaspin) (**Figure 2-18**). Deletion of the HBIS reproducibly lowered hHaspin protein levels compared to either WT or T128A for an unknown reason. Despite this reduced abundance, hHaspin Δ HBIS supported significantly higher levels of H3T3ph in interphase than either construct, indicating that the auto-inhibitory function of the HBIS is conserved in human cells.

A



B

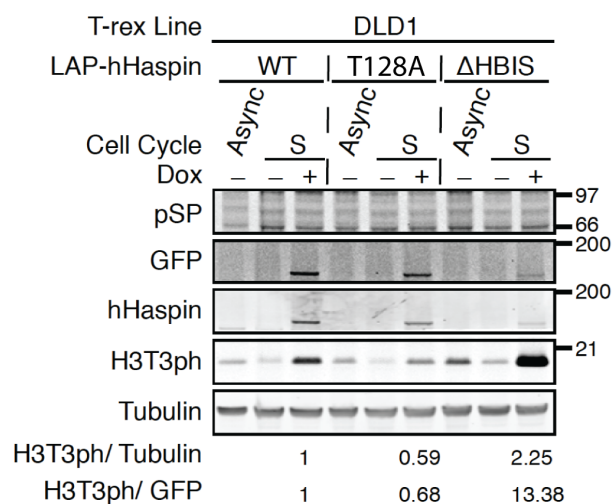


Figure 2-18: The hHaspin HBIS antagonizes H3T3ph in interphase

A, B) HeLa (A) and DLD1 (B) T-REx Flp-In cell lines expressing LAP-hHaspin (WT), LAP-hHaspin^{T128A}, or LAP-hHaspin ^{Δ HBIS} were synchronized in S phase by double thymidine block and processed for western blot analysis. The ratios of H3T3ph/GFP and H3T3ph/tubulin are reported relative to LAP-hHaspin (WT). Deletion of the HBIS stimulates H3T3ph in interphase.

2.3 Discussion

A model for coupling Haspin activation to the cell cycle

Timely recruitment of the CPC to chromatin is critical for cell division. During early mitosis, the CPC must be recruited to the centromere to support error correction and the SAC. Likewise, the CPC must be removed from chromatin following anaphase onset to allow proper chromosome decondensation and nuclear envelope reformation (Ramadan et al. 2007; Kelly et al. 2010). Cell cycle-dependent phosphorylation of H3T3 is one mechanism to coordinate CPC localization with mitotic progression. H3T3 is phosphorylated by Haspin during mitosis (Dai et al. 2005) and directly recruits the CPC to the centromere through Survivin (Jeyaprakash et al. 2011; Kelly et al. 2010; Yamagishi et al. 2010; F. Wang et al. 2010). Conversely, H3T3 is dephosphorylated by Repo-man/PP1 at anaphase onset, which is required to remove the CPC from chromatin (Qian et al. 2011). However, whether additional mechanisms exist to regulate cell cycle dependent phosphorylation of H3T3 is unclear.

Our results indicate that Haspin kinase activity is regulated with the cell cycle to promote robust H3T3ph specifically during mitosis (**Figure 2-19**). During interphase, the HBIS binds the xHaspin kinase domain in a sequence-dependent manner to inhibit its activation. Upon entry into mitosis, high levels of Cdk1-Cyclin B activity promote phosphorylation of xHaspin T206, creating a docking site for recruitment of Plx1/Plk1. Polo-dependent multisite phosphorylation of the

xHaspin N terminus promotes its binding to the HBIS, displacing the HBIS from the xHaspin kinase domain, which activates Haspin kinase activity and promotes H3T3ph during mitosis.

We also uncovered an additional layer of regulation in human cells. The BIR domain of Survivin directly binds H3T3ph and recruits the CPC to the inner centromere (Jeyaprakash et al. 2011; Kelly et al. 2010; Yamagishi et al. 2010; F. Wang et al. 2010). Local enrichment of the CPC promotes activation of Aurora B (Kelly et al. 2007), likely by auto-phosphorylation in trans (Sessa et al. 2005). Once active, at least two positive feedback loops can form. First, in line with previous work (F. Wang et al. 2011), we show that Aurora B-dependent phosphorylation of hHaspin supports H3T3ph. Second, Aurora B phosphorylates the activation loop of Plk1 to promote its kinase activity (Carmena, Pinson, et al. 2012) and thus Plk1-dependent phosphorylation of hHaspin. Together, this positive feedback promotes robust localization of the CPC during mitosis. At anaphase onset, the decrease in Cdk1-Cyclin B activity promotes HBIS-mediated inhibition of Haspin kinase activity, while the recruitment of Repo-man/PP1 to chromatin leads to dephosphorylation of H3T3 and transfer of the CPC to the spindle midzone.

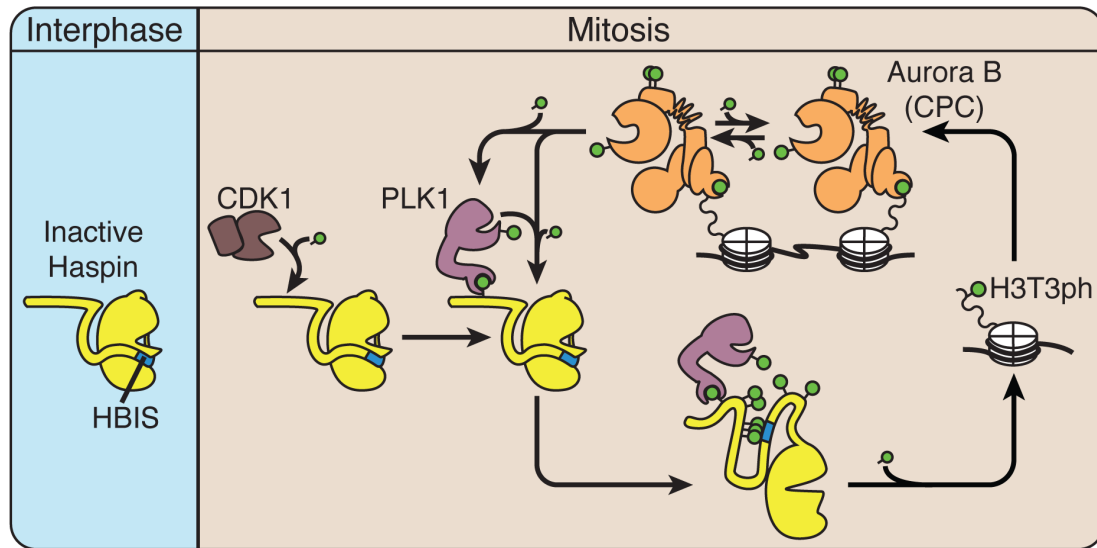


Figure 2-19: Molecular mechanism coupling activation of Haspin to the cell cycle

A schematic of the activation mechanism of Haspin and the chromatin-associated feedback loop. During interphase, Haspin kinase activity is inhibited by the HBIS. Upon entry into mitosis, activated Cdk1 phosphorylates the N terminus of Haspin (T206 in *Xenopus* and T128 in human). This is recognized by Plk1, which further phosphorylates the Haspin N terminus. The phosphorylated N terminus interacts with the HBIS, displacing it from the kinase domain in order to activate Haspin and promote H3T3 phosphorylation. Then, H3T3ph is recognized by the CPC, resulting in cluster-mediated autophosphorylation and autoactivation of Aurora B. Activated Aurora B phosphorylates the activation loop of Plk1 in order to stimulate its activity and also directly phosphorylates Haspin in order to promote H3T3 phosphorylation.

The mechanism of Haspin auto-inhibition in interphase

We demonstrate that xHaspin is inhibited in interphase by an HBIS upstream of its kinase domain. Several observations indicate that binding of the HBIS to the xHaspin kinase domain is likely dynamic. First, an HBIS peptide can inhibit purified xHaspin kinase domain (MBP-xHaspin Δ N730) *in vitro*, even though it contains an endogenous HBIS. This is consistent with the kinase domain alternating between HBIS-bound and –unbound states, at least *in vitro*. Second, while we can co-purify xHaspin-WT with HBIS beads, this is greatly enhanced by deleting the endogenous HBIS, suggesting that dynamic binding of the HBIS to the xHaspin kinase domain competes with binding of the exogenous peptide in extract, even when xHaspin is active during mitosis. Third, while we can deplete H3T3ph activity from extract by incubation with and removal of HBIS-coated beads, simply adding soluble or bead-bound HBIS-peptide to extract does not inhibit H3T3ph. This maybe due to proteolysis of the peptide or the relative concentration of the peptide versus xHaspin in extract; however, even 1mM of HBIS-peptide is insufficient to inhibit H3T3phh in CSF extract. An alternative explanation is that the HBIS-peptide interaction is too weak and/or dynamic in extract to sufficiently inhibit xHaspin kinase activity.

It remains unclear where the HBIS binds the xHaspin kinase domain. Mutation of the conserved acidic triplet in the Haspin kinase domain resulted in only a mild reduction in HBIS peptide binding and did not stimulate H3T3ph in interphase, as we would predict for mutating the HBIS binding site. One idea is

that binding of the HBIS to the xHaspin kinase domain occurs through a separate region in a sequence-dependent manner, but can be stabilized by the charge-based interaction of the HBIS with the acidic triplet. Sequence-specific inhibition is consistent with the ability of the HBIS-peptide, but not the SCR-peptide, to inhibit xHaspin Δ N730 *in vitro*, and the ability of the HBIS-peptide to co-purify xHaspin Δ HBIS much more effectively than SCR-peptide in extract. In the future, it will be important to map the HBIS binding site to better understand the mechanism of inhibition. Additionally, it will be important to determine whether the HBIS is capable of inhibiting xHaspin in cis, in trans, or both.

Why does MBP-xHaspin Δ N730 phosphorylate H3¹⁻⁴⁵-GST *in vitro*, even though the same construct cannot support H3T3ph when placed in extract? Ghenoiu demonstrated that this difference was not due to the MBP-tag or the difference in substrates between the two systems. One explanation is phosphatases in the extract remove H3T3 phosphorylation more rapidly than HBIS-inhibited xHaspin kinase domain can phosphorylate it. Alternatively, additional factors in the extract may facilitate HBIS-mediated inhibition, for example by regulating the conformation of the N terminus.

The mechanism of Haspin activation in mitosis

Cdk1-Cyclin B and Plx1/Plk1 phosphorylate the xHaspin N terminus to activate xHaspin during mitosis. Our results are mostly consistent with this activation being dependent on multisite phosphorylation. With the exception of

mutating S234, which produced only a mild reduction in H3T3ph, no single residue was critical for xHaspin activation except T206. While mutating five phosphorylation sites (S92, S298, S304, S305, S753) was insufficient to reduce H3T3ph, additional mutation of either S234 or T15 was enough to inhibit xHaspin activation. This result suggests that the number of phosphorylations, rather than the specific residues, is important for activation. Consistent with this, mutating a different set of five residues (T472, T490, S659, S662, S675) produced a mild but significant defect in H3T3ph.

An alternative explanation is that critical residues do exist but they were not mutated in our assay, either because they were not selected for analysis or were not identified by MS. The latter is likely given that our MS achieved only 50% peptide coverage of xHaspin-WT. In support of the idea of critical residues, I demonstrated that the ability of HBIS beads to bind xHaspin N730 is lost when the last 55aa of this construct are deleted. This region contained 7 putative Plx1 sites; however, our peptide coverage was too low in this region to identify phosphorylation sites. While this region maybe critical for binding HBIS peptide, this result is somewhat inconsistent with our phospho-site mutation data. xHaspin N530 was unable to interact with the HBIS, yet mutating various phosphorylation sites in this region was able to decrease H3T3ph in metaphase, consistent with phosphorylation in the N530 region contributing to binding and displacement of the HBIS. One explanation for this is that phosphorylations in the N530 region interact with the HBIS dependent on a conformational change that requires the

‘critical region’ downstream of N530. In the future, it will be important to determine whether a critical HBIS-binding region exists in the xHaspin N terminus and how this region supports HBIS-binding.

While our results clearly establish that Cdk1-Cyclin B and Plx1 support xHaspin activation through T206, we had difficulty identifying likely Plx1 phosphorylation sites. Our MS analysis of full-length xHaspin only identified 2 residues as being *bona fide* T206-dependent sites (S304, Y307), yet neither fit the Plx1 consensus motif. We identified an additional residue that had both sufficient peptide coverage and fit the Plx1 consensus (T472); however, it was dependent on xHaspin kinase activity, not T206. MS of *in vitro* phosphorylated xHaspin N520 identified two other residues that fit the Plx1 consensus (S234, S193), yet neither was found to be phosphorylated when this construct was incubated in *Xenopus* egg extract, suggesting that they were an artifact of *in vitro* phosphorylation.

One explanation for these results is that our ability to detect T206-dependent sites was limited by our low peptide coverage of xHaspin-WT by MS. Another possibility is that Polo sites on Haspin do not fit the canonical motif. Consistent with this, profiling of Plk1 sites in the proteome and peptide array analysis of the Plk1-substrate CENP-F indicate a high degree of flexibility in the Polo consensus motif (Santamaría et al. 2011). A final possibility is that phosphorylation of the xHaspin N terminus is more complex than being simply T206- and Plx1-dependent. Consistent with this, mutating five residues that were

dependent on xHaspin kinase activity (T472, T490, S659, S662, S675) diminishes H3T3ph, suggesting that xHaspin supports its own activation. Two additional residues (S92, S753) were dependent on both xHaspin kinase activity and T206, in line with Plx1-dependent phosphorylation stimulating xHaspin kinase auto-phosphorylation. Indeed, kinase dead xHaspin has a reduced mobility shift compared to xHaspin-WT. Interestingly, S92 can be phosphorylated by Plx1 *in vitro* in the absence of the xHaspin kinase domain. This suggests that xHaspin kinase activity may indirectly promote Plx1-dependent phosphorylation of S92. This could be through auto-phosphorylation priming xHaspin for activation, or through an indirect mechanism such as xHaspin-mediated activation of Plx1. It will be interesting to determine if these xHaspin kinase activity-dependent sites are *bona fide* auto-phosphorylation sites and how they contribute to xHaspin activation. Additionally, it will be important to determine if xHaspin phosphorylations that are independent of T206 and xHaspin kinase activity contribute to its activation.

Why is multisite phosphorylation necessary for xHaspin activation? One hypothesis is that the N terminus needs multiple negative charges to effectively bind and neutralize the HBIS, which contains a basic patch. This is supported by our peptide bead experiments indicating that the HBIS and SCR peptide, which share the same amount of positive charge but a scrambled sequence, co-purify equivalent amounts of the phosphorylated xHaspin N terminus. Given that

electrostatic interactions are sensitive to salt concentration, one way to test our model is to wash these beads with buffer containing increasing levels of salt.

The requirement for multisite phosphorylation has several implications. First, it is a general mechanism that could allow different kinases to activate Haspin in different species or physiological context. Indeed, while Aurora B is required for Haspin activation in human cells, it is dispensable in *Xenopus* egg extract. Second, it only allows activation of Haspin if a threshold level of activating kinase activity is present. If true, loss of Cdk1-dependent recruitment of Plk1 to Haspin at anaphase onset may help trigger rapid silencing of Haspin kinase activity to promote CPC delocalization. Finally, this mechanism does not require critical residues or conserved phosphorylation consensus motifs. While the Haspin kinase domain is highly conserved, the N terminus of Haspin is replete in serine/threonine residues and is highly divergent between species (Higgins 2001b). Thus, multisite phosphorylation may provide a general mechanism to activate Haspin despite changes in the sequence of its N terminus.

Polo and Aurora B support hHaspin activation in mitosis

How does Plx1- and/or Aurora B-dependent phosphorylation activate Haspin in mitosis? Ghenoiu demonstrated that Plx1-mediated phosphorylation of the HBIS on S753 weakly inhibited H3T3ph in metaphase, consistent with it contributing to but not being sufficient for xHaspin activation. Interestingly, in hHaspin, the homologous residue to S753 (hHaspin S389) as well as an adjacent residue that fits the consensus Aurora B phosphorylation motif ([R/K]x[S/T][no P];

hHaspin S387), are phosphorylated during mitosis (F. Wang et al. 2011). Thus, phosphorylation of Plk1- and Aurora B- specific residues in the HBIS may contribute to hHaspin activation.

While it was previously shown that Aurora B-dependent phosphorylation of hHaspin supported H3T3ph during mitosis (F. Wang et al. 2011), the molecular basis of activation was unknown. We demonstrate that multisite phosphorylation of the xHaspin N terminus promotes binding to the HBIS and activation of xHaspin kinase activity. Given that the majority of Aurora B-dependent phosphorylation is in the N terminus of hHaspin (F. Wang et al. 2011), Aurora B may support activation of hHaspin through a similar mechanism. Indeed, both Aurora B and Plk1 contribute independently to hHaspin mobility shift and H3T3ph, suggesting that they phosphorylate the N terminus of hHaspin at distinct sites.

Our results demonstrate that positive feedback between Haspin, Plk1 and Aurora B supports robust CPC recruitment to the centromere. We find that both Plk1- and Aurora B-dependent phosphorylation of Haspin independently promote H3T3ph and CPC localization, creating a positive feedback loop between Haspin and Aurora B. It has also been shown that Aurora B phosphorylates the activation loop of Plk1 to stimulate its activity (Carmena, Pinson, et al. 2012), creating further feedback between Plk1 and Aurora B through Haspin. This positive feedback loop at the inner centromere is further enhanced by indirect Aurora B-dependent recruitment of Bub1 to the kinetochore (Van Der Waal et al.

2012; Nijenhuis et al. 2013; Zhu et al. 2013; London et al. 2012; Shepperd et al. 2012; Yamagishi et al. 2012). Bub1 phosphorylates H2A T120 (Kawashima et al. 2010), which recruits Shugoshin 1 (Sgo1) (Kitajima et al. 2005; Tang et al. 2004), a protein that indirectly recruits the CPC through an interaction with Borealin (Yamagishi et al. 2010). Additionally, Sgo1 prevents degradation of centromeric cohesion (Kitajima et al. 2005; Tang et al. 2004), which may recruit Haspin to the centromere via its interaction with Pds5 (Yamagishi et al. 2010). The existence of feedback loops between multiple kinases at the centromere and kinetochore may be important for coupling Aurora B enrichment and activity to kinetochore-microtubule attachment status. In line with this, it was shown that both Plk1 and Aurora B activity were required for the CPC to enrich at the centromere of misaligned chromosomes in primary human tissue culture cell lines (Salimian et al. 2011). In the future, it will be important to understand how kinetochore-microtubule attachment status impinges on these positive feedback loops to regulate CPC localization and function.

Chapter 3: INCENP Detects Chromatin and Microtubules to Sustain the Mitotic Checkpoint and Alter Cell Fate

3.1 Introduction

Accurate chromosome segregation requires a pair of kinetochores on each chromosome to form bipolar attachments to the mitotic spindle. Because kMT attachments are formed stochastically, unattached kinetochores or erroneous configurations may occur. Either of these situations can lead to chromosome missegregation. Cells respond to these problems through two mechanisms: correction of erroneous attachments and activation of the spindle assembly checkpoint (SAC, or mitotic checkpoint) (Foley and Kapoor, 2012). Both processes are controlled through the phosphorylation of kinetochore and centromere proteins by the CPC (Carmena et al., 2012; Krenn and Musacchio, 2015; Ruchaud et al., 2007; Trivedi and Stukenberg, 2016). It has been proposed that the CPC is part of a tension sensing mechanism that monitors kMT attachment status to activate error correction and the SAC in the absence of bipolar attachment (Biggins and Murray, 2001; Tanaka et al., 2002). Aurora B-dependent phosphorylation is high on unattached or erroneously attached kinetochores, but low on bi-oriented kinetochores that are under microtubule-dependent tension (Deluca et al., 2011; Liu et al., 2009; Welburn et al., 2010). How Aurora B detects kMT-attachment status and couples this to phosphorylation of its substrates remains unclear.

Aurora B-dependent phosphorylation promotes error correction and the SAC through multiple mechanisms. First, Aurora B destabilizes kMT attachment by phosphorylating the N-terminal tail of the microtubule-binding protein Hec1 (Ndc80) (DeLuca et al., 2006; Welburn et al., 2010), generating unattached kinetochores that can signal the checkpoint (Pinsky et al., 2006). Second, Aurora B promotes the SAC by recruiting the kinase Mps1 to the Ndc80 tail (Nijenhuis et al., 2013; Saurin et al., 2011; van der Waal et al., 2012b; Zhu et al., 2013). Third, Aurora B promotes kinetochore recruitment of the KNL1 and the Ndc80 complexes through phosphorylation of Dsn1, a subunit of the Mis12 complex (Akiyoshi et al., 2013; Kim and Yu, 2015; Yang et al., 2008). Finally, Aurora B prevents PP1-mediated silencing of the SAC by phosphorylating the PP1 binding-motif on KNL1 to prevent PP1 localization (Liu et al., 2010; Rosenberg et al., 2011).

Aurora B activation depends on its interaction with INCENP, which targets the CPC to the inner centromere during early mitosis (Carmena et al., 2012). The N terminus of INCENP contains a centromere-targeting domain (CEN domain) that interacts with the CPC components Survivin and Borealin (Gassmann et al., 2004; Sampath et al., 2004), which interact with H3T3ph and H2A T120ph, respectively. The CPC also interacts weakly with spindle microtubules during early mitosis (Tseng et al., 2010). The interaction of Aurora B with EB1 (Banerjee et al. 2014) and UBASH3B/MKLP2 (Krupina et al. 2016) on microtubules promotes centromeric enrichment of the CPC in human cells through an

unknown mechanism. In addition, the CPC binds microtubules directly through a highly conserved single-alpha helix (SAH) domain (previously termed the putative coiled-coil domain) in the middle of INCENP (Samejima et al., 2015; Tseng et al., 2010; van der Horst et al., 2015; Mackay et al. 1993). The SAH domain is essential for viability in chicken DT40 cells (Samejima et al., 2015), for effective Dsn1 phosphorylation (Samejima et al., 2015) and for CPC relocation to the anaphase spindle midzone in human cells (van der Horst et al., 2015). In human cells, it was also reported that deleting the SAH domain attenuates the SAC in taxol (Vader et al., 2007). It remains unclear, however, if the interaction of the CPC with microtubules contributes to the SAC or to the recruitment of the CPC to the inner centromere.

Our goal was to characterize the molecular function of the SAH domain in the taxol-mediated SAC to determine how the CPC contributes to the checkpoint and how this function is regulated. Here we demonstrate that the INCENP SAH domain supports the taxol-mediated SAC in HeLa cells by interacting with microtubules. The SAH domain is also required for CPC localization and stability at the centromere independent of Borealin and Survivin. INCENP binding to either chromatin or microtubules stimulates the SAC, though both activities are required for a robust checkpoint response. We also find that INCENP microtubule binding is regulated by phosphorylation flanking the SAH domain and propose that kinetochore phosphatases locally regulate the activation and function of a kinetochore-proximal pool of CPC on microtubules. This work has been

submitted to the Journal of Cell Biology as a manuscript kentitled 'INCENP detects chromatin and microtubules to promote the mitotic checkpoint and alter cell fate'.

3.2 Results

The INCENP SAH domain is required for CPC localization and the SAC in *Xenopus* egg extracts

In *Xenopus* egg extract, the nocodazole-induced SAC depends on Aurora B (Gadea and Ruderman, 2005; Kallio et al., 2002). To determine if the INCENP SAH domain is required for the checkpoint in this system, we immunodepleted the CPC from M-phase extract and reconstituted it with GFP-tagged full-length *Xenopus laevis* INCENP (xINCENP) or xINCENP Δ SAH. The SAC was assayed by adding a high concentration of sperm chromatin (10,000 sperm/ μ L) and nocodazole to activate the checkpoint, followed by addition of calcium to release the cytostatic factor (CSF)-mediated arrest that normally maintains the *Xenopus* egg extract in M-phase (Minshull et al., 1994). M-phase specific H3T3ph was monitored to determine cell cycle stage (**Figure 3-1**). Mock-depleted extract remained in M-phase for the duration of the assay, indicative of a SAC arrest, while CPC-depleted extract (Δ CPC) lost H3T3ph within 30 min, indicative of release into interphase. This defect was fully rescued when the extract was reconstituted with CPC containing xINCENP, but not xINCENP Δ SAH, indicating the SAH domain is required for the SAC in *Xenopus* egg extract.

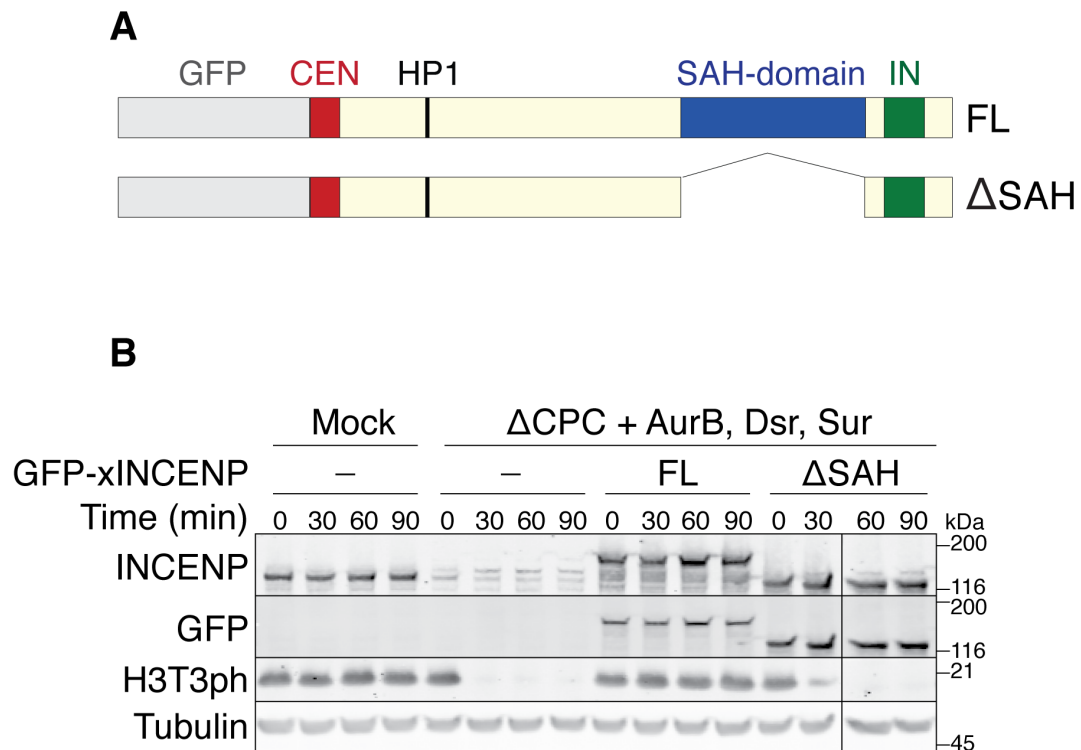


Figure 3-1: The xINCENP SAH domain supports the nocodazole-induced SAC in *Xenopus* egg extract.

A) Diagram of GFP-tagged full length xINCENP (FL) or xINCENP lacking the SAH domain (Δ SAH). GFP (gray); CEN, centromere targeting domain, which binds Survivin and Borealin (red); HP1, HP1 binding domain (black); SAH domain (blue); IN, IN-box, which binds Aurora B (green)

B) Nocodazole-induced SAC assay in *Xenopus* egg extracts either mock depleted or depleted of the CPC (Δ CPC) and reconstituted with xAurora B, xDasra A (the *Xenopus* Borealin homolog), xSurvivin and the indicated xINCENP construct. Time after calcium addition, which inactivates CSF, is indicated. Mitotic status is monitored by western blot for H3T3ph. Depleting the CPC or reconstituting extract with INCENP lacking the SAH domain lead to SAC silencing.

Mock= control IgG depletion, Δ CPC= CPC depletion. AurB= MBP-xAurora B protein, Dsr= xDasra A mRNA, Sur= xSurvivin mRNA

Since Aurora B activation is tightly coupled to its localization, we tested if the SAH domain contributes to chromatin localization of the CPC. We reconstituted extract with full-length xINCENP or xINCENP Δ SAH and performed immunofluorescence to visualize their distribution on sperm chromatin in the presence of nocodazole (**Figure 3-2A**). While xINCENP was broadly distributed along chromatin with enrichment near the centromere (xINCENP foci are in proximity to the centromere protein CENP-C, not shown), the level of xINCENP Δ SAH on chromatin was dramatically reduced. We observed a similar localization defect when we visualized the localization of xINCENP and xINCENP Δ SAH on preassembled CENP-A chromatin arrays added to M-phase extract (**Figure 3-2B**).

To test if the SAH domain binds chromatin, we expressed a GFP-tagged SAH domain fragment (xSAH) in M-phase extract and visualized its localization on sperm chromatin treated with nocodazole. Compared to GFP alone, we detected weak binding of the xSAH domain broadly on sperm chromatin (**Figure 3-3A**). This localization was independent of an interaction with endogenous INCENP as 6Myc-tagged xSAH localized to chromatin even after depletion of endogenous CPC (**Figure 3-3B**). Additionally, endogenous INCENP did not purify with the 6Myc-tagged xSAH domain via co-immunoprecipitation (**Figure 3-3C**). These results indicate that in addition to Survivin and Borealin, the SAH domain also interacts with chromatin to support robust localization of the CPC in *Xenopus* egg extract.

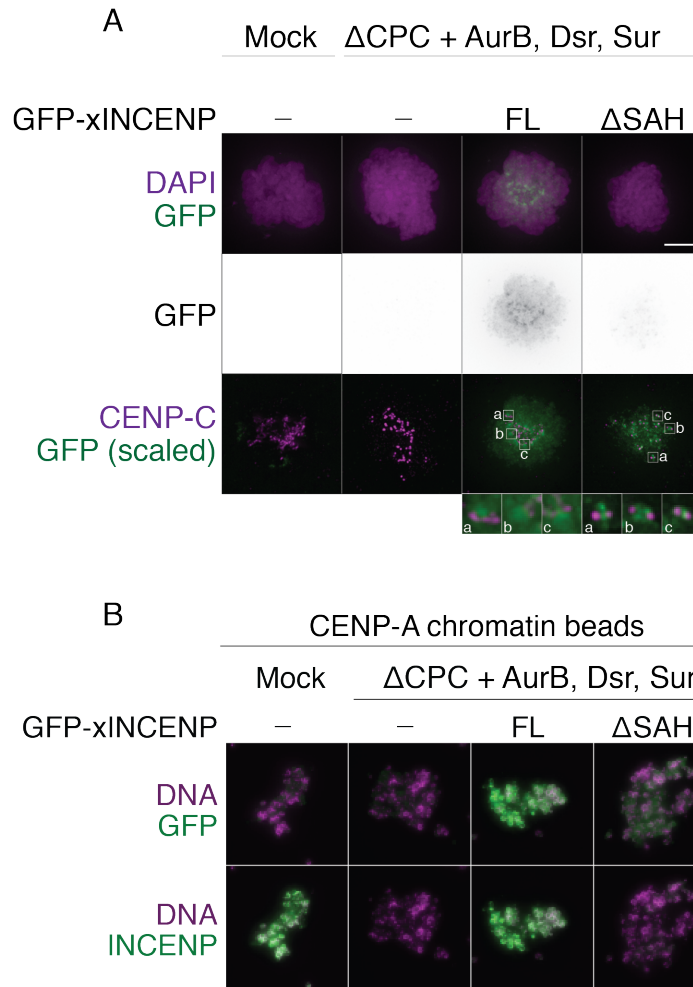


Figure 3-2: The xINCENP SAH domain supports CPC localization to chromatin in *Xenopus* egg extract.

A) Immunofluorescence visualizing GFP-xINCENP (green) abundance on sperm chromatin (top, purple) relative to the centromere protein CENP-C (bottom, purple; GFP for Δ SAH scaled to show residual xINCENP at centromere) in M-phase extract treated with nocodazole. Extracts were reconstituted as indicated. Scale bar, 5 μ m; Mock= control IgG depletion, Δ CPC= CPC depletion. AurB= MBP-xAurora B protein, Dsr/ Sur= xDasra A/ xSurvivin mRNA

B) Immunofluorescence visualizing GFP-xINCENP (green) on preformed CENP-A chromatin arrays (purple) incubated in M-phase extract reconstituted as indicated. GFP-xINCENP was detected by GFP (top). Endogenous INCENP and GFP-xINCENP were detected by a xINCENP antibody (bottom). Scale bar, 6 μ m

Figure 3-3: The xINCENP SAH domain interacts with chromatin independent of the INCENP CEN domain.

A) Quantification (left) and immunofluorescence (right) visualizing GFP or GFP-xSAH domain on sperm chromatin in M-phase extracts treated with nocodazole. GFP-xSAH domain is broadly distributed along sperm chromatin. Quantification of GFP intensity is normalized to the total amount of DAPI staining.

Representative images approximate the median, two-tailed Mann-Whitney t test, *** $p \leq 0.001$. Scale bar, 2 μm

B) Depletion efficiency (left), representative images (middle) and quantification (right) of 6Myc-xSAH localized to sperm chromatin in nocodazole following depletion of endogenous INCENP. 6Myc-xSAH (green) shows weak localization along sperm chromatin relative to a 6Myc-tagged protein that does not bind sperm chromatin (6Myc-Control) even when 95% of endogenous INCENP is depleted. CENP-A (purple) is a marker for the centromere. Quantification of Myc intensity is standardized to the total amount of DAPI staining. Representative images approximate the median, two-tailed Mann-Whitney t test, *** $p \leq 0.001$.

C) Total extract (Input) and immunoprecipitation (IP) of M-phase extract containing the indicated Myc-xSAH constructs. Extracts were immunoprecipitated with either anti-IgG (gray circles) or anti-Myc (black circles). Rabbit heavy chain (HC, red) is detected by the secondary antibody at the indicated molecular weight and partially obscures the detection of Myc-tagged xSAH constructs.

Endogenous INCENP (INCENP) does not co-purify with the xSAH domain. Scale bar, 2 μm

ΔCPC = CPC depletion

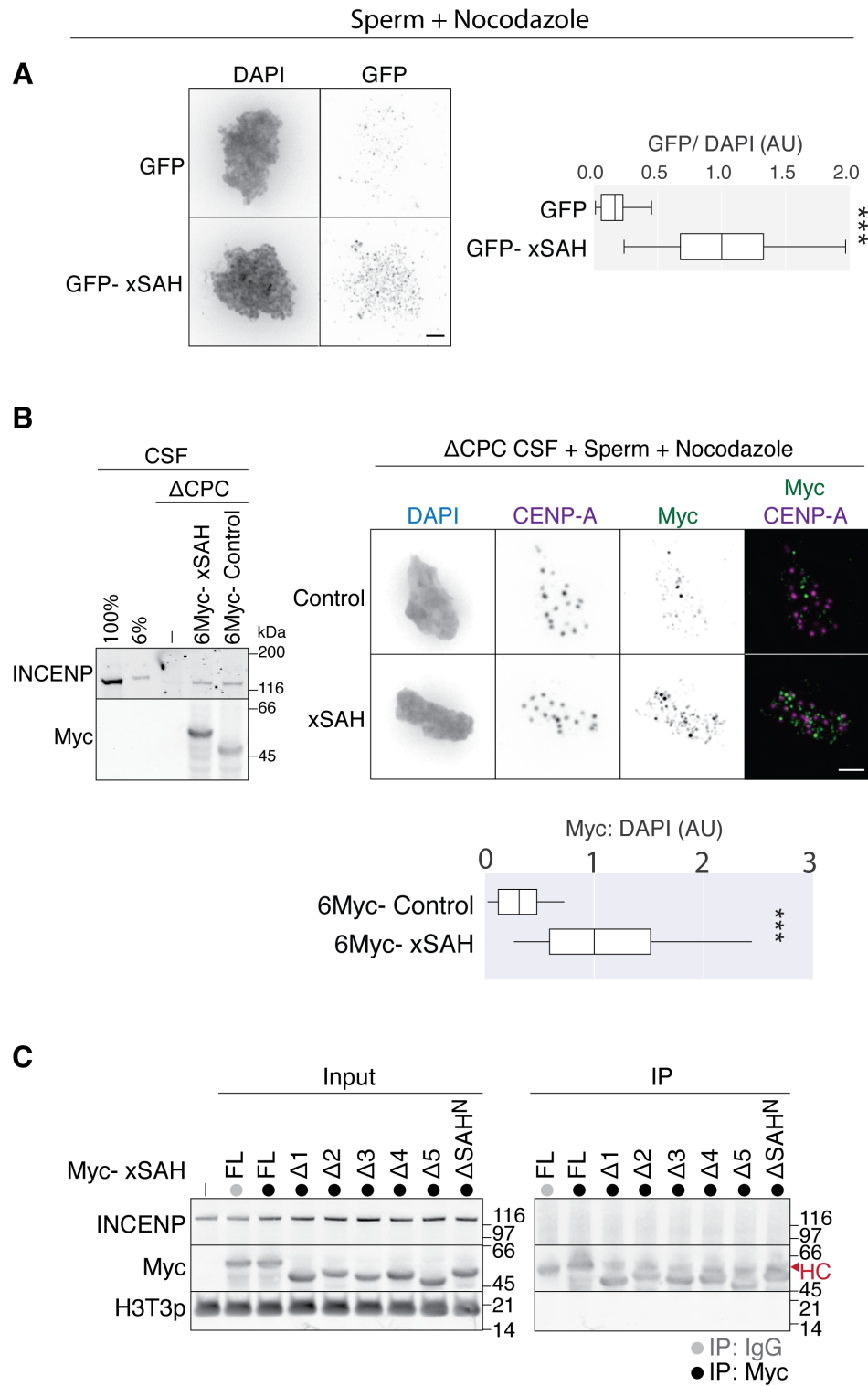


Figure 3-3: The xINCENP SAH domain interacts with chromatin independent of the INCENP CEN domain.

The SAH domain is required for CPC localization and dynamics in human cells

The importance of the INCENP SAH domain for robust CPC localization in *Xenopus* contrasts with qualitative data in human cells (U2OS, HeLa) and chicken DT40 cells, in which the SAH domain is dispensable for CPC localization to the centromere (Samejima et al., 2015; Vader et al., 2007; van der Horst et al., 2015). To determine the extent to which deleting the SAH domain affects CPC localization in human cells, we generated doxycycline-inducible HeLa T-REx cell lines containing full-length human INCENP (hINCENP) or hINCENP Δ SAH (**Figure 3-4A**). These constructs contain mutations that prevent their mRNA from binding a previously published INCENP siRNA (Vader et al., 2006) and contain an N-terminal fusion to the localization and purification (LAP) tag (Cheeseman and Desai, 2005). Treating these cells with INCENP siRNA reduced endogenous INCENP protein levels by 80%, while addition of doxycycline induced LAP-INCENP expression to near wild-type levels (**Figure 3-4B**). As previously published (Honda et al., 2003), knockdown of INCENP reduced the abundance of the entire CPC, including Aurora B, Borealin and Survivin. The stability of these components was rescued by expression of either hINCENP or hINCENP Δ SAH, indicating these constructs were incorporated into the CPC *in vivo*. This was confirmed by co-immunoprecipitation of the CPC subunits with hINCENP and hINCENP Δ SAH (**Figure 3-4C**).

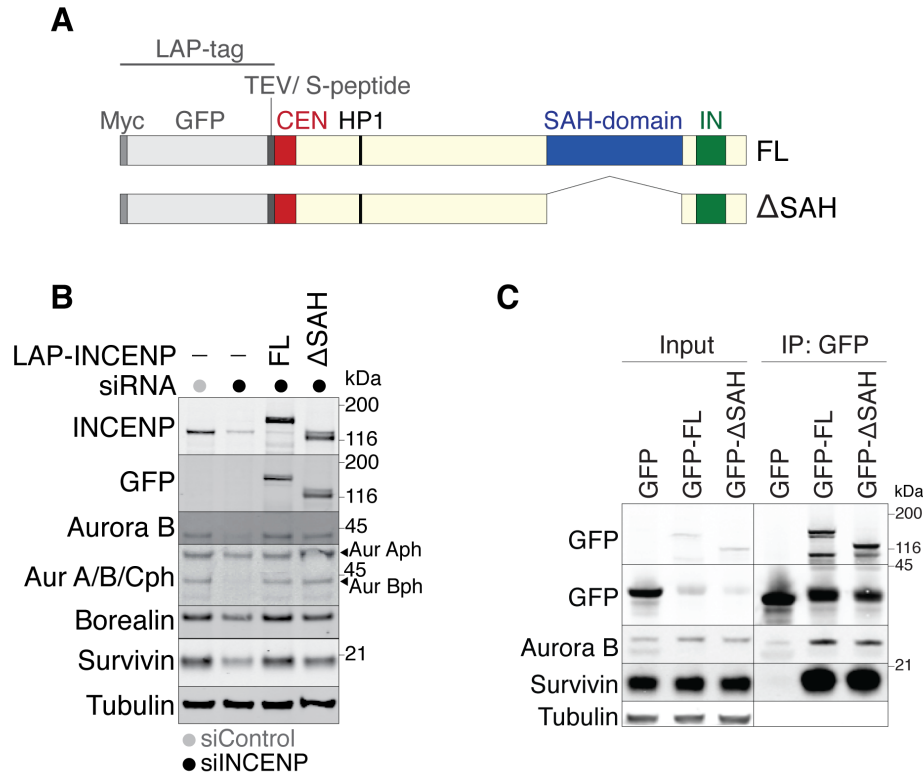


Figure 3-4: The CPC forms independent of the hINCENP SAH domain in HeLa cells.

A) Diagram of LAP-tagged full-length hINCENP (FL) and hINCENP lacking the SAH domain (hINCENP Δ SAH). LAP-tag, localization and purification tag, composed of Myc, GFP, a TEV protease site and S-peptide; CEN, centromere-targeting domain, which binds Survivin and Borealin; HP1, HP1-binding motif; SAH domain (blue); IN, IN-box, which binds Aurora B.

B) Western blot of mitotic HeLa cell extracts. Aur A/B/Cph detects the phosphorylated T-loop of Aurora A and Aurora B. Cells were treated with either siControl (gray circle), or siINCENP (black circle). Knockdown of INCENP destabilizes the other components of the CPC but is rescued by either hINCENP or hINCENP Δ SAH.

C) Western blot of total extract (Input) and anti-GFP immunoprecipitation (IP) from mitotic HeLa cell extracts containing the indicated construct. Survivin and Aurora B co-immunoprecipitate with hINCENP and hINCENP Δ SAH.

To determine if the SAH domain was required for CPC localization in human cells, we expressed hINCENP and hINCENP Δ SAH over endogenous INCENP and visualized their localization by immunofluorescence (**Figure 3-5**). Both constructs showed the appropriate spatiotemporal distribution, including enrichment at the inner centromere during pro/metaphase and transfer to the spindle midzone during anaphase. Compared to hINCENP, hINCENP Δ SAH appeared less abundant at the centromere and midzone, consistent with our observations in *Xenopus* (**Figure 3-2A**) and the published role of the hINCENP SAH domain in midzone localization (van der Horst et al., 2015), respectively.

To quantify the abundance of the CPC at the centromere during early mitosis, we depleted endogenous INCENP with siRNA, while simultaneously inducing expression of either hINCENP or hINCENP Δ SAH (**Figure 3-6A**). Immunofluorescence analysis indicated that in taxol-treated cells, expression of hINCENP Δ SAH significantly reduced the abundance of all tested CPC components (LAP-INCENP, Aurora B, Survivin) at the centromere relative to hINCENP (**Figure 3-6B**). A similar reduction in centromeric hINCENP Δ SAH was observed in nocodazole-treated cells (**Figure 3-6C**). Reduced CPC abundance at the centromere was accompanied by a slight reduction in centromeric H3T3ph and the appearance of H2A T120ph on chromosome arms (**Figure 3-6D**). These defects are consistent with the idea that reduced CPC abundance causes defects in Aurora B-dependent activation of the H3T3 kinase Haspin and Aurora B-dependent recruitment of the H2A T120 kinase Bub1 to the kinetochore.

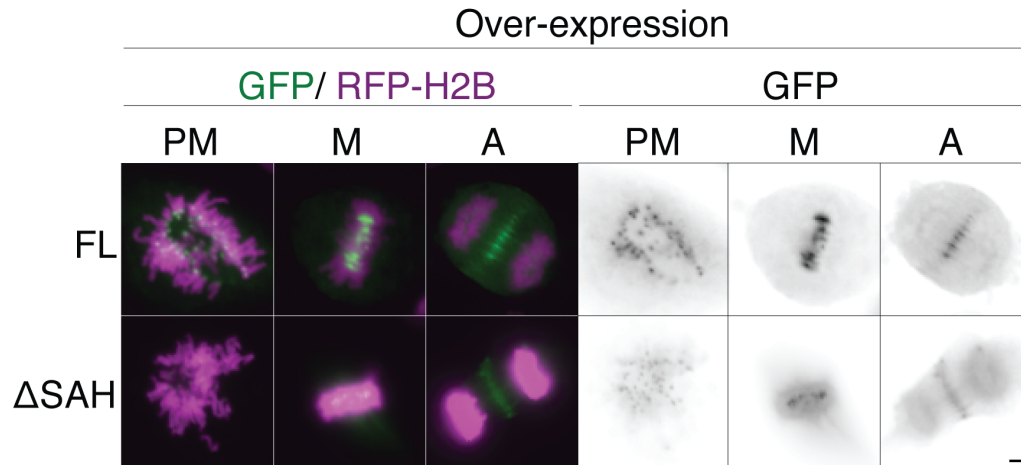


Figure 3-5: The hINCENP SAH domain is not required for the spatiotemporal distribution of the CPC in HeLa cells.

Immunofluorescence visualizing hINCENP and hINCENP Δ SAH expressed over endogenous INCENP in asynchronous cells. Both constructs show the correct cell cycle distribution, enriching at the centromere during early mitosis and transferring to the spindle midzone at anaphase. GFP (green), RFP-H2B (purple); PM, prometaphase; M, metaphase; A, anaphase; Scale bar, 2 μ m

Figure 3-6: The hINCENP SAH domain is necessary for robust enrichment of the CPC at the centromere in HeLa cells.

A) Experimental scheme for B-D. Cells were simultaneously treated with siRNA and doxycycline (to induce construct expression) for 24-36 hr then split onto chamber slides and allowed to adhere for 12 hr. To enrich for mitotic cells, I added the Cdk1 inhibitor RO-3306 for 12 hr to arrest cells at the G2/M transition, then performed a washout and release into media containing either taxol or nocodazole, at which point cells synchronously entered mitosis. After 4 hr, cells were fixed for immunofluorescence.

B) Whole cell integrated centromere intensity (left) was quantified for each epitope in taxol after treating cells with INCENP siRNA (siINCENP) and expressing the indicated LAP-tagged hINCENP construct. For each epitope, values were normalized to the median intensity of hINCENP- FL. Representative images (right) approximate the median value. Deletion of the SAH domain reduces the abundance of all three measured CPC components. $n \geq 28$ for each condition, two-tailed Mann-Whitney t test, $**p \leq 0.01$, $***p \leq 0.001$, Scale bar, 2 μ M

C) Same as B, but cells were treated with nocodazole

D) Quantification (left) and representative images (right) of the level of H3T3ph and H2A T120ph in cells expressing hINCENP (FL) or hINCENP Δ SAH (Δ SAH) following knockdown of endogenous INCENP and incubation with taxol (Similar to Figure C). H3T3ph shows only a minor reduction, while H2A T120p appears on chromosome arms. Representative images approximate the median, two-tailed Mann-Whitney t test, $*p \leq 0.05$, $***p \leq 0.001$, Scale bar, 2 μ m

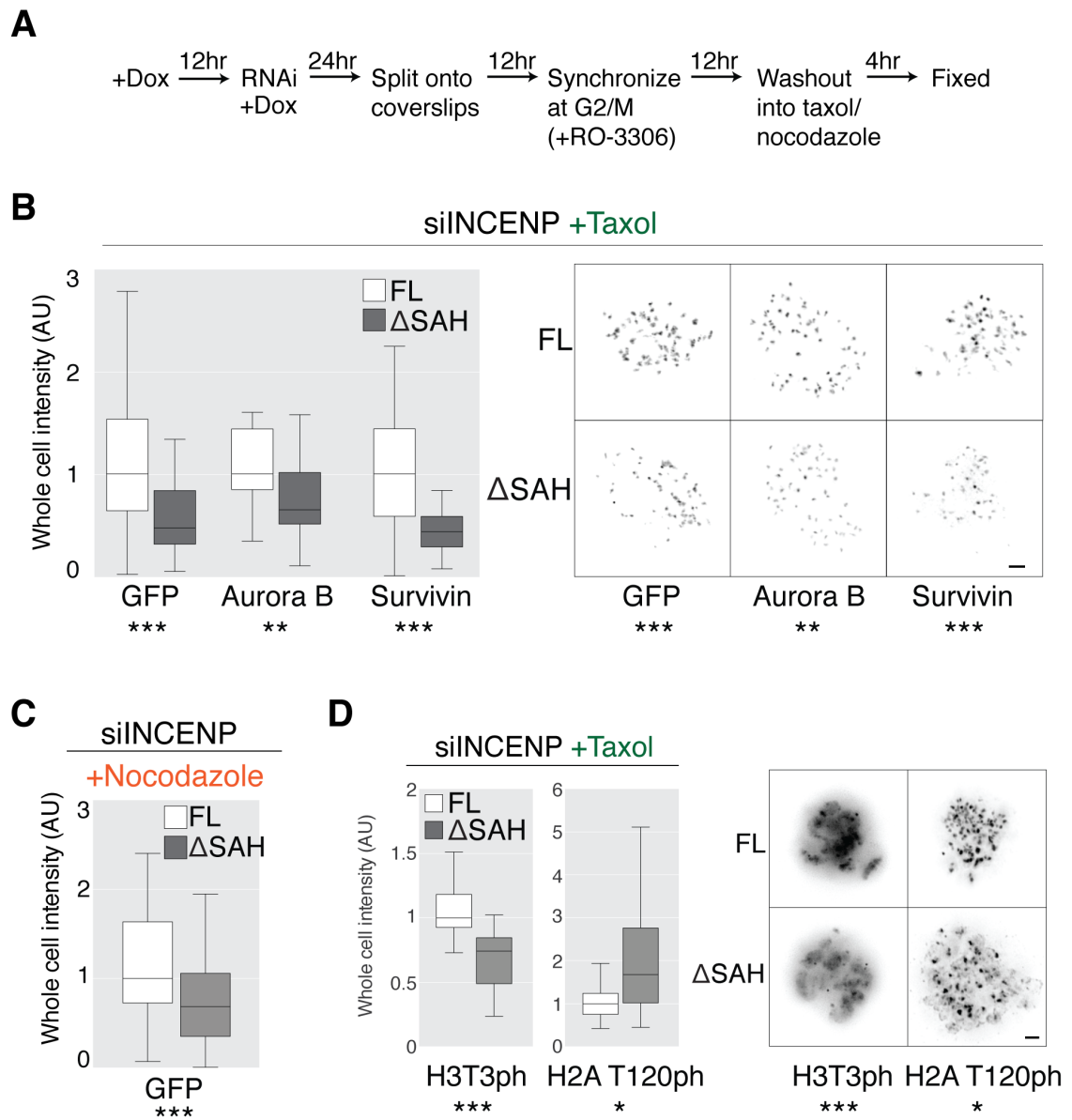


Figure 3-6: The hINCENP SAH domain is necessary for robust enrichment of the CPC at the centromere in HeLa cells.

To determine whether the SAH domain contributes to CPC stability at the centromere, we performed fluorescence recovery after photobleaching (FRAP) on centromeric foci of hINCENP or hINCENP Δ SAH in mitotic cells treated with taxol (**Figure 3-7A, 3-7C**). Consistent with the SAH domain being required for CPC stability at the centromere, hINCENP had a mean halftime of recovery ($t_{1/2}$) of 83.2 ± 33.5 s, while INCENP Δ SAH had a more rapid halftime of recovery (53.6 ± 33.1 s). These results were similar when cells were treated with nocodazole (**Figure 3-7B, 3-7C**) and in line with previously published results for INCENP in nocodazole (Ahonen et al., 2009). Taken together, these results demonstrate that, in addition to its capacity to bind microtubules, the SAH domain helps stabilize the CPC on centromeric chromatin in both *Xenopus* egg extracts and in human somatic cells.

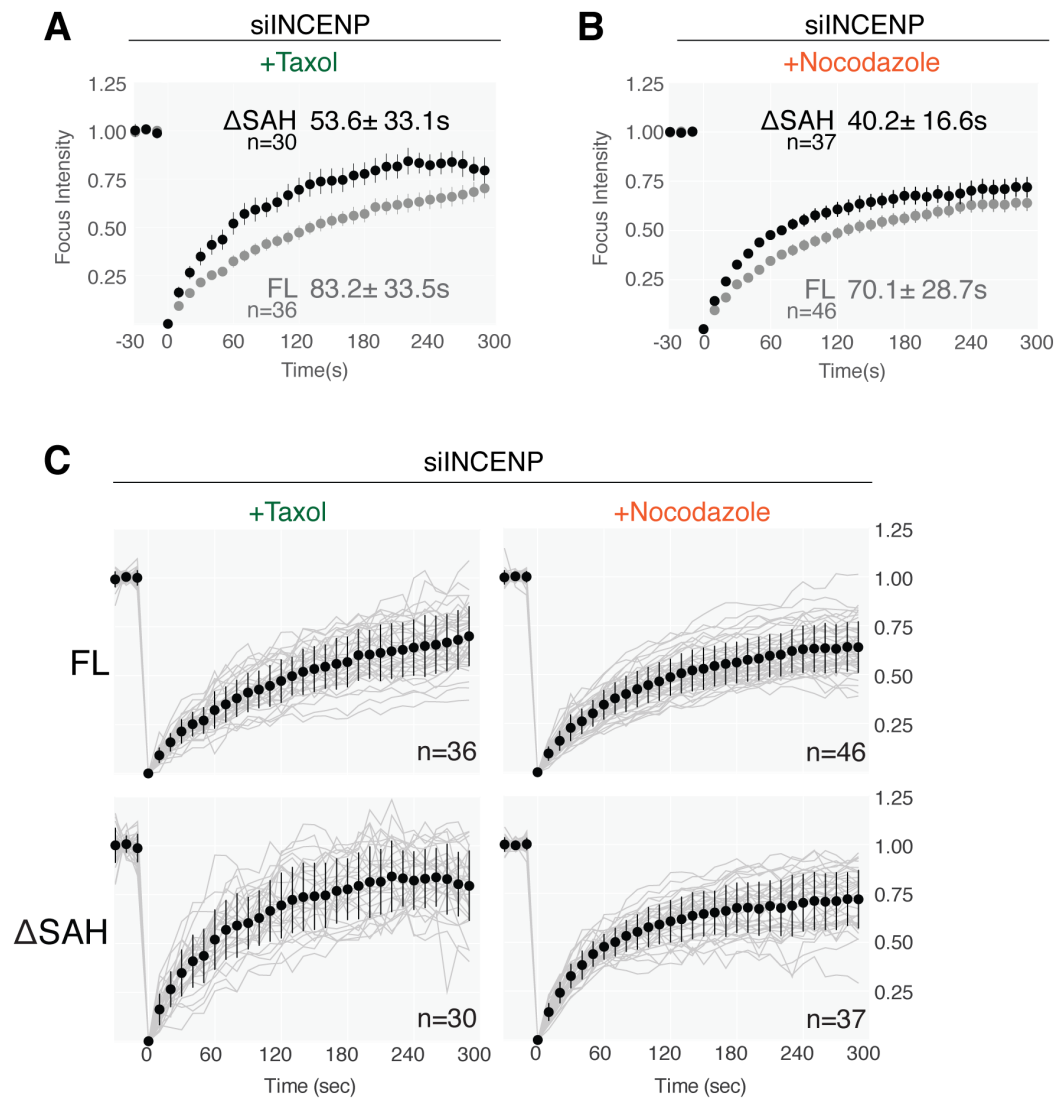


Figure 3-7: The hINCENP SAH domain stabilizes the CPC at the centromere in HeLa cells.

A, B) Fluorescence recovery after photobleaching (FRAP) of centromeric foci in taxol-treated (A) or nocodazole-treated (B) cells reconstituted with hINCENP or hINCENP ΔSAH . The mean FRAP recovery curve with a 95% confidence interval is displayed with the mean $t_{1/2} \pm \text{SD}$ for each sample, $n \geq 30$ centromeres for each condition. Deletion of the SAH domain decreases the $t_{1/2}$ of hINCENP in both taxol and nocodazole, consistent with increased dynamicity at the centromere.

C) Individual recovery curves for data in A and B. Mean curve (black) $\pm \text{SD}$.

The SAH domain is required for the SAC and cell death in taxol-treated human cells

A previous study investigating the role of SAH domain in the checkpoint used FACS to measure the relative abundance of mitotic cells (Vader et al., 2007). However, this analysis does not determine the duration of the mitotic arrest or how cells exit mitosis. Therefore, we measured the duration of mitosis (DoM) for single cells using live microscopy in the presence of 500 nM taxol, which is a concentration known to result in the longest DoM (Yang et al., 2009). We defined the DoM as the time from nuclear envelope breakdown to mitotic exit, which occurred either by slippage into interphase or death in mitosis. In taxol, all cells undergoing slippage produced a single, multinucleate cell due to an inability to undergo cytokinesis, while cells that died in mitosis exhibited blebbing followed by compaction into a crenulated spherical mass.

Cells treated with control siRNA showed a heterogeneous arrest time in taxol with a median DoM of 18.6 hr. Consistent with the CPC being required for SAC maintenance, INCENP siRNA decreased the median DoM to 8.3 hr. While expression of hINCENP fully rescued the DoM (18.7 hr), hINCENP Δ SAH did not (11.1 hr), confirming that the SAH domain is required to maintain the SAC in human cells (**Figure 3-8A**). Treating cells with monastrol, an Eg5 inhibitor that generates syntellic and merotelic attachments, demonstrated a similar requirement for the CPC and the SAH domain for the checkpoint (**Figure 3-8B**).

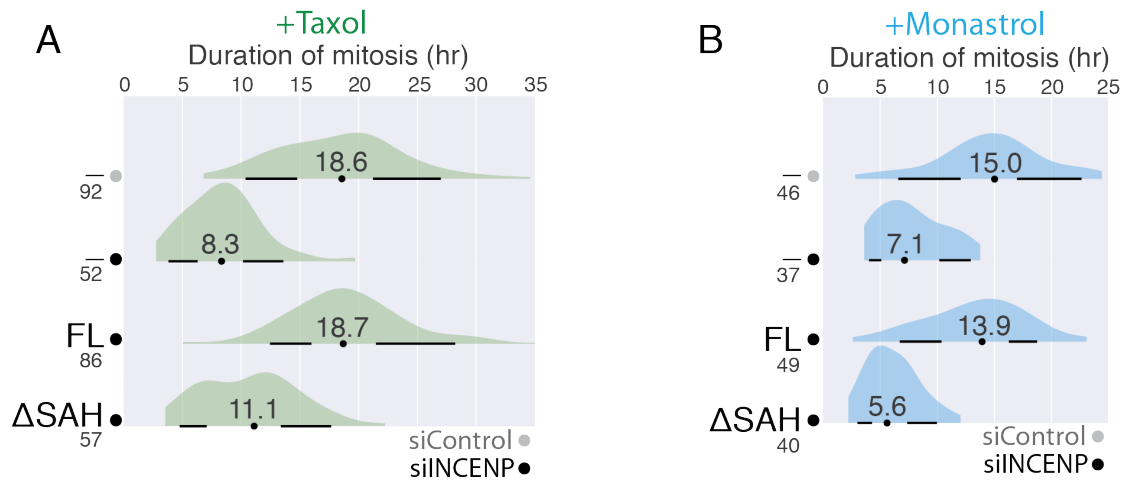


Figure 3-8: The hINCENP SAH domain is required for the taxol- and monastrol- induced SAC in HeLa cells.

A) Duration of mitosis for HeLa cells in taxol, treated with control siRNA (siControl) or INCENP siRNA (siINCENP) and complemented with siRNA-resistant full-length hINCENP (FL) or hINCENP-ΔSAH (ΔSAH). Data is displayed as a kernel density estimate of the duration of mitosis (DoM: time from nuclear envelope breakdown to mitotic exit by death or slippage) for all cells in each condition. A boxplot with a circle at the median and whiskers extending to $\pm 1.5^*$ interquartile range is under each density, n-values indicated under sample name.

B) Same as (A) except cells were treated with monastrol.

A cell undergoing SAC-dependent mitotic arrest in taxol has two distinct fates: mitotic slippage or cell death. The “competing-networks” hypothesis posits that this decision is determined in a competition between Cyclin B degradation, which promotes mitotic slippage, and the accumulation of pro-apoptotic signals, which trigger cell death (Gascoigne and Taylor, 2008; Topham and Taylor, 2013). More kinetochores activating the SAC generate a “stronger” response, which promotes slower degradation of Cyclin B (Collin et al., 2013; Dick and Gerlich, 2013). This results in a prolonged mitotic arrest, increasing the likelihood that enough pro-apoptotic signals accumulate to trigger death in mitosis (Topham and Taylor, 2013).

To investigate this hypothesis, we aggregated data from at least five independent replicates of our taxol-induced checkpoint experiment by normalizing the DoM for each construct to the median for that of hINCENP in the same replicate (**Figure 3-9A**). We then visualized the normalized DoM by cell fate (slippage or death) for each construct. Consistent with a defective SAC increasing cell survival, we find that while the majority of control cells (84%) or those expressing INCENP (71%) died in mitosis, the majority of cells lacking the CPC (75%) or containing INCENP Δ SAH (59%) underwent mitotic slippage. This shift is due to a defect in the SAC as cells initiated mitotic slippage in half as much time when expressing hINCENP Δ SAH relative to hINCENP. Expression of hINCENP Δ SAH reduced the median DoM of cells dying in mitosis, however, by

only 20%, consistent with the idea that the accumulation of cell death signals can be uncoupled from the degradation of Cyclin B (Topham and Taylor, 2013).

To better correlate the DoM with cell fate, we performed a linear regression of the median DoM against cell survival for every construct in every experiment in this paper, in addition to experiments not shown (**Figure 3-9B**). Consistent with the competing networks model, we see a strong positive correlation between the duration of mitosis and percentage of cells dying in mitosis. This trend holds even when we perform an independent regression for cells that undergo slippage ($r^2=0.61$) versus those that die in mitosis ($r^2= 0.37$). This indicates that the frequency of mitotic cell death, but not timing of cell death, strongly correlates with the capacity of INCENP to hold the SAC. Thus, the CPC and the INCENP SAH domain ensure a robust SAC-mediated mitotic arrest, which promotes mitotic death in cells treated with taxol.

Figure 3-9: The hINCENP SAH domain promotes mitotic cell death in taxol.

A) “Competing Networks” hypothesis for how cell fate is determined during mitotic arrest. Intrinsic and extrinsic factors determine the rate of Cyclin B degradation and cell death signal accumulation for each cell. If the level of Cyclin B (blue) goes below the threshold needed to maintain the cell in mitosis (slippage threshold), mitotic slippage occurs (left). If the accumulation of pro-apoptotic signals (red) goes above the threshold level to initiate cell death (death threshold), death in mitosis occurs (right). The result is a winner-take-all race determined by which event occurs first. Adapted from Gascoigne and Taylor, 2008.

B) Normalized duration of mitosis (DoM) for all cells (gray), and for cells undergoing death in mitosis (red) or mitotic slippage (blue). Data aggregated from at least 5 independent experiments. All values were normalized to the median of hINCENP in that experiment. Maximum height of each curve is proportional to percent composition of that class in the aggregate. Red numbers on the right indicate the overall percentage of cells dying in mitosis. The difference in the normalized DoM between cells complemented with hINCENP FL or Δ SAH is also indicated. Cells lacking the CPC or reconstituted with hINCENP lacking the SAH domain undergo mitotic slippage more frequently than death in mitosis.

C) Scatter plot of the median duration of mitosis (DoM) versus percent cell death. Each point represents a single sample from one experiment (including all experiments in this dissertation). Values for cells undergoing death in mitosis (red) or mitotic slippage (blue) are plotted separately for each sample against the total percent death for that sample. Shaded areas are kernel density estimates. The r^2 values for the linear regression are indicated in the top left. Across all samples, the DoM is proportional to the frequency of death in mitosis (% Death).

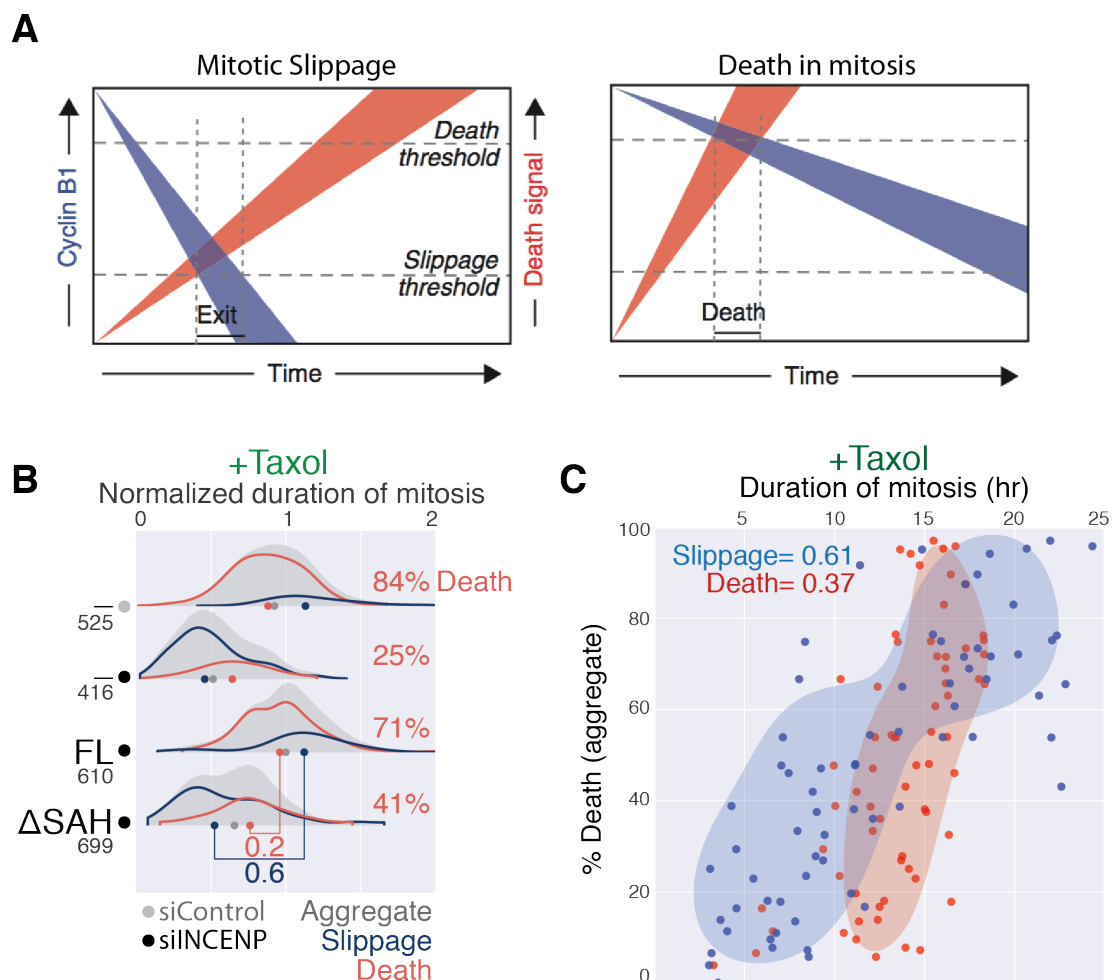


Figure 3-9: The hINCENP SAH domain promotes mitotic cell death in taxol.

The SAH domain is required for SAC protein recruitment and kinetochore phosphorylation in taxol-treated human cells

Next, we wanted to determine if the SAH domain was required to recruit SAC signaling proteins to the kinetochore. We quantified the abundance of Mad1, Bub1 and BubR1 at the kinetochore in cells expressing either hINCENP or hINCENP Δ SAH in the presence of taxol (**Figure 3-10A**). Whereas it was reported that BubR1 recruitment is not affected by deleting the SAH domain in U2OS cells (Vader et al., 2007), we found that cells expressing INCENP Δ SAH had a significant reduction in the amount of Mad1, Bub1 and BubR1 at the kinetochore compared to hINCENP. This is not due to a defect in kinetochore assembly, as hINCENP and hINCENP Δ SAH showed no difference in the amount of total CENP-A or Hec1 (**Figure 3-10B**).

Aurora B-mediated phosphorylation of the KMN (KNL1, Mis12, Ndc80) network promotes unattached kinetochores, which in turn recruit SAC proteins to the kinetochore (Funabiki and Wynne, 2013; Pinsky et al., 2006). To determine if the SAH domain supports Aurora B substrate phosphorylation in taxol, we performed immunofluorescence using previously published phospho-specific antibodies to assess Aurora B-dependent phosphorylation of centromere components (CENP-A S7ph), chromatin components (H3S10ph) and components of the KMN network (Dsn1 S100ph, KNL1 S24ph, Hec1 S44ph; **Figure 3-11**; Deluca et al., 2011; Hsu et al., 2000; Welburn et al., 2010; Zeitlin et al., 2001). hINCENP and hINCENP Δ SAH both supported robust Aurora B-

dependent phosphorylation of CENP-A at the centromere and H3S10 on chromatin, consistent with previous reports that the SAH domain is not required for general Aurora B activity (Vader et al., 2007) (**Figure 3-11A**). However, hINCENP Δ SAH had a reduced amount of Dsn1 S100ph and KNL1 S24ph at the kinetochore compared to INCENP (**Figure 3-11A**). A similar decrease was also seen using a phospho-specific antibody against Hec1 S44ph (**Figure 3-11B, C**). These results are consistent with a previous observation that the INCENP SAH domain influences Dsn1 phosphorylation (Samejima et al., 2015), and suggests that the SAH domain is required for the SAC by supporting Aurora B-dependent kinetochore phosphorylation and checkpoint protein recruitment.

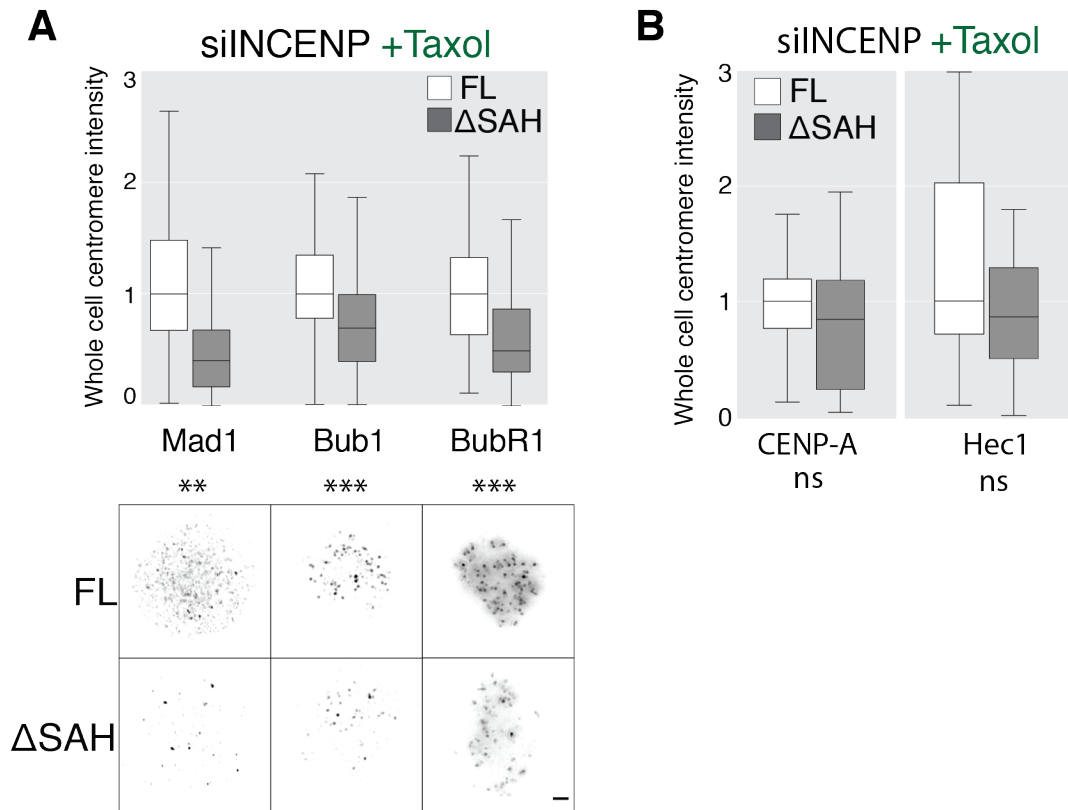


Figure 3-10: The hINCENP SAH domain supports SAC protein recruitment to the kinetochore.

A) Immunofluorescence quantification of SAC proteins in taxol-treated cells expressing hINCENP (FL) or hINCENP lacking the SAH domain (ΔSAH) following treatment with INCENP siRNA (siINCENP). Whole cell integrated intensity was quantified for Mad1, Bub1 and BubR1 with $n \geq 20$ cells per sample. Deletion of the SAH domain reduces the abundance of all three SAC proteins at the kinetochore in taxol. Representative images approximate the median, two-tailed Mann-Whitney t test, ns=not significant, $**p \leq 0.01$, $***p \leq 0.001$, Scale bar, 2 μm

B) Immunofluorescence quantification of whole cell integrated total CENP-A and total Hec1 in taxol-treated cells expressing hINCENP or hINCENP ΔSAH following treatment with INCENP siRNA (siINCENP). $n \geq 20$ cells per sample. A comparable amount of each protein is detected for hINCENP FL and ΔSAH, consistent with the SAH domain being dispensable for kinetochore assembly in HeLa cells.

Figure 3-11: The hINCENP SAH domain is required for Aurora B-dependent kinetochore phosphorylation in taxol.

A) Immunofluorescence quantification of Aurora B-dependent phosphorylation in taxol-treated cells expressing hINCENP (FL) or hINCENP lacking the SAH domain (Δ SAH) following treatment with INCENP siRNA (siINCENP). Whole cell integrated intensity was quantified for CENP-A S7ph, a centromeric substrate, and H3S10ph, a panchromosomal substrate, with $n \geq 20$ cells per sample.

Individual kinetochore intensity was quantified for Dsn1 S100ph and Knl1 S24ph using a kinetochore marker with $n \geq 1800$ individual kinetochores per sample.

Deletion of the SAH domain reduces the abundance of Aurora B-dependent phosphorylation at the kinetochore in taxol. Representative images approximate the median, two-tailed Mann-Whitney t test, ns=not significant, ** $p \leq 0.01$,

*** $p \leq 0.001$, Scale bar, 2 μ m

B) Immunofluorescence quantification of Hec1 S44ph, an Aurora B kinetochore phosphorylation site, at individual kinetochores standardized to total Hec1 at that kinetochore. n-values are indicated under the sample name. ZM, the Aurora B inhibitor ZM447439.

C) Representative images from B. A cell of representative intensity (right) and a zoom in of four representative kinetochore pairs (left). Scale bar (whole cell), 2 μ m, Scale bar (kinetochore pair), 0.25 μ m

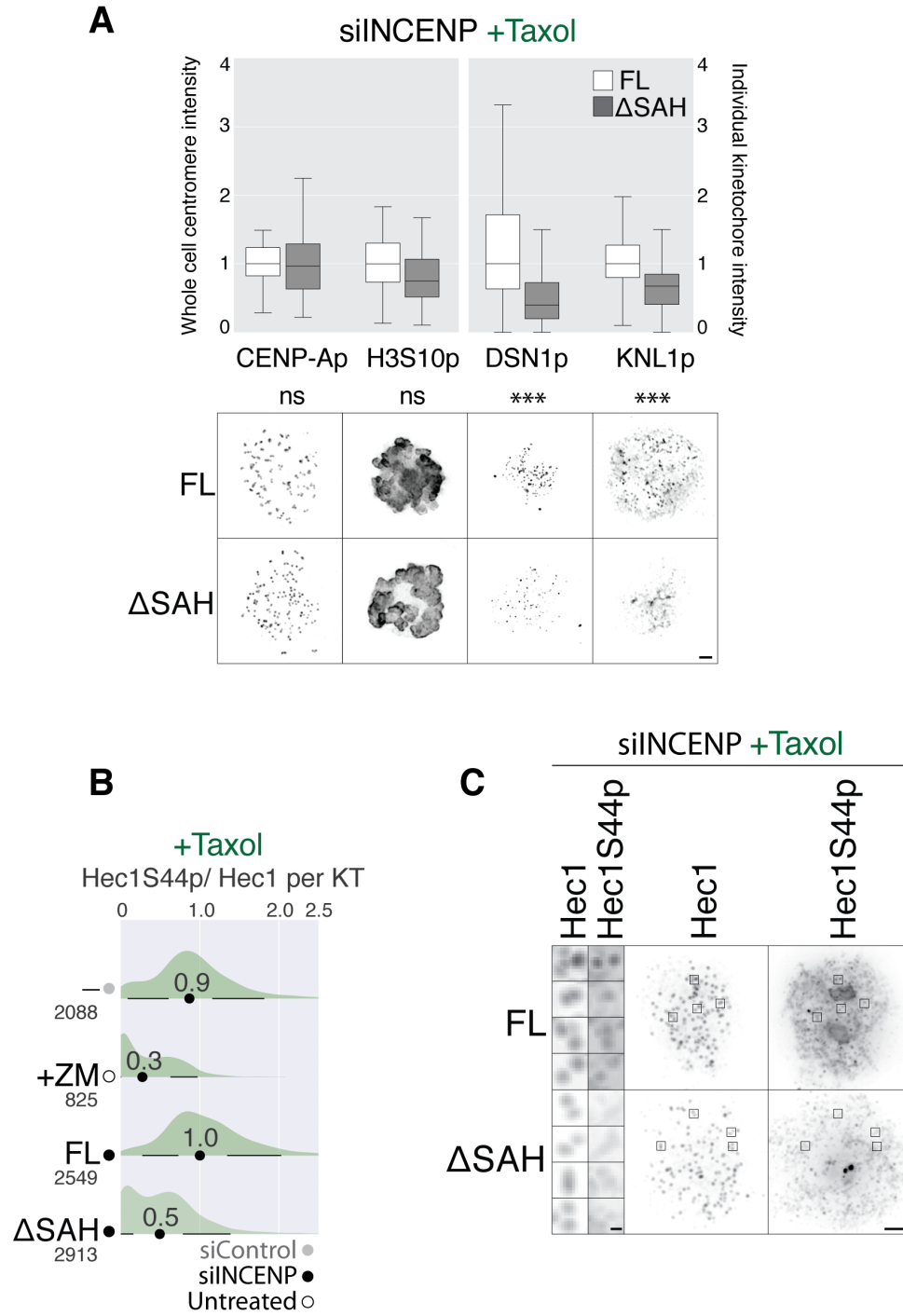


Figure 3-11: The hINCENP SAH domain is required for Aurora B-dependent kinetochore phosphorylation in taxol.

Neither cytoplasmic activation of Aurora B nor tethering INCENP to the centromere/kinetochore support a robust SAC

The observed reduction in Aurora B-dependent phosphorylation at the kinetochore may be due to defects in Aurora B catalytic activity or substrate accessibility. To address these possibilities, we first tested if artificial activation of Aurora B by forced dimerization could bypass the requirement of the SAH domain. As previously shown in *Xenopus* egg extracts (Tseng et al., 2010), replacing the SAH domain with the dimerization domain of GCN4 (hINCENP Δ SAH ∇ GCN4) dramatically increased the overall level of Aurora B auto-phosphorylation in human cells (**Figure 3-12A, B**). However, this construct mirrored hINCENP Δ SAH, failing to rescue the defect in CPC localization (**Figure 3-12C**) kinetochore phosphorylation (**Figure 3-12C**) and the SAC (**Figure 3-12D**). These results demonstrate that cytoplasmic activation of Aurora B is insufficient to support SAC maintenance and suggest that the SAH domain is not affecting the intrinsic activity of Aurora B.

Figure 3-12: Artificially activating Aurora B in the absence of the SAH domain is insufficient to support the taxol-mediated SAC.

A) Diagram of LAP-tagged hINCENP constructs in this figure. GCN4, leucine zipper dimerization domain of GCN4. CEN, centromere-targeting domain, which binds Survivin and Borealin; HP1, HP1-binding motif; SAH domain (blue); IN, IN-box, which binds Aurora B.

B) Western blot of anti-GFP immunoprecipitation of the indicated constructs from mitotic HeLa cell extract. Aurora Bph indicates activating phosphorylation on the Aurora B t-loop. Replacing the hINCENP SAH domain with the GCN4 dimerization domain stimulates Aurora B activation.

C) Immunofluorescence quantification of GFP, CENP-A S7ph, Dsn1 S100ph and BubR1 abundance at the centromere of cells expressing the indicated hINCENP construct in taxol following either knockdown of endogenous INCENP (siINCENP) or treatment with the Aurora B inhibitor ZM447439 (ZM). Expression of hINCENP Δ SAH ∇ GCN4 stimulates Aurora B activity, but does not rescue the defects in CPC localization (GFP), Aurora B-dependent phosphorylation (Dsn1 S100ph) or SAC protein recruitment (BubR1) from deleting the SAH domain (Δ SAH). Statistics are from a two-tailed Mann-Whitney t test, ns= not significant, * $p \leq 0.05$, ** $p \leq 0.01$, *** $p \leq 0.001$, $n \geq 25$ for each sample except ZM where $n=10$.

D) Duration of mitosis (DoM) for cells in taxol. Artificially activating Aurora B does not bypass the requirement for the hINCENP SAH domain.

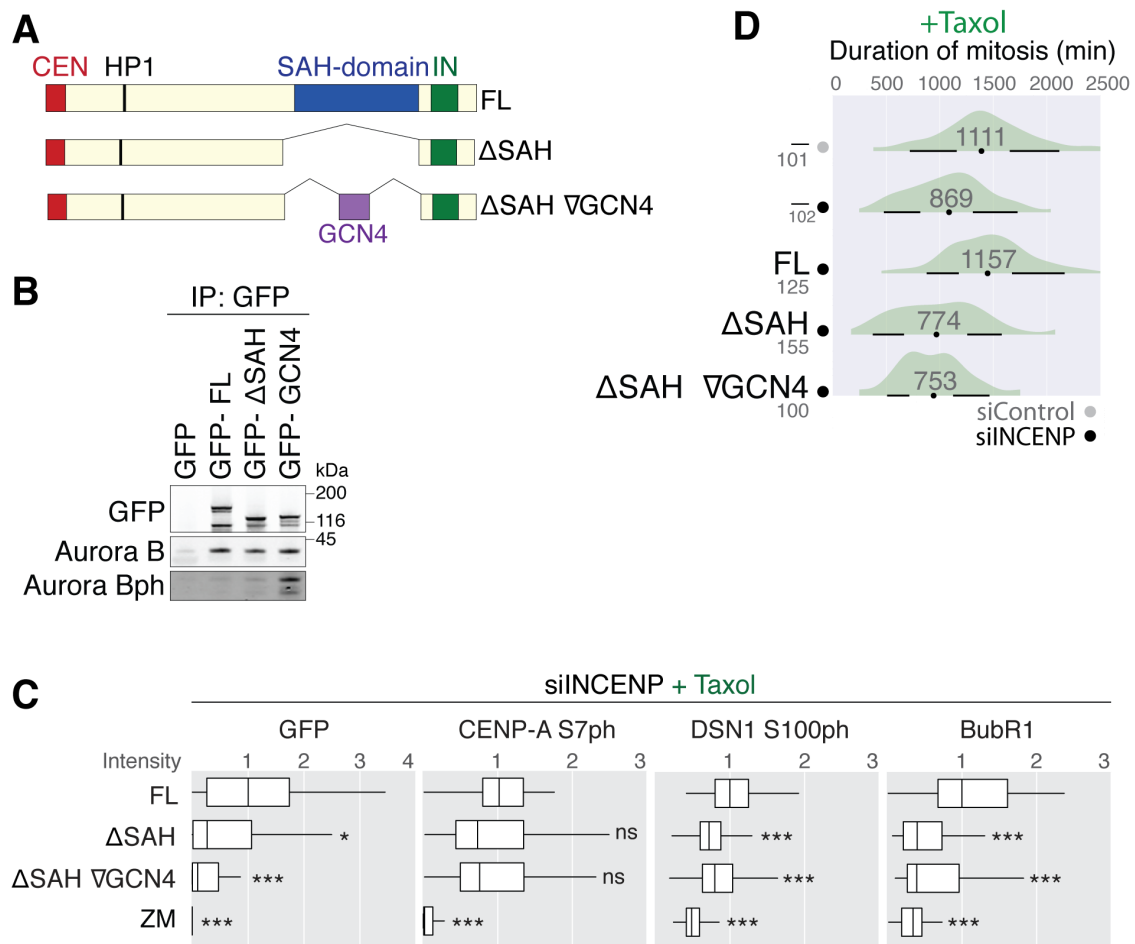


Figure 3-12: Artificially activating Aurora B in the absence of the SAH domain is insufficient to support the taxol-mediated SAC.

We next tested if tethering INCENP to the centromere or the kinetochore bypasses the requirement of the SAH domain. We generated HeLa T-REx lines where the N-terminal CEN-domain of INCENP was replaced with one of the following targeting modules: full length human Mis12 (Mis12-hINCENP Δ CEN) for kinetochore targeting, full length CENP-B (CB- hINCENP Δ CEN) for stable centromere targeting, or the CENP-B DNA binding domain (CB^{DBD}-hINCENP Δ CEN) for more dynamic centromere targeting (Liu et al., 2009; Wang et al., 2011a) (**Figure 3-13A**). We verified that these targeting chimeras localized as anticipated (**Figure 3-13B**). We then used siRNA to deplete endogenous INCENP, expressed the targeting chimeras, and monitored the DoM of these cells in taxol by live imaging (**Figure 3-14**). Surprisingly, we found that none of the INCENP targeting chimeras supported a robust SAC response in taxol. In fact, hINCENP Δ CEN had a significantly shorter DoM than cells treated with siINCENP alone, likely due to hINCENP Δ CEN sequestering Aurora B from any remaining endogenous INCENP supporting the checkpoint. Targeting INCENP to CENP-B chromatin or the kinetochore rescued the DoM relative to hINCENP Δ CEN, but was at best comparable to cells treated with siINCENP alone. This rescue was independent of the hINCENP SAH domain, as an identical set of targeting constructs lacking the SAH domain demonstrated a comparable rescue of the DoM in taxol (**Figure 3-15**). Thus, while targeting INCENP to the centromere or kinetochore cannot bypass the requirement for the CEN domain, it does stimulate the taxol-mediated SAC independent of the SAH domain.

Figure 3-13: Artificially targeting hINCENP to the centromere or kinetochore independent of the CEN domain.

A) Diagram of LAP-tagged hINCENP constructs. Mis12 (purple), full-length Mis12, a kinetochore protein; CB (orange), full-length CENP-B, a centromere protein; CD^{DBD}, CENP-B DNA binding domain, a fragment of CENP-B that binds the centromere but is more dynamic than the full-length protein. CEN, centromere-targeting domain, which binds Survivin and Borealin; HP1, HP1-binding motif; SAH domain (blue); IN, IN-box, which binds Aurora B.

B) Immunofluorescence visualizing the localization of constructs in A relative to CENP-A, a centromere marker. Each construct was expressed over endogenous INCENP. Constructs show the anticipated localization, with fusions to CENP-B and CENP-B^{DBD} associating with the centromere and fusions to Mis12 localizing to the kinetochore. Representative images are of a single cell (left) and a single kinetochore pair (right). GFP (green), CENP-A (purple); Scale bar (single cell), 2 μ m. Scale bar (centromere/kinetochore), 0.25 μ m

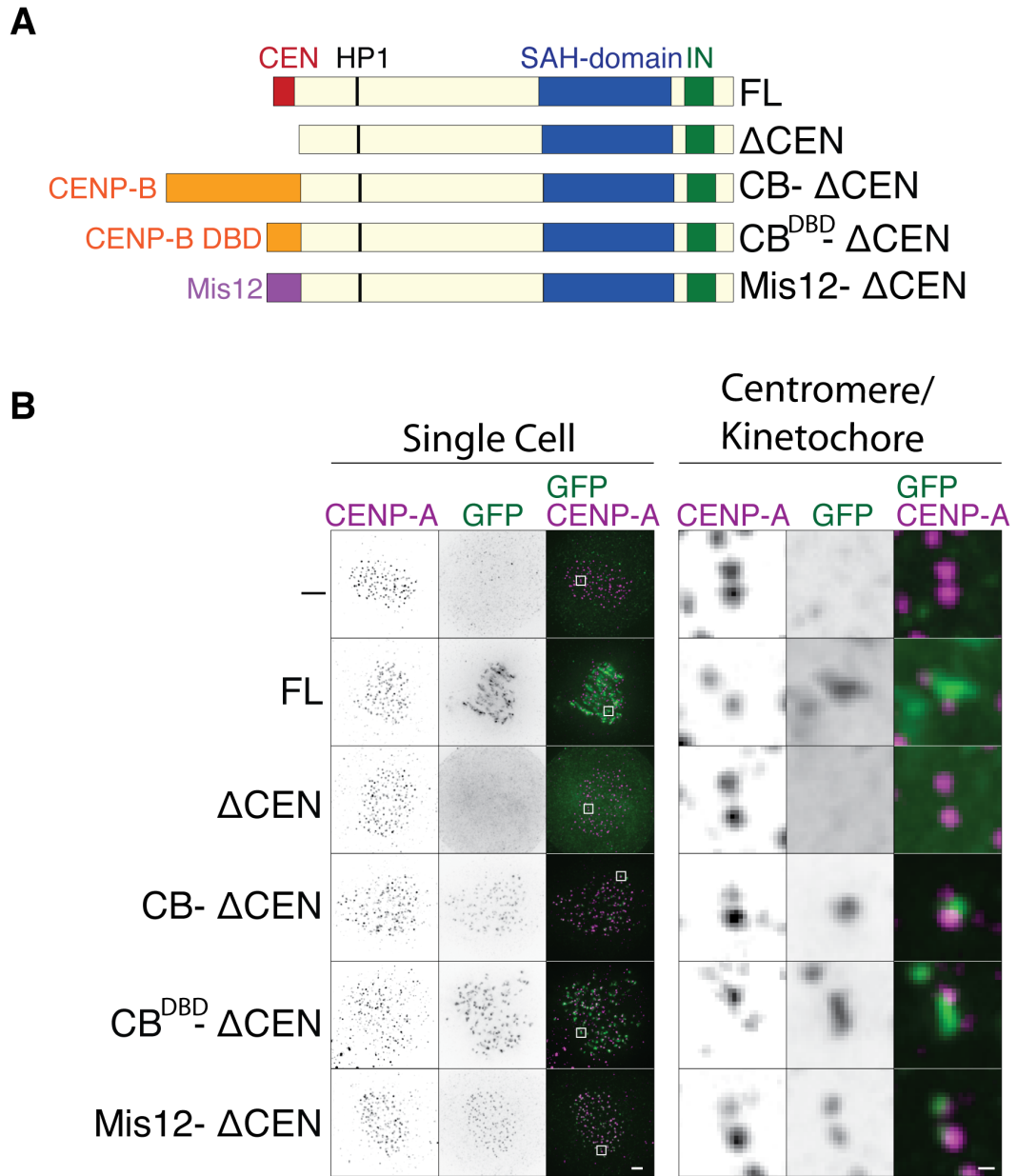


Figure 3-13: Artificially targeting hINCENP to the centromere or kinetochore independent of the CEN domain.

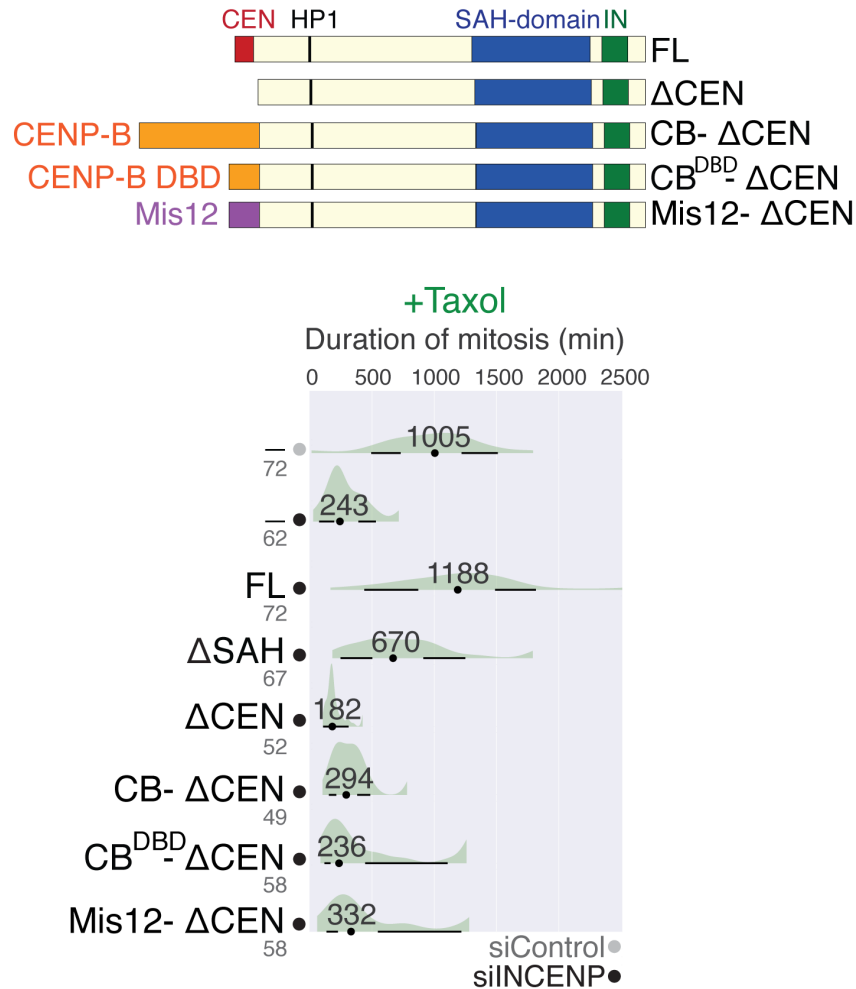


Figure 3-14: Targeting hINCENP to the centromere or kinetochore does not bypass the hINCENP CEN domain in the taxol-mediated SAC.

Duration of mitosis (DoM) for cells in taxol (bottom) expressing the indicated constructs (top) after treatment with Control siRNA (siControl) or INCENP siRNA (siINCENP). Deleting the CEN domain of INCENP greatly reduces the DoM in taxol and is only weakly rescued by artificially targeting this construct to the centromere (CENP-B fusions) or kinetochore (Mis12 fusion). Mis12, full-length Mis12, a kinetochore protein; CB, full-length CENP-B, a centromere protein; CB^{DBD}, CENP-B DNA binding domain, a fragment of CENP-B that binds the centromere but is more dynamic than the full-length protein

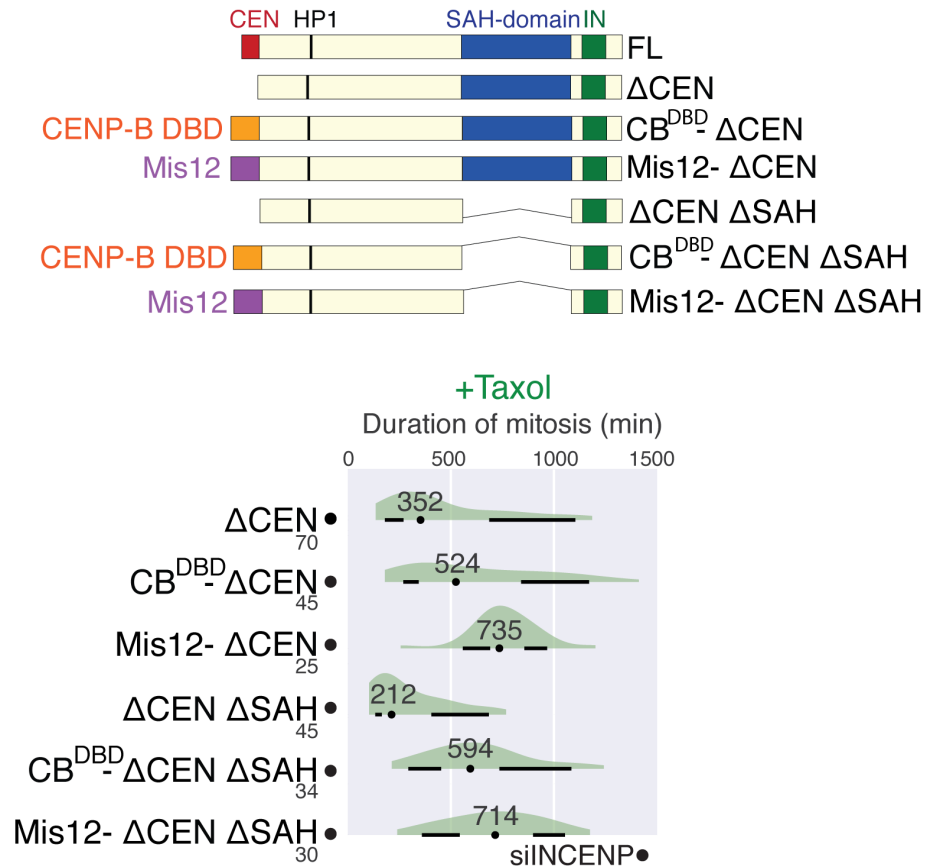


Figure 3-15: Targeting hINCENP to the centromere or kinetochore promotes the taxol-mediated SAC independent of the hINCENP SAH domain.

Duration of mitosis (DoM) for cells in taxol (bottom) expressing the indicated constructs (top) after treatment with INCENP siRNA (siINCENP). Deleting the CEN domain of INCENP reduces the DoM in taxol, but is partially rescued by targeting it to the centromere (CENP-B fusions) or kinetochore (Mis12 fusion). This rescue is independent of the hINCENP SAH domain. Mis12 (purple), full-length Mis12, a kinetochore protein; CB (orange), full-length CENP-B, a centromere protein; CD^{DBD}, CENP-B DNA binding domain, a fragment of CENP-B that binds the centromere but is more dynamic than the full-length protein. CEN, centromere-targeting domain, which binds Survivin and Borealin; HP1, HP1-binding motif; SAH domain (blue); IN, IN-box, which binds Aurora B.

Failure of these chimeric constructs to support the SAC was surprising, given that they are known to promote kMT destabilization and induce a mitotic delay when expressed in the presence of endogenous INCENP (Liu et al. 2009; Wang et al. 2011). To verify our constructs are not defective in these functions, we monitored the duration of this mitotic delay. We synchronized cells expressing these constructs at the G2/M transition with the Cdk inhibitor RO-3306, then released them into fresh media, at which point they synchronously entered mitosis (**Figure 3-16**). In cells expressing Mis12-hINCENP Δ CEN, 54% of cells arrested for at least 2 hr and 13% of cells arrested for at least 10 hr. This effect was independent of the SAH domain, as 56% and 19% of cells expressing Mis12-hINCENP Δ CEN Δ SAH arrested for at least 2 hr and 10 hr, respectively. This arrest was dependent on kinetochore targeting as 1% of cells expressing hINCENP Δ CEN and 0% of cell expressing hINCENP Δ CEN Δ SAH arrested for at least 10 hr. This result implies that the targeting construct can support Aurora B's function at the kinetochore independent of the SAH domain, at least in the presence of endogenous INCENP.

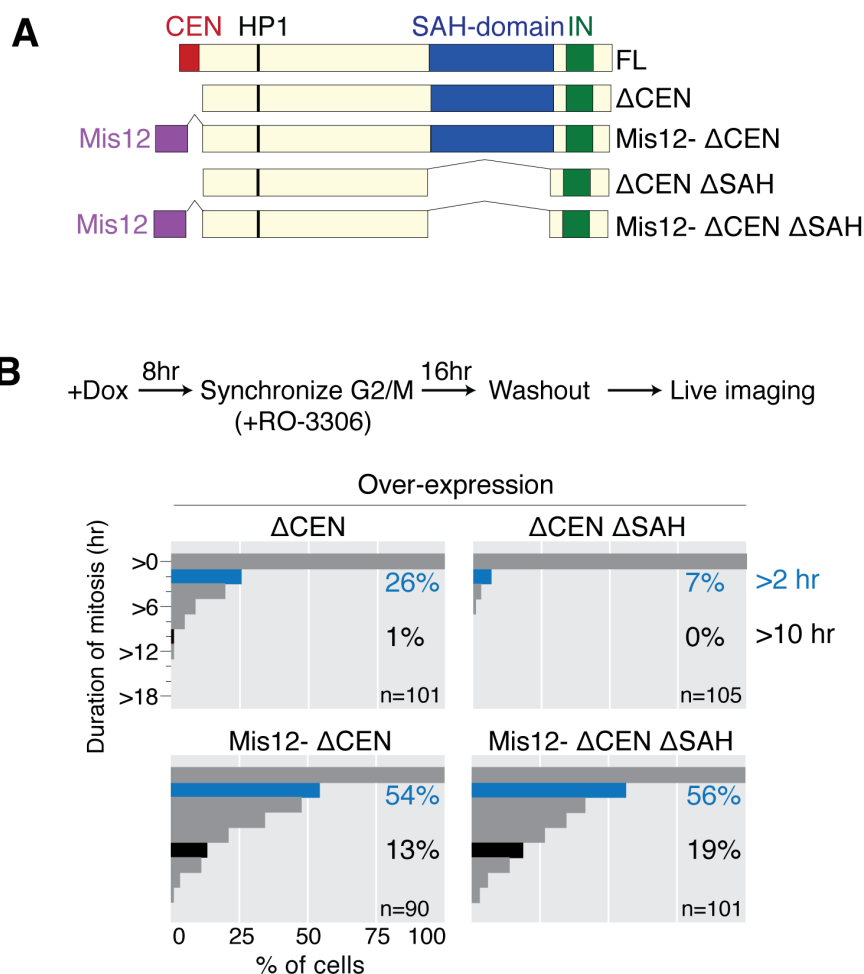


Figure 3-16: Targeting hINCENP to the kinetochore induces a prolonged mitotic delay independent of the SAH domain.

A) Diagram of LAP-tagged hINCENP constructs. Mis12 (purple), full-length Mis12, a kinetochore protein; CEN, centromere-targeting domain, which binds Survivin and Borealin; HP1, HP1-binding motif; SAH domain (blue); IN, IN-box, which binds Aurora B.

B) Cells were treated as indicated (top). Each construct was expressed over endogenous INCENP. Plots show the cumulative minimum duration of mitosis for each construct (bottom). Targeting hINCENP to the kinetochore induces a prolonged mitotic arrest independent of the SAH domain. Blue bars, arrested for at least 2h; black bars, arrested for at least 10h.

The SAH domain is a Cdk1-regulated microtubule-binding domain

Aurora B is critical in human cells for the SAC in the presence of microtubules (taxol, monastrol) (Hauf et al., 2003), but less important in the absence of microtubules (nocodazole) (Santaguida et al., 2011). Therefore, we wondered if the microtubule-binding capacity of the SAH domain contributes to the SAC. As a first step, we used *Xenopus* egg extract to test if a particular region of the SAH domain contributes to microtubule binding (**Figure 3-17A**). We found that 6Myc-tagged xSAH domain localized to the spindle with particular enrichment at the spindle poles. Using a series of sequential deletions, we mapped this spindle binding activity to the first ~100aa of the SAH domain. We also identified a shorter 35 aa deletion in the N terminus of the xSAH domain ($\Delta\text{SAH}^{\text{N}}$) that was unable to bind to the spindle. Thus, the N terminus of the *Xenopus* SAH domain binds the spindle, consistent with reports for the SAH domain of human and chicken (Samejima et al., 2015; van der Horst et al., 2015).

The enrichment of the xSAH domain at the spindle pole is distinct from that of xINCENP, which localizes along the entire spindle (Tseng et al., 2010) (**Figure 3-17B**). To identify elements flanking the SAH domain that might account for this difference, we aligned the protein sequence of 25 vertebrate INCENP homologs. We identified 4 putative Cdk-dependent phosphorylation sites ([S/T]P) upstream of the SAH domain and 2 sites downstream of the SAH domain that were widely conserved among vertebrates species; we named them phosphoregulatory domain (PRD) 1 and 2, respectively (**Figure 3-18**). Cdk-dependent

phosphorylation within the microtubule-binding region (MTBD) of the budding yeast INCENP homolog Sli15 is known to antagonize its association with the mitotic spindle (Pereira and Schiebel, 2003). While the Sli15 MTBD is distinct in amino acid composition from the vertebrate SAH domain, the C terminus of the MTBD aligns with the PRD1 containing four putative Cdk sites (**Figure 3-19**).

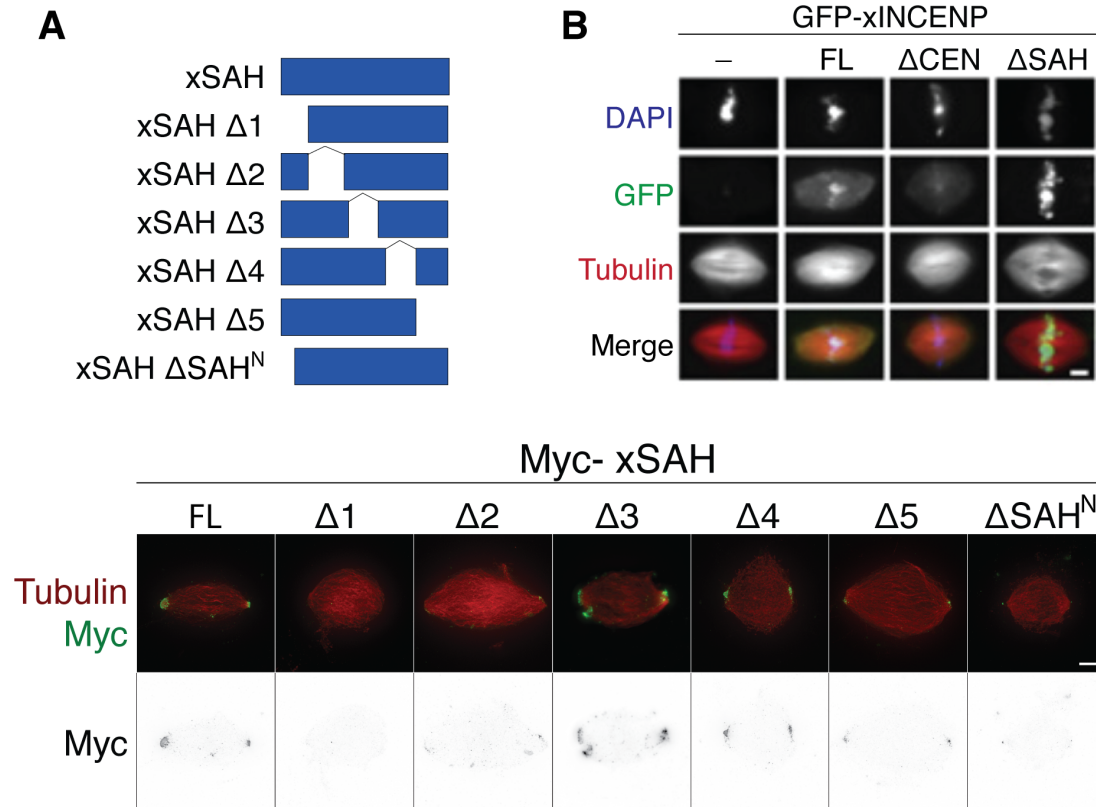


Figure 3-17: The xINCENP SAH domain associates with the spindle dependent on its N terminus in *Xenopus* egg extract.

A) Diagram of Myc-tagged xSAH domain constructs (left) and immunofluorescence (right) visualizing the indicated Myc-tagged constructs on the spindle in *Xenopus* egg extract. The xSAH domain associates with the spindle, with particular enrichment at the spindle poles, dependent on its N terminus. Tubulin (red), Myc (green); Scale bar, 5 μ m

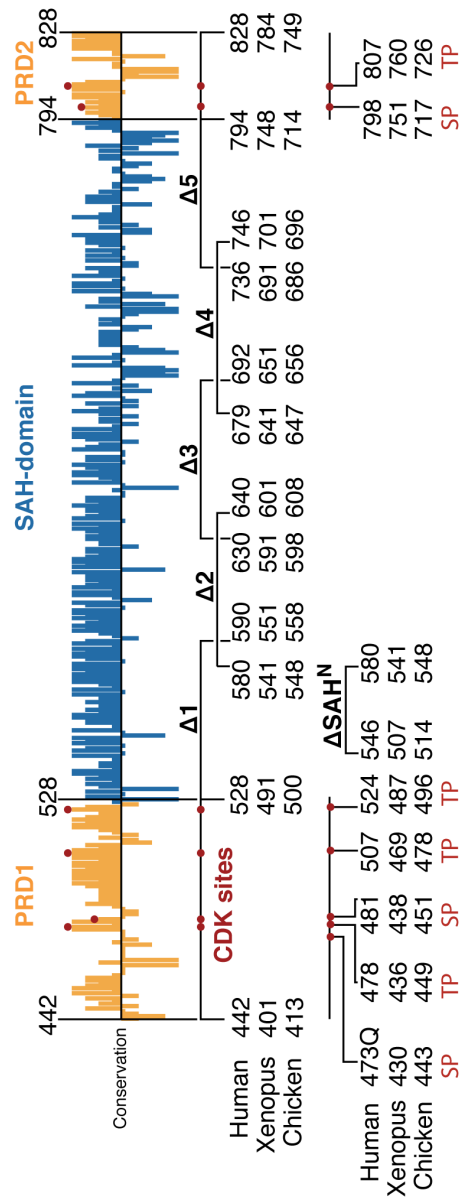
B) Immunofluorescence visualizing GFP-tagged full-length xINCENP (FL), xINCENP lacking the centromere targeting domain (xINCENP Δ CEN) or xINCENP lacking the SAH domain (xINCENP Δ SAH). xINCENP is uniformly distributed on the spindle. Tublin (red), GFP (green), DAPI (blue); reproduced from (Tseng et al. 2010).

Figure 3-18: Vertebrate INCENP contains six highly conserved putative Cdk1 phosphorylation sites flanking the SAH domain.

A) Conservation of each residue in PRD1, the SAH domain and PRD2 relative to the average conservation of residues in vertebrate INCENP (top). Conservation was determined using conSURF (Landau et al., 2005) with 25 vertebrate INCENP homologs. Putative Cdk sites conserved in at least 22 species are indicated (red circles). Deletions used to map xSAH domain microtubule binding are indicated.

B) Alignment of PRD1 and PRD2 among 25 vertebrate INCENP species. Alignment made using JalView 2.8.2 Tcoffee alignment with default settings. Putative Cdk sites (gray), cysteine (green), negatively charged residues (red) and positively charged residues (blue) are indicated.

A



B

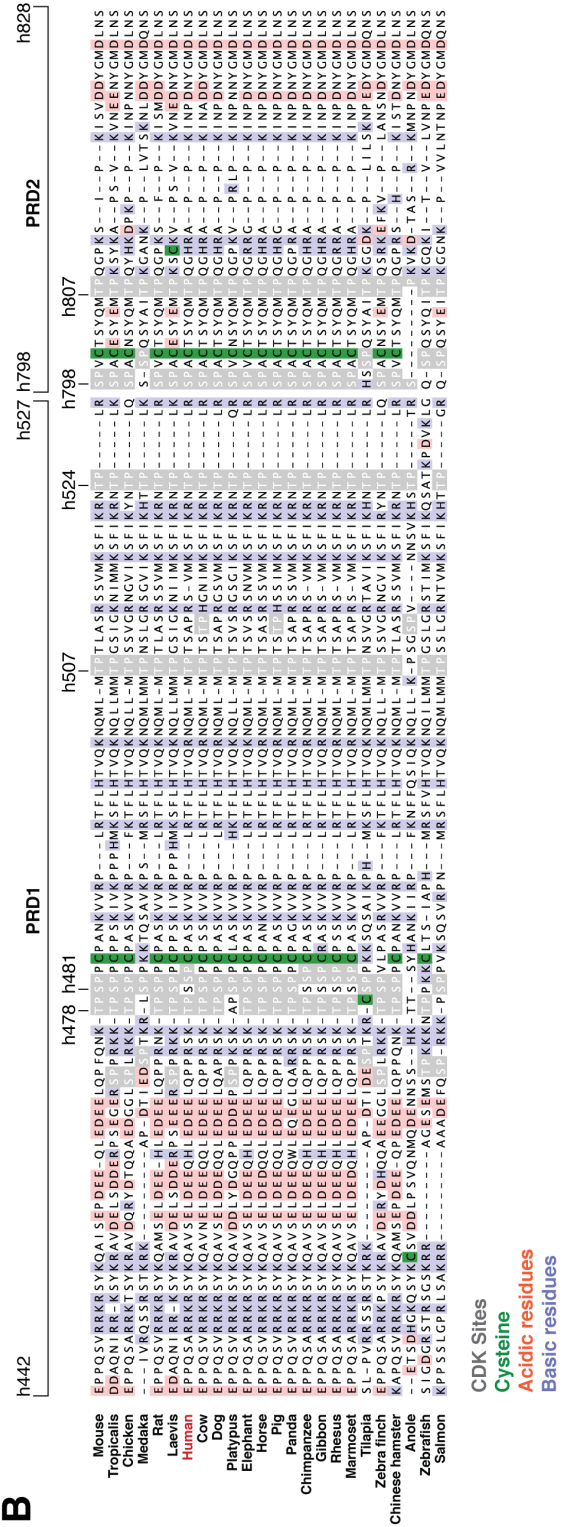
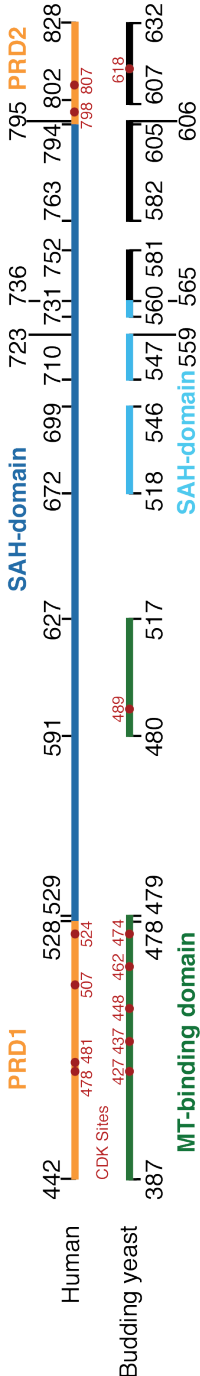


Figure 3-19: Alignment of human INCENP and the Budding yeast INCENP homolog Sli15.

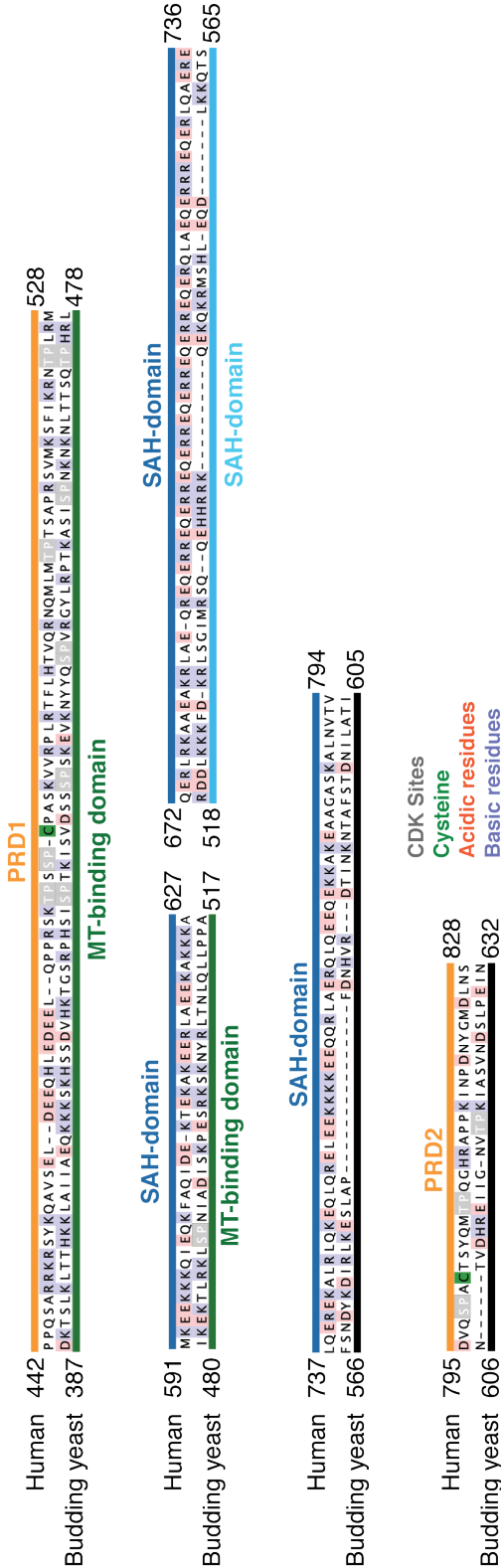
A) Diagrammatic representation of the alignment of the hINCENP PRD1 (yellow), SAH domain (dark blue) and PRD2 (yellow) with the budding yeast INCENP homolog Sli15. All gaps larger than 3aa are shown. The budding yeast microtubule-binding domain (green) and SAH domain (light blue) are indicated as well as putative Cdk1 sites ([S/T]P) in both species.

B) Alignment for select portions of A.

A



B



To determine if these putative Cdk-sites are phosphorylated in *Xenopus* egg extract, we prepared a larger fragment of the SAH domain encompassing PRD1 and PRD2 (PRD-xSAH), as well as versions where the six conserved putative Cdk sites, in addition to one SP site in PRD1 not conserved in humans, were made unphosphorylatable by mutation to alanine (PRD-xSAH 7A) or phosphomimetic by mutation to aspartic acid (PRD-xSAH 7D) (**Figure 3-20A**). These fragments were incubated in metaphase or interphase extracts, followed by treatment with or without phosphatases (**Figure 3-20B**). Western blot analysis demonstrates that the xSAH domain alone ran at a similar size regardless of cell cycle or phosphatase treatment. The PRD-xSAH fragment, which contains 24 serine/threonine residues including the putative Cdk sites, ran as a smear that collapsed to a single band upon phosphatase treatment, indicative of phosphorylation. Consistent with phosphorylation of the conserved [S/T]P residues being responsible for the majority of the observed mobility shift, the PRD-xSAH 7D fragment ran at the same size as the upper smear of PRD-xSAH and the PRD-xSAH 7A mutant ran at a similar size to the PRD-xSAH upon phosphatase treatment. The mobility shift of the PRD-xSAH fragment was greatly reduced in interphase, indicating cell cycle-dependent phosphorylation of these sites as expected for a Cdk substrate.

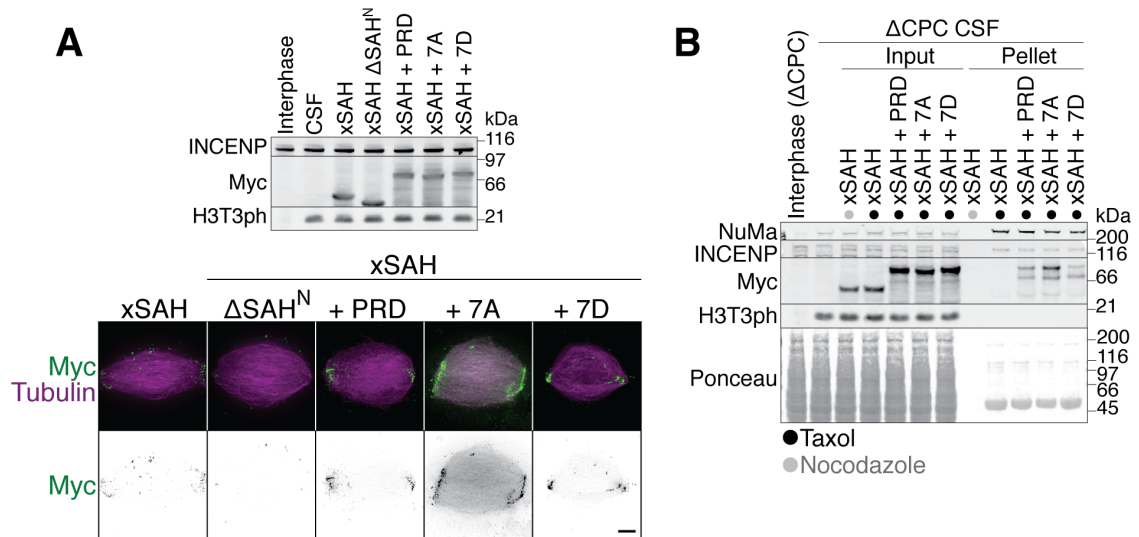


Figure 3-20: Phosphorylation of the PRD regulates xINCENP SAH domain binding to the spindle in *Xenopus* egg extract.

A) Immunofluorescence visualizing the indicated Myc-tagged constructs on the mitotic spindle in *Xenopus* egg extract. Western blot shows equal protein expression. Binding of the xSAH domain to the mitotic spindle is enhanced by making seven putative Cdk1 sites in the PRD unphosphorylatable (xSAH+7A). Tubulin (purple), Myc (green), Scale bar, 5 μ m

B) Microtubule pelleting assay with the indicated constructs following depletion of endogenous INCENP. Extract was incubated with nocodazole (a gray circle) or taxol (black circles) for 30 min, pelleted through a glycerol cushion, washed and resuspended for western blot. Inclusion of the PRD in the xSAH domain fragment enhances co-sedimentation with microtubules. This is further enhanced by making seven putative Cdk1 sites in the PRD unphosphorylatable (xSAH+7A). xNuMa, a microtubule binding protein, Ponceau, showing enrichment of protein(s) at the appropriate size for tubulin.

To determine if phosphorylation of the region flanking the SAH domain regulates microtubule binding, the M-phase localization of the PRD-xSAH fragments was assessed by immunofluorescence. While the SAH domain only weakly bound the spindle pole, the PRD-xSAH 7A mutant was highly enriched on the mitotic spindle and spindle pole (**Figure 3-21A**). The PRD-xSAH 7D mutant and the PRD-xSAH fragment localized to the spindle pole only slightly better than the xSAH domain alone.

To biochemically measure the microtubule binding activity of our SAH domain fragments, microtubule co-sedimentation assays were performed in M-phase extract (**Figure 3-21B**). The PRD-xSAH fragments, but not the xSAH domain alone, co-sedimented with taxol-stabilized microtubules, confirming that the regions flanking the SAH domain enhance microtubule binding. The PRD-xSAH 7A fragment exhibited an additional two-fold increase in sedimentation with microtubules compared to PRD-xSAH, which bound similar to PRD-xSAH 7D. These results indicate that the PRD and SAH domain promote microtubule binding, which is negatively regulated by Cdk-dependent phosphorylation at the PRD.

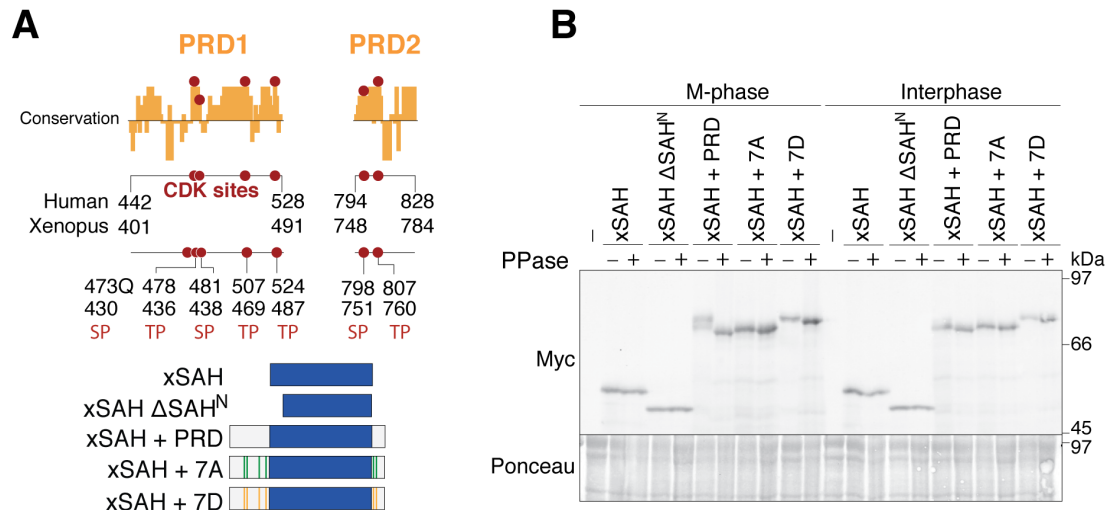


Figure 3-21: The xINCENP SAH domain is phosphorylated on the PRD in a cell-cycle-dependent manner in *Xenopus* egg extract.

A) Conservation of each residue in PRD1 and PRD2 relative to the average conservation of residues in INCENP (top). Conservation was determined using conSURF (Landau et al., 2005) with 25 vertebrate INCENP homologs. Putative Cdk sites conserved in at least 22 species are indicated (red circles). Diagrams of 6Myc-tagged constructs used in B (bottom).

B) Western blot visualizing the cell-cycle-dependent mobility shift of various Myc-tagged xSAH domain constructs. Samples were either taken from extract (-) or diluted in buffer containing lambda phosphatase and incubated at 30 °C for 40 min (+). The xSAH domain containing the PRD exhibits a phosphatase-sensitive mobility shift in M-phase. This shift is reduced by mutating seven putative Cdk1 sites in the PRD to alanine, making them unphosphorylatable, or by incubating the construct in interphase.

To determine if the PRD also regulates the microtubule binding of xINCENP, we generated versions of full length GFP-xINCENP containing the phospho-null (xINCENP 7A) and phospho-mimetic (xINCENP 7D) mutations either alone or in combination with the 35 aa deletion that attenuates xSAH domain microtubules binding (Δ SAH^N). Metaphase Δ CPC extracts were reconstituted with CPC containing these INCENP constructs and the microtubule co-sedimentation assay was performed (**Figure 3-22A**). As expected, xINCENP demonstrated robust microtubule binding. This was dependent on the N terminus of the SAH domain as neither xINCENP Δ SAH nor xINCENP Δ SAH^N co-sedimented with microtubules. xINCENP 7A showed an almost two-fold increase in microtubule binding, while xINCENP 7D co-sedimented similar to xINCENP. Incorporating Δ SAH^N into INCENP 7A abrogated microtubule binding, suggesting that the PRD is insufficient to bind microtubules in the absence of the SAH.

To determine if phosphorylation of the PRD regulates microtubule-dependent Aurora B activation (Tseng et al., 2010), we incubated reconstituted extracts with taxol to stabilize microtubules and monitored Aurora B auto-phosphorylation by western blot (**Figure 3-22B**). While xINCENP and xINCENP 7A demonstrated robust Aurora B auto-phosphorylation, deleting the microtubule-binding region of the SAH domain (xINCENP Δ SAH, Δ SAH^N, or 7A Δ SAH^N) or xINCENP 7D prevented activation of Aurora B. Thus, the SAH^N region and dephosphorylation of the PRD are required for microtubule-dependent activation of Aurora B.

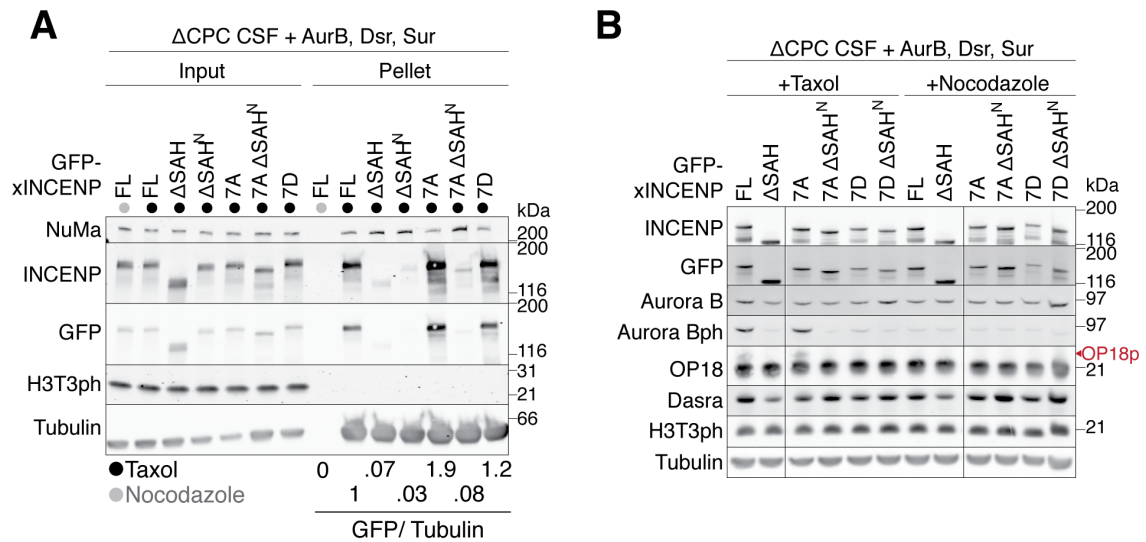


Figure 3-22: Phosphorylation of the PRD regulates xINCENP binding to microtubules and Aurora B activation.

A) Microtubule pelleting assay in extract reconstituted with the indicated GFP-xINCENP construct. Extract was incubated with nocodazole (a gray circle) or taxol (black circles) for 30 min, pelleted through a glycerol cushion, washed and resuspended for Western blot. Normalized quantitation of pelleted GFP-xINCENP constructs is shown at the bottom. The N terminus of the xINCENP SAH domain supports binding to microtubules. This binding is enhanced by making the putative Cdk1 sites in the xINCENP PRD unphosphorylatable (xINCENP 7A).

B) Western blot visualizing the microtubule-dependent activation of Aurora B. Extract was reconstituted with the indicated constructs, and then incubated in the presence of the indicated drug for 40 min. Aurora B activation is monitored by the appearance of OP18 hyperphosphorylation (OP18ph, red) and phosphorylation of the Aurora B activation loop (Aurora Bph). Taxol stimulated Aurora B activation, but not when the putative Cdk1 sites in the xINCENP PRD were made unphosphorylatable (xINCENP 7A). This is specific to the presence of microtubules as Aurora B remained inactive in nocodazole.

ΔCPC= CPC depletion. AurB= MBP_x-Aurora B protein, Dsr= xDasra A, Sur= xSurvivin mRNA

The SAH domain binds microtubules to maintain the SAC in taxol-treated cells

In *Xenopus* egg extract, the SAH domain can be functionally replaced with an exogenous microtubule-binding domain for its role in spindle assembly (Tseng et al., 2010). We adopted a similar strategy to determine if the SAH domain binds microtubules to sustain the SAC in taxol-treated HeLa cells. We replaced the SAH domain with the microtubule-binding domain from MAP4 (hINCENP Δ SAH ∇ MAP4; **Figure 3-23A**) and confirmed that this targeted hINCENP to both microtubules and chromatin by immunofluorescence (**Figure 3-23B**). While the median DoM for hINCENP Δ SAH in taxol was 10.9 hr, hINCENP Δ SAH ∇ MAP4 partially rescued this defect with a median DoM of 13.6 hr (**Figure 3-23C**), suggesting that the SAH domain supports the SAC through microtubule-binding.

Given that the SAH domain interacts with both chromatin and microtubules, we sought to more precisely disrupt microtubule binding. We deleted the 35 aa in the N terminus of the INCENP SAH domain required for microtubule binding in *Xenopus* (hINCENP Δ SAH^N). While hINCENP had a median DoM of 16.6 hr, hINCENP Δ SAH^N arrested for only 12.9 hr (**Figure 3-23A**). Three lines of evidence indicate that this defect was due to attenuated microtubule-binding activity, rather than a defect in chromatin binding. First, replacing the N terminus of the SAH domain with the MAP4-MTBD (hINCENP Δ SAH^N ∇ MAP4) completely rescued the SAC defect (**Figure 3-23A**). Second, while hINCENP Δ SAH^N was defective in recruitment of BubR1 to the kinetochore,

consistent with its checkpoint defect, its abundance at the centromere was indistinguishable from full-length hINCENP (**Figure 3-23D**). Finally, two larger deletions in the SAH domain downstream of the microtubule-binding region produced only minor defects in DoM relative to full-length hINCENP (**Figure 3-24**).

Figure 3-23: The hINCENP SAH domain binds microtubules to support the taxol-mediated SAC in HeLa cells.

- A)** LAP-tagged hINCENP constructs. MTBD, microtubule-binding domain from MAP4; CEN, centromere-targeting domain, which binds Survivin and Borealin; HP1, HP1-binding motif; SAH domain (blue); IN, IN-box, which binds Aurora B.
- B)** Immunofluorescence of hINCENP Δ SAH ∇ MAP4 expressed over endogenous INCENP in asynchronous cells. GFP signal (hINCENP) can be detected at the centromere (Hec1) and on the mitotic spindle (Tubulin).
- C)** Duration of mitosis (DoM) for cells in taxol. Red values are the percent cell death for each construct. Deleting the SAH domain (Δ SAH) or the N terminus of the SAH domain (Δ SAH^N), which is required for microtubule binding in xINCENP, attenuates the DoM in taxol and promotes mitotic slippage. These defects are rescued by inserting the microtubule-binding region from MAP4 into the deleted region in hINCENP.
- D)** Immunofluorescence quantification of GFP-INCENP, CENP-A S7ph, Dsn1 S100ph and BubR1 abundance at the centromere of cells expressing the indicated hINCENP construct in taxol following either knockdown of endogenous INCENP or treatment with the Aurora B inhibitor ZM447439 (ZM). A minimal deletion in the microtubule-binding region of INCENP (Δ SAH^N) does not affect GFP-INCENP localization, but is still defective in the checkpoint (C) and recruitment of the SAC protein BubR1. Statistics are from a two-tailed Mann-Whitney t test, ns= not significant, * $p \leq 0.05$, ** $p \leq 0.01$, *** $p \leq 0.001$, $n \geq 25$ for each sample except ZM where $n=10$.

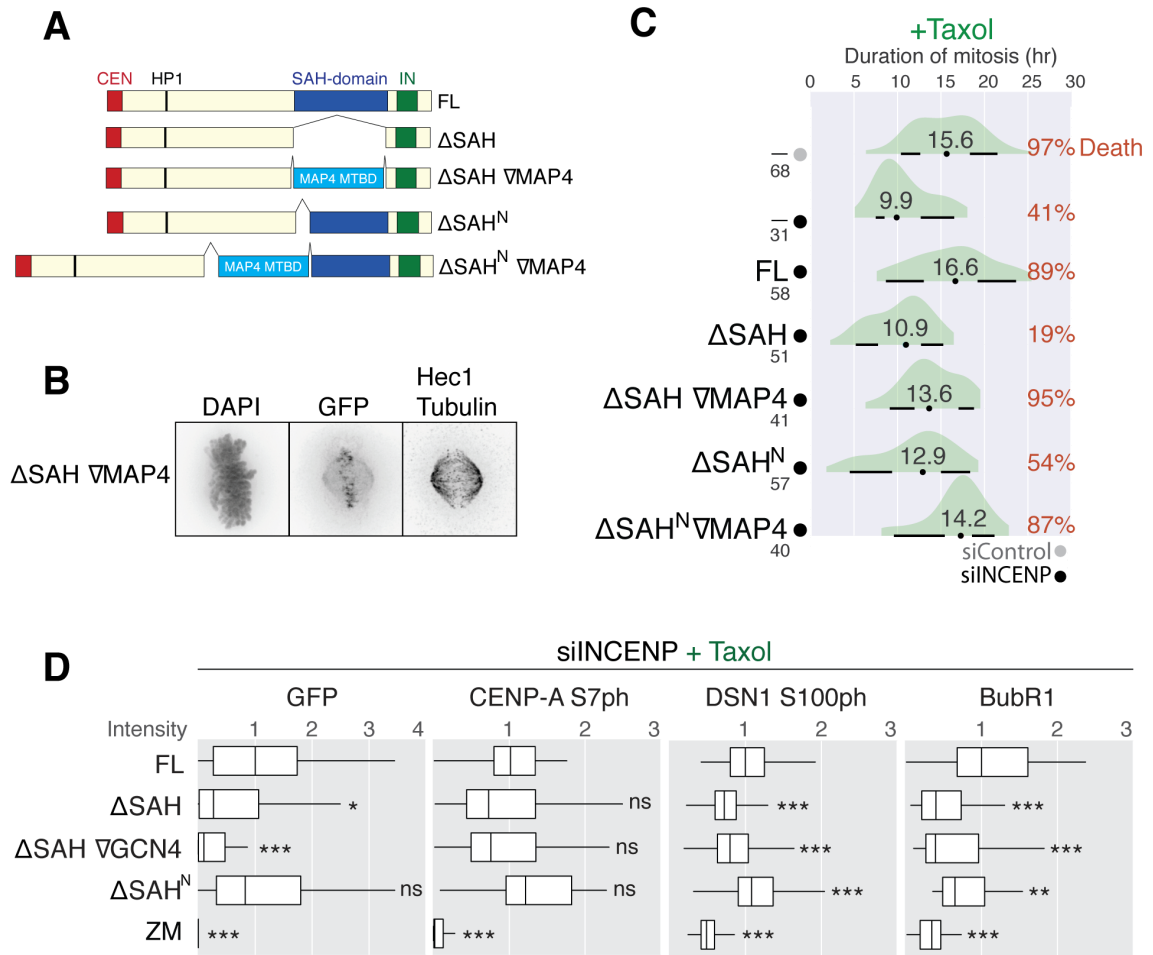


Figure 3-23: The hINCENP SAH domain binds microtubules to support the taxol-mediated SAC in HeLa cells.

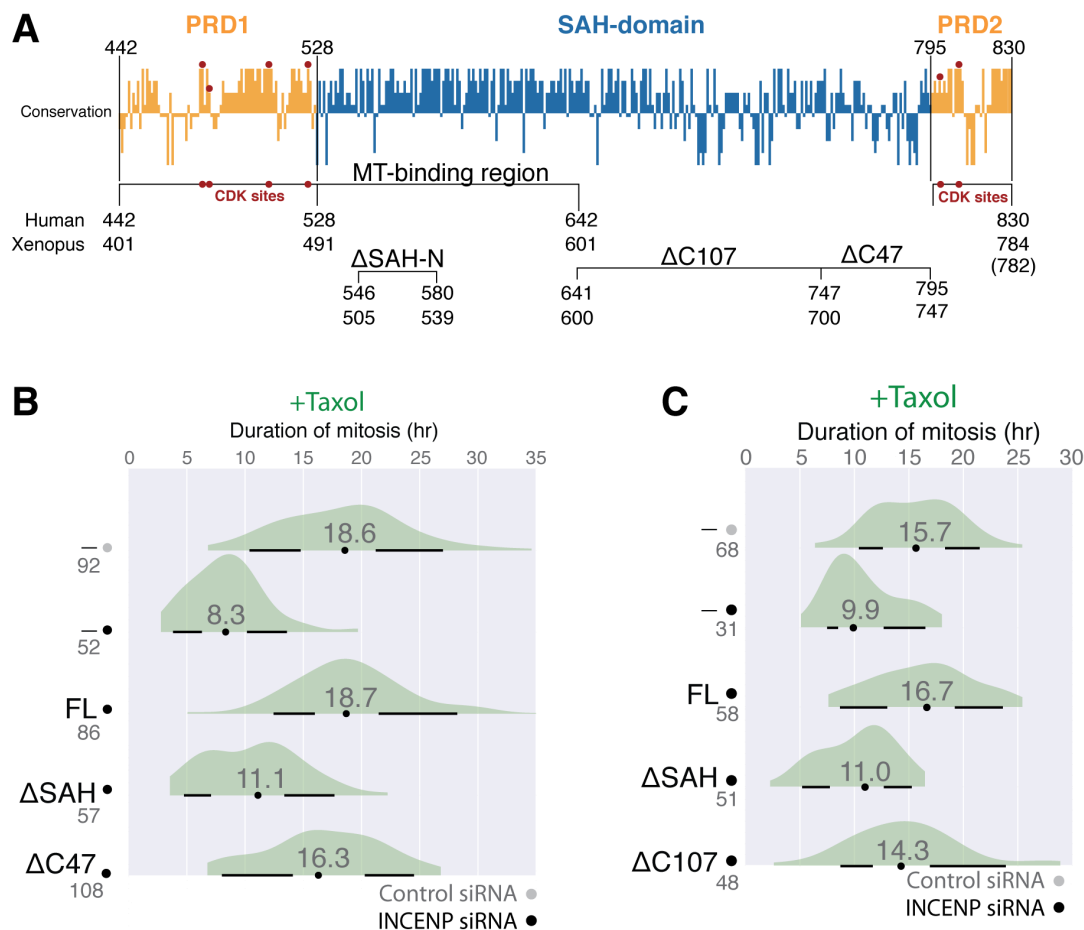


Figure 3-24: The C terminus of the hINCENP SAH domain is dispensable for the taxol-mediated SAC in HeLa cells.

A) Deletions in the hINCENP SAH domain used in B and C. Conservation of each residue in PRD1, the SAH domain and PRD2 relative to the average conservation of residues in vertebrate INCENP (top). Conservation was determined using conSURF (Landau et al., 2005) with 25 vertebrate INCENP homologs. Putative Cdk sites conserved in at least 22 species are indicated (red circles).

B, C) Duration of mitosis (DoM) for cells in taxol. Compared to deletion of the entire SAH domain (Δ SAH), deletion of 107aa (B; Δ C107) or 47aa (C; Δ C47) outside the microtubule-binding region shows only a minor defect in the DoM compared to full-length hINCENP (FL).

Next, we wanted to determine if the hINCENP PRD regulates microtubule-binding of the CPC and whether this binding was necessary for the taxol-mediated SAC in human cells. We generated unphosphorylatable (hINCENP 6A) and phospho-mimetic hINCENP (hINCENP 6D) and measured the DoM of cells expressing these constructs in taxol while simultaneously monitoring their distribution on chromatin (**Figure 3-25A, B**). hINCENP 6A supported a robust SAC arrest (17 hr) similar to hINCENP FL (19.3 hr), while hINCENP 6D prematurely silenced the checkpoint (13.5 hr). While all INCENP constructs appeared as foci on RFP-H2B chromatin, a subset of hINCENP 6A expressing cells had additional signal outside of chromatin, consistent with binding to taxol-stabilized microtubules (**Figure 3-25B**). We confirmed this by expressing these constructs over endogenous INCENP in taxol-treated cells and visualizing their distribution by immunofluorescence (**Figure 3-25C**). These observations suggest that phosphorylation of the hINCENP PRD regulates microtubule binding and the taxol-mediated SAC in human cells.

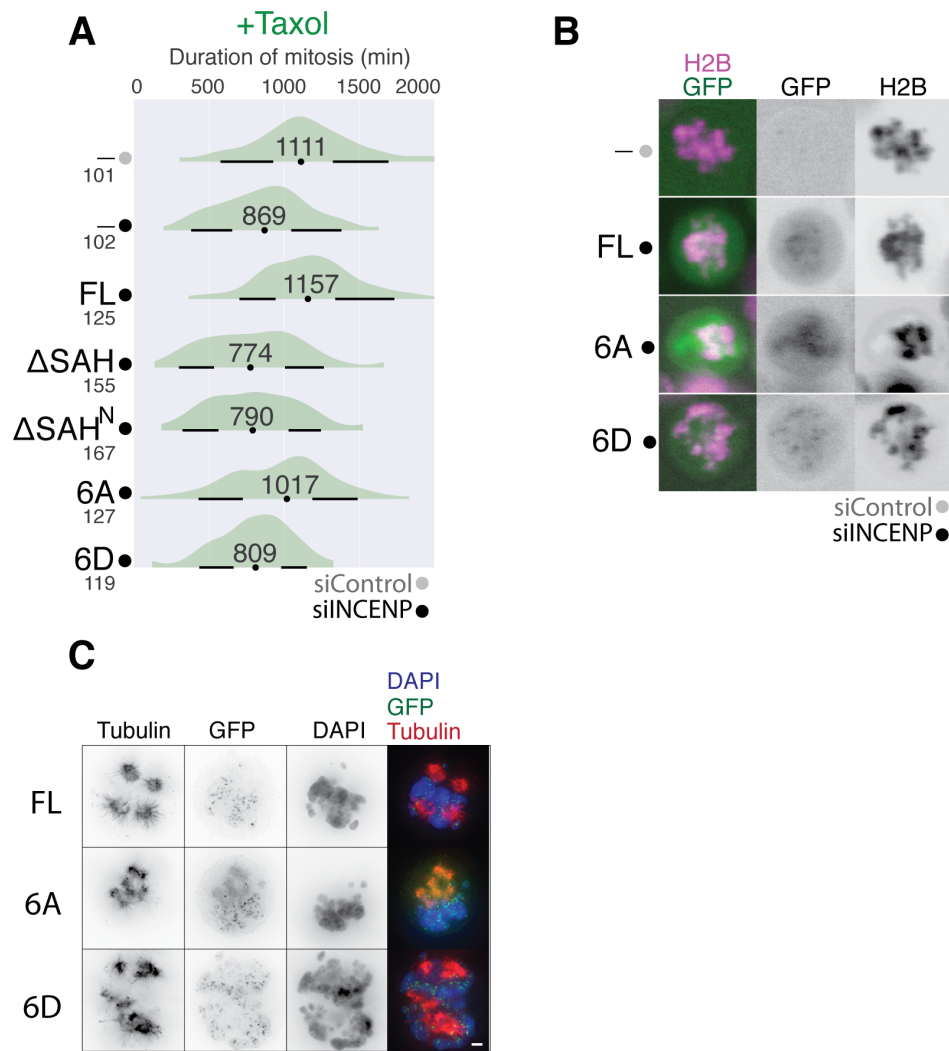


Figure 3-25: Phosphorylation of the hINCENP PRD regulates hINCENP microtubule binding and the taxol-mediated SAC in HeLa cells.

A) Duration of mitosis (DoM) for cells in taxol. Mutating six putative Cdk1 sites in the hINCENP PRD to mimic constitutive phosphorylation (6D) attenuates the SAC relative to making them unphosphorylatable by mutation to alanine (6A).

B) Immunofluorescence of the indicated constructs expressed over endogenous INCENP in taxol. hINCENP 6A enhances hINCENP spindle-binding relative to hINCENP or hINCENP 6D. Tubulin (red), GFP (green), DAPI (blue); Scale bar, 2 μ m

We then asked if targeting hINCENP to microtubules could support the SAC independently of chromatin binding. We mutated the putative Cdk1-sites in the PRD of hINCENP Δ CEN to tune INCENPs microtubules binding affinity (**Figure 3-26A**) and measured the ability of these constructs to support the taxol-induced SAC following depletion of endogenous INCENP with siRNA (**Figure 3-26B**). As we saw previously, expression of hINCENP Δ CEN reduced the median DoM relative to INCENP siRNA alone from 8.6 hr to 4.3 hr. hINCENP Δ CEN 6A localized to the mitotic spindle and increased the DoM to 5.8 hr. This was dependent on microtubule-binding, as the same construct with a deletion in the N terminus of the SAH domain (hINCENP Δ CEN 6A Δ SAH^N) failed to bind the spindle and didn't enhance the DoM (4 hr). Furthermore, hINCENP Δ CEN 6D, which localized only weakly to the mitotic spindle, had a median DoM identical to hINCENP Δ CEN. Taken together, these results indicate that targeting INCENP to the mitotic spindle can contribute to SAC maintenance independent of binding to chromatin, though it may be insufficient to fully support the SAC without centromere targeting.

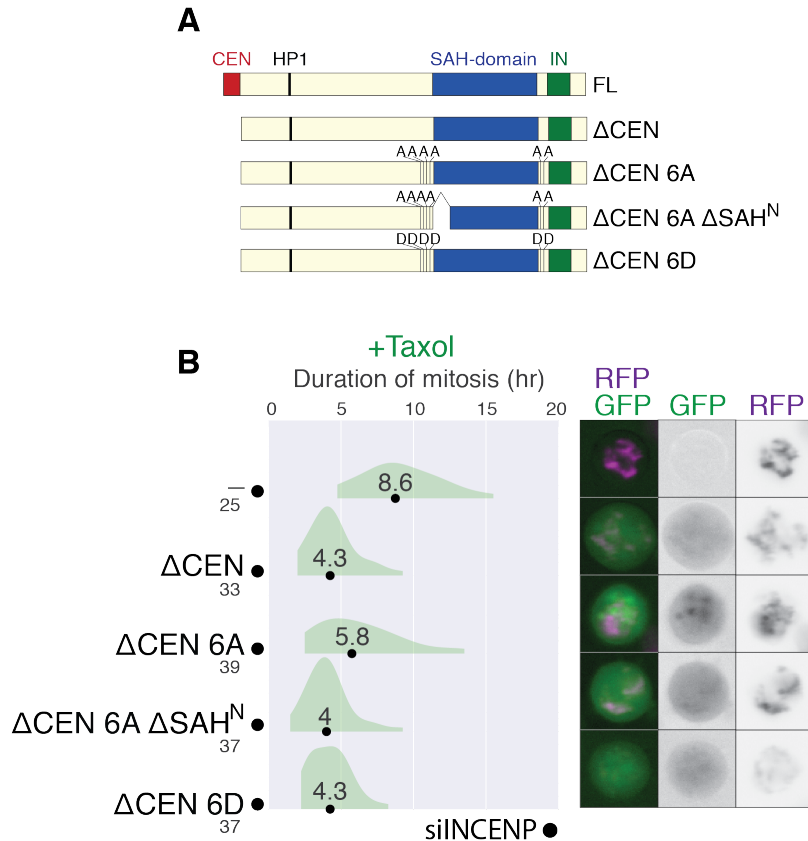


Figure 3-26: Targeting hINCENP to microtubules supports the taxol-mediated SAC independent of centromere targeting.

A) LAP-tagged hINCENP constructs. Mutation of six putative Cdk1 sites in the hINCENP PRD to alanine (6A) or glutamic acid (6D) is indicated. CEN, centromere-targeting domain, which binds Survivin and Borealin; HP1, HP1-binding motif; SAH domain (blue); IN, IN-box, which binds Aurora B

B) Duration of mitosis (DoM) for cells in taxol (left) and representative immunofluorescence images from the live imaging experiment (right). Deleting the centromere-targeting domain of hINCENP (ΔCEN) prevents binding to chromatin and reduces the DoM relative to cells treated with INCENP siRNA alone (siINCENP). hINCENP ΔCEN 6A enhances binding to the spindle and increases the DoM. Deleting the microtubule-binding region of this construct (ΔCEN 6A ΔSAH^N) reduces spindle-binding and mitigates the increase in the DoM over hINCENP ΔCEN. INCENP (green), RFP-H2B (purple).

If the SAH domain supports the SAC in taxol by binding microtubules, it should be dispensable for the SAC when microtubules are depolymerized by nocodazole. We tested this by measuring the DoM of cells expressing hINCENP-FL or hINCENP Δ SAH in a concentration of nocodazole previously published to depolymerizes all microtubules (Santaguida et al. 2011) (**Figure 3-27A**). While hINCENP Δ SAH had a 12% reduction in DoM relative to hINCENP-FL, this was substantially less than the 50% reduction we observed in taxol or monastrol. We also performed immunofluorescence to measure the amount of Aurora B substrate phosphorylation and checkpoint protein recruitment at the kinetochore (**Figure 3-27B, C**). Where as cells expressing hINCENP Δ SAH had over a 50% reduction in BubR1 and Dsn1 S100ph in taxol relative to hINCENP, we observed comparable levels of both epitopes between these constructs in nocodazole. We also observed a partial rescue of Hec1 S44ph in nocodazole, though the levels of Bub1 and Knl1 S24ph we observed in taxol were relatively unchanged by treatment with nocodazole. These defects may be due to the contribution of the SAH domain to CPC localization, rather than its role in microtubule binding. Taken together, is consistent with both chromatin- and microtubule-binding of INCENP promoting the SAC in human cells.

Figure 3-27: The hINCENP SAH domain is mostly dispensable for the SAC, SAC protein recruitment and kinetochore phosphorylation in nocodazole.

A) Duration of mitosis (DoM) for cells in nocodazole. The DoM of cells expressing hINCENP lacking the SAH domain (Δ SAH) is reduced by 12% relative to full-length hINCENP (FL), compared to a 40% reduction in taxol (**Figure 3-8**). Red values are the percent cell death for each construct.

B) Immunofluorescence quantification (top) and representative images (bottom) of SAC proteins and Aurora B-dependent phosphorylation in nocodazole-treated cells expressing hINCENP (FL) or hINCENP lacking the SAH domain (Δ SAH) following treatment with INCENP siRNA (siINCENP). Whole cell integrated intensity was quantified for the SAC proteins Bub1 and BubR1, with $n \geq 20$ cells per sample. Individual kinetochore intensity was quantified for Aurora B-dependent phosphorylation of Dsn1 S100ph and Knl1 S24ph using a kinetochore marker with $n \geq 1800$ individual kinetochores per sample. Representative images approximate the median, two-tailed Mann-Whitney t test, ns=not significant, * $p \leq 0.05$, ** $p \leq 0.01$, *** $p \leq 0.001$, Scale bar, 2 μ m

C) Immunofluorescence quantification of Aurora B-dependent phosphorylation of Hec1 (Hec1 S44ph) at individual kinetochores in nocodazole, standardized to total Hec1 at that kinetochore. n-values are indicated under the sample name. ZM, the Aurora B inhibitor ZM447439.

D) Representative images from C. A cell of representative intensity (right) and a zoom in of four representative kinetochore pairs (left). Scale bar (whole cell), 2 μ m, Scale bar (kinetochore pair), 0.25 μ m

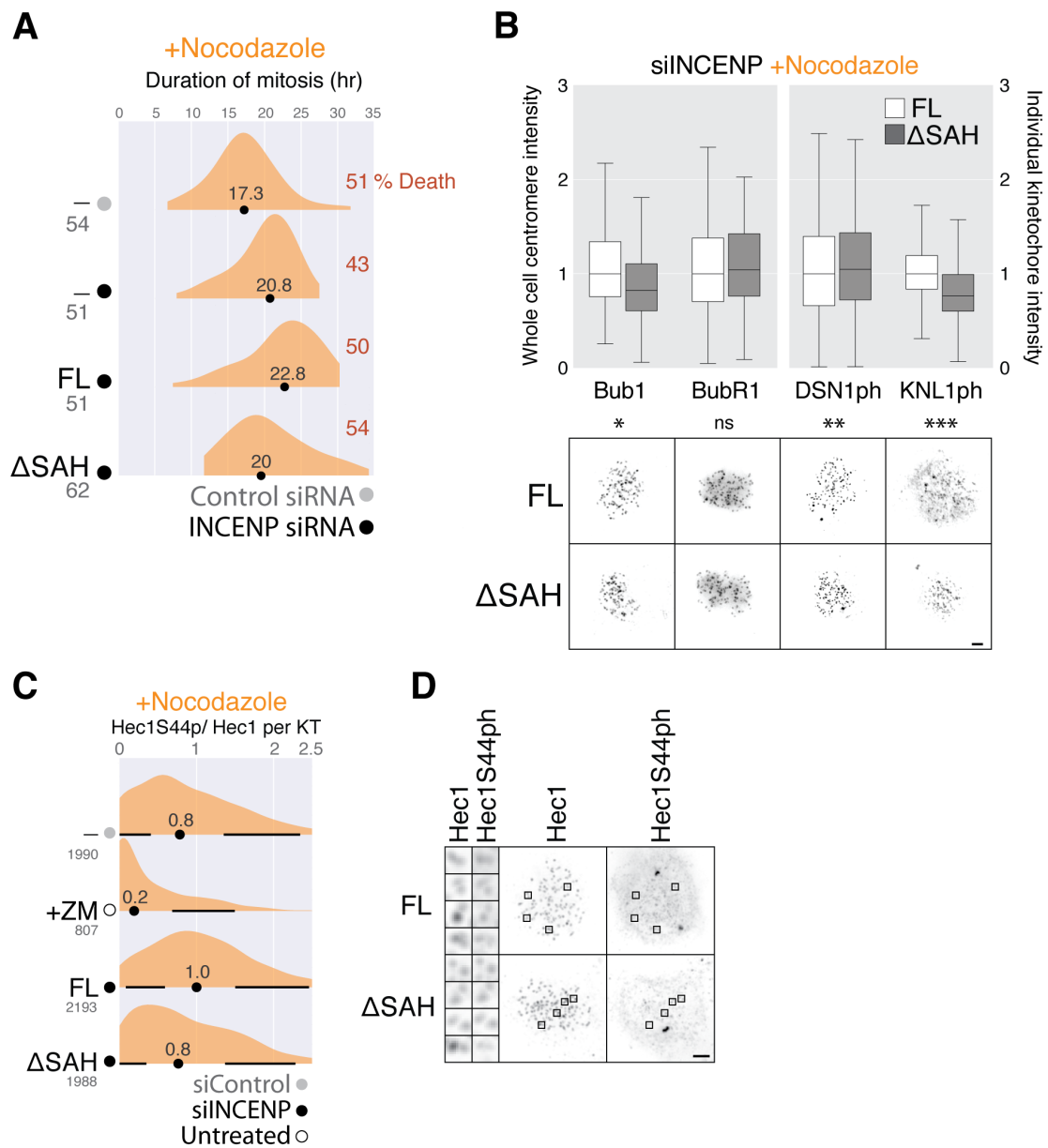


Figure 3-27: The hINCENP SAH domain is mostly dispensable for the SAC, SAC protein recruitment and kinetochore phosphorylation in nocodazole.

Given that the SAH domain is mostly dispensable for the nocodazole-induced SAC in HeLa cells, why is it required in *Xenopus* egg extract under similar conditions (**Figure 3-1**)? Recruitment of SAC proteins to the kinetochore in *Xenopus* requires high levels of Aurora B activity (Emanuele et al. 2008; Wynne & Funabiki 2015), which in turn requires CPC enrichment on chromatin. Given that deleting the xINCENP SAH domain reduces the abundance of CPC on chromatin by 90% (**Figure 3-2**), we hypothesized that the SAH domain supports the SAC in *Xenopus* primarily through CPC localization. To test this, we first determined whether xINCENP containing the minimal deletion in the SAH domain that attenuated microtubule binding (**Figure 3-28A**) had an effect on CPC localization or the nocodazole-induced SAC in *Xenopus* egg extract. Surprisingly, this deletion phenocopied both the checkpoint defect (**Figure 3-28B**) and localization defect (**Figure 3-28C**) of deleting the entire SAH domain, indicating that unlike in human cells, the N terminus of the SAH domain contributes to both chromatin- and microtubule-binding in *Xenopus*. To determine which of these activities was important for the SAC, we replaced the SAH domain with an exogenous microtubule-binding domain from Tau (xINCENP Δ SAH ∇ Tau) and replaced the N terminus of the SAH domain with an exogenous chromatin-binding domain from the chromokinesin xKid (xINCENP Δ SAH^N ∇ Kid). While xINCENP Δ SAH ∇ Tau targets the CPC to microtubules and can bypass the requirement for the SAH domain in spindle assembly (Tseng et al. 2010), it fails to support the SAC (**Figure 3-28D**). Conversely, xINCENP Δ SAH ∇ Kid bypasses

the requirement for the N terminus of the SAH domain for CPC localization and the SAC (**Figure 3-28D**). This data is consistent with the SAH domain promoting CPC localization to support the nocodazole-induced SAC in *Xenopus* egg extract.

Figure 3-28: The N terminus of the xINCENP SAH domain supports CPC localization on chromatin to maintain the nocodazole-mediated SAC in *Xenopus* egg extract

A) Localization of Myc-tagged xSAH domain (green) on the spindle (red) in *Xenopus* egg extract. Reproduced from (**Figure 3-15**). The xSAH domain binds the spindle dependent on its N terminus.

B) Nocodazole-induced SAC assay in *Xenopus* egg extracts either mock depleted or depleted of the CPC (Δ CPC) and reconstituted with xAurora B, xDasra A, xSurvivin and the indicated xINCENP construct. Time after calcium addition, which inactivates CSF, is indicated. Mitotic status is monitored by Western blot for H3T3ph. Depleting the CPC (Δ CPC) or reconstituting extract with INCENP lacking either the SAH domain (Δ SAH) or the N terminus of the SAH domain (Δ SAH^N) leads to SAC silencing. Mock= control IgG depletion, Δ CPC= CPC depletion. AurB= MBP-xAurora B protein, Dsr= xDasra A mRNA, Sur= xSurvivin mRNA

C) Representative images (left) and quantification (right) of immunofluorescence visualizing GFP-xINCENP (green) abundance on sperm chromatin (purple) in M-phase extract treated with nocodazole. Extracts were reconstituted as indicated. Scale bar, 5 μ m

D) Nocodazole-induced SAC assay, as in B. Replacing the xINCENP SAH domain with an exogenous microtubule-binding domain Tau (Δ SAH ∇ Tau) fails to rescue the checkpoint relative to xINCENP lacking the SAH domain (Δ SAH). While a minimal deletion in the N terminus of the xINCENP SAH domain (Δ SAH^N) is also defective in the checkpoint, inserting an exogenous DNA binding domain from the chromokinesin xKid into this construct rescues the defect (Δ SAH^N ∇ xKid).

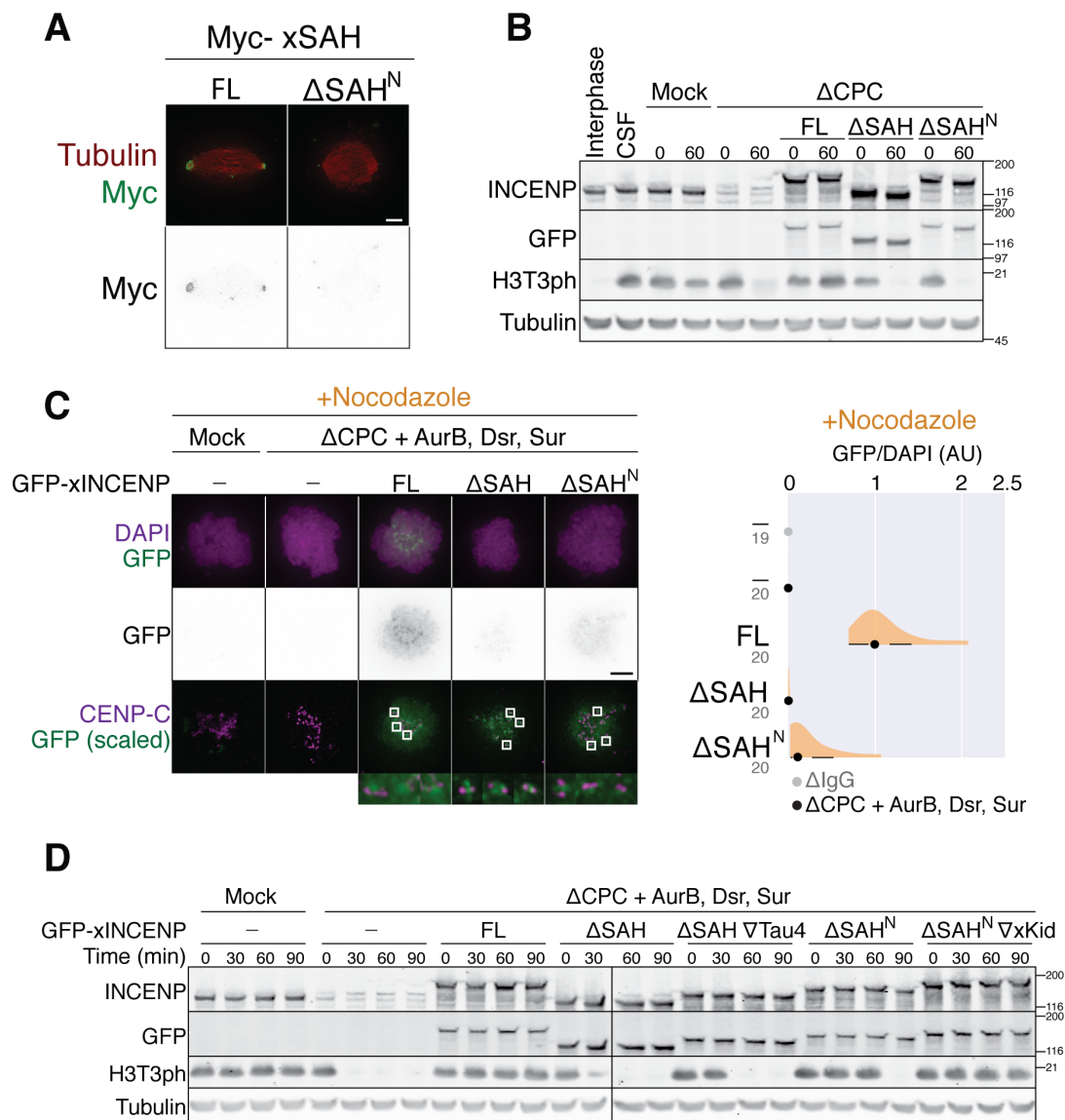


Figure 3-28: The N terminus of the xINCENP SAH domain supports CPC localization on chromatin to maintain the nocodazole-mediated SAC in *Xenopus* egg extract

3.3 Discussion

The INCENP SAH domain maintains the CPC on chromatin

It is thought that localization of the CPC to the inner centromere primarily depends on Survivin and Borealin (Carmena et al., 2012; Ruchaud et al., 2007). Here we demonstrate that the INCENP SAH domain also contributes to robust recruitment of the CPC to the inner centromere (**Figure 3-27**). Deletion of the SAH domain both reduces CPC abundance and enhances its dynamics at the inner centromere even in the absence of microtubules, indicating that this function is independent of the previously suggested role for the Aurora B-microtubule interaction in CPC enrichment at the centromere (Banerjee et al., 2014). Given that GFP-tagged xSAH domain is broadly distributed along sperm chromatin in *Xenopus* egg extract, the SAH domain may generally enhance the affinity of the CPC for chromatin.

Since local enrichment of the CPC stimulates the kinase activity of Aurora B (Kelly et al., 2007), it is surprising that artificially targeting INCENP Δ CEN to the centromere (CENP-B fusion) or kinetochore (Mis12 fusion) does not bypass the requirement of the CEN domain for the taxol-induced checkpoint (**Figure 3-15**). However, these constructs do cause a mitotic delay when they are expressed in the presence of endogenous Aurora B (**Figure 3-16**). These observations may be explained if endogenous Aurora B activated at the centromere supports activation of the artificially targeted Aurora B. Since Borealin promotes CPC dimerization (Bourhis et al., 2009) (Bekier et al., 2015), it is tempting to speculate

that chromatin targeting of the CPC by Survivin/Borealin and the SAH domain may change the conformation of pre-existing CPC dimers and facilitate Aurora B autophosphorylation. Thus, targeting INCENP Δ CEN to the kinetochore or centromere may not support Aurora B activation due to a loss of Borealin-mediated dimerization. Our results are consistent with a model where Aurora B is activated at the inner centromere to phosphorylate kinetochore substrates and to stimulate SAC signaling. However, as we discuss below, robust SAC maintenance also requires binding of the SAH domain to microtubules.

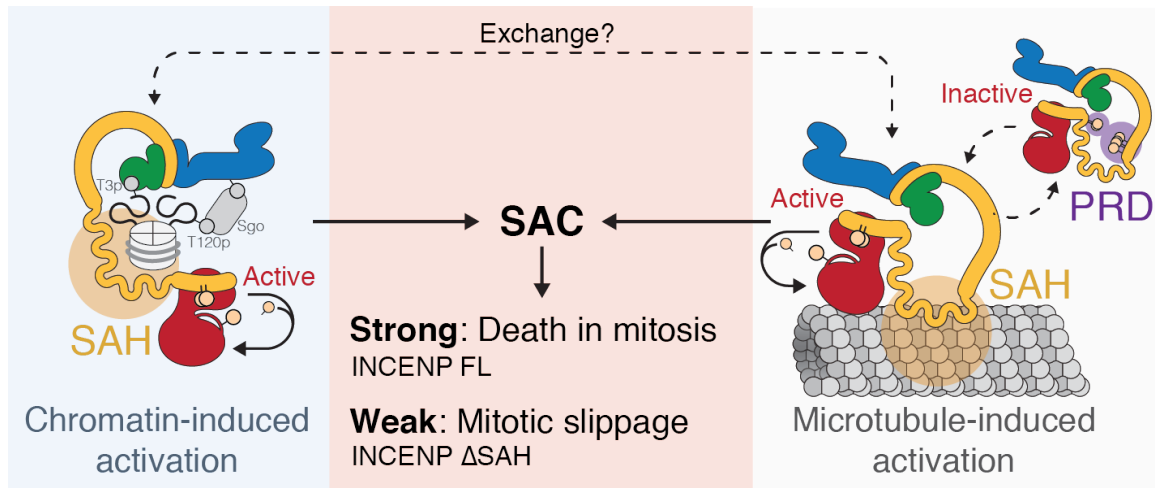


Figure 3-29: A model for the CPC in the taxol-mediated SAC.

The SAH domain (SAH) interacts with chromatin (blue) and microtubules (gray) to support activation of Aurora B (red; active) by autophosphorylation *in trans* (black curved arrows). While chromatin- and microtubule- induced activation of Aurora B independently support the SAC (left arrow and right arrow, respectively), both are required for a robust SAC arrest in taxol. Taxol-treated cells expressing INCENP-FL elicit a strong SAC arrest where the majority of cells die in mitosis; conversely, cells expressing INCENP ΔSAH elicit a weaker SAC arrest where the majority of cells undergo mitotic slippage. The microtubule binding capacity of the INCENP SAH domain is antagonized by Cdk-dependent phosphorylation of the INCENP PRD (purple), which decreases its association with microtubules, prevents activation of Aurora B (inactive), and attenuates the SAC. Regulated phosphorylation of the PRD (dashed circle arrows) may couple CPC function to kinetochore-microtubule attachment status. Additionally, CPC on chromatin and on microtubules may dynamically exchange (dashed arrows) to support the diverse functions of the CPC during early mitosis. T3p= H3T3ph, T120p= H2A T120ph, Sgo= Shugoshin.

The INCENP SAH domain binds microtubules prior to anaphase to support the SAC in taxol-treated cells

Our current studies in *Xenopus* are consistent with observations in chicken and human cells that the N-terminal segment of the SAH domain directly binds microtubules (Samejima et al., 2015; van der Horst et al., 2015). This domain was previously shown to target the CPC to the spindle midzone during anaphase to facilitate cytokinesis (van der Horst et al., 2015). Ample evidence indicates that the CPC-microtubule interaction also plays a role prior to anaphase, even though the majority of the CPC is visualized at the inner centromere. In human cells, Aurora B interacts with EB1 and UBASH3B on microtubules to promote localization of the CPC to the inner centromere (Banerjee et al., 2014; Krupina et al., 2016). In budding yeast, Sli15 lacking the centromere-targeting domain could support error correction, but not when the microtubule-binding region of Sli15 was deleted (Campbell and Desai, 2013). Finally, we have demonstrated that the INCENP SAH domain binds microtubules to support microtubule-dependent Aurora B activation and spindle assembly in *Xenopus* egg extract (Tseng et al., 2010). Here we show that the MAP4 microtubule binding domain bypasses the requirement of the SAH domain (**Figure 3-23**), strongly suggesting that the microtubule-binding capacity of the SAH domain is important for SAC activation/maintenance in response to the aberrant kMT attachments generated by taxol or monastrol.

How does targeting the CPC to microtubules sustain the SAC in taxol-treated cells? Taxol-stabilized microtubules activate Aurora B through the INCENP SAH domain (**Figure 3-22**) (Tseng et al., 2010). This suggests that targeting Aurora B to microtubules generates a local pool of active Aurora B (**Figure 3-29A**). It has been suggested that the interaction of Aurora B with microtubules facilitates CPC enrichment at the centromere (Banerjee et al., 2014; Krupina et al., 2016), which is important for the SAC. However, the SAH domain must contribute to the SAC independent of this mechanism as a 35 aa-deletion in its microtubule-binding region (hINCENP Δ SAH^N) attenuates the SAC without affecting localization to the centromere. We suggest that the microtubule-binding capacity of the CPC may be critical for the SAC in at least two ways: first, to regulate kinetochore substrates including those involved in kMT attachment (Ndc80, Knl1, Dsn1), checkpoint activation (Ndc80), and checkpoint silencing (Knl1, Zwint1) and second, to regulate microtubule dynamics through phosphorylating microtubule associated proteins, such as the Ska complex (Chan et al., 2012), mDia3 (Cheng et al., 2011), EB2 (limori et al., 2016) and the Astrin-SCAP complex (Schmidt et al., 2010) (**Figure 3-29B**). Indeed, we have previously shown that Aurora B-dependent phosphorylation can be detected on mitotic spindle (Tseng et al., 2010), and an *in vitro* study has shown that INCENP-microtubule interaction preferentially promotes Aurora B-dependent phosphorylation of microtubule-bound substrates over unbound substrates (Banerjee et al., 2014).

INCENP chromatin- and microtubule-binding independently contribute to the SAC in taxol

Localization of Aurora B to the centromere is critical for its role in kinetochore phosphorylation and the SAC; however, Aurora B has also been detected at the kinetochore (Deluca et al. 2011; Posch et al. 2010) and on microtubules (Banerjee et al. 2014; Krupina et al. 2016) in human cells. Whether these non-centromeric pools of CPC exist is controversial, and how they contribute to CPC function remains unclear. Here, we demonstrate that INCENP chromatin-binding and microtubule-binding independently promote the SAC in taxol. Deleting the INCENP CEN domain (hINCENP Δ CEN) prevents chromatin binding and attenuates the checkpoint. This can be rescued by either artificially tethering INCENP to the centromere/kinetochore (**Figure 3-15**) or mutating the PRD to target INCENP to spindle microtubules (hINCENP Δ CEN 6A) (**Figure 3-26**). Tethering INCENP Δ CEN to the centromere/kinetochore promotes the SAC even when the SAH domain is deleted, indicating that chromatin-binding is sufficient to stimulate the checkpoint. Conversely, incorporating a minimal microtubule-binding deletion into INCENP Δ CEN 6A prevents it from binding spindle microtubules and mitigates its rescue of the SAC relative to INCENP Δ CEN, indicating microtubule-binding is sufficient to stimulate the SAC. Importantly, neither chromatin- nor microtubule-binding alone was sufficient for a checkpoint arrest comparable to hINCENP, suggesting that both activities are necessary for a robust SAC. Altogether, we suggest that the CPC must interact

with both centromeric chromatin and microtubules to support a robust checkpoint arrest. In the future, it will be interesting to determine if the CPC interacts simultaneously with chromatin and microtubules and if microtubule-bound Aurora B phosphorylates specific substrates on microtubules.

Cdk1-dependent regulation of the INCENP SAH domain

In budding yeast, phosphorylation of the INCENP homolog Sli15 by Cdk1 prevents binding to the mitotic spindle prior to anaphase (Pereira and Schiebel, 2003); however, there is a conflict in the literature as to whether phosphorylation of Sli15 supports or inhibits the SAC (Makrantonis et al., 2014; Mirchenko and Uhlmann, 2010). In human cells, it was previously shown that Cdk1 phosphorylation indirectly inhibits INCENP microtubule binding by preventing it from binding to MKLP2, which targets the CPC to anaphase spindle midzone (Gruneberg et al., 2004; Hummer and Mayer, 2009). Here, we demonstrate that the PRD enhances SAH-dependent microtubule binding and that Cdk1-dependent phosphorylation of the PRD reduces the binding of INCENP to microtubules (**Figure 3-22**). The interaction of microtubules with either reconstituted budding yeast CPC, xINCENP⁴⁹¹⁻⁸⁷³-xAurora B, or the hINCENP SAH domain occurs through electrostatic interactions with the negatively charged e-hooks of tubulin (Cormier, Drubin, and Barnes 2013; Noujaim et al., 2014; van der Horst et al., 2015). We speculate that the PRD helps orient positively charged residues in the SAH domain to promote microtubule binding, while Cdk1-

dependent phosphorylation introduces negative charges that either create electrostatic repulsion with microtubules or neutralize the capacity of the PRD to stimulate microtubule-binding activity of the SAH.

Given that Cdk1-Cyclin B activity is high in early mitosis, it may be counterintuitive that dephosphorylation of the PRD helps sustain the SAC. However, phosphatases are active in mitosis; among five Cdk1-dependent phosphorylation sites on the N terminus of Cdc20, three threonine residues are dephosphorylated by PP2A to activate Cdc20, while two serine residues remain phosphorylated in metaphase *Xenopus* egg extracts (Labit et al., 2012). Similarly, the INCENP PRD may be targeted for context-dependent dephosphorylation to locally control Aurora B activity. Dephosphorylation of INCENP at the centromere, for example by Aurora B-dependent recruitment of PP2A to the centromere (Tanno et al., 2010), may activate INCENP's microtubule-binding activity, allowing it to bind and destabilize merotelic attachments passing by the centromere. At the outer kinetochore, PP2A recruited to BubR1 could facilitate CPC-mediated regulation of kinetochore-proximal microtubules (Kruse et al., 2013; Suijkerbuijk et al., 2012; Xu et al., 2013).

Regulation of local Aurora B activity on kMTs by INCENP dephosphorylation may contribute to the mechanism that couples Aurora B substrate phosphorylation to kinetochore tension. If tension at the kinetochore can stabilize kinetochore-microtubule attachments in a manner independent of Aurora B, as has been shown using purified yeast kinetochores (Akiyoshi et al.,

2010), this stabilized attachment may competitively remove Mps1 from Ndc80 (Hiruma et al., 2015; Ji et al., 2015), leading to removal of the Bub3-Bub1-BubR1-PP2A axis (Suijkerbuijk et al., 2012). Upon dissociation of PP2A from bi-oriented kinetochores (Foley et al., 2011), Cdk1 may rephosphorylate the INCENP PRD and inhibit Aurora B action on microtubules, facilitating microtubule stabilization. To validate this hypothesis, future studies are needed to test if PP2A on BubR1 or Sgo1 promotes dephosphorylation of the PRD in a tension-sensitive manner.

The CPC sustains the SAC to promote death in mitosis

Our live-imaging analyses show that the CPC and the INCENP SAH domain sustain the SAC in taxol to promote cell death. We see a strong, linear increase between the duration of mitosis and percentage of cells dying in mitosis (**Figure 3-9C**). We find that the amount of time it takes a cell to die in mitosis is similar under all conditions, consistent with the hypothesis that the timing of mitotic cell death can be largely uncoupled from the strength of checkpoint. The median time for cells to die in mitosis appears to be reduced when the checkpoint is compromised; however, this is likely due to selective loss of cells that take the longest to die in mitosis, as they are unable to remain arrested long enough to die without a functional checkpoint. This hypothesis is consistent with the competing-networks model where the decision to undergo slippage or death in mitosis is a winner-take-all race between cyclin B degradation (triggering

slippage) and accumulation of pro-apoptotic signals (triggering death) (Gascoigne and Taylor, 2008; Topham and Taylor, 2013) (**Figure 3-9A**). Under control conditions or when cells are expressing INCENP-FL, a small fraction of cells (10-30%) undergo mitotic slippage. Interestingly, these cells remain in mitosis well past the time most cells die in mitosis (**Figure 3-9B**). Although this may be explained by heterogeneity in the rate of pro-apoptotic signaling or genetic/epigenetic variation within the cell line, we cannot rule out the possibility that a robust SAC arrest can delay cell death. Regardless of the mechanism, our data indicate that even a mild reduction in SAC strength, for example by weakening the microtubule-binding capacity of INCENP, can have a dramatic impact on mitotic cell fate in the presence of taxol.

Chapter 4: Perspectives

4.1 Broader Implications

This dissertation focuses on understanding the molecular mechanisms regulating CPC localization and function. Together with Cristina Ghenoiu, I discovered how the kinase activity of Haspin is coupled to M-phase to promote timely recruitment of the CPC to the centromere. Subsequently, I identified a regulated interaction between the INCENP SAH domain and microtubules critical for kinetochore phosphorylation and the spindle assemble checkpoint in taxol-treated cells. This work both elaborates the current paradigm of spatiotemporal regulation of the CPC and highlights a previously unappreciated role for the CPC interacting with microtubules to support kinetochore phosphorylation and the SAC. Below, I discuss the implications of these findings in the broader context of mitosis and Aurora B regulation.

Haspin detects Plk1 activity to regulate cohesion during mitosis

During entry into mitosis, Plk1- and Aurora B-dependent phosphorylation promote dissociation of the cohesin complex from chromosome arms (Hauf et al. 2005; Nishiyama et al. 2013). Meanwhile, Aurora B also supports recruitment of Shugoshin proteins and PP2A to the inner centromere (Tanno et al. 2010), which is required to protect centromeric cohesin prior to anaphase. Haspin knockdown has been reported to lead to precocious sister chromatid separation (Dai et al. 2006), presumably through loss of Aurora B-dependent protection of cohesin at

the centromere. The protein Pds5, which associates with the cohesin complex and protects centromeric cohesin, interacts with and targets the budding yeast homolog of Haspin (Hrk1) to chromatin to support H3T3ph (Yamagishi et al. 2010). Based on these observations, it has been suggested that Haspin, Plk1 and the CPC are part of a pathway that coordinates removal of arm cohesion and protection of centromeric cohesion during early mitosis (Trivedi & Stukenberg 2016).

Based on our results, one interesting idea is that Plk1-and Aurora B-dependent Haspin activation is important for coordinating cohesin removal. Upon entry into mitosis, Haspin may be targeted to cohesin by its interaction with Pds5 and phosphorylated by Cdk1, which promotes binding to Plk1 and phosphorylation of H3T3. H3T3ph would then locally recruit Aurora B, placing both Aurora B and Plk1 in proximity to cohesin. On chromosome arms, this would facilitate rapid removal of cohesin. At the centromere, this would promote Aurora B-dependent recruitment of Shugoshin and PP2A to oppose Aurora B- and Plk1-mediated removal of cohesin, thus preventing sister chromatid separation. Therefore, activation of Haspin by Aurora B and Plk1 may help support the rapid degradation of arm cohesion while protecting centromeric cohesion upon mitotic entry.

Positive feedback in CPC localization: The chicken and the egg

CPC enrichment at the inner centromere involves a complex positive feedback loop between Aurora B, Plk1 and Haspin. Plk1 and Bub1 support Aurora B activation by targeting it to the inner centromere, while Aurora B-dependent phosphorylation promotes activation of Plk1 (Carmena, Pinson, et al. 2012) and indirectly recruits Bub1 to the kinetochore (Van Der Waal et al. 2012). Which of these pathways is initiated first to establish CPC localization and positive feedback? Bub1-dependent H2A T120ph is unlikely to establish the CPC at the inner centromere. Aurora B facilitates Bub1 recruitment indirectly by promoting rapid recruitment of Mps1 to the kinetochore upon mitotic entry (Saurin et al. 2011). After mitotic entry, Aurora B inhibition no longer causes a defect in Mps1 localization. This result is consistent with Aurora B already being localized/active at the centromere prior to Bub1-dependent positive feedback.

It is more complicated to determine whether Aurora B at the inner centromere precedes or follows Haspin activation by Plk1. Haspin is recruited to cohesion and HP1 (Yamagishi et al. 2010), both of which interact with chromatin prior to mitotic entry, though H3T3ph is not present at this time (Polioudaki et al. 2004). Plk1-dependent phosphorylation of Haspin directly stimulates Haspin kinase activity *in vitro* (Ghenoiu et al. 2013) and indirectly promotes its centromeric localization by supporting Haspin binding to the SUMOylated tail of Topoisomerase II (Yoshida et al. 2016). This requires priming phosphorylation on Haspin (T206 in *Xenopus*, T128 in humans) (**Figure 2-3**), suggesting it occurs

upon mitotic entry. While Plx1 can support Haspin activation independent of Aurora in *Xenopus* egg extract (**Figure 2-1**), Plk1 requires Aurora B-mediated phosphorylation of its activation loop for full activation in *Drosophila* and human cells (Carmenta, Pinson, et al. 2012), suggesting Plk1-dependent Haspin activation is downstream of Aurora B recruitment, at least in these systems.

Consistent with this, Aurora B is enriched on pericentromeric heterochromatin in late G2 via INCENP binding to HP1 (Kang et al. 2011; Ainsztein et al. 1998), potentially placing it in close proximity to Haspin which also interacts with HP1 (Yamagishi et al. 2010). This suggests that pericentromeric Aurora B promotes CPC localization to the centromere through Haspin, followed by downstream activation of Plk1 and recruitment of Bub1. Consistent with this mechanism, pericentromeric phosphorylation of the Aurora B substrate H3S10 can be detected in late G2 (Hayashi-Takanaka et al. 2009), indicating Aurora B is active prior to mitotic entry. Depletion of HP1 protein in non-transformed human cell lines decreases Aurora B-dependent phosphorylation of the kinetochore substrates Dsn1 and Knl1 (Abe et al. 2016), suggesting that in the absence of HP1-mediated CPC recruitment, Bub1 recruitment/ Plk1 activation may be impaired. However, this function could be indirect as HP1 also recruits Shugoshin to the centromere (Tanno et al. 2015), which recruits the CPC through Bub1-mediated phosphorylation of H2A T120ph. Therefore, while Mps1-dependent CPC recruitment is likely to occur last in the

positive feedback loop, it remains unclear whether Haspin- or HP1-dependent recruitment of the CPC is first.

An additional mechanism supports CPC localization to the centromere

The current paradigm for CPC localization at the inner centromere is dual recognition of phosphorylated histones by Borealin and Survivin (Yamagishi et al. 2010; Kelly et al. 2010; F. Wang et al. 2010; Tsukahara et al. 2010). The spatiotemporal distribution of H3T3ph and H2A T120ph are consistent with these marks being sufficient to enrich the CPC at the inner centromere during early mitosis. My work with Ghenoiu defined how Haspin activity is coupled to the cell cycle to ensure timely phosphorylation of H3T3 during mitosis. Additionally, the interaction of H3T3ph with the BIR domain of Survivin has been crystalized and characterized, including the determinants that enhance its specificity over the unphosphorylated H3 tail (Du et al. 2012; Niedzialkowska et al. 2012). The interaction of Borealin with H2A T120ph is more enigmatic. It is unclear how Bub1 at the kinetochore phosphorylates H2A at the centromere and the molecular details of binding between Shugoshin and Borealin are unknown. Additionally, HP1 may contribute to CPC recruitment through this pathway, as its been shown to interact with and recruit both Shugoshin and INCENP to the centromere in human cells (X. Liu et al. 2014; Kang et al. 2011; Tanno et al. 2015).

My work has identified a third determinant of CPC localization to the centromere: the INCENP SAH domain. Deleting the SAH domain reduces the abundance of CPC on chromatin by over 90% in *Xenopus* egg extract (**Figure 3-28**) and 50% in HeLa cells (**Figure 3-6**). Despite these large defects in CPC localization, we detect no decrease in global H3T3ph by western blot in *Xenopus* and only a minor defect in H3T3ph and H2A T120ph by immunofluorescence in human cells (**Figure 3-6**). These results are consistent with the SAH domain supporting CPC localization independent of stimulating Haspin- or Bub1-dependent CPC recruitment. Additionally, I observe GFP- or Myc-tagged SAH domain broadly distributed along sperm chromatin by immunofluorescence in *Xenopus* (**Figure 3-3**), consistent with an idea that it interacts with chromatin independently of Borealin and Survivin.

How does the SAH domain interact with chromatin? The broad distribution of the GFP-SAH domain along sperm chromatin suggests that the domain recognizes a general feature of chromatin rather than a specific DNA sequence or chromatin state. One explanation is the SAH-domain interacts with other chromatin proteins, such as histones; however, immunopurification of GFP-SAH domain from metaphase *Xenopus* egg extract failed to identify proteins with known DNA- or chromatin-binding capacity. An alternative explanation is that the interaction is electrostatic, similar to how the SAH domain binds microtubules (Samejima et al. 2015). Interestingly, preliminary results in *Xenopus* indicate the chromatin- and microtubule- binding regions of GFP-SAH overlap (**Figure 3-28**).

Thus, basic residues within the SAH domain, which are important for binding to the negatively charged e-hook of tubulin, may also interact with negative charges on phosphorylated chromatin proteins or the phosphate backbone of DNA.

The SAH domain is primarily composed of small clusters of basic and acidic residues that alternate along the length of the domain and are predicted to stabilize its single alpha helix structure. The sequential stacking of basic and acidic residues with each turn of the helix could lead to an alternating distribution of charge that may facilitate electrostatic interactions with either the positively charged tails of histones or the negatively charged backbone of DNA.

To characterize the potential interaction of the SAH domain with DNA/nucleosomes, I would purify recombinant SAH domain and perform an *in vitro* binding assay. Our lab has developed a method to reliably assemble DNA-coated beads with or without nucleosomes, allowing me to identify which substrate the SAH domain may prefer. If the SAH domain prefers nucleosomal DNA, I would then determine if this interaction was dependent on histone tails by removing them via transient exposure to trypsin. Next, I would assess the ability of the SAH domain to directly bind recombinant nucleosome octamers, as well as H2A:H2B dimers and H3:H4 tetramers. Once I had determined which substrate interacts with the SAH domain, I could determine if this binding was sensitive to increasing salt concentration, as would be predicted for an electrostatic interaction. Finally, I would purify SAH domain deletion mutants and use them to map the interaction site on the SAH domain. If the SAH domain failed to interact

with any of these substrates *in vitro*, it may indicate that binding is indirect, potentially through a protein-protein interaction or perhaps binding to RNA, which has been implicated in CPC localization and activation (Jambhekar et al. 2014) (Becker et al. 2010; Blower 2016).

While the SAH domain is required for chromatin localization of the CPC in *Xenopus* egg extract and human cells, the extent of the requirement seems different. In *Xenopus*, deletion of the SAH domain reduces CPC abundance on chromatin by over 90% and can be phenocopied by the minimal deletion in the N terminus of the SAH domain that attenuates microtubule binding (**Figure 3-28**). In human cells however, deletion of the SAH domain reduces CPC abundance by a relatively modest 40% (**Figure 3-6**), while INCENP lacking the N terminus of the SAH domain localizes to the centromere indistinguishable from full-length INCENP (**Figure 3-23**). Why does CPC localization in *Xenopus* egg extract appear more dependent on the SAH domain than in human cells?

One explanation is that the CPC is more weakly associated with chromosomes in *Xenopus*, where it is more broadly distributed along chromosomes than in human cells, where it is primarily enriched at the centromere. Clustering at the centromere may support robust feedback between Aurora B and Haspin in human cells, a mechanism that is dispensable in *Xenopus* egg extract (**Figure 2-1**). Additionally, while H3T3ph is broadly distributed along chromatin with some enrichment at the centromere, H2A T120ph is restricted to the centromere (Yamagishi et al. 2010; Williams et al.

2016; Kelly et al. 2010), suggesting that centromeric CPC may be inherently more stable than CPC on chromosome arms, which lack H2A T120ph. Given that a higher fraction of the CPC is localized at the centromere in human cells, and that this binding may be more stable, it makes sense that deletion of the SAH domain has a smaller impact in this system. Conversely, the stabilizing effect of the SAH domain may be more important in *Xenopus* where a larger fraction of the CPC is associated with chromosome arms and only overlaps with H3T3ph. Consistent with this idea, the only CPC remaining on chromatin in *Xenopus* in the absence of the SAH domain is associated with the centromere (**Figure 3-28**).

This difference may also explain why INCENP Δ SAH^N phenocopies the localization defect of INCENP Δ SAH in *Xenopus*, but not in human cells. If deletion of the N terminus of the SAH domain only partially removes the chromatin-binding activity of the SAH domain, this may not produce an effect in human cells where CPC localization is more robust. One way to test this hypothesis is to reduce H3T3ph or H2A T120ph in human cells and determine if INCENP Δ SAH^N now demonstrates a CPC localization defect. An alternative explanation for this difference is a species-specific difference in how the SAH domain binds chromatin in human cells versus *Xenopus*. While the SAH domain is highly conserved among vertebrates, human INCENP contains a primate specific expansion of a 'QERRE' motif in its C terminus that is highly predicted to form a SAH domain and may provide additional chromatin-binding capacity in this system.

Why are there different requirements of the SAH domain in nocodazole versus taxol in human cells and *Xenopus* egg extract?

The INCENP SAH domain is required for the nocodazole-induced SAC in *Xenopus* egg extract (**Figure 3-1**), yet mostly dispensable for this arrest in HeLa cells (**Figure 3-27**). These results mirror the requirement for Aurora B activity in maintenance of the nocodazole-induced SAC in these systems. In *Xenopus*, the role of Aurora B in this checkpoint was established using microinjection of Aurora B antibodies into *Xenopus* XTC cells (Kallio et al. 2002) and subsequently confirmed by chemical inhibition using ZM in *Xenopus* egg extracts (Gadea & Ruderman 2005). Conversely, while early reports using the Aurora B inhibitor ZM447439 demonstrated a similar requirement in human cells (Ditchfield et al. 2003), conflicting reports made the role of Aurora B in the nocodazole-induced SAC in human cells controversial until recently, in part because a low amount of residual Aurora B activity seems sufficient for the SAC (Santaguida et al. 2011). Thus, it seems the nocodazole-induced SAC requires a high level of Aurora B activity in *Xenopus* egg extract and a much lower level of Aurora B activity in human cells.

What is the molecular basis for this difference? One likely explanation is that assembly of the kinetochore is much more sensitive to Aurora B activity in *Xenopus* egg extracts than in human cells. Depleting Aurora B protein or inhibiting its kinase activity prevents the recruitment of outer kinetochore proteins required to assemble the SAC signaling platform including Knl1, Mad1, Mad2 and

BubR1 (Emanuele et al. 2008; Wynne & Funabiki 2015). This effect is rapid and potent, as within 10 min of adding the Aurora B inhibitor Hesperadin, 95% of Ndc80 is lost from the kinetochore in *Xenopus* egg extract. Conversely, adding Hesperadin or ZM447439 alone to human A549 lung epithelial cells had no effect on Ndc80 recruitment. Combining both inhibitors had an additive effect on Aurora B inhibition, eventually resulting in a 60% decrease in Ndc80 kinetochore recruitment (Emanuele et al. 2008). Thus, *Xenopus* egg extract requires a high level of Aurora B activity to assemble the kinetochore-based SAC signaling platform, while human cells require potent Aurora B inhibition to reveal a similar requirement.

These observations may explain why the SAH domain is required for the nocodazole-induced SAC in *Xenopus* but not HeLa cells. Deletion of the SAH domain in *Xenopus* reduces CPC abundance on chromatin by over 90%. Given that Aurora B activation is coupled to its localization and that high Aurora B activity is needed to assemble the kinetochore in *Xenopus*, the SAH domain may silence the checkpoint because there isn't enough CPC on chromatin to support Aurora B-dependent kinetochore assembly. If true, retargeting the CPC to chromatin should rescue the SAC defect upon deleting the SAH domain. While INCENP Δ SAH^N phenocopies the localization and checkpoint defect of deleting the SAH domain in *Xenopus* egg extract, preliminary results indicate that inserting the DNA-binding domain of the chromokinesin xKid into this construct (xINCENP Δ SAH ∇ xKid DBD) rescues both CPC localization and the SAC in

nocodazole (**Figure 3-28**). This result suggests that the SAH-domain supports the SAC in *Xenopus* primarily through promoting CPC localization to chromatin.

Conversely, the SAH domain is mostly dispensable for the SAC in human cells treated with nocodazole (**Figure 3-27**). There is a 12% reduction in the DoM of cells expressing hINCENP Δ SAH relative to hINCENP, but only a minor reduction in Bub1 and no noticeable difference in BubR1, Mad1, or total Hec1 recruitment. This minor defect is coincident with a 40% reduction in the abundance of centromeric CPC (**Figure 3-6**) and a 10-20% reduction in Aurora B-dependent kinetochore phosphorylation (**Figure 3-27**). Thus, while the SAH domain may support the SAC in nocodazole by promoting CPC localization similar to *Xenopus* egg extract, it is mostly dispensable for the checkpoint under this condition.

In taxol- or monastrol-treated human cells, however, deleting the SAH domain dramatically attenuates the SAC (**Figure 3-8**). This defect can be rescued by replacing the SAH domain with an exogenous microtubule binding domain (**Figure 3-23**), providing strong evidence that the SAH domain must interact with microtubules to support the SAC rather than support CPC localization at the centromere. It is impossible to determine if a similar requirement exists in *Xenopus* egg extract as this system fails to elicit a checkpoint response in a high dose of taxol (Minshull et al. 1994). A tempting idea is that the CPC-microtubule indirectly prevents taxol-induced activation of the SAC in *Xenopus* egg extracts. Taxol stabilizes a large number of microtubule asters in *Xenopus* egg extract that

might sequester the CPC from chromatin, leading to defects in kinetochore assembly and an inability to mount a checkpoint response. Indeed, the CPC can bind taxol-stabilized microtubules in extract (**Figure 3-22**) and binding of the CPC to chromatin is competitive with binding to microtubules in human cells (van der Horst et al. 2015). Additionally, replacing the SAH domain with a dimerization domain from GCN4 stimulates Aurora B activity but is defective in chromatin localization and is insufficient to support the nocodazole-induced SAC in *Xenopus* (unpublished data, B.S. Tseng), suggesting Aurora B activity must be coupled to chromatin. This hypothesis predicts that xINCENP Δ SAH^N ∇ xKid DBD, which has a defect in microtubule binding but can bind to chromatin, might support kinetochore assembly in *Xenopus* egg extract incubated with taxol and allow a SAC-dependent response. Testing this may provide an answer to the longstanding question of why the *Xenopus* egg extract system does not respond to taxol.

CPC localization dynamics at the centromere

The INCENP SAH domain is required for CPC stability at the centromere in human cells. I find that hINCENP-FL has a $T_{1/2}$ of 70.1 ± 28.7 s in nocodazole and 83.2 ± 33.5 s in taxol (**Figure 3-7**), similar to previous reports for GFP-INCENP in porcine LLC-PK cells (nocodazole: 108 ± 31 , taxol: 107 ± 34) and *Xenopus* S3 cells (nocodazole: 69 ± 2) (Ahonen et al. 2009). Deleting the SAH domain decreases the $T_{1/2}$ of INCENP by $\sim 40\%$ in both taxol and nocodazole, indicating

that this domain contributes to CPC stability independent of microtubules, which have been reported to promote CPC localization at the centromere (Banerjee et al. 2014).

Putting these results in context is difficult given that few studies have measured the dynamics of the CPC at the centromere. Only two studies report $t_{1/2}$ for their samples (summarized in **Figure 4-1**), albeit from 5-10 centromeres per measurement, while the remaining reports focus on qualitative differences in fluorescence recovery (Delacour-Larose et al. 2004; Delacour-Larose et al. 2007). This lack of quantitative data makes interpretation difficult. However, at least three trends are consistent across these studies: First, INCENP and Aurora B have similar dynamics when measured by a single group, second, Survivin is more dynamic than all other CPC components and three, Aurora B activity regulates Survivin dynamicity.

Protein	Construct	Cell Cycle Stage	Cell line	Treatment	t1/2 (s)	Recovery
Aurora B	xAurB-YFP	Metaphase	Xeno S3		43±7	88±18
...	MG132	31±5	69±11
INCENP	GFP-xINCENP	Metaphase	Xeno S3		53±19	83±8
...	MG132	38±9	80±13
...	...	Prometaphase	...	Nocodazole	69±21	86±10
...	LLC-PK		115±32	76±14
...	Nocodazole	108±31	72±9
...	Taxol	107±34	72±9
...	...	Metaphase	...		100±37	85±16
...	MG132	83±26	77±10
Survivin	Survivin-GFP	G2	HeLa		1860±600	84±11
...	...	Prometaphase	...		7.2±4.2	79±8
...	Nocodazole	31.3±9.8	71±10
...	...	Telophase	...		144±42	9±5
...	...	G2	LLC-PK		2940±480	89±12
...	...	Prophase	...		7.2±4.4	92±9
...	...	Prophase***	...		6.8±3.1	82±9
...	...	Metaphase	...		5.3±3.5	93±8
...	...	Prometaphase	...		4.6±1.1	79±8
...	Nocodazole	74.2±18.1	77±11
...	ZM/ MG132	67.1±27.2	17±13
...	MG132	4.4±2.1	83±8
...	Taxol	10.3±8	78±9
...	...	Anaphase	...		87±23	8±4
...	...	Telophase	...		204±108	11±3

Figure 4-1: Summary of FRAP recovery data for CPC componenets from previous publications

Summary of quantitative FRAP recovery data of various CPC components. Xeno-S3 is a *Xenopus* tissue culture cell line. LLC-PK cells are porcine kidney epithelial cells. In all cases, the centromere was bleached with the following exceptions: telophase and anaphase were bleached at the midzone and midbody, respectively. Aurora B and INCENP data from (Ahonen et al. 2009). Survivin data from (Beardmore et al. 2004). *** indicates bleaching on the chromosome arm.

The observation that INCENP and Aurora B have similar dynamics is consistent with them forming a stable complex. Interestingly, while INCENP and Survivin display similar dynamics in porcine LLC-PK cells treated with nocodazole (INCENP: 108 ± 31 , Survivin: 74.2 ± 18.1), Survivin is at least an order of magnitude more dynamic in taxol (INCENP: 107 ± 34 , Survivin: 10.3 ± 8) or when cells are arrested at metaphase with MG132 (INCENP: 83 ± 26 , Survivin 4.4 ± 2.1) (**Figure 4-1**). Given that Survivin is more dynamic in taxol and MG132 relative to nocodazole, these results may suggest that kMT attachment alters the dynamicity of the CPC at the centromere, generating a form of negative feedback between kMT attachment and CPC localization. While tempting, it is inconsistent with the fact that INCENP dynamics do not change in nocodazole or taxol (**Figure 3-7, Figure 4-1**). Moreover, while untransformed human cells do demonstrate enhanced CPC localization in nocodazole relative to MG132, this enrichment depends on increased phosphorylation of H2A T120 and not H3T3ph (Salimian et al. 2011). Thus, the functional significance of this difference in dynamics remains unclear.

Nonetheless, it is surprising that INCENP is more stable than Survivin at the centromere, given that INCENP localization is dependent on forming a triple-helix bundle with Survivin and Borealin (Jeyaprakash et al. 2007). One explanation is that the CPC remains associated with the centromere via Borealin even as Survivin exchanges with H3T3ph and/or the INCENP CEN domain. However, it has been demonstrated that CPC reconstituted with a Borealin point

mutant that excludes Survivin from the triple-helix bundle fails to localize to the centromere, suggesting this mechanism is unlikely (Jeyaprakash et al. 2007). A second explanation is that two pools of Survivin exist at the centromere, a slow-exchanging pool incorporated into the CPC and a fast-exchanging pool that is independent of the CPC. However, no group has fit a double exponential to their Survivin FRAP data or empirically tested this idea. A third explanation is that the INCENP SAH domain retains INCENP at the centromere even as Survivin exchanges with the INCENP CEN domain. This is consistent with the idea that CPC localization is specified by Survivin/Borealin and stabilized by the SAH-domain. Future studies performing careful kinetic analysis of CPC components under different conditions may provide novel insight into the molecular dynamics of CPC localization at the centromere.

Localization and function of the CPC on microtubules in early mitosis

My work demonstrates that INCENP interacts with microtubules prior to anaphase and that this interaction is important for CPC function. Mutating six putative Cdk1 sites on hINCENP to alanine to mimic dephosphorylation (hINCENP 6A) targets hINCENP to the mitotic spindle in taxol, yet still supports the SAC (**Figure 3-25**). Conversely, attenuating the interaction of hINCENP with microtubule by mimicking constitutive phosphorylation (hINCENP 6D) results in an attenuated DoM relative to hINCENP 6A. These results imply that during a normal mitotic arrest in taxol, INCENP interacts with microtubules to promote the SAC.

These observations are consistent with the observation that Aurora B-dependent phosphorylation occurs on the mitotic spindle in human cells during early mitosis (Tseng et al. 2010). They are also in line with previous reports that the interaction of the CPC with microtubules prior to anaphase is functionally important in human cells. Aurora B interacts with EB1 on kinetochore-proximal microtubules and this interaction supports localization of the CPC at the inner centromere, presumably through stimulating H2A T120ph via Bub1 recruitment to the kinetochore (Banerjee et al. 2014). Similarly, ubiquitinated Aurora B interacts with the ubiquitin receptor protein UBASH3B in complex with Mklp2 on microtubules, and this interaction is important for preventing CPC accumulation on chromosome arms and promoting robust localization at the inner centromere (Krupina et al. 2016). This group also visualized Aurora B on kinetochore-proximal microtubules in prometaphase cells, albeit ambiguously given the physical overlap of chromosomes and the robust localization of CPC at the inner centromere.

What are the function(s) of CPC on microtubules in early mitosis? EB1 and UBASH3B support CPC localization to the inner centromere. Interestingly, depleting either of these proteins also strongly reduces H3T3ph and H2A T120ph, indicating a defect in the positive feedback loops that support CPC localization. While the SAH domain supports CPC localization, this is independent of underlying histone marks or its interaction with microtubules. Both EB1 and UBASH3B may be important for Aurora B-dependent error correction,

as EB1 depletion reduces levels of Aurora B-dependent phosphorylation of Knl1 while UBASH3B depletion leads to an increase in chromosome missegregation. My results are consistent with this, as the SAH domain supports Dsn1, Knl1 and Hec1 phosphorylation at the kinetochore in taxol (**Figure 3-11**). This could be directly tested using a cold-stable microtubule assay or monastrol washout assay to determine if the SAH domain contributes to error correction. While I demonstrate that the SAH domain is also essential for the taxol-mediated SAC, the role of EB1 and UBASH3B in the SAC was never assessed. Given that deleting the SAH domain or depleting EB1 or UBASH3B may produce distinct phenotypes, it is interesting to speculate that the CPC interacts with microtubules through different proteins to promote different functions.

It is important to note that these studies do not provide a consensus model on how the CPC-microtubule interaction supports CPC localization at the centromere. While depletion of UBASH3B reduces the abundance of CPC and H3T3ph at the centromere, addition of 3 μ M nocodazole ameliorates both effects, suggesting microtubules have an activity that in the absence of UBASH3B prevents accumulation of the CPC at the centromere. Stukenberg and colleagues, who identified the interaction with EB1, reported that while 0.33 μ M nocodazole had no effect on Aurora B localization, 3 μ M nocodazole decreased Aurora B localization to the inner centromere. My own results indicate that relative to taxol, CPC localization is enhanced at the centromere by about 20% in nocodazole. This is similar to previous reports demonstrating that exposure of

untransformed human RPE cells to nocodazole enhances Aurora B recruitment to the centromere (Salimian et al. 2011). These differences are not due to different cell lines *per se*, as all experiment in my study were performed in HeLa cells using the same concentration of nocodazole. Thus, future work is necessary to better characterize the interaction of the CPC with microtubules and how this promotes CPC localization.

While my results seem distinct from work on EB1 and UBASH3B, they are consistent with several observations in budding yeast. Mutating putative Cdk1 sites to alanine in the budding yeast INCENP homolog Sli15 (Sli15-6A) targets it the anaphase spindle (Mirchenko & Uhlmann 2010). Similarly, mutation of 20 putative Ipl1 phosphorylation sites to alanine (Sli15-20A) targets Sli15 to the spindle, but demonstrates no defect in error correction or ability to maintain the SAC in response to defective tension (Makrantonis et al. 2014). It has also been shown that Sli15 lacking the CEN domain retargets to mitotic spindles, but is competent for error correction and the SAC in response to defective tension (Campbell & Desai 2013). In line with the importance of the CPC-microtubule interaction, attenuating the binding of Sli15 to microtubules, either by mimicking constitutive phosphorylation of Ipl1 sites (Sli15-20D) or deleting the microtubule-binding region of Sli15 lacking the CEN domain, silences the tension-dependent checkpoint and leads to a defect in chromosome segregation, respectively. Although there is a potential conflict in the budding yeast literature that while the Sli15-20A and Sli15 Δ CEN mutants maintains the SAC in response to defective

tension, Sli15-6A does not (Mirchenko & Uhlmann 2010), these results are consistent with my observations in human cells and suggest that the interaction of the CPC with microtubules is an evolutionarily conserved mechanism to promote the SAC. Understanding the basis of this requirement in the genetically tractable budding yeast system may provide key insights to verify in higher vertebrates.

Regulation of the CPC at the kinetochore and on microtubules

The interaction of the CPC with microtubules may support cluster-dependent activation of Aurora B near the kinetochore. This idea is in line with previous work identifying a pool of active Aurora B at the outer kinetochore (Deluca et al. 2011; Posch et al. 2010), though the existence and function of this pool remains controversial. Recently, it has been reported that this kinetochore-proximal pool of CPC requires dimerization of Borealin (Bekier et al. 2015). Dimerization of INCENP through the CEN domain, where Borealin binds, increases the affinity of the CPC for microtubules (van der Horst et al. 2015), consistent with microtubule-dependent Aurora B activation supporting a kinetochore-proximal pool of CPC. How could this kinetochore pool of Aurora B be regulated?

Mps1-dependent phosphorylation of the Borealin dimerization domain promotes Aurora B-dependent error correction during an unperturbed mitosis (Jelluma et al. 2008). It also prevents Borealin dimerization *in vitro* (Bourhis et al.

2009), which may decrease the affinity of the INCENP SAH domain for microtubules (van der Horst et al. 2015). These observations are in line with a mechanism whereby Aurora B is activated by clustering on microtubules before diffusing to locally phosphorylate substrates at the kinetochore (**Figure 3-29**).

Alternatively, PP1 and PP2A are known to oppose Aurora B activity at the kinetochore and may be critical for regulating kinetochore-proximal CPC. In particular, PP2A in complex with a B56 regulatory subunit is localized to the kinetochore during prometaphase where it regulates Aurora B-dependent kinetochore phosphorylation to promote kMT attachment (Foley et al. 2011). PP2A-Shugoshin also localizes to the centromere in an Aurora B-dependent manner (Tanno et al. 2010) and locally regulates activation of Aurora B by dephosphorylating Thr232 on its activation loop (Meppelink et al. 2015). Interestingly, the activation loop of Aurora B is protected from PP2A-mediated dephosphorylation at the kinetochore by virtue of its interaction with EB1 (Sun et al. 2008) and by acetylation of its kinase domain by TIP60 (Mo et al. 2016). If these proteins protect Aurora B from inactivation by PP2A, how then does PP2A oppose Aurora B activity at the kinetochore?

One idea is that PP2A inhibits Aurora B activity by promoting activation of PP1, which unlike PP2A can dephosphorylate the activation loop of Aurora B in complex with EB1 (Sun et al. 2008). B56-PP2A depletion increases both Aurora B- and Plk1-dependent phosphorylation at the kinetochore (Foley et al. 2011). While loss of B56-PP2A also destabilizes kMT attachment, this affect can be

rescued by inhibition of either Aurora B or Plk1 (Foley et al. 2011), suggesting they may be in the same pathway promoting KMT destabilization. Consistent with this, Plk1 promotes Aurora B activity at the kinetochore by opposing PP1 via phosphorylation of the PP1 regulatory subunit Sds22 (Duan et al. 2016). If B56-PP2A depletion enhances Plk1-dependent inhibition of Sds22-PP1, this may be mechanistically similar to depletion of Sds22, which increases both Aurora B T232 at the kinetochore and the frequency of lagging chromosomes (Posch et al. 2010). Thus, PP2A may oppose Plk1 to promote PP1-mediated dephosphorylation of Aurora B at the kinetochore. This mechanism would allow PP2A to indirectly inactivate Aurora B, even if TIP60 and EB1 prevent direct dephosphorylation of Aurora B T232.

What is the functional significance of making Aurora B refractory to dephosphorylation by PP2A? One idea is PP2A dephosphorylates the INCENP PRD to promote Aurora B localization/ activation on microtubules, which is important for the SAC in taxol (**Figure 3-25**). It has been suggested that PP2A preferentially dephosphorylates threonine residues during mitosis (Labit et al. 2012) and 4/6 residues in the PRD are threonine in most vertebrate species (**Figure 3-18**). During early mitosis, this activity might oppose phosphorylation of the PRD by Cdk1-Cyclin B to promote clustering and activation of Aurora B on kinetochore-proximal microtubules. EB1 and TIP60 may be critical to allow PP2A to target the CPC to microtubules without also inactivating Aurora B. Upon bi-orientation, PP2A is removed from the kinetochore (Foley et al. 2011), which

would prevent the INCENP-microtubule interaction and decrease the kinetochore pool of active Aurora B. Decreased Aurora B activity would promote binding of PP1, which could then reinforce stable kMT attachment and checkpoint silencing. While highly speculative, this model suggests how kinetochore proximal CPC could be activated and regulated with kMT attachment to support CPC function at the kinetochore.

4.2 Concluding Remarks: CPC at the centromere and beyond

The current paradigm for how the CPC promotes accurate cell division focuses on the importance of its localization at the centromere. The first half of my graduate work elaborated this canonical pathway, culminating in a mechanism that couples the activity of Haspin to the cell cycle to promote timely recruitment of the CPC during mitosis. Subsequently, I identified the INCENP SAH domain as a previously unappreciated molecular determinant of CPC localization to the centromere. Moreover, this domain also targets the CPC to microtubules during early mitosis, an interaction that is critical for maintaining the SAC. INCENPs ability to bind both chromatin and microtubules is necessary for a robust SAC, suggesting new complexity in the localization and regulation of Aurora B-dependent phosphorylation at the kinetochore. This work establishes the importance of regulated localization of the CPC beyond the centromere as an exciting new mechanism for understanding how CPC function is regulated to promote accurate chromosome segregation.

Chapter 5: Material and Methods

5.1 General Techniques

Plasmid construction

Data on all constructs is in **Table 2**. All Haspin constructs were prepared from xHaspin-FL (Kelly et al. 2010). All GFP-tagged xINCENP constructs and xSAH-domain constructs were prepared from GFP-xINCENP-FL (Tseng et al. 2010). Full-length siRNA-resistant hINCENP was a gift from S. Lens. All human constructs were cloned into a pcDNA5-FRT-TO plasmid containing the LAP-tag gifted by R. Gassmann. Full-length hCENP-B and hCENP-B DNA-binding domain were gifted by M. Lampson (E. Wang et al. 2011). Full-length hMis12 and a plasmid containing the MAP4-MTBD were gifted by T. Kapoor (Tan & Kapoor 2011). All human phospho-site mutants were generated using the QuikChange Multi Site-Directed Mutagenesis kit (Agilent) per the manufacturers recommendations. *Xenopus* phospho-site mutants were generated using Gibson Assembly (Gibson et al. 2009) with synthesized DNA fragments corresponding to the desired mutations. All constructs were cloned using either QuikChange Site-Directed Mutagenesis (Aglient), a PCR-based digestion/ ligation strategy using a pair of unique restriction sites in the pcDNA5-FRT-TO plasmid, or were generated using Gibson Assembly. The coding frame of all constructs was verified by DNA sequencing prior to insertion into T-REx cell lines.

Immunoblotting

Mitotic cell extracts were prepared by placing cells in 0.33 μ M nocodazole for 6-8 hr followed by mitotic shake-off. Cells were pelleted at 200 g, rinsed twice in PBS and resuspended in 2x Laemmli Buffer. Extracts were sonicated at 4 °C in a Bioruptor water bath (Diagenode) at medium intensity cycling 30s on/ 60s off for a total of 10 min. Samples were denatured, the protein concentration was determined using 260/280 on a NanoDrop 2000 and an equal amount of each sample was run on a precast 4-12% Bis-Tris gel (Thermo Fisher) followed by transfer to a nitrocellulose membrane overnight at 30 V. For *Xenopus* egg extract, samples were diluted in sample buffer, denatured, run on a precast gel as above, and transferred to a nitrocellulose membrane overnight at 15 V.

Membranes were blocked in sterile 4% nonfat milk in PBS for at least 30 min, followed by incubation with primary antibody diluted in 5% BSA for 1-6 hr at room temperature. After 3x 5 min washes in PBST, the membranes were incubated for 1 hr with IRDye 800CW and 680LT secondary antibodies diluted in Odyssey Blocking Buffer with 0.1% Tween. Membranes were then washed 3x 5min in PBST, and detected using the Odyssey Infrared Imaging System (LI-COR Biosciences). All antibody information is located in **Table 3, 4**.

Immunofluorescence image acquisition and processing

Immunofluorescence images were acquired on a DeltaVision Image Restoration Microscope (Applied Precision) using an Inverted Olympus IX-70 stage, pco.edge sCOS camera (PCO), Insight SSI solid state illumination system (Applied Precision), 20x/0.75 air and 100x/1.4 oil objectives (Olympus) and running SoftWoRx v6.1 software (Applied Precision). Wavelengths used are 435, 525, 594 and 676. All images were acquired as z-stacks with 0.4 μm optical sectioning and deconvolved using SoftWoRx constrained iterative deconvolution with default settings. All images within an experiment used identical acquisition settings. Images for Chapter 2 were acquired similarly, but with a CoolSNAP QE CCD camera (Photometrics).

Deconvolved stacks were exported as 16-bit TIFFS and quantified using MetaMorph. For all samples, a maximum projection of the DAPI channel was used to generate a DAPI mask around the channel of interest. Centromere intensity was quantified by integrated the signal intensity in each plane of the Z-stack above a threshold that specifically captured centromeric signal. Kinetochore intensity of phospho-specific kinetochore antibodies was quantified using a marker channel to manually place a circle of defined size around each kinetochore. These kinetochore regions were then used to quantify the signal intensity from a maximum projection of the phospho-specific antibody channel.

Data presentation

Broken violin plots were generated using a custom script in Python 2.7. Briefly, a kernel density estimate of the underlying data was determined using the `scipy.stats.gaussian_kde` module with a bandwidth determined by the 'Scott' method. The integrated area underneath each density estimate is equal between all samples in a plot unless otherwise indicated. For visualization, density estimates were cut at the minimum and maximum value of the underlying data. Beneath each density is a minimalist boxplot with a lower whisker from $-1.5 \times \text{IQR}$ to the 1st quartile, a circle at the median, and an upper whisker from the 3rd quartile to $+1.5 \times \text{IQR}$. Data was organized using the Pandas module, programmatically visualized using the matplotlib and seaborn modules, and labeled and formatted in Adobe Illustrator CC.

Representative images are no more than $\pm 20\%$ of the median value of the construct based on quantification. Representative images from qualitative experiments were chosen based on morphology. Graphs were generated using Python or Prism software. All boxplots are Tukey boxplots with whiskers extending $\pm 1.5 \times$ interquartile range. For visual simplicity, points past the whiskers (considered statistical outliers) are omitted. All statistical analyses were conducted in Prism using a two-tailed Mann-Whitney test. Individual p-values and n-values are indicated in figure legends.

5.2 Human Tissue Culture

Cell culture, siRNA and drug treatments

RPE1-hTERT cells were cultured at 37 °C with 5% CO₂ in DMEM:F12 (ATCC) with 10% FBS. HeLa cells were cultured at 37 °C with 5% CO₂ in Dulbecco's Modified Eagle Media (Thermo Fisher) supplemented with 10% tetracycline-free FBS (Atlanta Biologicals) and non-essential amino acids (Thermo Fisher). HeLa and DLD1 T-Rex cell lines were generated using the manufacturers protocol from a parental line containing a single FRT integration site and stably integrated RFP-H2B (a gift of A. Desai and R. Gassmann) (Gassmann et al. 2010).

For live cell imaging experiments, 300,000 cells were seeded onto glass bottom dishes No. 1.5 thickness (MatTek). After 12-16 hr, 100 mg/ml doxycycline was added to induce construct expression and siRNA was transfected using Lipofectamine RNAiMax (Thermo Fisher) and 60 pmol of either ON-TARGETplus control siRNA (GE Healthcare) or a previously described siRNA against the coding region of human INCENP (5'-UGACACGGAGAUUGCCAAC-3') (Vader et al. 2006). After 24-36 hr, cells were transferred to fresh media prior to imaging.

For live cell imaging synchronization and release experiments, cells were plated as above and allowed to adhere in the presence of doxycycline for 6 hr, before the addition of RO-3306 for 16-18 hr. Cells were rinsed 3 times in DPBS and placed in fresh media prior to imaging.

For fixed cell immunofluorescence, cells were seeded in 10 cm dishes, adhered for 12-16 hr, treated with doxycycline and siRNA for 24-36 hr, then split onto poly-D-lysine coated Millicell EZ glass chamber slides (Millipore) and a 6 cm dish (processed in parallel and used to prepare mitotic extracts for immunoblotting). After adhering for 12 hr, cells were synchronized with RO-3306 for 12 hr, followed by 3 washes in DPBS and addition of fresh media containing either nocodazole or taxol for 2-4 hr before fixation. When used, ZM447439 was added 1 hr prior to fixation.

For expression of LAP-hHaspin constructs in interphase, cells were grown in thymidine for 18 hr, released into fresh media for 9 hr, then placed in media containing thymidine and 25 ng/ml doxycyclin for 24 hr. Cells were collected by trypsinization and processed for western blot analysis.

Drug concentrations for human tissue culture cells, unless otherwise indicated: 9 μ M RO-3306 (Sigma), 3.3 μ M nocodazole (Sigma), 500nM taxol (Millipore), 100 μ M monastrol (Tocris), 2 μ M ZM447439 (Chemietek), 10 μ M MG132, 100 nM Bi2536, 2mM thymidine

Immunoprecipitation

For immunoprecipitation from mitotic HeLa cell extracts, construct expression was induced by doxycycline in a confluent 15 cm dish for 8 hr followed by the addition of 100 ng/ml nocodazole for 16 hr. Mitotic cells were collected by shake-off, rinsed in PBS, resuspended in 50 μ L PBS, then incubated

in lysis buffer (50mM Tris pH 8, 150 mM NaCl, 1% NP-40, 0.5 mM PMSF, 5 mM beta-glycerol phosphate, phosphatase inhibitor cocktail (Roche) and EDTA-free protease inhibitor (Sigma)) for 30 min. Samples were sonicated in a water bath 5x 10 s on/ 10 s off and passaged through a 25¼ gauge needle. Samples were clarified by spinning for 10 min at maximum speed in a tabletop centrifuge. Clarified lysate was incubated with magnetic beads cross-linked to Rabbit IgG or Rabbit anti-GFP antibodies for 1.5 hr with constant agitation. Beads were removed, rinsed once in lysis buffer, resuspended in sample buffer and boiled. Half the sample was loaded for western blot analysis. All steps were performed at 4 °C.

Live cell imaging and analysis

Live cell imaging was performed at 37 °C in 5% CO₂ in a LCV110U VivaView FL incubator microscope (Olympus) equipped with an X-Cite-exacte illumination source (Excelitas Technologies) and Orca-R2 CCD camera (Hamatsu). For SAC experiments, spindle poisons diluted in media were added to each dish at least 20 min prior to imaging. For RO synchronization and release experiments, samples were imaged directly after the final washout. Images were acquired with a 20x objective every 15 min for 48-72 hr in the DIC, RFP and GFP channel. Individual cells were manually analyzed using the CellCognition browser. The duration of mitosis and class at exit from mitosis were inferred from DIC and RFP morphology. For SAC experiments, only cells observed

transitioning from interphase to mitosis during the first 16 hr of the movie were analyzed. The duration of mitosis was calculated as the time from nuclear envelope breakdown until either slippage into interphase or cell death.

For live cell imaging synchronization and release experiments, each sample was imaged prior to washout to verify that >95% of cells were in interphase. Following washout, cells in prophase/prometaphase at the beginning of the movie or those seen transitioning into mitosis within the first 6 hr of the movie were analyzed. The duration of mitosis was calculated as the time from nuclear envelope breakdown until chromosome segregation or cell death.

Immunofluorescence

HeLa cells were fixed in 2% PFA in PBS pH 7.4 or 1% PFA + 0.2% Triton X-100 (for DSN1 S100ph, KNL1 S24ph; gifts of I. Cheeseman and Hec1 S44ph; a gift of J. Deluca) for 10 min at room temperature. Cells were then washed twice in PBS, permeabilized in PBS + 0.2% Triton X-100 for 10 min, rinsed twice in PBS, then blocked for at least 30 min in 5% BSA + 0.2% Tween 20 (Blocking). Cells were incubated in primary antibody diluted in blocking for at least 1 hr, rinsed twice in PBST, and then incubated in secondary antibody in blocking for at least 1 hr. Cells were rinsed twice in PBST, incubated for at least 5 min in PBS + 1 µg/ml DAPI, rinsed once in PBS and mounted with ProLong Gold antifade mountant (Thermo Fisher). All primary and secondary antibodies are listed in **Table 3, 4.**

For immunofluorescence of human cells in Chapter 2: Cells were mitotic shake-off and resuspended in ice-cold PBS. Cells were placed on poly-L-lysine coated slides by cytocentrifugation (Stat Spin Cytofuge 2) for 4 min at 850 RPM and fixed for 10 min in 2% PFA in PBS pH 7.7. After rinsing in PBS, cells were permeabilized for 10 min in 0.5% Triton, rinsed 2x 5 min in PBS, then blocked for 1 hr in blocking solution (10% FBS, 10 mM Tris pH 8, 120 mM KCl, 20 mM MgCl_2 , 0.5 mM EDTA). Cells were incubated with primary antibody for 1 hr in blocking solution with 0.1% triton x-100, rinsed 3x 5 min in wash buffer (10 mM Tris pH8, 120 mM KCl, 20 mM MgCl_2 , 0.5 mM EDTA, 0.1% triton x-100), then incubated with secondary for 30 min in blocking solution + 0.1% triton x-100. After a 3x 5 min rinse in wash buffer and a 5 min rinse in PBS, cells were mounted with 6 μL vectashield with DAPI. Coverslips were sealed with nailpolish and slides were stored at 4 °C.

Fluorescence recovery after photobleaching (FRAP)

Following 36-48 hr siRNA treatment and construct induction, cells were treated with 3.3 μ M nocodazole or 500 nM taxol for 1 hr then placed in a 37 °C chamber mounted on a Deltavision Image Restoration System microscope (see 'Image acquisition and processing'). FRAP was performed using SoftWoRx v6.1 software and a 488 QLM laser pulse to bleach 3 centromeric foci per cell. Images were acquired at 60x/1.42 oil objective from a single z-section every 10 s for 30 s before and 5 min after bleaching. Quantification was performed in ImageJ using a circle of defined size to quantify the integrated intensity of each bleached focus, a same-sized background focus, and the entire cell. Only foci remaining in the focal plane for the duration of the movie were quantified. Full-scale normalization and single-exponential fitting was performed in MATLAB using the easyFRAP module (Rapsomaniki et al. 2012) to determine the $t_{1/2}$ of each focus.

5.3 *Xenopus* egg extract

***Xenopus* egg extract depletion and reconstitution**

A published protocol was used to prepare CSF extracts (Murray 1991). Depletion of endogenous CPC and reconstitution was previously described (Tseng et al. 2010). For depletion, magnetic protein A Dynabeads (Invitrogen) were coupled and cross-linked to either Rabbit anti-IgG or Rabbit anti-xINCENP beads using BS_3 (Pierce) according to the manufacturers recommendations. CSF extract was incubated with the appropriate beads in a 1:1 ratio for 1 hr at 4 °C then beads were removed to yield depleted extract. The CPC was reconstituted in Δ CPC extract by the addition of 500 nM recombinant MBP- xAurora B, 0.3 $\mu\text{g}/\mu\text{l}$ of mRNA for the appropriate GFP-xINCENP construct, and 0.075 $\mu\text{g}/\mu\text{l}$ each of mRNA encoding xSurvivin and xDasra A. To translate these mRNA constructs, extract was cycled into interphase by the addition of 300 μM calcium chloride for 1.5 hr at 22 °C then driven back into metaphase by adding an equal volume of fresh CSF extract and incubating for 30-45 min at 22 °C. mRNA was prepared using the SP6 mMessage mMachine RNA transcription kit (Ambion). All xSAH-domain fragments were expressed from mRNA added to extract at 0.15-0.3 $\mu\text{g}/\mu\text{l}$ and cycled as above. Immunoprecipitation of GFP and GFP-xSAH was performed similar to CPC depletion using Rabbit anti-GFP antibodies.

xHaspin was depleted from CSF extracts containing cycloheximide (100 $\mu\text{g}/\text{ml}$) using anti-xHaspin-coated protein A-Dynabeads (Invitrogen), following an immunodepletion protocol as described (Kelly et al. 2010). To complement

Δ xHaspin extracts by full-length or mutant xHaspin, we produced the proteins using the transcription-coupled translation rabbit reticulocyte lysate system (Promega). The reactions were incubated for 2.5 hr at 30 °C in the presence of ³⁵S-labeled methionine. The samples were diluted 1:10 into either CSF or interphase extracts and incubated for 60–90 min.

Plx1 was depleted from CSF extract using two sequential rounds of immunodepletion at a 1:1 ratio of anti-Plx1-beads (without crosslinking) to extract. The antibody beads were incubated with extract for 1 hr, on ice, then the beads were removed and the procedure was repeated with the second set of antibody beads. Extracts treated with protein A-beads coated with rabbit IgG were used as control extracts.

Immunofluorescence

Immunofluorescence of spindles and sperm chromatin was performed as previously published (Tseng et al. 2010; Desai et al. 1999). Briefly, extract was diluted in fixative (1x BRB80, 2% formaldehyde) for 5 min, layered over a glycerol cushion and then pelleted onto a stage containing a circular coverslip for 15 min at 5.1K RPM in a Sorval HS7 swinging-bucket rotor. The cushion was rinsed twice with 1x BRB80 and aspirated away. The coverslip was removed, fixed in ice cold methanol for 5 min, rinsed 2x in 10 mM TBS pH 7.4 + 0.1% Triton-X100, then incubated with Abdil (10 mM TBS pH 7.4, 150 mM NaCl, 0.1% Triton-X100, 2% BSA) overnight at 4 °C. Samples were incubated with primary and secondary

antibodies diluted in Abdil for at least 1 hr, with a 2x PBST rinse after each incubation. Samples were washed once in PBS then mounted with VectaShield antifade mountant containing DAPI (Vector laboratories).

For immunofluorescence on nocodazole treated sperm chromatin, 1000-2000 sperm/ μ l were added prior to calcium addition. After incubation with fresh CSF, samples were incubated with 33 μ M nocodazole for 30 min prior to processing for immunofluorescence.

Spindle Assembly Checkpoint

The spindle assembly checkpoint assay was performed similar to (Minshull et al. 1994). Briefly, samples were reconstituted as above. CSF extract was then incubated with 10,000 sperm/ μ L and 33 μ M nocodazole for 45 min, followed by addition of 600 μ M calcium chloride. Western blot samples were taken at 30 min intervals following the addition of calcium chloride.

Microtubule Pelleting Assay

Microtubule pelleting assays were modified from (Xue et al. 2013). Extract was incubated for 30 min with 33 μ M nocodazole or 10 μ M taxol at 22 °C. An input sample was taken and 20 μ L of extract was diluted in fixative (1x BRB80, 30% glycerol, 0.1% Triton X-100, phosphatase inhibitor) and layered over a glycerol cushion (1x BRB80, 40% glycerol). Samples were spun in a tabletop centrifuge at room temperature for 15 min at maximum speed. The cushion was

washed twice with 1x BRB80, aspirated away, and the pellet was resuspended in 1x BRB80 + 0.1% Triton X-100 and transferred to a fresh tube. The sample was spun again for 15 min and the pellet resuspended in 40 µl sample buffer.

Phosphatase Treatment

For phosphatase treatment, samples were diluted in buffer containing lambda phosphatase for 40 min at 30 °C (NEB).

CENP-A nucleosome arrays

(by D. Wynne)

CENP-A nucleosome arrays were assembled according to (Guse et al. 2011). Briefly, chromatin was assembled by salt dialysis of 3.6 µM human CENP-A/ *Xenopus laevis* H4 dimers that had been co-purified from bacteria using hydroxyapatite (Bio-Rad) and HiTrap SP (GE) columns, 4.0 µM *Xenopus laevis* H2A/H2B dimers generated by purifying his-tagged constructs separately from inclusion bodies using Ni-NTA (Qiagen) and dialyzed together after cleavage of the His tags using TEV protease (Zierhut et al. 2014), and 0.2 µg/µl of a DNA fragment containing 19 copies of the 601 nucleosome positioning sequence, which had been biotinylated on both ends using Klenow (NEB) in the presence of biotin-14-dATP, thio-dTTP and thio-dGTP. Plasmids encoding this DNA template and for CENP-A/H4 co-expression were gifts from A. Straight. Plasmids for expression of His-H2A and His-H2B were gifts from C. D. Allis.

Coupling to Dynabeads M-280 Streptavidin (Life Technologies) at a concentration in which 1 μ g of DNA was coupled to 10 μ l of bead slurry for 1 hr was done just prior to addition to extract. To assay CPC localization, array-coupled beads were added to a final volume of 100 μ l control (Δ IgG), CPC-depleted, or CPC-reconstituted extract. Extracts were then cycled to express RNA (see above) and 33 μ M nocodazole was added. Beads were then removed from extract with a magnet, washed in ice cold CSF-XB with 0.05% Triton X-100, fixed for 5 min in 2% formaldehyde, washed with Abdil, added to acid-washed, poly-L-lysine coated coverslips, and then processed for immunofluorescence in the same manner as sperm chromosomes (see above).

Immunoprecipitation

RNAs encoding wild-type or various xHaspin mutants carrying a C-terminal GFP tag were synthesized using the SP6 mMessage mMachine RNA transcription kit (Ambion). These mRNAs were added at 0.1 μ g/ μ l to CSF-arrested or interphase extracts and incubated for 60-90 min to allow expression. Then protein G-beads coated with GFP antibody (2 μ g of GFP antibody for 50 μ l of beads) were incubated with the extract on ice for 1 hr. The beads were removed and washed 5x with ice cold wash buffer (1xPBS, 1% Triton X-100, 0.5 mM PMSF, 5 mM b-glycerophosphate, 1x phosphatase inhibitor cocktail 2 (P5726 Sigma)).

Importin b beads were prepared by coupling 12 μ l of the nuclear transport factor p97, mAB (3E9) (Enzo, ALX-804-025) to 33 μ l of prewashed protein G beads. As a control we used the Mouse IgG antibody from Sigma diluted in PBS with 50% glycerol. The extract was incubated with 0.1 μ g/ μ l of xHaspin mRNA for 45 min at room temperature. At this point the extract was divided into two tubes, one was maintained in CSF for another 60 min, while to the other we added calcium and induced interphase at room temperature. Cyclohexamide was added to both samples to stop further xHaspin translation. To 40 μ l of extracts we added 15 μ l of Importin b coupled beads. They were incubated at room temperature with occasional mixing for 1 hr. Prior to removing the beads we took the input western blot sample. The beads were removed by placing them on a magnet for 2 min. The supernatant western blot sample was taken at this point. Immediately 150 μ l of wash buffer was added to the beads to avoid drying. The beads were washed 5 times in ice cold buffer containing: 1xPBS, 1% Triton, 0.5 mM PMSF, phosphatase inhibitor cocktail [Sigma, p2850]), 5 mM β -glycerophosphate, 1xLPC. The beads were resuspended in an equal volume of sample buffer and boiled prior to running on a polyacrylamide gel.

MBP-xHaspin N420 constructs were incubated with extract at 2 mM for 60 min. They were subsequently captured using protein G-Dyna beads coated with anti-MBP antibody (NE Biolabs #E8032S), 3 μ g of antibody for 30 μ l of beads. They were washed and prepared as above.

Synthetic Peptides and Bead Pulldowns

Biotinylated peptides corresponding to the xHaspin HBIS (biotin-HWLRLRAALSLHRKKKVQATD) or a scrambled version of the sequence (biotin-ARDQKLWSKARTHVAHLKLLR) were synthesized by the Rockefeller University Proteomics Resource Center. Peptides were >95% pure by analytical HPLC and ESI MS.

Peptide beads were prepared similar to (Kelly et al. 2010) but with the following modifications. Streptavidin-coated magnetic beads (Invitrogen) were washed three times in PBS + 0.01% triton, resuspended in PBS, then incubated for 45 min at room temperature without peptide or with 10-fold excess (2 nmol peptide/mg beads) of scrambled or HBIS peptide. Beads were rinsed five times in PBS +0.01% triton and three times in sperm dilution buffer.

Peptide bead pulldowns were performed similar to (Kelly et al. 2010). For each sample, 50-100 μ l beads (100-200 pmol peptide) were incubated with 30 μ l CSF extract for 60 min at 4 °C mixing every 20 min. An input sample was taken before placing the extract on a magnetic rack for 10 min. Extract was removed and beads were washed three times in an equal volume of bead wash buffer (20 mM HEPES pH 8, 250 mM NaCl, 0.05 % Igal CA-630, 10% glycerol, 0.1 mM TCEP, 0.5 mM PMSF, 10 ng/ml LPC) with phosphatase inhibitors (1 mM b-glycerophosphate, 1x phosphatase inhibitor cocktail from Sigma) and twice in plain wash buffer. All wash steps were performed at 4 °C. Beads and inputs were treated with lambda phosphatase for 45 min at 30 °C. Beads were then mixed

with 4X SDS loading buffer and denatured at 100 °C for 5 min before running on a 7.5-15 % SDS-PAGE gel. Peptides and streptavidin were visualized by Coomassie.

Mass spectrometry

LC-MS/MS analysis on xHaspin fragments phosphorylated in metaphase *Xenopus* egg extracts and *in vitro* with Plk1 and Cdk1-Cyclin B was performed by the Rockefeller University Proteomics Resource Center. LC-MS/MS analysis on full-length xHaspin-GFP constructs was performed by MS Bioworks (Ann Arbor, MI).

LC-MS/MS analysis on xHaspin fragments phosphorylated in metaphase Xenopus egg extracts and in vitro with Plk1 and Cdk1-Cyclin B, performed by the Rockefeller University Proteomics Resource Center

Protein in-solution was reduced (Dithiothreitol) and alkylated (iodoacetamide) prior to trypsination (Promega trypsin, Promega, Madison, WI). Generated peptides were desalted and concentrated (Rappsilber et al., 2007) prior to analysis by nano LCMS/MS using an Q-Exactive (Thermo, San Jose, CA) mass spectrometer. MS/MS data were extracted using ProteomeDiscoverer v. 1.4 (Thermo, Bremen, Germany) and queried against a data base, containing xHaspin, common observed contaminants and background proteome (5,177 sequences), using MASCOT 2.3 (Matrixscience, London, UK). Mass tolerance of

20 ppm and 20 mDa were used for peptide precursors and peptide fragments, respectively. For peptide spectrum matches the median precursor mass accuracy was 0.46 ppm. Phosphorylations of serine, threonine and tyrosine were allowed as variable modifications together with oxidized methionine. All cysteines were treated as being iodoacetamidated.

For the identification and validation of phosphopeptides the following strategy was followed: Phosphopeptides were not enriched prior to LC-MS/MS analysis which allowed for 1) validation of lower quality phosphopeptide spectra by comparison to high quality spectra of corresponding non-phosphorylated peptides and 2) an approximate ranking of the phosphorylated peptides based on phosphorylation level. The latter was achieved by comparing the ratio of area under curve for the phosphorylated peptide and the corresponding non-phosphorylated peptides. Differences in ionization of phosphorylated versus non-phosphorylated peptides were not taken into account. For peptides containing multiple potential phosphorylation sites phosphoRS was used to calculate probability for the different residues (Olsen et al., 2006).

LC-MS/MS analysis on full-length xHaspin-GFP constructs, performed by MS Bioworks (Ann Arbor, MI)

In gel digestion was performed using a ProGest robot (DigiLab) with the following protocol: 1) Washed with 25 mM ammonium bicarbonate followed by acetonitrile. 2) Reduced with 10 mM dithiothreitol at 60 °C followed by alkylation

with 50 mM iodoacetamide at room temperature. 3) Digested with sequencing grade trypsin (Promega) at 37 °C for 4 hr. 4) Quenched with formic acid and the supernatant was analyzed directly without further processing.

The sample was analyzed by nano LC/MS/MS with a Waters NanoAcquity HPLC system interfaced to a ThermoFisher Q Exactive mass spectrometer. 30 µl of sample was loaded on a trapping column and eluted over a 75 µm analytical column at 350 nl/min; both columns were packed with Jupiter Proteo resin (Phenomenex). The mass spectrometer was operated in data- dependent mode, with MS performed at 70,000 FWHM resolution and MS/MS performed at 17,500 FWHM. The fifteen most abundant ions were selected for MS/MS.

Data were searched using a local copy of Mascot with the following parameters: Enzyme: Trypsin Database: NCBI *Xenopus laevis* (Appended with common contaminants, reversed and concatenated) Fixed modification: Carbamidomethyl (C) Variable modifications: Oxidation (M), Acetyl (N-term), Pyro-Glu (N-term Q), Deamidation (N,Q), Phospho (S,T,Y) Mass values: Monoisotopic Peptide Mass Tolerance: 10 ppm Fragment Mass Tolerance: 0.015 Da Max Missed Cleavages: 2 Mascot DAT files were parsed into the Scaffold software for validation, filtering and to create a non-redundant list per sample. For protein identification the data were filtered using a minimum protein value of 80 %, a minimum peptide value of 50% (Prophet scores) and requiring at least two unique peptides per protein. For phosphosite identification only one unique peptide was required.

5.4 Recombinant proteins/ *in vitro* assays:

Recombinant proteins

(by C. Ghenoiu)

MBP-xHaspin Δ N729 and MBP-xHaspin Δ N729 Δ HBIS were expressed in BL21 *E.coli* and purified by Ni-NTA standard methods, followed by gel filtration (S200) and dialyzed into 50 mM HEPES pH 8, 300 mM NaCl, 10% glycerol. MBP-xHaspin N420 and MBP-xHaspin N520 were purified similarly to the kinase domain constructs except a higher salt concentration was used (500 mM NaCl vs. 300mM) and an extra wash step was applied with MgCl₂/ATP (50 mM Tris pH 8, 500 mM NaCl, 2.5 mM ATP, 10 mM MgCl₂, 10 mM b-mercaptoethanol). MBP-hHaspin was bacterially expressed using pMALc2/coHaspin (codon optimized, a generous gift from Jonathan Higgin), and was purified following a standard MBP/amylose chromatography protocol, using 1M NaCl column buffer. The protein was stored in 50 mM HEPES pH 8, 300 mM NaCl, 10% glycerol. The kinase was stored at 4 °C after purification and the *in vitro* kinase experiments were performed within two days of purification. We noted that liquid nitrogen freezing and storing at -80 °C resulted in protein degradation upon thawing. GST-Plx1-PBD-His was purified by Ni-NTA standard methods and dialyzed into protein binding buffer (50 mM HEPES pH 8, 300 mM NaCl, 0.1% Tween 20, 4 % w/v skim milk, 10 % glycerol, 1 mM DTT). His₆-tagged IBB was generated and purified from a plasmid generously provided by Karsten Weis following a published procedure (Weis et al. 1996).

Far western blots

(by C. Ghenoïu)

Protein phosphorylation was performed at room temperature using 173 pmols of the various substrates, 0.2 ng/μl Cdk1/Cyclin B (Millipore #14-450), 250 μM cold ATP in a final volume of 30 μl 1x kinase buffer (10x kinase buffer: 200 mM HEPES-KOH pH 7.7, 1.5 M NaCl, 100 mM MgCl₂, 10 mM DTT, phosphatase inhibitor cocktail [Sigma, p2850]). The reaction was quenched by addition of 10 μl 4xSDS buffer and heat and the samples were run on a polyacrylamide gel and transferred to nitrocellulose membrane (Whatman Protran BA79). The membrane was blocked for 1 hr using Odyssey blocking buffer (LICOR 927-40000). The bait concentration (either PBDWT or PBDH532A/K534A) was set to 5 μg/ml. The bait was incubated in protein binding buffer (50 mM HEPES pH 8, 300 mM NaCl, 0.1% Tween 20, 4% w/v skim milk, 10% glycerol, 1mM DTT) for 10 hr at room temperature. The membrane was washed twice with PBST for 10 min and incubated with primary antibody (anti-Plx1) for 1 hr and after two more washes in PBST, an IRDye 800CW goat anti-rabbit IgG (LICOR) secondary antibody was applied for 1 hr. The membrane was washed three times in PBST (10 min) and twice in PBS (10 min) before imaging it using the Odyssey LICOR system.

Kinetic analysis of H3T3ph

(by C. Ghenoiu)

We analyzed kinetic data from anti-phospho H3T3 Western blots by adapting a method published by (Good et al. 2009). Briefly, to generate the standard H3T3ph curve, we incubated 10 μ M of H31-45-GST (produced from plasmids, generously provided by J. Higgins) (Dai et al. 2005) with 2 μ M MBP-xHaspin- Δ 729 overnight at 16 °C to ensure complete phosphorylation of the substrate. Serial dilutions of fully phosphorylated H31- 45-GST were analyzed by quantitative western blot with anti-H3T3ph antibody. To determine the linear range of the western blot signal, several dilution series of the anti- H3T3ph antibody were employed. For kinetic analysis, we set up a reaction mix that contained 1 nM of either MBP-xHaspin- Δ 729 or MBP-xHaspin- Δ 729 Δ HBIS, 750 μ M ATP, varying concentrations of GST-H3 1 to 45 (0, 50, 100, 200, 400, 800, 1600 nM) in 1x Kinase buffer (20 mM HEPES pH 8, 150 mM NaCl, 10 mM MgCl₂, 1 mM DTT) on ice. The reaction was initiated by addition of ATP and the substrate and it was allowed to proceed on ice. Samples were collected at 1, 3.5 and 7 min and quenched by adding 4x SDS sample buffer containing 50 mM EDTA followed by boiling. The samples were run on a polyacrylamide gel and subjected to western blotting analysis using as primary antibody anti-phospho H3T3ph 1:10000 (Millipore # 07-424) that was optimized to be in the linear range and as secondary antibody goat anti-rabbit IgG LICOR IRDye 800. The blots were scanned and quantified on LICOR Odyssey Imaging system. The data was exported to Prism 5 and rate plots (AU/min) were generated, all with an R² >

0.95. Using the standard curve mentioned above, we estimated the absolute concentration of phosphorylated substrates to obtain the rate plots in nM/min. Triplicate data sets were fit to the Michaelis-Menten equation with Prism to calculate K_m and k_{cat} for each curve.

***In vitro* kinase assays with recombinant proteins**
(by C. Ghenoiu)

To check the ability of Cdk1 and Plk1 to phosphorylate the xHaspin N terminus (MBPxHaspin- N520) *in vitro*, we set up 25 μ l reactions, at room temperature, in the presence of 250 μ M cold ATP and 2.5 μ Ci per reaction of γ -³³P ATP. The substrate, MBPxHaspin- N520 was added to the reaction at 0.3 μ M. Cdk1-Cyclin B (Millipore #14 450) was added to the reaction at 0.2 ng/ μ l. Plk1 (SignalChem # P41-10H-10) was added to the reaction at 32 ng/ μ l. Co-incubation of Cdk1-Cyclin B and Plk1 was performed as follows: MBP-xHaspin-N520 was allowed to pre-incubate with Cdk1-CyclinB in the presence of cold ATP only, for 1 hr at room temperature. Then, the Cdk1 inhibitor RO- 3306 (Enzo, ALX-270-463) was added to the reaction to 10 μ M final concentration and allowed to incubate for 30 min. To this reaction we added Plk1 together with γ -³³P ATP. To phosphorylation recombinant hHaspin by Plk1 and Cdk1-Cyclin B, 1 μ M MBPhHaspin was incubated in a mixture of 1x Kinase buffer with either 3 ng/ μ l Cdk1-Cyclin B (Millipore #14-450), 32 ng/ μ l Plk1 (SignalChem # P41-10H-10), or both kinases, 250 μ M cold ATP, 3.75 μ Ci per reaction of γ -³³P ATP for 2 hr at room temperature. Then, the reaction was diluted in 1x Kinase buffer to 25

nM MBP-hHaspin and placed on ice for 30 min to cool. This pre-phosphorylated MBP-hHaspin was added in 1:10 (2.5 nM final) to another *in vitro* kinase reaction that was kick started by the addition of 300 nM GST-H3 and 750 μ M cold ATP. At 8, 12 and 20 min, 20 μ l were removed and added to 8 μ l of 4xSDS buffer. These samples were boiled and processed for western blot analysis. The LICOR Odyssey Imaging system was used to quantify the H3T3ph signal. The ability of Plk1 to phosphorylate either the N-terminal tail (1-45 aa) of histone H3 or a positive control, namely dephosphorylated Casein (SignalChem, C03-54BN), was assessed in the presence of 250 μ M cold ATP and 2.5 μ Ci per reaction of γ -³³P ATP.

Antibody beads kinase assay (by C. GhenoIU)

To perform the *in vitro* kinase assay involving full length xHaspin, wild-type or kinase inactive xHaspin K862A, tagged with GFP, were expressed and purified from interphase *Xenopus* egg extracts following the protocol described in the Immunoprecipitations section. After washing, the beads were resuspended in an equal volume of sperm dilution buffer (SDB: 1 mM MgCl₂, 100 mM KCl, 150 mM sucrose, 5 mM HEPES, 100 μ g/ml cytochalasin B), 10 μ l of these beads were pre-incubated with either Cdk1-Cyclin B, Plk1 or both. 25 μ l reactions were assembled to contain 250 μ M cold ATP, 10 μ l of xHaspin beads, 2 ng/ μ l Cdk1-Cyclin B (Millipore #14-450), 32 ng/ μ l Plk1 (SignalChem # P41-10H-10). These reactions were incubated for 1.5 hr at room temperature. Following this

incubation, the 25 μ l reaction was placed on ice for 30 min. Then to start the reaction, the 25 μ l were added to 115 μ l of an ice cold 1x Kinase buffer mixture containing 200 nM GST-H31-45, 750 μ M cold ATP. At 0, 1, 3, 5, and 10 min, 20 μ l were removed and added to 8 μ l of 4xSDS buffer. These samples were boiled and processed for western blot analysis. The LICOR Odyssey Imaging system was used to quantify the H3T3ph signal.

Quantification of H3T3ph activity exhibited by xHaspin phosphorylation mutants

(by C. GhenoIU)

The expression level of Haspin phosphorylation mutants were quantified based on the 35 S intensity present in the 0 min input sample by using the Odyssey 2.1.10 quantification software (LICOR). In multiple experiments we confirmed that performing the quantification using the 35 S intensity present at the 60 min gave the same result, and since quantifying a sharp band was less technically challenging, we reported the results using the 0 min input. The H3T3ph levels were quantified in a similar manner. The data was processed by first normalizing the H3T3ph level to the 35 S level of each mutant. Subsequently, the mutant activity was expressed as a percentage of the wild-type activity. P-values were determined using a one-way ANOVA followed by a Bonferroni post-hoc test.

Appendix: Tables

Table 1: Identification of phosphorylation sites on xHaspin

[illegible]

Number of phosphorylated peptide (Number of unphosphorylated peptide)										
Flanking Sequence@	mRNA expressed xHaspin-GFP in metaphase extract				Recombinant MBP-xHaspin N520 in vitro	Recombinant MBP-xHaspin fragments in extract				
	WT	T206A	Kinase Dead	N520		N520 in metaphase	N520 T206A in metaphase	ΔN729 in metaphase	N520 in metaphase	N520 in T206A in metaphase
VIRT*YGR	1 (1)	0 (0)	0 (0)	HIT		1 (1)	1 (5)	0 (4)		0 (4)
RIQT*QT*WFS*PVN	2 (4)	3 (5)	2 (4)	4 (9)		0 (10)	0 (15)	0 (2)	0 (13)	0 (18)
GRS*NIP	6 (14)	0 (10)	0 (12)	3 (14)		5 (10)	3 (11)	0 (3)	0 (11)	0 (20)
NPAS*P*LT*V*PFR	5 (10)	7 (16)	4 (8)	14 (16#3)						
FVT*VRR	4 (7)	0 (2)	0 (1)	2 (2)					0 (1)	0 (1)
DIRS*ILNS*PT*EIS*HS*PLQ	4 (3#1)	8 (8#2)	4 (4#1)	11 (20#2)		2 (4)	4 (5)		4 (12)	2 (6)
LQKS*PLLS*P*TP*P*VLL	5 (6#1)	0 (0)	7 (6#2)	6 (11)		3 (5)	0 (6)	0 (1)	0 (16)	0 (4)
LCET*LEES*VVR	0 (1)	0 (5)	0 (1)	4 (16)		0 (2)	0 (4)		0 (8)	0 (10)
PQVY*EQLET*FNT*P*EED				3 (10)			1 (1)		0 (3)	0 (3)
PIRSSQKS										
RLRS*AHC	2 (3)	1 (2)	0 (1)							
DFIS*QOS*NQR	2 (13)	1 (9)	2 (9)	3 (10)		0 (3)	0 (7)	0 (3)	0 (3)	0 (7)
RGVS*P*HY*AEP	4 (12)	0 (11)	2 (10)	2 (3)		1 (2)	0 (2)	0 (2)	0 (2)	0 (3)
APVT*LS*P*CAS*QOS*VIC				2 (8)			0 (1)		0 (1)	0 (1)
RGNS*QVLCLS*SELS*EDDDHS*KT*PSH	0 (2)	2 (6)	0 (0)	3 (10)			0 (1)		0 (2)	0 (4)
NADS*VMQY*FOS*RING	1 (10)	0 (11)	1 (6)	7 (23)		0 (3)	0 (7)	0 (1)	0 (5)	0 (6)
NGPS*VS*LLT*NT*QAE	1 (5)	0 (6)	0 (1)	19 (26#4)		0 (5)	0 (5)		0 (8)	0 (9)
FNHT*VVPPS*KDGDHVT*P*PCHT*NKR	6 (12)	6 (26)	0 (9)	4 (5#1)		2 (3)	0 (1)	0 (12)	0 (12)	3 (16)
QPN*AT*PKCF	2 (6)	3 (10)	2 (8)	1 (6)		1 (2)	1 (4)		0 (3)	0 (6)
NLPT*PCP	1 (2)	1 (5)	0 (1)							
RNIS*PLLES*IT*KT*PNLAES*RT*TERK	7 (20)	11 (29#1)	3 (15)							
KVQS*CS*P*RAQ	2 (5)	0 (3)	0 (3)							
AQAS*VGT*GRK	4 (7)	1 (4)	2 (5)							
VCIS*GFS*AKR	12 (22#1)	5 (14)	1 (11)							
LKKT*RT*QQQ	2 (6)	3 (13)	0 (3)							
AALS*LHR	13 (20)	0 (9)	1 (10)							
ADRS*LALQS*PPS*VNV								8 (13)		
RCLS*ACA	0 (2)	1 (4)	0 (3)					0 (15)		
IIDY*TT*LSR	1 (6)	0 (6)	0 (4)					0 (10)		
KKPS*P*ALQ	2 (10)	1 (8)	1 (9)					0 (6)		

Table 2: Constructs

Construct name	N-terminal tag	Construct
hINCENP FL	LAP-tag	hINCENP 1:918
hINCENP ΔSAH	LAP-tag	hINCENP Δ528:795
hINCENP ΔSAH ΔGCN4	LAP-tag	hINCENP Δ528:795 ΔscGCN4 250:281
hINCENP ΔSAH ΔMAP4	LAP-tag	hINCENP Δ528:795 ΔhMAP4 590:964
hINCENP ΔSAH ^N	LAP-tag	hINCENP Δ546:580
hINCENP ΔSAH ^N ΔMAP4	LAP-tag	hINCENP Δ546:580 ΔhMAP4 590:964
hINCENP 6A	LAP-tag	hINCENP (T478A, S481A, T507A, T524A, S798A, T807A)
hINCENP 6D	LAP-tag	hINCENP (T478D, S481D, T507D, T524D, S798D, T807D)
hINCENP ΔSAH ⁶⁴¹⁻⁷⁴⁷	LAP-tag	hINCENP Δ641:747
hINCENP ΔSAH ⁷⁴⁸⁻⁷⁹⁸	LAP-tag	hINCENP Δ748:798
hINCENP ΔCEN	LAP-tag	hINCENP Δ1:47
CB- hINCENP ΔCEN	LAP-tag	hCENP-B 1:599- hINCENP Δ1:47
CB ^{DBD} - hINCENP ΔCEN	LAP-tag	hCENP-B 1:167- hINCENP Δ1:47
Mis12- hINCENP ΔCEN	LAP-tag	hMis12 1:205- hINCENP Δ1:47
hINCENP ΔCEN ΔSAH	LAP-tag	hINCENP Δ1:47 Δ528:795
CB- hINCENP ΔCEN ΔSAH	LAP-tag	hCENP-B 1:599- hINCENP Δ1:47 Δ528:795
CB ^{DBD} - hINCENP ΔCEN ΔSAH	LAP-tag	hCENP-B 1:167- hINCENP Δ1:47 Δ528:795
Mis12- hINCENP ΔCEN ΔSAH	LAP-tag	hMis12 1:205- hINCENP Δ1:47 Δ528:795
hINCENP ΔCEN 6A	LAP-tag	hINCENP Δ1:47 (T478A, S481A, T507A, T524A, S798A, T807A)
hINCENP ΔCEN 6A ΔSAH ^N	LAP-tag	hINCENP Δ1:47 Δ546:580 (T478A, S481A, T507A, T524A, S798A, T807A)
hINCENP ΔCEN 6D	LAP-tag	hINCENP Δ1:47 (T478D, S481D, T507D, T524D, S798D, T807D)
xINCENP FL	GFP	xINCENP 1:871
xINCENP ΔSAH	GFP	xINCENP Δ491:748
xINCENP ΔSAH ^N	GFP	xINCENP Δ505:539
xINCENP 7A	GFP	xINCENP (S430A, T436A, S438A, T469A, T487A, S751A, T760A)
xINCENP 7A ΔSAH ^N	GFP	xINCENP Δ505:539 (S430A, T436A, S438A, T469A, T487A, S751A, T760A)
xINCENP 7D	GFP	xINCENP (S430D, T436D, S438D, T469D, T487D, S751D, T760D)
GFP	GFP	
xSAH	GFP	xINCENP 491:748
xSAH	6x Myc	xINCENP 491:748
xSAH Δ1	6x Myc	xINCENP 491:748 Δ491:551
xSAH Δ2	6x Myc	xINCENP 491:748 Δ552:601
xSAH Δ3	6x Myc	xINCENP 491:748 Δ591:651
xSAH Δ4	6x Myc	xINCENP 491:748 Δ641:701
xSAH Δ5	6x Myc	xINCENP 491:748 Δ691:748
xSAH ΔSAH ^N	6x Myc	xINCENP 491:748 Δ505:539
xSAH + PRD	6x Myc	xINCENP 401:784
xSAH + 7A	6x Myc	xINCENP 401:784 (S430A, T436A, S438A, T469A, T487A, S751A, T760A)
xSAH + 7D	6x Myc	xINCENP 401:784 (S430D, T436D, S438D, T469D, T487D, S751D, T760D)
xDasra A		xDasra A 1:296
xSurvivin		xSurvivin 1:160

Table 3: Primary antibodies

Epitope	Source	IF dilution	WB dilution	Species	Catalog #	Epitope origin	Type	PMID
Hec1	Abcam	1000		Mo	ab3613	Hs	monoclonal	
Hec1 S44ph	Jennifer Deluca	1000		Rb		Hs	polyclonal	21266467
DSN1 S100ph	Ian Cheeseman	1000		Rb	19A2	Hs	polyclonal	20471944
GFP	Molecular Probe	400		Rb	A11122		polyclonal	
GFP	Roche	400	200	Mo	11814460001		monoclonal	
Aurora B	BD Transduction	500-2000	1000	Mo	611082	Hs	monoclonal	
Survivin	Novus Biologicals	500	1000	Rb	NB500-201	Hs	polyclonal	
INCENP	Abcam		1000	Rb	ab134112	Hs	monoclonal	
MAD2	Covance	200		Rb	PRB-452C-200	Hs	polyclonal	
Bub1	Millipore	500		Mo	MAB3610	Hs	monoclonal	
BubR1	Millipore	500		Mo	MAB3612	Hs	monoclonal	
Borealin	Santa Cruz		500	Mo	sc-376635	Hs	monoclonal	
Histone H3 T3ph	Millipore		3000	Rb	07-424	Hs	polyclonal	
Histone H3 T3ph	Upstate	12500	10000	Rb				
Aurora A/B/C T288ph	Cell Signaling		400	Rb	2914S	Hs	monoclonal	
alpha-Tubulin	Sigma		10000	Mo	T9026	Gg	monoclonal	
CENP-C	Hiroshi Kimura	1000-2000		Gp		Hs	polyclonal	11884609
KNL1 S24ph	Ian Cheeseman	500-1000		Rb	59A2	Hs	polyclonal	20471944
Myc	Millipore		1000	Mo	05-724	Hs	monoclonal	
NUMA	Rebecca Heald		1000	Rb		Xl	polyclonal	15102852
CENP-A S7ph	Millipore	500-1000		Rb	07-232	Hs	polyclonal	
CENP-A	Millipore	500		Rb	07-574	Hs	polyclonal	
Histone H3 S10ph	Cell Signaling	2000-3000		Rb	3377	Hs	monoclonal	
xSurvivin	Funabiki		3000	Rb	RU1594	Xl	polyclonal	20627073
xINCENP	Funabiki		1mg/mL	Rb	RU1720	Xl	polyclonal	15260989
xAurora B	Funabiki		1mg/mL	Rb	RU1050	Xl	polyclonal	17199039
xINCENP	Funabiki		1mg/mL	Rb	RU1718	Xl	polyclonal	15260989
xDasra A	Funabiki		1mg/ml	Rb	RU982	Xl	polyclonal	15260989
CREST		400		Hu		Hu	polyclonal	
xOP18	Funabiki					Xl		
Pan CDK1 S/Tp	Cell Signaling		1000	Rb	2324		polyclonal	
Importin β	BD Transduction		1000	Mo	610560	Mo		
MBP	NEBiolabs		10000	Mo	E8032S		monoclonal	
Pix1	Funabiki		0.2ug/mL	Rb		Xl	polyclonal	
xHaspin	Funabiki		1ug/mL	Rb		Xl	polyclonal	

Table 4: Secondary antibodies

Secondary for IF	Fluorophore	IF dilution
GP	Dylight 594	1000
Rb	Alexa 488	1000
Rb	Cy5	1000
Mo	Alexa 488	1000
Mo	Cy5	1000
Hu	Dylight 649	400

References

- Abe, Y. et al., 2016. HP1-Assisted Aurora B Kinase Activity Prevents Chromosome Segregation Errors., 36(5), pp.487–497.
- Adams, R.R. et al., 2000. INCENP binds the Aurora-related kinase AIRK2 and is required to target it to chromosomes, the central spindle and cleavage furrow. *Current Biology*, 10(17), pp.1075–1078.
- Ahonen, L.J. et al., 2009. Perturbation of Incenp function impedes anaphase chromatid movements and chromosomal passenger protein flux at centromeres. *Chromosoma*, 118(1), pp.71–84.
- Ainsztein, A.M. et al., 1998. INCENP centromere and spindle targeting: identification of essential conserved motifs and involvement of heterochromatin protein HP1. *The Journal of Cell Biology*, 143(7), pp.1763–1774.
- Akiyoshi, B. et al., 2009. Analysis of Ipl1-mediated phosphorylation of the Ndc80 kinetochore protein in *Saccharomyces cerevisiae*. *Genetics*, 183(4), pp.1591–1595.
- Akiyoshi, B. et al., 2010. Tension directly stabilizes reconstituted kinetochore-microtubule attachments. *Nature*, 468(7323), pp.576–579.
- Akiyoshi, B., Nelson, C.R. & Biggins, S., 2013. The aurora B kinase promotes inner and outer kinetochore interactions in budding yeast. *Genetics*, 194(3), pp.785–789.
- Alfieri, C. et al., 2016. Molecular basis of APC/C regulation by the spindle assembly checkpoint. *Nature*, 536(7617), pp.431–436.
- Aravamudhan, P., Goldfarb, A.A. & Joglekar, A.P., 2015. The kinetochore encodes a mechanical switch to disrupt spindle assembly checkpoint signalling. *Nature*, 17(7), pp.868–879.
- Banerjee, B., Kestner, C.A. & Stukenberg, P.T., 2014. EB1 enables spindle microtubules to regulate centromeric recruitment of Aurora B. *The Journal of Cell Biology*, 204(6), pp.947–963.
- Barisic, M. et al., 2010. Spindly/CCDC99 is required for efficient chromosome congression and mitotic checkpoint regulation. *Molecular biology of the cell*, 21(12), pp.1968–1981.
- Bayliss, R. et al., 2012. On the molecular mechanisms of mitotic kinase activation. *Open biology*, 2(11), pp.120136–120136.

- Beardmore, V.A. et al., 2004. Survivin dynamics increases at centromeres during G2/M phase transition and is regulated by microtubule-attachment and Aurora B kinase activity. *Journal of cell science*, 117(Pt 18), pp.4033–4042.
- Becker, M. et al., 2010. Centromere localization of INCENP-Aurora B is sufficient to support spindle checkpoint function. *Cell cycle (Georgetown, Tex)*, 9(7), pp.1360–1372.
- Bekier, M.E. et al., 2015. Borealin dimerization mediates optimal CPC checkpoint function by enhancing localization to centromeres and kinetochores. *Nature communications*, 6, p.6775.
- Biggins, S. & Murray, A.W., 2001. The budding yeast protein kinase Ipl1/Aurora allows the absence of tension to activate the spindle checkpoint. *Genes & development*, 15(23), pp.3118–3129.
- Biggins, S. et al., 1999. The conserved protein kinase Ipl1 regulates microtubule binding to kinetochores in budding yeast. *Genes & development*, 13(5), pp.532–544.
- Bishop, J.D. & Schumacher, J.M., 2002. Phosphorylation of the carboxyl terminus of inner centromere protein (INCENP) by the Aurora B Kinase stimulates Aurora B kinase activity. *The Journal of biological chemistry*, 277(31), pp.27577–27580.
- Blower, M.D., 2016. Centromeric Transcription Regulates Aurora-B Localization and Activation. *Cell reports*, 15(8), pp.1624–1633.
- Bohnert, K.A. et al., 2009. A link between aurora kinase and Clp1/Cdc14 regulation uncovered by the identification of a fission yeast borealin-like protein. *Molecular biology of the cell*, 20(16), pp.3646–3659.
- Bokros, M. & Wang, Y., 2016. Spindle assembly checkpoint silencing and beyond. *Cell cycle (Georgetown, Tex)*, 15(13), pp.1661–1662.
- Bourhis, E. et al., 2009. Phosphorylation of a borealin dimerization domain is required for proper chromosome segregation. *Biochemistry*, 48(29), pp.6783–6793.
- Buffin, E. et al., 2005. Recruitment of Mad2 to the kinetochore requires the Rod/Zw10 complex. *Current Biology*, 15(9), pp.856–861.
- Campbell, C.S. & Desai, A., 2013. Tension sensing by Aurora B kinase is independent of survivin-based centromere localization. *Nature*, 497(7447), pp.118–121.

- Carmena, M. et al., 2014. Polo kinase regulates the localization and activity of the chromosomal passenger complex in meiosis and mitosis in *Drosophila melanogaster*. *Open biology*, 4(11), pp.140162–140162.
- Carmena, M., Pinson, X., et al., 2012. The chromosomal passenger complex activates polo kinase at centromeres. *PLoS biology*, 10(1), p.e1001250.
- Carmena, M., Wheelock, M., et al., 2012. The chromosomal passenger complex (CPC): from easy rider to the godfather of mitosis. *Nature reviews Molecular cell biology*, 13(12), pp.789–803.
- Carretero, M. et al., 2013. Pds5B is required for cohesion establishment and Aurora B accumulation at centromeres. *The EMBO Journal*, 32(22), pp.2938–2949.
- Chan, C.S. & Botstein, D., 1993. Isolation and characterization of chromosome-gain and increase-in-ploidy mutants in yeast. *Genetics*, 135(3), pp.677–691.
- Chan, Y.W. et al., 2009. Mitotic control of kinetochore-associated dynein and spindle orientation by human Spindly. *The Journal of Cell Biology*, 185(5), pp.859–874.
- Cheeseman, I.M. et al., 2006. The conserved KMN network constitutes the core microtubule-binding site of the kinetochore. *Cell*, 127(5), pp.983–997.
- Ciferri, C. et al., 2008. Implications for kinetochore-microtubule attachment from the structure of an engineered Ndc80 complex. *Cell*, 133(3), pp.427–439.
- Cimini, D. et al., 2006. Aurora kinase promotes turnover of kinetochore microtubules to reduce chromosome segregation errors. *Current Biology*, 16(17), pp.1711–1718.
- Clute, P. & Pines, J., 1999. Temporal and spatial control of cyclin B1 destruction in metaphase. *Nature Publishing Group*, 1(2), pp.82–87.
- Collin, P. et al., 2013. The spindle assembly checkpoint works like a rheostat rather than a toggle switch. *Nature*, 15(11), pp.1378–1385.
- Cooke, C.A., Heck, M.M. & Earnshaw, W.C., 1987. The inner centromere protein (INCENP) antigens: movement from inner centromere to midbody during mitosis. *The Journal of Cell Biology*, 105(5), pp.2053–2067.
- Dai, J. et al., 2005. The kinase haspin is required for mitotic histone H3 Thr 3 phosphorylation and normal metaphase chromosome alignment. *Genes & development*, 19(4), pp.472–488.

- Dai, J., Sullivan, B.A. & Higgins, J.M.G., 2006. Regulation of mitotic chromosome cohesion by Haspin and Aurora B., 11(5), pp.741–750.
- De Antoni, A. et al., 2005. The Mad1/Mad2 complex as a template for Mad2 activation in the spindle assembly checkpoint. *Current Biology*, 15(3), pp.214–225.
- Delacour-Larose, M. et al., 2004. Distinct dynamics of Aurora B and Survivin during mitosis. *Cell cycle (Georgetown, Tex)*, 3(11), pp.1418–1426.
- Delacour-Larose, M. et al., 2007. Role of survivin phosphorylation by aurora B in mitosis. *Cell cycle (Georgetown, Tex)*, 6(15), pp.1878–1885.
- DeLuca, J.G. et al., 2006. Kinetochore microtubule dynamics and attachment stability are regulated by Hec1. *Cell*, 127(5), pp.969–982.
- DeLuca, K.F., Lens, S.M.A. & DeLuca, J.G., 2011. Temporal changes in Hec1 phosphorylation control kinetochore-microtubule attachment stability during mitosis. *Journal of cell science*, 124(Pt 4), pp.622–634.
- Desai, A. et al., 1999. The use of *Xenopus* egg extracts to study mitotic spindle assembly and function in vitro. *Methods in cell biology*, 61, pp.385–412.
- Dick, A.E. & Gerlich, D.W., 2013. Kinetic framework of spindle assembly checkpoint signalling. *Nature*, 501(7466), pp.1370–1377.
- Ditchfield, C. et al., 2003. Aurora B couples chromosome alignment with anaphase by targeting BubR1, Mad2, and Cenp-E to kinetochores. *The Journal of Cell Biology*, 161(2), pp.267–280.
- Du, J. et al., 2012. Structural Basis for Recognition of H3T3ph and Smac/DIABLO N-terminal Peptides by Human Survivin. *Structure (London, England : 1993)*, 20(1), pp.185–195.
- Duan, H. et al., 2016. Phosphorylation of PP1 regulator Sds22 by PLK1 ensures accurate chromosome segregation. *The Journal of biological chemistry*, p.jbc.M116.745372.
- Dumont, J., Oegema, K. & Desai, A., 2010. A kinetochore-independent mechanism drives anaphase chromosome separation during acentrosomal meiosis. *Nature*, 465(7302), pp.894–901.
- Earnshaw, W.C. & Cooke, C.A., 1991. Analysis of the distribution of the INCENPs throughout mitosis reveals the existence of a pathway of structural changes in the chromosomes during metaphase and early events in cleavage furrow formation. *Journal of cell science*, 98 (Pt 4), pp.443–461.

- Elia, A.E.H., Cantley, L.C. & Yaffe, M.B., 2003. Proteomic screen finds pSer/pThr-binding domain localizing Plk1 to mitotic substrates. *Science (New York, NY)*, 299(5610), pp.1228–1231.
- Elia, A.E.H., Rellos, P., et al., 2003. The molecular basis for phosphodependent substrate targeting and regulation of Plks by the Polo-box domain. *Cell*, 115(1), pp.83–95.
- Emanuele, M.J. et al., 2008. Aurora B kinase and protein phosphatase 1 have opposing roles in modulating kinetochore assembly. *The Journal of Cell Biology*, 181(2), pp.241–254.
- Espt, A. et al., 2014. PP2A-B56 opposes Mps1 phosphorylation of Knl1 and thereby promotes spindle assembly checkpoint silencing. *The Journal of Cell Biology*, 206(7), pp.833–842.
- Eswaran, J. et al., 2009. Structure and functional characterization of the atypical human kinase haspin. *Proceedings of the National Academy of Sciences of the United States of America*, 106(48), pp.20198–20203.
- Etemad, B., Kuijt, T.E.F. & Kops, G.J.P.L., 2015. Kinetochore-microtubule attachment is sufficient to satisfy the human spindle assembly checkpoint. *Nature communications*, 6, p.8987.
- Foley, E.A. & Kapoor, T.M., 2013. Microtubule attachment and spindle assembly checkpoint signalling at the kinetochore. *Nature reviews Molecular cell biology*, 14(1), pp.25–37.
- Foley, E.A., Maldonado, M. & Kapoor, T.M., 2011. Formation of stable attachments between kinetochores and microtubules depends on the B56-PP2A phosphatase. *Nature*, 13(10), pp.1265–1271.
- Gadea, B.B. & Ruderman, J.V., 2006. Aurora B is required for mitotic chromatin-induced phosphorylation of Op18/Stathmin. *Proceedings of the National Academy of Sciences of the United States of America*, 103(12), pp.4493–4498.
- Gadea, B.B. & Ruderman, J.V., 2005. Aurora kinase inhibitor ZM447439 blocks chromosome-induced spindle assembly, the completion of chromosome condensation, and the establishment of the spindle integrity checkpoint in *Xenopus* egg extracts. *Molecular biology of the cell*, 16(3), pp.1305–1318.
- Gascoigne, K.E. & Taylor, S.S., 2008. Cancer cells display profound intra- and interline variation following prolonged exposure to antimitotic drugs. *Cancer cell*, 14(2), pp.111–122.

- Gassmann, R. et al., 2008. A new mechanism controlling kinetochore-microtubule interactions revealed by comparison of two dynein-targeting components: SPDLC-1 and the Rod/Zw10/Zw10 complex. *Genes & development*, 22(17), pp.2385–2399.
- Gassmann, R. et al., 2004. Borealin: a novel chromosomal passenger required for stability of the bipolar mitotic spindle. *The Journal of Cell Biology*, 166(2), pp.179–191.
- Gassmann, R. et al., 2010. Removal of Spindly from microtubule-attached kinetochores controls spindle checkpoint silencing in human cells. *Genes & development*, 24(9), pp.957–971.
- Ghenoiu, C., Wheelock, M.S. & Funabiki, H., 2013. Autoinhibition and Polo-dependent multisite phosphorylation restrict activity of the histone H3 kinase Haspin to mitosis. *Molecular cell*, 52(5), pp.734–745.
- Gibson, D.G. et al., 2009. Enzymatic assembly of DNA molecules up to several hundred kilobases. *Nature methods*, 6(5), pp.343–345.
- Good, M. et al., 2009. The Ste5 scaffold directs mating signaling by catalytically unlocking the Fus3 MAP kinase for activation. *Cell*, 136(6), pp.1085–1097.
- Griffis, E.R., Stuurman, N. & Vale, R.D., 2007. Spindly, a novel protein essential for silencing the spindle assembly checkpoint, recruits dynein to the kinetochore. *The Journal of Cell Biology*, 177(6), pp.1005–1015.
- Gruneberg, U. et al., 2004. Relocation of Aurora B from centromeres to the central spindle at the metaphase to anaphase transition requires MKlp2. *The Journal of Cell Biology*, 166(2), pp.167–172.
- Guimaraes, G.J. et al., 2008. Kinetochore-microtubule attachment relies on the disordered N-terminal tail domain of Hec1. *Current Biology*, 18(22), pp.1778–1784.
- Guse, A. et al., 2011. In vitro centromere and kinetochore assembly on defined chromatin templates. *Nature*, 477(7364), pp.354–358.
- Hauf, S. et al., 2005. Dissociation of cohesin from chromosome arms and loss of arm cohesion during early mitosis depends on phosphorylation of SA2. R. S. Hawley, ed. *PLoS biology*, 3(3), p.e69.
- Hauf, S. et al., 2003. The small molecule Hesperadin reveals a role for Aurora B in correcting kinetochore-microtubule attachment and in maintaining the spindle assembly checkpoint. *The Journal of Cell Biology*, 161(2), pp.281–294.

- Hayashi-Takanaka, Y. et al., 2009. Visualizing histone modifications in living cells: spatiotemporal dynamics of H3 phosphorylation during interphase. *The Journal of Cell Biology*, 187(6), pp.781–790.
- Heinrich, S. et al., 2014. Mad1 contribution to spindle assembly checkpoint signalling goes beyond presenting Mad2 at kinetochores. *EMBO reports*, 15(3), pp.291–298.
- Higgins, J.M., 2001a. Haspin-like proteins: a new family of evolutionarily conserved putative eukaryotic protein kinases. *Protein science : a publication of the Protein Society*, 10(8), pp.1677–1684.
- Higgins, J.M., 2001b. The Haspin gene: location in an intron of the integrin alphaE gene, associated transcription of an integrin alphaE-derived RNA and expression in diploid as well as haploid cells. *Gene*, 267(1), pp.55–69.
- Higgins, J.M.G., 2003. Structure, function and evolution of haspin and haspin-related proteins, a distinctive group of eukaryotic protein kinases. *Cellular and Molecular Life Sciences*, 60(3), pp.446–462.
- Hiruma, Y. et al., 2015. CELL DIVISION CYCLE. Competition between MPS1 and microtubules at kinetochores regulates spindle checkpoint signaling. *Science (New York, NY)*, 348(6240), pp.1264–1267.
- Hoffman, D.B. et al., 2001. Microtubule-dependent changes in assembly of microtubule motor proteins and mitotic spindle checkpoint proteins at PtK1 kinetochores. *Molecular biology of the cell*, 12(7), pp.1995–2009.
- Honda, R., Körner, R. & Nigg, E.A., 2003. Exploring the functional interactions between Aurora B, INCENP, and survivin in mitosis. *Molecular biology of the cell*, 14(8), pp.3325–3341.
- Howell, B.J. et al., 2001. Cytoplasmic dynein/dynactin drives kinetochore protein transport to the spindle poles and has a role in mitotic spindle checkpoint inactivation. *The Journal of Cell Biology*, 155(7), pp.1159–1172.
- Hummer, S. & Mayer, T.U., 2009. Cdk1 negatively regulates midzone localization of the mitotic kinesin Mklp2 and the chromosomal passenger complex. *Current biology : CB*, 19(7), pp.607–612.
- Jambhekar, A. et al., 2014. RNA stimulates Aurora B kinase activity during mitosis. D. L. Silver, ed. *PLoS ONE*, 9(6), p.e100748.
- Jelluma, N. et al., 2008. Mps1 phosphorylates Borealin to control Aurora B activity and chromosome alignment. *Cell*, 132(2), pp.233–246.

- Jelluma, N. et al., 2010. Release of Mps1 from kinetochores is crucial for timely anaphase onset. *The Journal of Cell Biology*, 191(2), pp.281–290.
- Jeyaprakash, A.A. et al., 2011. Structural basis for the recognition of phosphorylated histone h3 by the survivin subunit of the chromosomal passenger complex. *Structure (London, England : 1993)*, 19(11), pp.1625–1634.
- Jeyaprakash, A.A. et al., 2007. Structure of a Survivin-Borealin-INCENP core complex reveals how chromosomal passengers travel together. *Cell*, 131(2), pp.271–285.
- Ji, Z., Gao, H. & Yu, H., 2015. CELL DIVISION CYCLE. Kinetochore attachment sensed by competitive Mps1 and microtubule binding to Ndc80C. *Science (New York, NY)*, 348(6240), pp.1260–1264.
- Kaitna, S. et al., 2000. Incenp and an aurora-like kinase form a complex essential for chromosome segregation and efficient completion of cytokinesis. *Current Biology*, 10(19), pp.1172–1181.
- Kalab, P., et al. 2002. Visualization of a Ran-GTP gradient in interphase and mitotic *Xenopus* egg extracts. *Science*, 295(5564), pp.2452-2456.
- Kallio, M.J. et al., 2002. Inhibition of aurora B kinase blocks chromosome segregation, overrides the spindle checkpoint, and perturbs microtubule dynamics in mitosis. *Current Biology*, 12(11), pp.900–905.
- Kang, J. et al., 2011. Mitotic centromeric targeting of HP1 and its binding to Sgo1 are dispensable for sister-chromatid cohesion in human cells. *Molecular biology of the cell*, 22(8), pp.1181–1190.
- Kasuboski, J.M. et al., 2011. Zwint-1 is a Novel Aurora B Substrate Required for the Assembly of a Dynein-binding Platform on Kinetochores. *Molecular biology of the cell*.
- Kato, H. et al., 2013. A conserved mechanism for centromeric nucleosome recognition by centromere protein CENP-C. *Science (New York, NY)*, 340(6136), pp.1110–1113.
- Kawashima, S.A. et al., 2010. Phosphorylation of H2A by Bub1 prevents chromosomal instability through localizing shugoshin. *Science (New York, NY)*, 327(5962), pp.172–177.
- Kawashima, S.A. et al., 2007. Shugoshin enables tension-generating attachment of kinetochores by loading Aurora to centromeres. *Genes & development*, 21(4), pp.420–435.

- Kelly, A.E. & Funabiki, H., 2009. Correcting aberrant kinetochore microtubule attachments: an Aurora B-centric view. *Current opinion in cell biology*, 21(1), pp.51–58.
- Kelly, A.E. et al., 2007. Chromosomal enrichment and activation of the aurora B pathway are coupled to spatially regulate spindle assembly., 12(1), pp.31–43.
- Kelly, A.E. et al., 2010. Survivin reads phosphorylated histone H3 threonine 3 to activate the mitotic kinase Aurora B. *Science (New York, NY)*, 330(6001), pp.235–239.
- Kim, J.-H., Kang, J.S. & Chan, C.S., 1999. Sli15 associates with the ipl1 protein kinase to promote proper chromosome segregation in *Saccharomyces cerevisiae*. *The Journal of Cell Biology*, 145(7), pp.1381–1394.
- Kim, S. & Yu, H., 2015. Multiple assembly mechanisms anchor the KMN spindle checkpoint platform at human mitotic kinetochores. *The Journal of Cell Biology*, 208(2), pp.181–196.
- Kirschner, M. & Mitchison, T., 1986. Beyond self-assembly: from microtubules to morphogenesis. *Cell*, 45(3), pp.329–342.
- Kitajima, T.S. et al., 2005. Human Bub1 defines the persistent cohesion site along the mitotic chromosome by affecting Shugoshin localization. *Current Biology*, 15(4), pp.353–359.
- Kops, G.J.P.L. et al., 2005. ZW10 links mitotic checkpoint signaling to the structural kinetochore. *The Journal of Cell Biology*, 169(1), pp.49–60.
- Krenn, V. & Musacchio, A., 2015. The Aurora B Kinase in Chromosome Bi-Orientation and Spindle Checkpoint Signaling. *Frontiers in oncology*, 5(Pt 12), p.225.
- Krupina, K. et al., 2016. Ubiquitin Receptor Protein UBASH3B Drives Aurora B Recruitment to Mitotic Microtubules., 36(1), pp.63–78.
- Kruse, T. et al., 2014. A direct role of Mad1 in the spindle assembly checkpoint beyond Mad2 kinetochore recruitment. *EMBO reports*, 15(3), pp.282–290.
- Kulukian, A., Han, J.S. & Cleveland, D.W., 2009. Unattached kinetochores catalyze production of an anaphase inhibitor that requires a Mad2 template to prime Cdc20 for BubR1 binding., 16(1), pp.105–117.
- Labit, H. et al., 2012. Dephosphorylation of Cdc20 is required for its C-box-dependent activation of the APC/C. *The EMBO Journal*, 31(15), pp.3351–3362.

- Lampson, M.A. & Cheeseman, I.M., 2011. Sensing centromere tension: Aurora B and the regulation of kinetochore function. *Trends in cell biology*, 21(3), pp.133–140.
- Lampson, M.A. et al., 2004. Correcting improper chromosome-spindle attachments during cell division. *Nature Publishing Group*, 6(3), pp.232–237.
- Lange, A. et al., 2007. Classical nuclear localization signals: definition, function, and interaction with importin alpha. *The Journal of biological chemistry*, 282(8), pp.5101–5105.
- Li, X. & Nicklas, R.B., 1995. Mitotic forces control a cell-cycle checkpoint. *Nature*, 373(6515), pp.630–632.
- Liu, D. et al., 2010. Regulated targeting of protein phosphatase 1 to the outer kinetochore by KNL1 opposes Aurora B kinase. *The Journal of Cell Biology*, 188(6), pp.809–820.
- Liu, D. et al., 2009. Sensing chromosome bi-orientation by spatial separation of aurora B kinase from kinetochore substrates. *Science (New York, NY)*, 323(5919), pp.1350–1353.
- Liu, H. et al., 2015. Mitotic Transcription Installs Sgo1 at Centromeres to Coordinate Chromosome Segregation. *Molecular cell*, 59(3), pp.426–436.
- Liu, X. et al., 2014. Chromatin protein HP1 interacts with the mitotic regulator borealin protein and specifies the centromere localization of the chromosomal passenger complex. *The Journal of biological chemistry*, 289(30), pp.20638–20649.
- London, N. & Biggins, S., 2014. Mad1 kinetochore recruitment by Mps1-mediated phosphorylation of Bub1 signals the spindle checkpoint. *Genes & development*, 28(2), pp.140–152.
- London, N. et al., 2012. Phosphoregulation of Spc105 by Mps1 and PP1 regulates Bub1 localization to kinetochores. *Current biology : CB*, 22(10), pp.900–906.
- Luo, X. et al., 2004. The Mad2 spindle checkpoint protein has two distinct natively folded states. *Nature structural & molecular biology*, 11(4), pp.338–345.
- Maciejowski, J. et al., 2010. Mps1 directs the assembly of Cdc20 inhibitory complexes during interphase and mitosis to control M phase timing and spindle checkpoint signaling. *The Journal of Cell Biology*, 190(1), pp.89–100.

- Mackay, A.M. et al., 1993. Molecular analysis of the INCENPs (inner centromere proteins): separate domains are required for association with microtubules during interphase and with the central spindle during anaphase. *The Journal of Cell Biology*, 123(2), pp.373–385.
- Magidson, V. et al., 2015. Adaptive changes in the kinetochore architecture facilitate proper spindle assembly. *Nature*, 17(9), pp.1134–1144.
- Magidson, V. et al., 2016. Unattached kinetochores rather than intrakinetochore tension arrest mitosis in taxol-treated cells. *The Journal of Cell Biology*, 212(3), pp.307–319.
- Makrantonis, V. et al., 2014. Phosphorylation of Sli15 by Ipl1 is important for proper CPC localization and chromosome stability in *Saccharomyces cerevisiae*. B. G. Mellone, ed. *PLoS ONE*, 9(2), p.e89399.
- Maldonado, M. & Kapoor, T.M., 2011. Constitutive Mad1 targeting to kinetochores uncouples checkpoint signalling from chromosome biorientation. *Nature*, 13(4), pp.475–482.
- Malvezzi, F. et al., 2013. A structural basis for kinetochore recruitment of the Ndc80 complex via two distinct centromere receptors. *The EMBO Journal*, 32(3), pp.409–423.
- Mansfeld, J. et al., 2011. APC15 drives the turnover of MCC-CDC20 to make the spindle assembly checkpoint responsive to kinetochore attachment. *Nature*, 13(9), pp.1–11.
- Mapelli, M. et al., 2007. The Mad2 conformational dimer: structure and implications for the spindle assembly checkpoint. *Cell*, 131(4), pp.730–743.
- Maresca, T.J. & Salmon, E.D., 2009. Intrakinetochore stretch is associated with changes in kinetochore phosphorylation and spindle assembly checkpoint activity. *The Journal of Cell Biology*, 184(3), pp.373–381.
- Maresca TJ, et al., 2009. Spindle assembly in the absence of a RanGTP gradient requires localized CPC activity. *Curr Biol*, 19(14), pp.1210–1215.
- Maresca, T.J. & Salmon, E.D., 2010. Welcome to a new kind of tension: translating kinetochore mechanics into a wait-anaphase signal. *Journal of cell science*, 123(Pt 6), pp.825–835.
- McEwen, B.F. et al., 1997. Kinetochore fiber maturation in PtK1 cells and its implications for the mechanisms of chromosome congression and anaphase onset. *The Journal of Cell Biology*, 137, pp.1567–1580.

- Meppelink, A. et al., 2015. Shugoshin-1 balances Aurora B kinase activity via PP2A to promote chromosome bi-orientation. *Cell reports*, 11(4), pp.508–515.
- Miller, S.A., Johnson, M.L. & Stukenberg, P.T., 2008. Kinetochore attachments require an interaction between unstructured tails on microtubules and Ndc80(Hec1). *Current Biology*, 18(22), pp.1785–1791.
- Minshull, J. et al., 1994. A MAP kinase-dependent spindle assembly checkpoint in *Xenopus* egg extracts. *Cell*, 79(3), pp.475–486.
- Mirchenko, L. & Uhlmann, F., 2010. Sli15(INCENP) dephosphorylation prevents mitotic checkpoint reengagement due to loss of tension at anaphase onset. *Current biology : CB*, 20(15), pp.1396–1401.
- Mo, F. et al., 2016. Acetylation of Aurora B by TIP60 ensures accurate chromosomal segregation. *Nature chemical biology*, 12(4), pp.226–232.
- Moyle, M.W. et al., 2014. A Bub1-Mad1 interaction targets the Mad1-Mad2 complex to unattached kinetochores to initiate the spindle checkpoint. *The Journal of Cell Biology*, 204(5), pp.647–657.
- Murray, A.W., 1991. Cell cycle extracts. *Methods in cell biology*, 36, pp.581–605.
- Musacchio, A., 2015. The Molecular Biology of Spindle Assembly Checkpoint Signaling Dynamics. *Current biology : CB*, 25(20), pp.R1002–18.
- Musacchio, A. & Salmon, E.D., 2007. The spindle-assembly checkpoint in space and time. *Nature reviews Molecular cell biology*, 8(5), pp.379–393.
- Nagpal, H. & Fukagawa, T., 2016. Kinetochore assembly and function through the cell cycle. *Chromosoma*, pp.1–15.
- Nakajima, Y. et al., 2009. Nbl1p: a Borealin/Dasra/CSC-1-like protein essential for Aurora/Ipl1 complex function and integrity in *Saccharomyces cerevisiae*. *Molecular biology of the cell*, 20(6), pp.1772–1784.
- Niedzialkowska, E. et al., 2012. Molecular basis for phosphospecific recognition of histone H3 tails by Survivin paralogues at inner centromeres. *Molecular biology of the cell*, 23(8), pp.1457–1466.
- Nijenhuis, W. et al., 2013. A TPR domain-containing N-terminal module of MPS1 is required for its kinetochore localization by Aurora B. *The Journal of Cell Biology*, 201(2), pp.217–231.
- Nijenhuis, W. et al., 2014. Negative feedback at kinetochores underlies a responsive spindle checkpoint signal. *Nature*, 516(7532), pp.1257–1264.

- Nishino, T. et al., 2013. CENP-T provides a structural platform for outer kinetochore assembly. *The EMBO Journal*, 32(3), pp.424–436.
- Nishino, T. et al., 2012. CENP-T-W-S-X forms a unique centromeric chromatin structure with a histone-like fold. *Cell*, 148(3), pp.487–501.
- Nishiyama, T. et al., 2013. Aurora B and Cdk1 mediate Wapl activation and release of acetylated cohesin from chromosomes by phosphorylating Sororin. *Proceedings of the National Academy of Sciences of the United States of America*, 110(33), pp.13404–13409.
- Norden, C. et al., 2006. The NoCut pathway links completion of cytokinesis to spindle midzone function to prevent chromosome breakage. *Cell*, 125(1), pp.85–98.
- Nozawa, R.-S. et al., 2010. Human POGZ modulates dissociation of HP1alpha from mitotic chromosome arms through Aurora B activation. *Nature*, 467(727), pp.719–727.
- Overlack, K. et al., 2015. A molecular basis for the differential roles of Bub1 and BubR1 in the spindle assembly checkpoint. *eLife*, 4, p.e05269.
- Pereira, G. & Schiebel, E., 2003. Separase regulates INCENP-Aurora B anaphase spindle function through Cdc14. *Science (New York, NY)*, 302(5653), pp.2120–2124.
- Pinsky, B.A. et al., 2006. The Ipl1-Aurora protein kinase activates the spindle checkpoint by creating unattached kinetochores. *Nature Publishing Group*, 8(1), pp.78–83.
- Polioudaki, H. et al., 2004. Mitotic phosphorylation of histone H3 at threonine 3. *FEBS letters*, 560(1-3), pp.39–44.
- Posch, M. et al., 2010. Sds22 regulates aurora B activity and microtubule-kinetochore interactions at mitosis. *The Journal of Cell Biology*, 191(1), pp.61–74.
- Primorac, I. et al., 2013. Bub3 reads phosphorylated MELT repeats to promote spindle assembly checkpoint signaling. *eLife*, 2, p.e01030.
- Przewloka, M.R. et al., 2011. CENP-C is a structural platform for kinetochore assembly. *Current biology : CB*, 21(5), pp.399–405.
- Qian, J. et al., 2013. Aurora B defines its own chromosomal targeting by opposing the recruitment of the phosphatase scaffold Repo-Man. *Current biology : CB*, 23(12), pp.1136–1143.

- Qian, J. et al., 2011. PP1/Repo-man dephosphorylates mitotic histone H3 at T3 and regulates chromosomal aurora B targeting. *Current biology : CB*, 21(9), pp.766–773.
- Ramadan, K. et al., 2007. Cdc48/p97 promotes reformation of the nucleus by extracting the kinase Aurora B from chromatin. *Nature*, 450(7173), pp.1258–1262.
- Rapsomaniki, M.A. et al., 2012. easyFRAP: an interactive, easy-to-use tool for qualitative and quantitative analysis of FRAP data. *Bioinformatics (Oxford, England)*, 28(13), pp.1800–1801.
- Rauh, N.R. et al., 2005. Calcium triggers exit from meiosis II by targeting the APC/C inhibitor XErp1 for degradation. *Nature*, 437(7061), pp.1048–1052.
- Rieder, C.L. & Khodjakov, A., 2003. Mitosis through the microscope: advances in seeing inside live dividing cells. *Science (New York, NY)*, 300(5616), pp.91–96.
- Rieder, C.L. et al., 1994. Anaphase onset in vertebrate somatic cells is controlled by a checkpoint that monitors sister kinetochore attachment to the spindle. *The Journal of Cell Biology*, 127(5), pp.1301–1310.
- Rieder, C.L. et al., 1995. The checkpoint delaying anaphase in response to chromosome monoorientation is mediated by an inhibitory signal produced by unattached kinetochores. *The Journal of Cell Biology*, 130(4), pp.941–948.
- Rodriguez-Bravo, V. et al., 2014. Nuclear pores protect genome integrity by assembling a premitotic and Mad1-dependent anaphase inhibitor. *Cell*, 156(5), pp.1017–1031.
- Romano, A. et al., 2003. CSC-1: a subunit of the Aurora B kinase complex that binds to the survivin-like protein BIR-1 and the incenp-like protein ICP-1. *The Journal of Cell Biology*, 161(2), pp.229–236.
- Rosenberg, J.S., Cross, F.R. & Funabiki, H., 2011. KNL1/Spc105 recruits PP1 to silence the spindle assembly checkpoint. *Current biology : CB*, 21(11), pp.942–947.
- Ruchaud, S., Carmena, M. & Earnshaw, W.C., 2007. Chromosomal passengers: conducting cell division. *Nature reviews Molecular cell biology*, 8(10), pp.798–812.
- Salimian, K.J. et al., 2011. Feedback Control in Sensing Chromosome Biorientation by the Aurora B Kinase. *Current Biology*, 21(13), pp.1158–1165.

- Samejima, K. et al., 2015. The Inner Centromere Protein (INCENP) Coil Is a Single α -Helix (SAH) Domain That Binds Directly to Microtubules and Is Important for Chromosome Passenger Complex (CPC) Localization and Function in Mitosis. *The Journal of biological chemistry*, 290(35), pp.21460–21472.
- Sampath, S.C. et al., 2004. The chromosomal passenger complex is required for chromatin-induced microtubule stabilization and spindle assembly. *Cell*, 118(2), pp.187–202.
- Santaguida, S. & Musacchio, A., 2009. The life and miracles of kinetochores. *The EMBO Journal*, 28(17), pp.2511–2531.
- Santaguida, S. et al., 2011. Evidence that Aurora B is implicated in spindle checkpoint signalling independently of error correction. *The EMBO Journal*, 30(8), pp.1508–1519.
- Santamaría, A. et al., 2011. The Plk1-dependent phosphoproteome of the early mitotic spindle. *Molecular & cellular proteomics : MCP*, 10(1), pp.M110.004457–M110.004457.
- Saurin, A.T. et al., 2011. Aurora B potentiates Mps1 activation to ensure rapid checkpoint establishment at the onset of mitosis. *Nature communications*, 2, p.316.
- Schmidt, A. et al., 2005. Xenopus polo-like kinase Plx1 regulates XErp1, a novel inhibitor of APC/C activity. *Genes & development*, 19(4), pp.502–513.
- Screpanti, E. et al., 2011. Direct binding of Cenp-C to the Mis12 complex joins the inner and outer kinetochore. *Current biology : CB*, 21(5), pp.391–398.
- Sessa, F. et al., 2005. Mechanism of Aurora B activation by INCENP and inhibition by hesperadin. *Molecular cell*, 18(3), pp.379–391.
- Shepperd, L.A. et al., 2012. Phosphodependent recruitment of Bub1 and Bub3 to Spc7/KNL1 by Mph1 kinase maintains the spindle checkpoint. *Current biology : CB*, 22(10), pp.891–899.
- Silió, V., McAinsh, A.D. & Millar, J.B., 2015. KNL1-Bubs and RZZ Provide Two Separable Pathways for Checkpoint Activation at Human Kinetochores., 35(5), pp.600–613.
- Simonetta, M. et al., 2009. The influence of catalysis on mad2 activation dynamics. D. Pellman, ed. *PLoS biology*, 7(1), p.e10.

- Skoufias, D.A. et al., 2001. Mammalian mad2 and bub1/bubR1 recognize distinct spindle-attachment and kinetochore-tension checkpoints. *Proceedings of the National Academy of Sciences of the United States of America*, 98(8), pp.4492–4497.
- Speliotes, E.K. et al., 2000. The survivin-like *C. elegans* BIR-1 protein acts with the Aurora-like kinase AIR-2 to affect chromosomes and the spindle midzone. *Molecular cell*, 6(2), pp.211–223.
- Steigemann, P. et al., 2009. Aurora B-mediated abscission checkpoint protects against tetraploidization. *Cell*, 136(3), pp.473–484.
- Stern, B.M. & Murray, A.W., 2001. Lack of tension at kinetochores activates the spindle checkpoint in budding yeast. *Current biology : CB*, 11(18), pp.1462–1467.
- Sudakin, V., Chan, G.K. & Yen, T.J., 2001. Checkpoint inhibition of the APC/C in HeLa cells is mediated by a complex of BUBR1, BUB3, CDC20, and Mad2. *The Journal of Cell Biology*, 154(5), pp.925–936.
- Suijkerbuijk, S.J.E. et al., 2012. Integration of kinase and phosphatase activities by BUBR1 ensures formation of stable kinetochore-microtubule attachments., 23(4), pp.745–755.
- Sun, L. et al., 2008. EB1 promotes Aurora-B kinase activity through blocking its inactivation by protein phosphatase 2A. *Proceedings of the National Academy of Sciences of the United States of America*, 105(20), pp.7153–7158.
- Suzuki, A. et al., 2011. Spindle microtubules generate tension-dependent changes in the distribution of inner kinetochore proteins. *The Journal of Cell Biology*, 193(1), pp.125–140.
- Suzuki, A. et al., 2014. The architecture of CCAN proteins creates a structural integrity to resist spindle forces and achieve proper Intrakinetochore stretch., 30(6), pp.717–730.
- Tan, L. & Kapoor, T.M., 2011. Examining the dynamics of chromosomal passenger complex (CPC)-dependent phosphorylation during cell division. *Proceedings of the National Academy of Sciences of the United States of America*, 108(40), pp.16675–16680.
- Tanaka, H. et al., 2001. Cloning and characterization of human haspin gene encoding haploid germ cell-specific nuclear protein kinase. *Molecular human reproduction*, 7(3), pp.211–218.

- Tanaka, H. et al., 1999. Identification and characterization of a haploid germ cell-specific nuclear protein kinase (Haspin) in spermatid nuclei and its effects on somatic cells. *The Journal of biological chemistry*, 274(24), pp.17049–17057.
- Tanaka, T. et al., 2000. Cohesin ensures bipolar attachment of microtubules to sister centromeres and resists their precocious separation. *Nature Publishing Group*, 2(8), pp.492–499.
- Tanaka, T.U. et al., 2002. Evidence that the Ipl1-Sli15 (Aurora kinase-INCENP) complex promotes chromosome bi-orientation by altering kinetochore-spindle pole connections. *Cell*, 108(3), pp.317–329.
- Tang, Z. et al., 2004. Human Bub1 protects centromeric sister-chromatid cohesion through Shugoshin during mitosis. *Proceedings of the National Academy of Sciences of the United States of America*, 101(52), pp.18012–18017.
- Tanno, Y. et al., 2010. Phosphorylation of mammalian Sgo2 by Aurora B recruits PP2A and MCAK to centromeres. *Genes & development*, 24(19), pp.2169–2179.
- Tanno, Y. et al., 2015. The inner centromere-shugoshin network prevents chromosomal instability. *Science (New York, NY)*, 349(6253), pp.1237–1240.
- Tauchman, E.C., Boehm, F.J. & DeLuca, J.G., 2015. Stable kinetochore-microtubule attachment is sufficient to silence the spindle assembly checkpoint in human cells. *Nature communications*, 6, p.10036.
- Tooley, J.G., Miller, S.A. & Stukenberg, P.T., 2011. The Ndc80 complex uses a tripartite attachment point to couple microtubule depolymerization to chromosome movement. *Molecular biology of the cell*, 22(8), pp.1217–1226.
- Trivedi, P. & Stukenberg, P.T., 2016. A Centromere-Signaling Network Underlies the Coordination among Mitotic Events. *Trends in Biochemical Sciences*, 41(2), pp.160–174.
- Tseng, B.S. et al., 2010. Dual detection of chromosomes and microtubules by the chromosomal passenger complex drives spindle assembly., 18(6), pp.903–912.
- Tsukahara, T., Tanno, Y. & Watanabe, Y., 2010. Phosphorylation of the CPC by Cdk1 promotes chromosome bi-orientation. *Nature*, 467(7316), pp.719–723.
- Uchida, K.S.K. et al., 2009. Kinetochore stretching inactivates the spindle assembly checkpoint. *The Journal of Cell Biology*, 184(3), pp.383–390.

- Uren, A.G. et al., 2000. Survivin and the inner centromere protein INCENP show similar cell-cycle localization and gene knockout phenotype. *Current Biology*, 10(21), pp.1319–1328.
- Vader, G. et al., 2006. Survivin mediates targeting of the chromosomal passenger complex to the centromere and midbody. *EMBO reports*, 7(1), pp.85–92.
- Vader, G. et al., 2007. The chromosomal passenger complex controls spindle checkpoint function independent from its role in correcting microtubule kinetochore interactions. *Molecular biology of the cell*, 18(11), pp.4553–4564.
- van der Horst, A. et al., 2015. Inter-domain Cooperation in INCENP Promotes Aurora B Relocation from Centromeres to Microtubules. *Cell reports*, 12(3), pp.380–387.
- Van Der Waal, M.S. et al., 2012. Mps1 promotes rapid centromere accumulation of Aurora B. *EMBO reports*, 13(9), pp.847–854.
- Villa, F. et al., 2009. Crystal structure of the catalytic domain of Haspin, an atypical kinase implicated in chromatin organization. *Proceedings of the National Academy of Sciences of the United States of America*, 106(48), pp.20204–20209.
- Wan, X. et al., 2009. Protein architecture of the human kinetochore microtubule attachment site. *Cell*, 137(4), pp.672–684.
- Wang, E., Ballister, E.R. & Lampson, M.A., 2011. Aurora B dynamics at centromeres create a diffusion-based phosphorylation gradient. *The Journal of Cell Biology*.
- Wang, F. et al., 2011. A positive feedback loop involving Haspin and Aurora B promotes CPC accumulation at centromeres in mitosis. *Current biology : CB*, 21(12), pp.1061–1069.
- Wang, F. et al., 2012. Haspin inhibitors reveal centromeric functions of Aurora B in chromosome segregation. *The Journal of Cell Biology*, 199(2), pp.251–268.
- Wang, F. et al., 2010. Histone H3 Thr-3 phosphorylation by Haspin positions Aurora B at centromeres in mitosis. *Science (New York, NY)*, 330(6001), pp.231–235.
- Wang, Y. et al., 2014. The current view for the silencing of the spindle assembly checkpoint. *Cell cycle (Georgetown, Tex)*, 13(11), pp.1694–1701.

- Waters, J.C. et al., 1998. Localization of Mad2 to kinetochores depends on microtubule attachment, not tension. *The Journal of Cell Biology*, 141(5), pp.1181–1191.
- Weis, K., Ryder, U. & Lamond, A.I., 1996. The conserved amino-terminal domain of hSRP1 alpha is essential for nuclear protein import. *The EMBO Journal*, 15(8), pp.1818–1825.
- Welburn, J.P.I. et al., 2010. Aurora B phosphorylates spatially distinct targets to differentially regulate the kinetochore-microtubule interface. *Molecular cell*, 38(3), pp.383–392.
- Wheatley, S.P. et al., 2001. INCENP is required for proper targeting of Survivin to the centromeres and the anaphase spindle during mitosis. *Current Biology*, 11(11), pp.886–890.
- Williams, S.J., Abrieu, A. & Losada, A., 2016. Bub1 targeting to centromeres is sufficient for Sgo1 recruitment in the absence of kinetochores. *Chromosoma*, pp.1–8.
- Wojcik, E. et al., 2001. Kinetochore dynein: its dynamics and role in the transport of the Rough deal checkpoint protein. *Nature Publishing Group*, 3(11), pp.1001–1007.
- Wynne, D.J. & Funabiki, H., 2015. Kinetochore function is controlled by a phospho-dependent coexpansion of inner and outer components. *The Journal of Cell Biology*, 210(6), pp.899–916.
- Xue, J.Z. et al., 2013. Chromatin-bound Xenopus Dppa2 shapes the nucleus by locally inhibiting microtubule assembly., 27(1), pp.47–59.
- Yamagishi, Y. et al., 2012. MPS1/Mph1 phosphorylates the kinetochore protein KNL1/Spc7 to recruit SAC components. *Nature*, 14(7), pp.746–752.
- Yamagishi, Y. et al., 2010. Two histone marks establish the inner centromere and chromosome bi-orientation. *Science (New York, NY)*, 330(6001), pp.239–243.
- Yang, M. et al., 2007. p31comet blocks Mad2 activation through structural mimicry. *Cell*, 131(4), pp.744–755.
- Yang, Y. et al., 2008. Phosphorylation of HsMis13 by Aurora B kinase is essential for assembly of functional kinetochore. *The Journal of biological chemistry*, 283(39), pp.26726–26736.

- Yang, Z. et al., 2009. Cells satisfy the mitotic checkpoint in Taxol, and do so faster in concentrations that stabilize syntelic attachments. *The Journal of Cell Biology*, 186(5), pp.675–684.
- Yoshida, M.M. et al., 2016. SUMOylation of DNA topoisomerase II α regulates histone H3 kinase Haspin and H3 phosphorylation in mitosis. *The Journal of Cell Biology*, 213(6), pp.665–678.
- Yoshimura, Y. et al., 2001. Nested genomic structure of haploid germ cell specific haspin gene. *Gene*, 267(1), pp.49–54.
- Zhang, G. et al., 2015. Distinct domains in Bub1 localize RZZ and BubR1 to kinetochores to regulate the checkpoint. *Nature communications*, 6, p.7162.
- Zhu, T. et al., 2013. Phosphorylation of microtubule-binding protein Hec1 by mitotic kinase Aurora B specifies spindle checkpoint kinase Mps1 signaling at the kinetochore. *The Journal of biological chemistry*, 288(50), pp.36149–36159.
- Zierhut, C. et al., 2014. Nucleosomal regulation of chromatin composition and nuclear assembly revealed by histone depletion. *Nature structural & molecular biology*, 21(7), pp.617–625.